CRPP

CENTRE DE RECHERCHES EN PHYSIQUE DES PLASMAS
FACULTÉ DES SCIENCES DE BASE
ASSOCIATION EURATOM - CONFÉDÉRATION SUISSE

ÉCOLE POLYTECHNIQUE
FÉDÉRALE DE LAUSANNE

ANNUAL REPORT

2009

Table of content

Préface

Cher Lecteur,

C'est un privilège de présenter le Rapport Annuel 2009 du Centre de Recherches en Physique des Plasmas.

Nos activités de recherche se sont focalisées sur l'avancement de la science et de la technologie de la fusion, ainsi que sur ITER et l' «Approche Elargie». Il est important de noter que la Suisse a rejoint formellement en 2009 le projet ITER et l'Approche Elargie au travers de l'Euratom. Cette décision du Conseil Fédéral, ratifiée par le Parlement, est un signe clair de l'engagement de la Suisse pour le développement de l'énergie de fusion. Pour nous tous, la «génération ITER» de jeûnes diplômés et doctorants, le personnel technique et scientifique, ceci est un encouragement à continuer nos efforts dans la quête d'une source d'énergie inépuisable et respectueuse de l'environnement. Le dévouement de tous mes collègues a permis de maintenir le CRPP au premier plan de la recherche comme un des laboratoires à l'avant-garde de la science et de la technologie de la fusion. Je voudrais remercier chacun pour ses efforts.

La recherche en fusion nécessite un financement important. Plusieurs institutions, publiques et privées, suisses et internationales, ont soutenu nos activités. Je voudrais ici leur exprimer mes plus grands remerciements

Prof. M.Q. Tran
Directeur Général

Foreword

Dear Reader,

It is a privilege for me to present the 2009 Annual Report of the Centre de Recherches en Physique des Plasmas.

Our research activities were focused on the advancement of fusion science and technology and on ITER and Broader Approach. It is important to note that, in 2009, Switzerland joined formally ITER and the Broader Approach through Euratom. This decision of the Swiss Federal Council, ratified by the Parliament, is a clear sign of the commitment of Switzerland to the development of fusion energy. For all of us, the "ITER generation" of young Master students and PhD candidates, the technical and scientific staff, it is an encouragement to continue our effort in the quest of a sustainable, environment-friendly source of energy. The dedication of all my colleagues has allowed maintaining the CRPP at the forefront of research and as one of the leading laboratories in fusion science and technology. I would like to thank each and all of them for their effort.

Research in Fusion requires important funding. Many institutions, public and private, Swiss and international, have supported our activities. I would like to express here all my deepest thanks to them.

Prof. M.Q. Tran
General Director

Vorwort

Liebe Leserinn und Leser,

Es ist ein Privileg für mich, Ihnen hiermit den Jahresbericht 2009 des Centre de Recherches en Physique des Plasmas (CRPP) vorlegen zu können.

Wie bereits in den vergangenen Jahren, waren unsere wissenschaftlichen Aktivitäten auf Fusionsforschung und –technologie, die Unterstützung des ITER-Projekts sowie des erweiterten Forschungsprogramms zur Fusion ("broader approach") ausgerichtet. Es ist wichtig zu erwähnen, dass die Schweiz im Jahr 2009 ihren Beitrag zu ITER und dem erweiterten Programm zur Fusion als EURATOM-Partner formell bestätigt hat. Diese Entscheidung des Schweizerischen Bundesrats, die vom Parlament ratifiziert wurde, ist ein deutliches Zeichen dafür, dass sich die Schweiz für die Entwicklung der Kernfusion als zukünftiger Energiequelle einsetzt. Für uns alle, Wissenschaftler und Ingenieure, aber insbesondere für die junge "ITER-Generation" von Studenten und Doktoranden, bedeutet dies eine Ermutigung, die Anstrengungen zur Entwicklung einer dauerhaften und umweltfreundlichen Energiequelle fortzuführen.

Der unermüdliche Einsatz der Kollegen und Mitarbeiter hat dazu beigetragen, dass das CRPP zu den führenden Forschungsinstituten in der Kernfusion zählt und Beiträge zur Spitzenforschung leistet. Bei dieser Gelegenheit möchte allen Mitarbeitern meine dankbare Anerkennung aussprechen.

Die Fusionsforschung ist auf erhebliche finanzielle Unterstützung angewiesen. Zahlreiche Institutionen aus dem öffentlichen und privaten Bereich haben unsere Forschungstätigkeiten gefördert. Dafür möchte ich mich an dieser Stelle nochmals ausdrücklich bedanken.

Prof. M.Q. Tran
General Direktor

Prefazione

Caro lettore,

È per me un privilegio presentare il Rapporto Annuale del Centro di Ricerca in Fisica dei Plasmi per il 2009.

Le nostre attività di ricerca si sono concentrate sugli aspetti sia scientifici che tecnologici della fusione, su ITER e sul cosiddetto "Broader Approach" (programma internazionale globale di ricerca sulla fusione). Merita una menzione particolare il fatto che nel 2009 la Svizzera è divenuta un membro ufficiale del progetto ITER e del "Broader Approach" attraverso l'Euratom. Questa decisione del Consiglio Federale Svizzero, ratificata dal Parlamento, è una chiara dimostrazione dell'impegno della Svizzera nello sviluppo dell'energia da fusione nucleare. Per tutti noi, la "generazione di ITER" di giovani studenti di Master e di dottorato cosí come il personale tecnico e scientifico, questo impegno costituisce un incoraggiamento a proseguire i nostri sforzi alla ricerca di una sorgente di energia sostenibile e rispettosa dell'ambiente. La dedizione di tutti i miei colleghi ha permesso al CRPP di

mantenersi all'avanguardia e di rimanere uno dei laboratori principali della scienza e tecnologia della fusione. Desidero perció ringraziare ognuno di loro per il loro impegno.

La ricerca sulla fusione richiede finanziamenti importanti. Molte istituzioni, pubbliche e private, svizzere e internazionali, hanno sostenuto le nostre attivitá e desidero esprimere loro in quest'occasione la mia profonda gratitudine.

Prof. M.Q. Tran
Direttore Generale

1 INTRODUCTION

1.1 The international frame and its relation to the Swiss programme

1.1.1 ITER

The participation of Switzerland in ITER as a member of the Euratom Party was ratified by the Swiss Parliament in 2008 and entered into force in 2009. In parallel, Switzerland also became full member of the ITER European Domestic Agency, the Joint Undertaking Fusion for Energy.

Regarding ITER, the assessment on cost, time schedule, technical and managerial aspects were at the centre of the international discussions. It is expected that in 2010, the so-called "Baseline" of ITER, which includes not only the scientific objectives, but also cost and planning, will be approved by the seven Parties (China, EU, India, Japan, Korea, Russia and USA).

In parallel, the construction of the machine is progressing with the signature of many procurement arrangements concerning major equipments to be delivered in kind by the Parties.

1.1.2 Euratom

It was decided to continue the operation of JET in 2011, until the end of the present Euratom framework programme. This will allow the scientific exploitation of the set of major upgrades, which concern the heating systems, the beryllium wall and the use of tungsten in the divertor.

Due to Euratom financial constraints, the Associations will see their support by Euratom decrease significantly in 2011. This decrease was already felt in 2009 and will continue in 2010-2011. While its support to fusion remains very strong and the importance of national fusion programmes - in particular the Swiss one - is recognized, because of the tight financial means the Euratom expects a stronger participation of member and associated states in their national programme. This vision has been expressed to the Swiss counterparts (the State Secretariat for Education and Research, the Council of Swiss Federal Institute of Technology, the Swiss Federal Institute of Technology Lausanne and the CRPP). The analysis and the Swiss strategy in response to the European approach are still under discussion.

In 2009, under the auspices of the European Fusion Development Agreement (EFDA) and a new EFDA Implementing Agreement, a new high performance computing (HPC) platform solely dedicated to European fusion research was put into operation. While the signature process by Switzerland is not yet completed, CRPP-led projects have been allocated a significant fraction of CPU time (~16%) of this 100 Teraflops supercomputer.

1.2 A brief summary of the CRPP activities

The research activities at the CRPP during 2009 followed the strategy which was proposed and endorsed by the Evaluation Panel set up by the School of Basic Science in 2005. They are focused on the contributions to ITER construction and on the advancement of plasma science in preparation for the scientific exploitation of ITER and for DEMO. Besides these activities, the CRPP also continued to work on tasks allocated to Switzerland in the frame the Broader Approach R&D, and on plasma processes. Last but not least, education and training are also two important items of 2009 activities.

The 2009 annual report gives the details of our achievements. They have been the subjects of more than hundred publications or presentations in international conferences. As highlights, we can note:

- the realisation on TCV of a new divertor configuration (called “snowflake” due to the analogy of the magnetic field lines separatrix shape with that of a snowflake) and the evidence of edge transport barriers in this configuration;

- the evidence of the coupling of electron heating (by electron cyclotron wave) and ion heating via ion acoustic waves;

- the further development of highly efficient first principle based turbulence numerical simulation codes for HPC platforms;

- on TORPEX, a specialized basic plasma device, the studies were focused on the propagation of plasma “blobs” and the interaction between energetic ion population and turbulence;

- a qualification of ITER superconducting cables was performed on SULTAN;

- for Broader Approach tasks, the CRPP continued the design of the creep fatigue test cell to be implemented on IFMIF and the R&D on Small Sample Test Technology;

- the development of industrial processes has continued in 2009 with the same success as in the past.

1. INTRODUCTION

1.1 La situation internationale en relation avec le programme Suisse

1.1.1 ITER

La participation de la Suisse à ITER, en tant que membre de l'Euratom a été ratifiée par le parlement en 2008 et a été mise en œuvre en 2009. Parallèlement à cela, la Suisse est également devenue membre à part entière de l'Agence Intérieure Européenne d'ITER, l'entreprise commune « Fusion For Energy ».

En ce qui concerne ITER, l'évaluation des coûts, du calendrier et des aspects techniques et de direction ont été au centre des discussions internationales. On s'attend à ce qu'en 2010 la « Ligne de Référence » pour ITER, qui inclut non seulement les objectifs scientifiques, mais aussi les coûts et la planification, soit approuvée par les sept Partenaires (la Chine, l'Union Européenne, l'Inde, le Japon, la Corée du Sud, la Russie et les Etats-Unis).

En parallèle, la construcition de la machine a progressé, avec la signature de plusieurs arrangements pour l'approvisionnement des pièces principales, qui seront livrées en nature par les Partenaires.

1.1.2 Euratom

Il a été décidé de continuer l'opération de JET en 2011, jusqu'à la fin du programme cadre actuel de l'Euratom. Ceci va permettre l'exploitation scientifique d'un ensemble d'améliorations significatives concernant les systèmes de chauffage, la paroi de béryllium et l'utilisation de tungstène dans le diverteur.

A cause de contraintes financières de l'Euratom, les Associations verront leur support décroître significativement en 2011. Cette décroissance a déjà été ressentie en 2009 et continuera dans les années 2010-2011. Alors que son support de la fusion reste très fort, et que l'importance des programmes nationaux de la fusion, et en particulier celui de la Suisse, est reconnue, l'Euratom s'attend à une plus forte participation des états membres et associés à leur programme national. Cette vision a été exprimée aux partenaires suisses)le Secrétariat d'Etat à l'Education et à la Recherche, le Conseil des Ecoles Polytechniques Fédérales, l'Ecole Polytechnique Fédérale de Lausanne et le CRPP), L'analyse et la stratégie de la Suisse en réponse à l'approche européenne sont encore en discussion.

En 2009, sous les auspices de l'EFDA (European Fusion Development Agreement) et d'un nouvel accord d'implémentation, une nouvelle plateforme de calcul à haute performance (HPC), dédiée uniquement à le recherche européenne sur la fusion, a été mise en service. Alors que le processus de signature par la Suisse n'est pas encore terminé, les projets conduits par le CRPP se sont vus allouer une portion significative (16%) du temps de calcul sur ce super-ordinateur de 100 TeraFlops.

1.2 Un bref résumé des activités du CRPP

Les activités de recherche au CRPP en 2009 ont suivi la stratégie proposée par le panel d'experts établi par la Faculté des Sciences de Base de l'EPFL en 2005. Elles se sont focalisées sur des contributions à la construction d'ITER, l'avancement de la science des plasmas en préparation de l'exploitation scientifique d'ITER et pour DEMO. Outre ces activités, le CRPP a continué à travailler aux tâches de recherche & développement attribuées à la Suisse dans le cadre de l'Approche Elargie, ainsi que sur les procédés plasma. Enfin et surtout, l'enseignement et la formation ont été deux activités importantes en 2009.

Ce rapport annuel 2009 donne les détails de nos réalisations. Elles ont fait l'objet de plus d'une centaine de publications et présentations à des conférences internationales. Comme points saillants, nous pouvons noter :

- La réalisation dans TCV d'une nouvelle configuration de diverteur (appelée « flocon de neige » par analogie de la forme de la séparatrice des lignes de champ magnétique), et la mise en évidence de barrières de transport dans cette configuration ;
- La démonstration du couplage du chauffage des électrons (par ondes cyclotroniques électroniques) et du chaiffage des ions, par l'intermédiaire des ondes acoustiques ioniques ;
- Le développement et l'amélioration de codes de simulations numériques de la turbulence, basés sur les premiers principes, et hautement efficaces sur des plateformes de calcul à haute performance (HPC) ;
- Sur TORPEX, une expérience spécialisée de plasmas de base, les études se sont focalisées sur la propagation de « blobs » de plasma et sur l'interaction entre la population d'ions énergétiques et la turbulence ;
- La qualification des câbles supraconducteurs pour ITER a été accomplie sur SULTAN ;
- Pour les tâches de l'Approche Elargie, le CRPP a continué le design de la cellule de test de fluage qui sera implémentée sur IFMIF et la R&D sur la technologie de test de petits échantillons ;
- Le développement des procédés plasmas a continué en 2009 avec le même succès que par le passé.

1 EINLEITUNG

1.1 Der internationale Rahmen und die Beziehung zum schweizerischen Forschungsprogramm

1.1.1 ITER

Die gesetzlichen Grundlagen zur Beteiligung der Schweiz als EURATOM-Mitglied am ITER-Programm wurden im Jahr 2008 vom Parlament ratifiziert und traten im Jahr 2009 in Kraft. Gleichzeitig erhielt die Schweiz den Status eines vollwertigen Mitglieds innerhalb der europäischen ITER-Agentur, dem sogen. "Joint Undertaking Fusion for Energy".

Die international geführte Diskussion in Bezug auf ITER konzentrierte sich auf die Beurteilung von Kostenaufwand, Zeitplan und technischer sowie organisatorischer Aspekte.
Es wird erwartet, dass im Jahr 2010 das sogen. Basisprogramm von ITER, das nicht nur die wissenschaftlichen Ziele, sondern auch Kosten und Planung beinhaltet, von den sieben Partnern (China, Europäische Union, Indien, Japan, Korea, Russische Föderation und USA) angenommen wird.

Zur gleichen Zeit geht es in der Bauphase von ITER voran; mehrere Verträge zur Bereitstellung von bedeutenden Komponenten durch die ITER-Partner wurden unterzeichnet.

1.1.2 EURATOM

Nach jüngsten Entscheidungen soll der Betrieb von JET (Joint European Torus) bis zum Ablauf des gegenwärtigen EURATOM Rahmenprogramms fortgeführt werden. Auf diese Weise kommen einige bedeutende technische Erweiterungen wie zusätzliche Heizung, Berylliumbeschichtung der ersten Wand und Divertorkomponenten aus Wolfram genutzt werden.

Wegen der finanziellen Rahmenbedingungen von EURATOM werden allerdings die Zuwendungen an die Assoziationen im Jahr 2011 deutlich reduziert werden. Der Rückgang war bereits 2009 spürbar und wird in den Jahren 2010 bis 2011 anhalten. Innerhalb von EURATOM ist zwar die Unterstützung der Fusionsforschung weiter hin stark und die Bedeutung der nationalen Forschungsprogramme, darunter auch dasjenige der Schweiz, werden anerkannt, aber man erwartet, dass die Assoziationen einen grösseren Anteil ihrer nationalen Programme selbst finanzieren. Die zuständigen Stellen in der Schweiz (Staatssekretariat für Bildung und Forschung, Rat der ETHs, ETH-Lausanne und CRPP) wurden über diese Auffassung informiert. Die Analyse der Sachlage ist noch im Gang und über eine Strategie der Schweiz, die diesen veränderten Bedingungen angepasst ist, wird noch diskutiert.

Im Jahr 2009 wurde unter der Patenschaft von EFDA (European Fusion Development Agreement) und als Folge eines neuen EFDA-Abkommens ein neues Hochleistungs-Rechenzentrum eingeweiht, das speziell der Fusionsforschung in Europa zur Verfügung steht. Obwohl die Unterschrift der Schweiz zu diesem

Abkommen noch aussteht, konnte das CRPP bereits einen bedeutenden Anteil der verfügbaren Rechenzeit (ca. 16% der CPU Zeit) dieses 100-Teraflop-Rechners nutzen.

1.2 Eine Zusammenfassung der Forschungsergebnisse des CRPP

Auch im Jahr 2009 folgten die Forschungsaktivitäten am CRPP der empfohlenen und anerkannten Strategie einer Expertengruppe, die im Jahr 2005 von der Fakultät für Basis-Wissenschaften der ETH-L einberufen worden war. Die Schwerpunkte sind Mitarbeit am ITER-Projekt, Beiträge zum Fortschritt in der Plasmaforschung in Vorbereitung and als Unterstützung für ITER und DEMO. Darüber hinaus verfolgt das CRPP weiterhin Aufgaben, die der Schweiz im Rahmen des erweiterten Programms zur Fusion zugewiesen wurden und ist auf dem Gebiet der Plasmatechnologie tätig. Ausbildung und Weiterbildung nehmen nach wie vor einen wichtigen Platz ein.

Der Jahresbericht 2009 gibt einen Ueberblick der Tätigkeiten und erbrachten Leistungen. Die Forschungsergebnisse waren Gegenstand von mehr als hundert Veröffentlichungen und Konferenzbeiträgen. Herausragende Ergebnisse sind :

- die Verwirklichung einer neuartigen Divertor-Konfiguration (“snowflake” wegen der Aehnlichkeit des magnetischen Flussfächenprofils im Separatrixbereich mit einer Schneeflocke) und gleichzeitiger Erzeugung einer Transportbarriere am Plasmarand
- Nachweis einer Kopplung der Heizung von Elektronen und Ionen (über ionenakustische Wellen) bei Anwendung von Elektronenzyklotronheizung
- Weiterentwicklung von leistungsfähigen numerischen Simulationen der Plasmaturbulenz (ausgehend von einer allgemein gültigen Beschreibung) für den Einsatz auf Hochleistungsrechnern
- Untersuchungen zur Ausbreitung von turbulenten Strukturen (sogen. “blobs”) und zur Wechselwirkung zwischen energiereichen Ionen und Instabilitäten am Experiment TORPEX (Experiment für Grundlagenforschung)
- Untersuchungen und Bewertungen von Supraleitern im Prüfstand SULTAN
- Entwicklung einer Testzelle für Materialprüfungen im Rahmen des erweiterten Programms zur Fusion (Projekt IFMIF) und weitere Beiträge zur Technologie der Materialprüfung an kleinen Testobjekten.
- Erfolgreiche Weiterentwicklung von Prozessen in der Plasmatechnologie.

1. INTRODUZIONE

1.1 La situazione internazionale in relazione al programma svizzero

1.1.1 ITER

La partecipazione della Svizzera ad ITER in qualitá di membro dell'Euratom è stata ratificata dal Parlamento svizzero in 2008 ed è divenuta ufficiale in 2009. In parallelo, la Svizzera è anche divenuta membro a pieno titolo dell'Ente Europeo per ITER, l'Impresa Comune "Fusion for Energy".

Per quanto riguarda ITER, la valutazione dei costi, della pianificazione e della gestione sono stati al centro delle discussioni internazionali. È previsto che nel 2010 il cosiddetto "Baseline" (strategia di riferimento) di ITER, comprendente non solo gli obiettivi scientifici ma anche i costi e la pianificazione, sia approvato dalle sette parti (Cina, UE, India, Giappone, Corea, Russia e Stati Uniti).

In parallelo, la costruzione della macchina progredisce grazie alla firma di svariati contratti di appalto, in natura, per componenti di base che saranno forniti dalle sette parti contraenti.

1.1.2 Euratom

È stata presa la decisione di continuare l'operazione di JET nel 2011, fino al termine dell'attuale programma quadro Euratom. Questo permetterà l'utilizzo scientifico di diverse importanti modifiche, che coinvolgono i sistemi di riscaldamento, il muro ricoperto di berillio e l'uso del tungsteno nel divertore.

Le attuale ristrettezze finanziarie comporteranno una riduzione imponente del sostegno delle Associazioni da parte dell'Euratom nel 2011, continuando un andamento già iniziato nel 2009. Benché rimanga un forte sostenitore della fusione e riconosca l'importanza dei programmi nazionali di fusione e di quello svizzero in particolare, l'Euratom richiede oggi una maggiore partecipazione degli Stati membri e associati a causa dei problemi finanziari. Questa prospettiva è stata espressa alle istanze svizzere (la Segreteria di Stato per l'educazione e la ricerca, il Consiglio dei Politecnici Federali di Zurigo e Losanna e il CRPP), che stanno attualmente analizzando la situazione e discutendo della strategia svizzera in risposta al nuovo approccio europeo.

Nel 2009, sotto gli auspici dell'Accordo Europeo per lo Sviluppo della Fusione (EFDA) e di un nuovo accordo di applicazione EFDA, è entrato in operazione un nuovo centro di calcolo ad alte prestazioni (HPC) interamente dedicato alla ricerca europea sulla fusione. Benché le procedure per la firma dell'accordo da parte della Svizzera non siano state ancora completate, progetti gestiti dal CRPP hanno ottenuto una percentuale elevata di tempo CPU (~16%) su questo supercomputer da 100 Teraflops.

1.2 Breve riassunto delle attività del CRPP

Le attività di ricerca al CRPP durante il 2009 hanno seguito la strategia proposta e approvata dal comitato di valutazione convocato dalla Facoltà di Scienze di Base nel 2005. Queste attività sono concentrate sui contributi alla costruzione di ITER e sulla promozione della ricerca scientifica sul plasma in vista dell'utilizzo scientifico di ITER e di DEMO. Il CRPP ha anche continuato ad eseguire progetti assegnati alla Svizzera nel quadro di Ricerca e Sviluppo nel Broader Approach e ad occuparsi di processi al plasma. Vanno menzionate infine le attività fondamentali di educazione e di formazione.

Il Rapporto Annuale 2009 espone i dettagli dei nostri risultati, che sono confluiti in oltre cento pubblicazioni o presentazioni a congressi internazionali. Si possono evidenziare alcuni risultati principali:

- la realizzazione in TCV di una nuova configurazione di divertore (detta "fiocco di neve" per via della somiglianza tra quest'ultimo e la forma delle line di campo che formano la separatrice) e la scoperta di barriere di trasporto al bordo in questa configurazione;

- la dimostrazione di un accoppiamento tra il riscaldamento degli elettroni (da parte di onde ciclotroniche elettroniche) e degli ioni attraverso onde acustiche ioniche;

- il continuo sviluppo a partire da principi primi di programmi ad alta efficienza di simulazione numerica della turbolenza per centri HPC;

- su TORPEX, un dispositivo specializzato per plasmi di base, gli studi si sono concentrati sulla propagazione di "blobs" (grumi di plasma) e sull'interazione tra una popolazione di ioni ad alta energia e la turbolenza;

- una qualificazione di cavi superconduttori per ITER è stata effettuata su SULTAN;

- nel contesto del Broader Approach, il CRPP ha proseguito la progettazione della camera di prova per studi di fatica e deformazioni per l'IFMIF e la ricerca sulla tecnologia di prova su piccoli campioni;

- lo sviluppo di processi industriali nel 2009 ha continuato ad avere lo stesso successo che nel passato.

2 RESEARCH ACHIEVEMENTS OF THE CRPP IN 2009

2.1 The TCV tokamak

The TCV general scientific programme aims at broadening the physical parameter range of reactor relevant regimes for ITER and DEMO, by exploring fundamental tokamak plasma physics questions and by investigating new plasma shapes and control tools.

The 2009 TCV experimental campaign started around mid-March, after a shut down period lasting about four months, mostly dedicated to the repair of the excitation transformer of the TCV flywheel generator, as well as to the implementation of a number of diagnostic improvements.

The 2009 campaign was conducted according to the missions defined in 2008 during discussions within the TCV Team and with its European and International collaborators. These missions aim at exploiting TCV unique capabilities, such as plasma shaping and Electron Cyclotron Heating and Current Drive (ECH, ECCD) tools, and are structured according to six themes:

- Advanced scenarios with internal transport barriers and large bootstrap currents (of interest for a steady-state operation of tokamaks)
- Physics of H-mode (the reference scenario for Q=10 operation in ITER)
- Transport and rotation
- ECH and ECCD physics
- Real time control of plasma and heating systems (including new plasma shapes and configurations)
- Plasma edge physics

The text follows this structure and highlights the main results obtained in 2009, both from new experiments and from analysis of previously obtained data.

In parallel with the scientific exploitation of TCV, part of the team investigated possible medium term developments and upgrades, along the lines depicted in the European Facilities review, conducted in the frame of the European Fusion Development Agreement. These developments include the possibility of direct ion heating by Neutral Beam Injection (NBI), of increasing the ECRH third harmonic (X3) power, of installing additional tools for error fields and Edge Localized Mode (ELM) control, and of performing fast ion physics experiments on TCV, as detailed in Section 3.4.

2.1.1 Scenarios with internal transport barriers

A few experimental sessions were dedicated to internal transport barriers studies in 2009, with two main aims. The first was to take advantage of the updated Thomson system, which now has a significantly better radial resolution. The second was to study the ion and impurity behaviours and rotation profiles in electron internal transport barriers sustained by ECH/ECCD. The sharp gradients in the electron temperature profiles that characterize plasmas with eITBs in TCV had motivated an upgrade of the Thomson scattering diagnostic in 2008. For a selected number of

channels (covering the barrier region for typical TCV plasma configurations) the spatial resolution has been increased by a factor of two. Since the beginning of 2009 the improved system is fully operational. However, the profile measurements now only cover the range from Z=-17 to +66cm. An example of an improved resolution in the profile reconstruction is given in Fig. 2.1.1.

Several internal transport barrier, with varying degree of confinement improvement have been sustained in TCV, with the aim of diagnosing precisely the barrier width and the resulting bootstrap current profile and peaked position. In the past, the barrier width was of the same order as the diagnostic spatial resolution. The results of this year measurements show that the width and gradients inferred from the previous system are confirmed. Although this implies that we had actually just about enough resolution, we can now better determine the role of the bootstrap current and of its position with respect to the barrier position. This study will be performed using the data obtained in 2009.

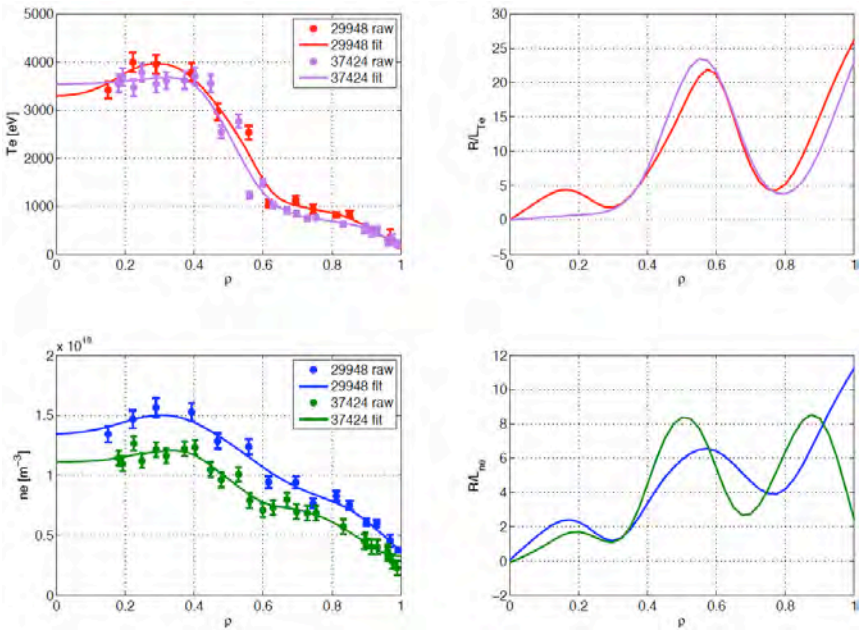

Fig. 2.1.1 *Left: Comparison of electron temperature and density profiles measured with low (TCV-29948) and high spatial resolution (TCV-37424). Right: Gradient scale lengths R/L_{Te}, R/L_{ne} as obtained from these measurements.*

To study the ion and impurity behaviours and rotation profiles, the experiments have been separated into two stages. In the first stage, eITB plasmas need to be developed at the TCV equator, z=0, in order to be aligned with the CXRS diagnostics. This is different with respect to what was done in the recent past, with eITBs developed near z=23cm to be optimal with respect to the gyrotron launchers and guarantee maximum efficiency and flexibility for off-axis current drive and profile control.

On the other hand, at z=0, the upper launchers are further away and the control of the driven current density profile is more difficult. Nevertheless we have been able to develop a set of good eITBs at z=0, which are now being studied in detail with respect to ion and impurity transport. We will also be able to measure toroidal and poloidal rotation in these plasmas and assess their role with electron barriers.

2.1.2 H-mode physics

Further experiments were performed to characterise and understand more fully X3 heated H-modes. With respect to previous campaigns (2003, 2005) the toroidal magnetic field and plasma current directions were reversed. In principle this lowered the threshold power required to attain the H-mode. Due to the failure of one X3 gyrotron only approximately 900kW of additional heating power was available at the plasma.

The most striking result of the campaign was the ease with which Type I ELMs were attained with only 900kW additional power. Type I ELMs were systematically obtained whenever more than 600kW of X3 power was coupled to the plasma. This is in stark contrast to campaigns with the magnetic field in the opposite direction in which more than 900kW coupled X3 power was required to achieve Type I ELMs. With less than this coupled power, the plasma transited to an ELM-free H-mode with a resultant loss of density control.

The capability of using ECH at the 3rd harmonic for additional heating opened the path for studies of the transition from type-III to type I ELMs of on TCV. Making use of the improved spatial resolution of the Thomson scattering diagnostic for a selected number of channels (10 channels covering the range Z=0.51m to 0.63m with a resolution of 12mm), the changes in electron density (n_e) and temperature (T_e) profiles near the plasma edge have been measured. As for previous experiments with ohmic heating only, the height and width of the pedestal and the gradient scale length have been quantified. With vertical power injection from 2 gyrotrons (900kW), the pedestal T_e increased from 200 to 450eV at comparable values of the pedestal n_e. Due to the increase in heating power, the averaged relative energy loss per ELM increased from 5% to near 15% (based on measurements by the DiaMagnetic Loop (DML)). The observed variation in ELM frequency with additional heating power indicates a transition to ELMs of type I.

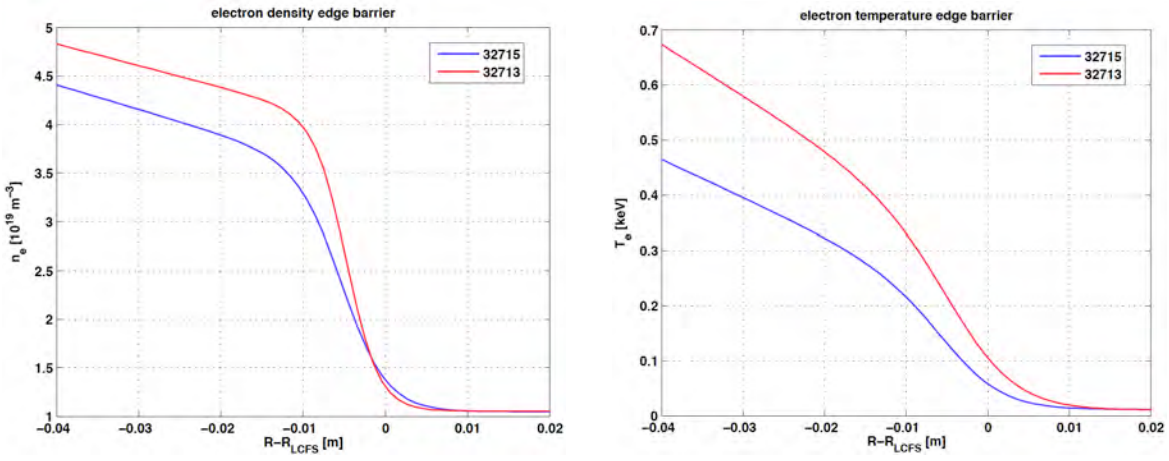

Fig. 2.1.2 *Comparison of T_e and n_e profiles in the pedestal region for Ohmic (32715) and X-3 heated H-mode plasmas (32713)*

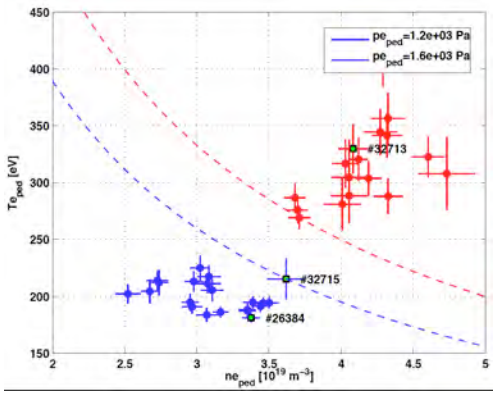

Fig. 2.1.3 *Parameter space (pedestal temperature and density) for ELMs with ohmic heating only and additional heating by X3 ECRH.*

Detailed measurement of the divertor radiation were made. In particular, divertor radiation contours and divertor tiles temperature were estimated using a fast imaging Infra-red camera on loan from Culham laboratory. Filaments were clearly observed in the infra-red images.

2.1.3 Plasma rotation

Rotation measurements on TCV

Over the last year, the Charge exchange Recombination Spectroscopy (CXRS) measurement system has benefitted from the increased resolution resulting from an upgrade of the observation cameras. Profiles of toroidal and poloidal rotation have been obtained up to the plasma edge with up to 40 radial points along a minor axis.

A new operational mode was developed where, following a sawtooth crash, the evolution of toroidal rotation up until the next sawtooth crash was measured by conditional sampling, time resolved but averaged over many sawteeth events. In order to achieve this, two developments were required: a restructure of the CCD acquisition algorithm to acquire up to 4 tracks from each side of the CCD in less than 2ms, and an algorithm for the new TCV real-time system that detects the sawtooth crash and sends a synchronous series of trigger pulses to the CCD camera.

With these features, many sawteeth spectra were acquired and re-synchronised to the sawteeth crash in discharges where the sawtooth repetition time was extended to ~15ms using resonant ECH just inside the sawteeth inversion radius. This experiment showed for the first time the evolution of intrinsic toroidal rotation between sawteeth. This study will be extended in 2010 with the purchase of faster CCD cameras with on-chip gain that will allow the conditional averaging process to be repeated over fewer sawteeth events.

In another set of experiments, in collaboration with Warwick University, UK, a theoretical hypothesis was tested in which up-down asymmetry generates an additional radial flux (anomalous, i.e. associated with turbulent transport) of toroidal momentum. Theory predicts a change in sign of this additional flux if the plasma current, the main toroidal field or the plasma shape are reversed.

Using TCV shape flexibility, mirror discharges were produced with opposite shape and the toroidal rotation profile measured. Initial results, shown in Fig. 2.1.4 and 2.1.5, are highly encouraging, with a difference in the toroidal rotation of the same order of magnitude and the same sign as that predicted. In the context of intrinsic toroidal rotation, in which a theoretical description that can describe the range of profiles and values measured experimentally is missing, this is particularly encouraging in that at least one term in the total momentum equilibrium appears to be modelled correctly. From the representation of the experimental rotation data as a function of poloidal flux, the increased radial resolution of the new optical system can readily be noticed.

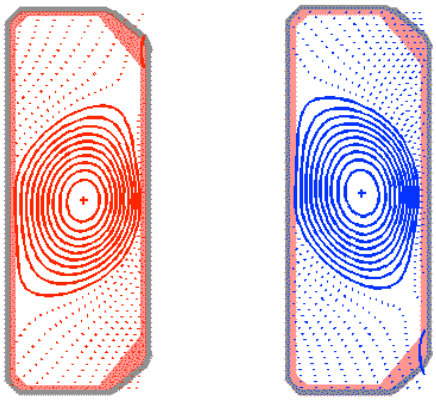

Fig. 2.1.4 *Two plasma shapes on TCV with opposite shapes. The plasma current and magnetic field are in the same direction.*

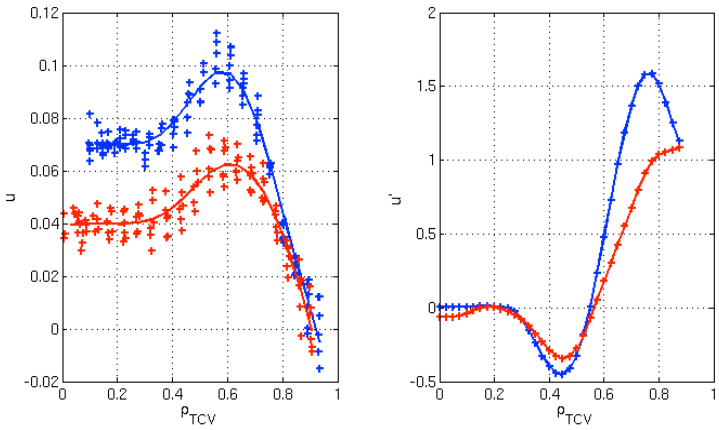

Fig. 2.1.5 *Effect observed on the toroidal rotation u and its radial gradient u' (both normalised to the thermal ion velocity).*

Collaboration with Alcator C-mod

Following initial experiments on the Alcator C-mod machine at MIT, USA, early in 2008, CRPP staff visited the MIT group late in 2008 for more detailed analysis of the results. The discharges showed a reversal of the toroidal rotation, in agreement with the TCV observations. We were able to analyse the edge charge exchange diagnostic data and phase contrast data to look for a possible co-incidence of turbulence.

It was noted that the C-mod discharges were close to being diverted and/or limited, so that a clear comparison with TCV data, where the configuration was always

clearly defined, was difficult. Since C-mod was in the middle of a long shutdown, two courses of action were initiated.

First, we reproduced the C-mod plasma shape in the TCV vessel. Here, the plasma rotation was observed during a change from limited to diverted configuration by programming a horizontal plasma shift during the discharge. The results agreed with the C-mod data, demonstrating that the toroidal velocity reversal observed on TCV is a robust feature that can be reproduced on other tokamaks.

Second, we defined and planned new experiments on C-mod with a definite diverted and limited series of discharges to compare more explicitly to the TCV data. With the delays in re-commissioning C-mod and further problems with one of the most important C-mod diagnostics, these experiments are now expected to take place early in 2010.

2.1.4 Heat and particle transport in TCV

Particle and impurity transport in TCV

Particle transport in electron internal transport barriers, e-ITB's

Electron ITBs appear in fully EC current driven discharges in TCV where and when the magnetic shear reverses. In the strongest eITBs, strong electron density gradients are also observed. Since there is no central particle source, this cannot simply be attributed to a reduced particle diffusivity, but an inward pinch must also be present. Transport analysis using linear calculations with the GS2 gyrokinetic code show that the gradients are such that both the TEM and the ITG modes are unstable. In this situation the dominant thermo-diffusive component of the inward particle pinch is maximised, such that $\sigma_e=L_{Te}/L_{ne}\cong 0.35$. The experimental observation provides $\sigma_e\cong 0.45$ for the strongest barriers (Fig. 2.1.6). This increased peaking in the presence of electron heating contrasts with L-modes, where central electron heating causes density profile flattening.

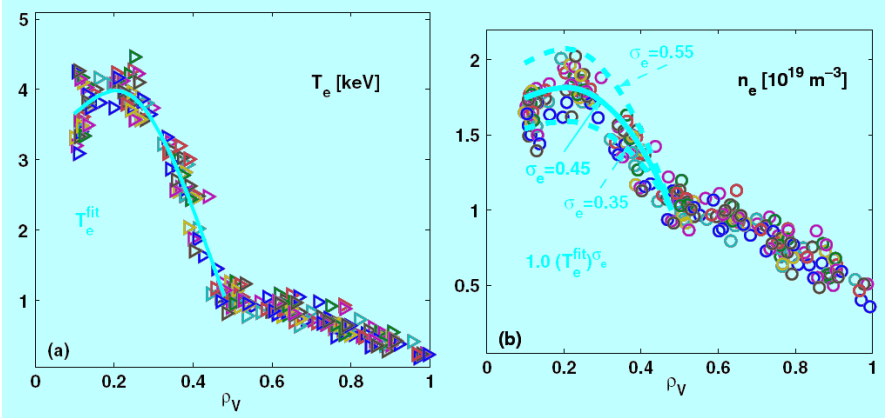

Fig. 2.1.6 *Electron temperature and density profiles in a stationary TCV eITB discharge. The different colours refer to different times at which Thomson scattering measurements were performed.*

Carbon profiles in TCV L-modes

Experimental observations from TCV Ohmic L–modes show that both the electron and the carbon density profiles are fairly flat inside the sawtooth inversion radius and similar (for all plasma currents, i.e. all values if q_{95}) outside the sawtooth inversion radius. This can be seen in Fig. 2.1.7, where the profiles have been normalised to their value at ρ_ψ=0.8. The normalised gradients of the carbon density profiles are higher than those of the electron density profiles, leading to substantially more peaked carbon profiles at low plasma currents (i.e. high edge safety factor).

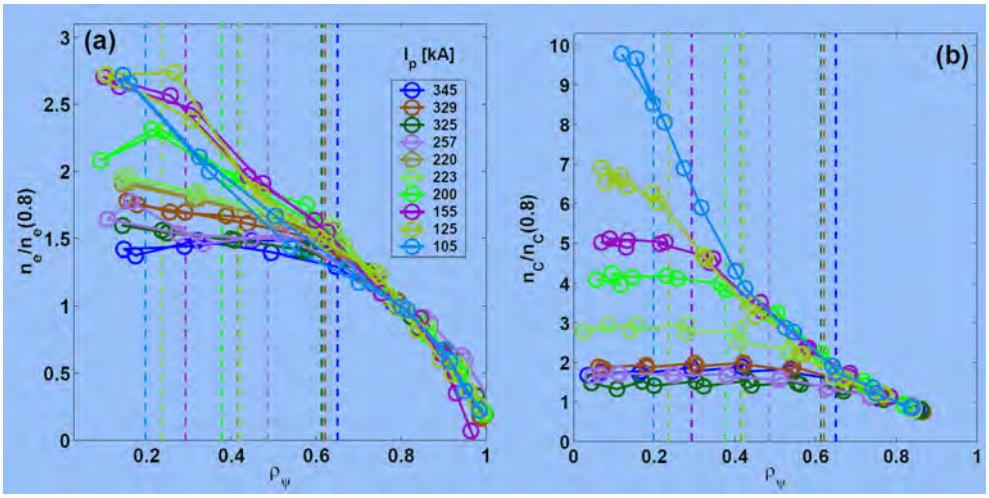

Fig. 2.1.7 *Electron density (a) and carbon density profiles from charge exchange recombination spectroscopy (b) in Ohmic L-mode discharges with different plasma currents.*

When core electron heating is applied, both profiles are flattened, with the carbon density profile showing a stronger flattening. According to gyrokinetic theory the thermodiffusive pinch is reversed (inward directed) in Trapped Electron Mode (TEM) dominated turbulence and outward and weak for Ion Temperature Gradient (ITG) driven turbulence. There is a second contribution to the pinch due to parallel and perpendicular ion dynamics, which is opposite in sign to the former. The simulations show that in the above Ohmic cases, the Ware pinch also plays a non-trivial role, pushing the discharges towards a TEM dominated state, where the thermodiffusive pinch is directed inward for carbon. The addition of ECH strongly reduces the Ware pinch and indirectly the TEM drive, thereby reducing the peaking of the carbon profiles.

Density profiles in electron-heated H-modes

Following the successful modelling of density peaking in JET last year, modelling of particle transport in TCV H-modes using GS2 is underway. The fairly high peaking of Ohmic H-modes at high collisionality, which contrasts with the relatively flat density profiles observed at high collisionality in JET, appears to be attributable to an interplay of the Ware pinch with anomalous transport. The Ware pinch is inherently more important with Ohmic heating alone and in smaller devices than e.g. at JET. The large scatter of density peaking observed at low collisionality with X3 ECH heating in TCV is still not understood in a satisfactory manner.

Core turbulence measured by correlation-ECE

Temperature fluctuations are measured on TCV by cross-correlating two radially separated channels of the Electron Cyclotron Emission (ECE) diagnostics. Broadband electron temperature fluctuations are found in Ohmically heated (OH) and Electron Cyclotron Resonance heated (ECRH) discharges, between typically 20kHz and 150kHz, and extending radially between 0.3<r/a<0.8, as measured from the equatorial mid-plane from the low field side (LFS).

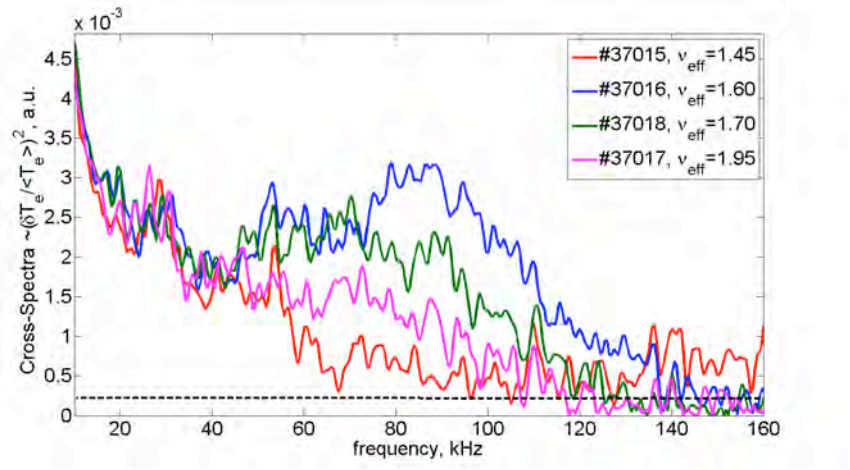

Fig. 2.1.8 *Cross-spectra (a.u.) for different values of collisionality measured at ρ_V=0.55.*

Figure 2.1.8 shows the cross-spectra measured for different densities at the normalised radius ρ_V=0.55, which corresponds to the frequency of 69.5GHz of the second harmonic X-mode ECE ($B_T(0)$=1.43T, local B_T=1.235T). The two radiometer channels were separated by 240MHz to minimise the contribution of thermal noise. Broadband turbulence is clearly seen here between 40–120kHz. Its amplitude decreases with increasing density, i.e. with increasing collisionality. The squared amplitudes of the broadband turbulence, obtained from the analysis of the cross-correlation function of two filtered signals, and integrated over the range 30-140kHz, are shown for different collisionality values in Fig. 2.1.9. The general trend is that the amplitude decreases with increasing density, or collisionality.

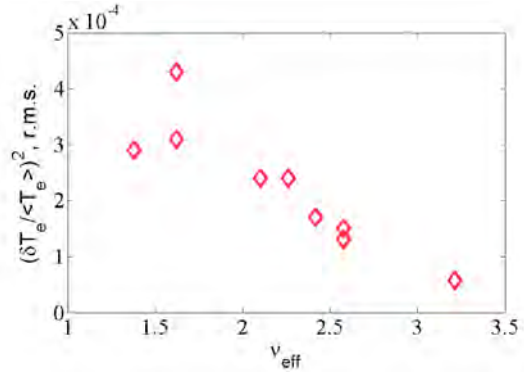

Fig. 2.1.9 *Broadband mode squared amplitude, calculated from the cross-correlation function, as a function of collisionality*

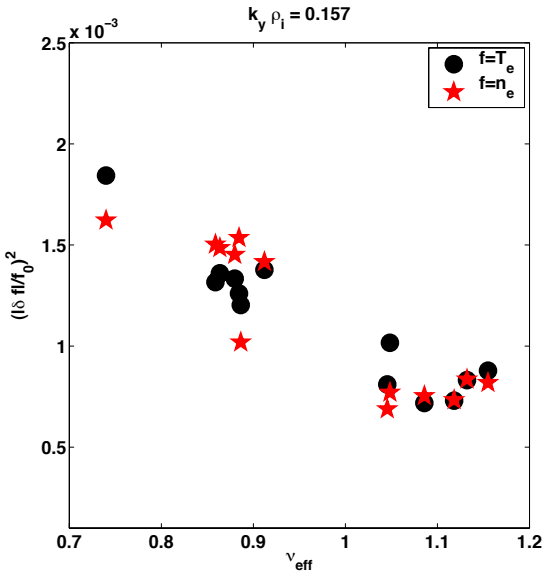

Fig. 2.1.10 *The amplitude of the normalized fluctuation level, squared, for electron temperature (circles) and density (stars) obtained from GS2 quasi-linear calculations and extracted for modes at $k_y\rho_i$ = 0.157, versus collisionality ν_{eff}.*

A radial scan between he plasma centre and ρ_V=0.6 yields the radial distribution of the turbulence amplitude. Two branches of enhanced temperature fluctuations were identified, one inside ρ_V=0.2, where the plasma is optically thick, τ>3, and a second one outside ρ_V>0.3, where τ<3. Thus in the core, the temperature fluctuations do not contain contributions from density fluctuations, whereas in the outer plasma regions, both kinds of fluctuations contribute to the correlation functions. The relative fluctuation amplitude does not exceed 1.5% (taking the square root of the correlation functions at null time delay). The correlation length for the broadband turbulence at ρ_V~0.5 is found to be more than 1.5cm and depends on the value of the density. Even at large channel separation (2GHz, i.e. ~2cm), is the broadband mode clearly visible.

The dependence of the fluctuations amplitude upon collisionality is also explored theoretically by means of a quasi-linear model, which uses results from linear calculations performed with the GS2 gyrokinetic code. The amplitude of the temperature fluctuations decreases with increasing electron density, both in experiment and in the quasi-linear gyro-kinetic calculation. Thus, the mixing length heat diffusivity calculated from GS2 decreases with increasing collisionality, as does the corresponding experimental quantity, measured from power balance analysis. In addition, electron temperature and density fluctuations are both found to decrease similarly with increasing collisionality, as shown in Fig. 2.1.10. The main reason for the reduction of the turbulence level seems therefore to be the increase in collisionality. Moreover, this is due both to a reduction in the mode growth rate and to an increase in the perpendicular wave number, the latter linked to the mode being more extended on the field lines at higher collisionality. The real frequency of the mode stays positive over the explored range of collisionalities. This is suggestive of dominant TEM turbulence activity, which is reduced by collisional de-trapping.

Influence of plasma shape on heat transport and plasma turbulence from correlation-ECE in the TEM domain

The earlier observed dependencies of the electron thermal diffusivity on triangularity (direct) and collisionality (inverse) have been qualitatively reproduced by linear global and nonlinear local gyro-kinetic simulations and shown to be associated with Trapped Electron Mode (TEM) turbulence. Both in the linear and non-linear phases, negative triangularity is found to have a stabilizing influence on

the TEM by modifying the toroidal precessional drift of trapped electrons that resonantly drive the modes. In addition, negative triangularity increases the perpendicular wave number (presumably by modifying the curvature and Shafranov shift), which, following a mixing length argument, should reduce the transport. Heat transport measurements from power balance as well as gyrokinetic simulations demonstrate the stabilising effect of both electron-ion collisions and negative triangularity. The influence of collisions is confirmed by the turbulence measurements obtained from correlation ECE.

By looking at the turbulence level, the correlation ECE diagnostics enables the study of the previously found heat transport dependence with triangularity measured from power balance at a microscopic level. Turbulence features, like amplitude, radial correlation length and orientation of the potential cells, which are predicted to change with plasma shape and up/down-asymmetries, can now be measured through the correlation lengths along a horizontal ECE line of sight.

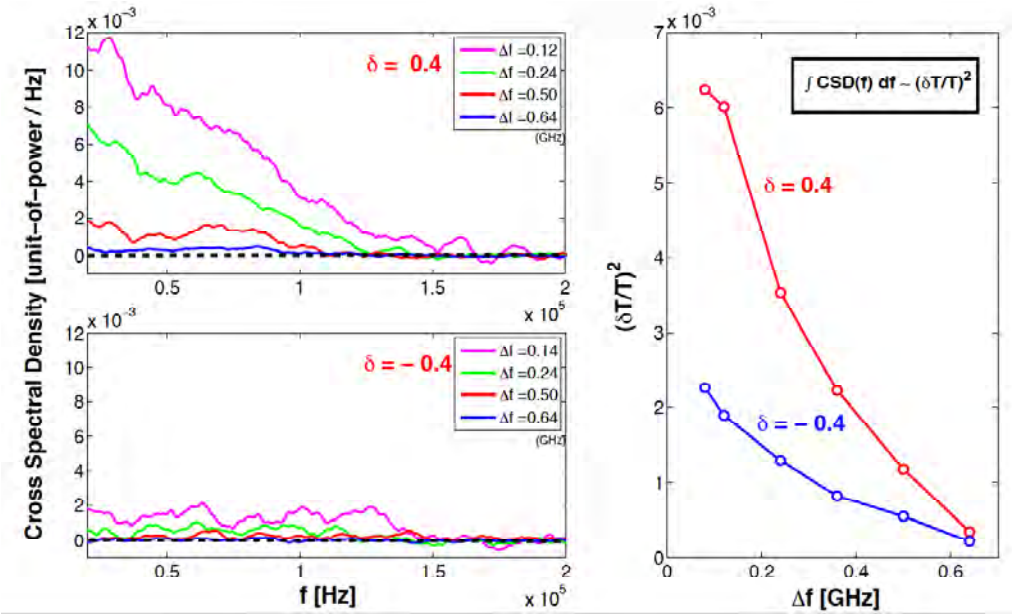

Fig. 2.1.11 *a) and b) Cross-spectral density (CDS) measured on the LFS equator at ρ~0.55 after subtraction of noise level for a) δ~+0.4 and b) δ~-0.4. Note the different amplitude vs. frequency behavior of the CSD, with a strong contribution of the low frequencies at δ~+0.4, whereas all frequencies between 30-130kHz contribute evenly and at a lower level at δ~-0.4.*
c) RMS amplitude of the fluctuations from the integration of the CSD between 30-130kHz, as a function of the radial channel separation Δf (1GHz~1cm).

The cross-spectral density (CSD) is measured on the LFS equator in positive and negative triangularity Ohmic discharges, δ=±0.4 (Fig.2.1.11). The CSD for similar spatial separation is significantly higher at positive triangularity. Integrating over the full turbulence spectrum, in the range 30-130kHz (Fig.2.1.11c), leads to amplitudes that are higher by a factor 2-3 for the positive triangularity case. In other words, at a given $(\delta T/T)^2$, the radial correlation extends typically over a factor of two further in the positive triangularity case. It is interesting to note that at negative triangularity, the CSD is relatively flat between 30-130kHz (Fig.2.1.11b), whereas for the positive triangularity, low frequencies provide a clearly dominating contribution to the CSD amplitude (Fig.2.1.11a). This suggests that low-frequency,

low-*n* TEM modes play a significant role in the change of transport with triangularity.

2.1.5 Physics of ECH, ECCD and of suprathermal electrons

Suprathermal ions in ECCD discharges

Turbulent ion heating in X2 ECCD plasmas on TCV

X2-ECRH TCV plasmas with EC driven currents (ECCD) have the particularity of a bulk population of electrons whose bulk population is 10 – 35 times hotter than the bulk ion population. In contrast, the EC driven current is sustained by a non-negligible fraction of electrons with parallel drift speeds approaching the weakly relativistic velocity range. In such scenarios, ion-acoustic waves, emitted by the circulating electrons, can grow (Fig. 2.1.12), potentially transferring their energy to the ions through Landau damping. Fast ion populations are routinely observed in such scenarios with the Neutral Particle Analysers (NPA). These measurements show that, in steady-state ECCD plasmas, the turbulence and the fast ion populations saturate, reaching temperatures $T_{i,hot}$ 10 times higher than the ion bulk $T_{i,bulk}$ and fractions of up to 20 % of the ions.

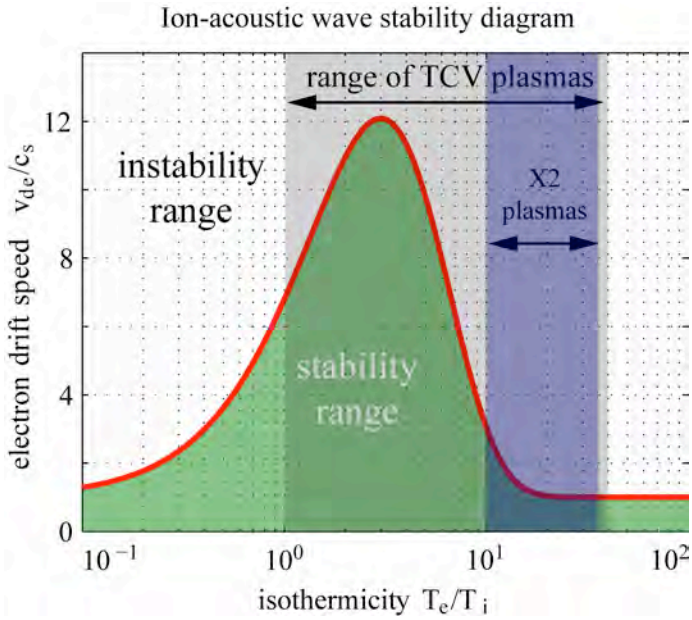

Fig. 2.1.12 *If* $T_e >> T_i$, *ion acoustic waves are destabilised for electron drift speeds* v_{de} *as low as the ion sound speed* c_s.

Recent quasilinear modelling of ion acoustic turbulence has successfully modelled the experimentally observed properties of the fast ions. An example of the modelled ion velocity distribution function at the turbulence saturation stage is shown in Fig. 2.1.13. A suprathermal population in the tail of the distribution is clearly visible and the anisotropy extends into the direction of the noninductively driven ECCD current (positive parallel velocity direction). The experimental investigation of this anisotropy will be investigated using a new, toroidally looking, line-of-sight of the Compact NPA for comparison with the initial view which observes the particles leaving the plasma along a major radius i.e perpendicularly. Observations with

forward and reversed plasma current directions with forward and reversed ECCD will then be compared to the model predictions. A second, vertically viewing, NPA spectrometer will be used to ensure comparable plasma conditions between measurements.

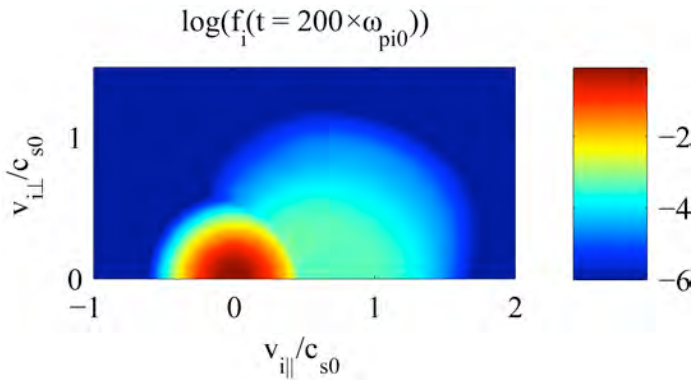

Fig. 2.1.13 *Anisotropy of the high energy tail of the ion velocity distribution function after 200 turbulence cycles.*

Real-time control using EC actuators

MHD instabilities in tokamak plasmas, such as sawteeth and neoclassical tearing modes (NTMs) can degrade the plasma performance or even terminate entirely the plasma discharge in a disruption. Techniques for controlling these instabilities are currently the subject of worldwide research to minimise or even prevent their formation and growth. One method relies upon injecting a microwave beam (ECRH) into the plasma in the close vicinity of the instability in order to change the local plasma current profile, thereby modifying the stability properties of the plasma. At TCV, the microwave heating systems are now controllable in real time, including the launcher injection angles and the power levels, and we have been investigating techniques to control these MHD instabilities. The sawtooth is a repeating crash of the central plasma pressure which limits the plasma pressure and may also trigger NTMs in the plasma. Algorithms which control the period of the sawtooth crash, by obtaining sawteeth of a pre-determined period and by maximising the period have been developed and tested on TCV.

Control of the plasma profiles is one of the main challenges for steady-state operation of ITER. Real-time control techniques are under investigation using the ECRH system. As a first step, line integrated soft X-ray channel measurements are used as an indication of the plasma pressure profile, which is controlled in real-time by varying the power of gyrotrons depositing power in different locations. This approach has allowed us to control both the peak and the width of the profile simultaneously. This work is being extended towards more general control of several profile parameters, including parameters describing the current density profile, and also towards control of profiles during eITBs.

EC stabilisation of Neoclassical Tearing Modes

Neoclassical Tearing Modes (NTMs) are expected to significantly reduce the performance of ITER. The study and understanding of their onset and evolution are therefore of great importance. NTMs have been observed on TCV in particular situations in which ECCD causes local changes to the current density profile and thus the safety profile (q), sufficient to render a tearing mode "classically" unstable, i.e. making the mode appear without an external trigger such as a sawtooth or

another plasma event. It is important to understand this triggering mechanism for two reasons. First, to provide an important benchmark of the physics models currently used for extrapolation to ITER. In particular, while ECCD deposition perfectly aligned with a mode is expected to suppress it, a misaligned gyrotron could very well cause further destabilization because of this classical triggering effect. Second, if localized q profile modifications can trigger a mode, some other local changes in the q profile can well stabilize it. This could make certain q profiles inherently more stable to tearing modes when external triggers such as sawteeth or ELMs are present.

To investigate the physics behind this phenomenon, an effort is underway to model the NTMs observed on TCV and investigate them experimentally. Modelling efforts, combining q profiles obtained from the ASTRA transport code with the MHD code PEST III, confirmed the sensitivity of the classical tearing mode stability to localized changes in the q profile, and in its first and second derivatives. In particular, the second derivative is observed to play an important role and strongly depends on the position of the deposited ECCD with respect to the rational surface.

On the experimental side, it was shown that by changing the deposition location only by a very small amount, a tearing mode was triggered. This confirms the modelling results and provides an indication that more can be learnt from experiments of this kind. This work will continue in 2010 with the aim of modelling self-consistently the appearance of NTMs, including the effect of ECCD and of the mode itself on the profiles. Experimentally, if the NTM destabilizing effect due to ECCD can be offset by a second (stabilizing) gyrotron at a different location, this would provide proof of the competition of these two effects and reinforce our confidence in our understanding of the physics behind these modes.

2.1.6 Electron Bernstein Wave Heating and Current Drive

In preparation of electron Bernstein waves (EBW) experiments via O-SX-B mode conversion in TCV, a systematic analysis of the EBW heating and current drive performances is carried out using the Antenna-Mode-conversion-Ray-tracing code (AMR) coupled to the Fokker-Planck solver LUKE. Special attention was given to the code implementation in terms of the exact field configuration and launching geometry. In AMR, the O-SX mode-conversion efficiency is calculated solving the full-wave equation in a cold plasma slab along the density gradient. This mode conversion calculation is more accurate than the standard analytical formula and has been successfully benchmarked with a previous experimental injection angle scan. The dispersion function along the ray path remains close to zero (~10^{-7}), i.e. at least seven orders of magnitude lower than with a formerly used numerical tool.

The simulations are performed for an overdense ELM-free H-mode equilibrium. The vertical position of the magnetic axis is scanned artificially and single rays are injected from a launcher located at the equator of the vessel. For each configuration, the optimum injection angles for the O-SX-B double mode conversion are determined, the EBW ray-tracing is performed and the quasi-linear wave-plasma interaction is calculated.

With the plasma in front of the antenna (Z_p 4cm), the parallel refractive index $N_{||}$ remains small and allows central deposition at ρ_V=0.1 at low-Doppler-shifted resonance (Fig. 2.1.14). The sign of $N_{||}$ changes along the ray, which may limit the driven current I_{CD} by cancellation of co- and counter-current drive. The latter effect is observed when Z_p=4cm: the $N_{||}$ upshift along the ray is strong enough for the wave to be partly absorbed with $N_{||}$>0 generating a current I_{CD}=-3.9kA

(Fig. 2.1.15). The remaining power in the wave is deposited with $N_{||}<0$, thus decreasing the net driven current to I_{CD}=-2.6kA. With the plasma away from the antenna (Z_p=8cm), only one wave-plasma interaction location remains with positive $N_{||}$ and a counter-current I_{CD}=-3.3kA is driven due to Fisch-Boozer mechanism with high normalized current drive efficiency $\xi_{CD}=32.7(n_{20}I_A R_m)/(P_W T_{keV})$=-0.41. With the plasma further away, the deposition location moves further off-axis. The effect of the lower electron temperature is stronger than the effect of the larger $N_{||}$, yielding lower I_{CD} and ξ_{CD}.

Thus, the poloidal position of the power injection strongly influences the EBW trajectory and absorption. Central power deposition for optimum EBW heating efficiency is possible with injection at the equator of the plasma. For optimum EBW current drive, an injection slightly away from the plasma equator is necessary to avoid multiple deposition locations. However, the current-drive amplitude remains small at this magnetic field.

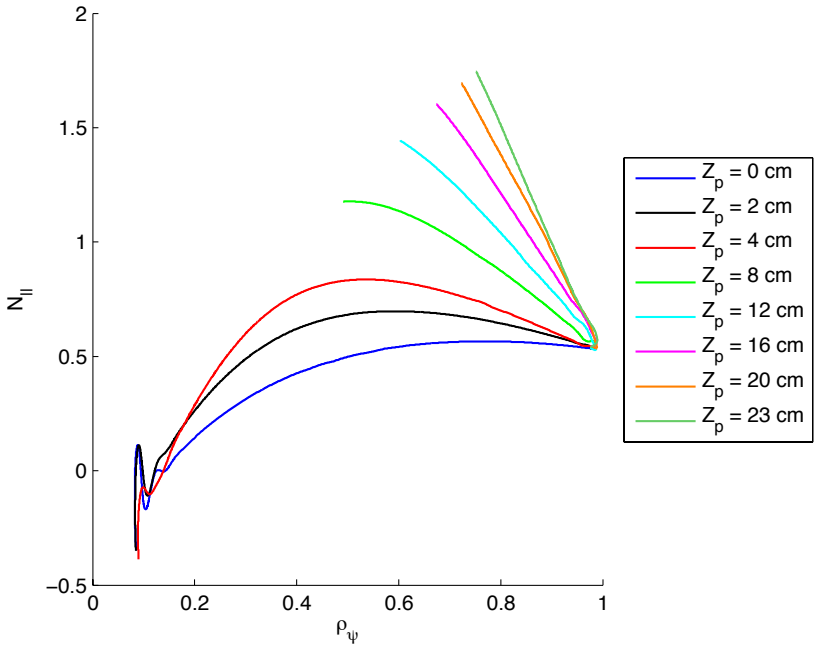

Fig. 2.1.14 *Evolution of the parallel refractive index* $N_{||}$ *for single EBW rays launched from an antenna located at the vessel equator. The ELM-free H-mode target is displaced at different vertical positions* Z_p *above the antenna, yielding different* $N_{||}$ *upshifts. Here,* B_t*=1.45T.*

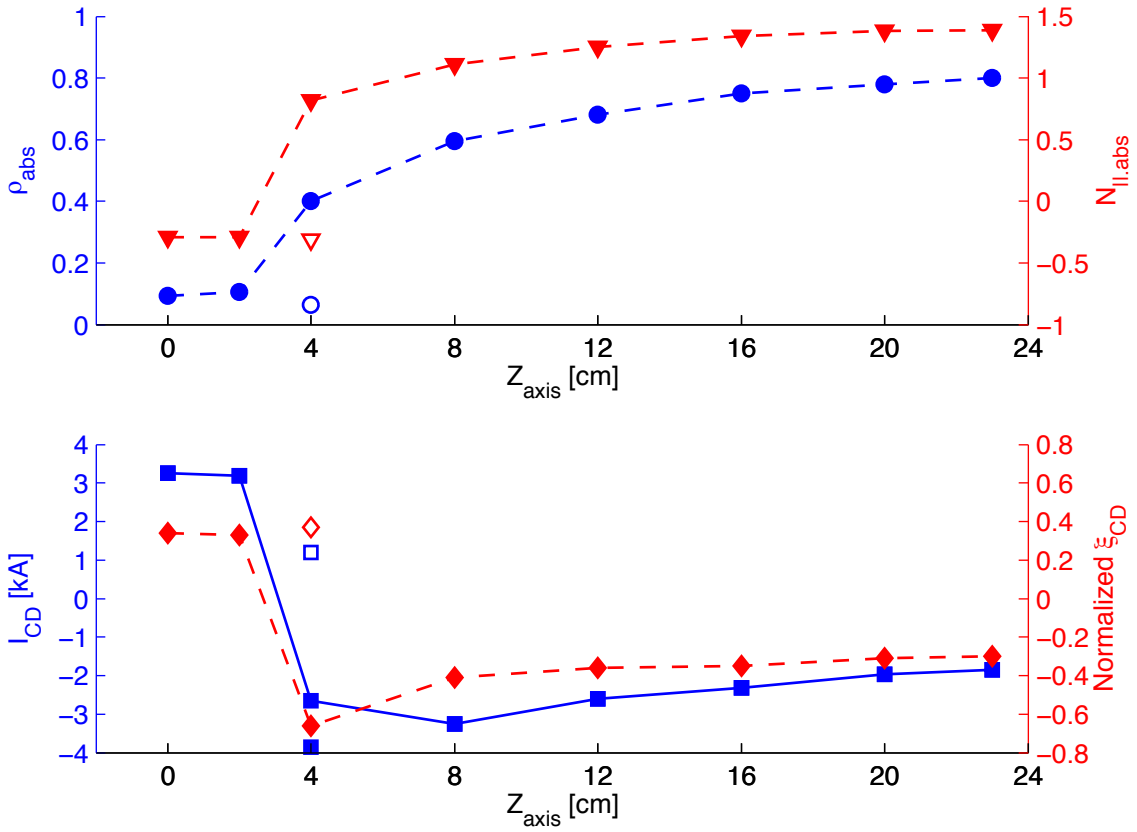

Fig. 2.1.15 *Normalized radius ρ_{abs} and parallel refractive index $N_{//abs}$ at the absorption location (top), driven current I_{CD} and normalized current drive efficiency ξ_{CD} (bottom) versus the vertical position of the magnetic axis. The isolated empty symbols correspond to the secondary power deposition in the case Z_p=4cm. I_{CD} values from both deposition locations are summed to obtain the net driven current.*

2.1.7 Exploration of new shapes and configurations: snowflake divertor

In future experimental nuclear fusion reactors, power exhaust handling and plasma wall interaction must be controlled to a level compatible with wall materials. Tokamak operation will thus feature highly radiative edges. On the other hand, radiation in the core plasma must be minimized to preserve the energy content.

Many solutions have been proposed to reduce the plasma-wall interaction by acting on the magnetic field topology in diverted plasmas. One of these solutions is the so-called snowflake (SF) divertor. The basic concept of the snowflake divertor (SF) is illustrated in Fig. 2.1.16.

In a standard X-point configuration the poloidal magnetic field vanishes at the X-point (first order null). A SF diverted configuration is characterized by a second order null, i.e. the first derivatives of the magnetic field also vanish at the null point and the separatrix divides the poloidal plane into six sectors, Fig. 2.1.16(b). Perturbing the exact SF configuration produces the magnetic configurations that are shown in Fig. 2.1.16(a) and Fig. 2.1.16(c). In these two configurations, the first derivatives of the poloidal magnetic field are small compared to those of a standard

X-point (single null configuration, SN). We will refer to these two configurations as of snowflake-plus (SF+) and snowflake-minus (SF-) respectively.

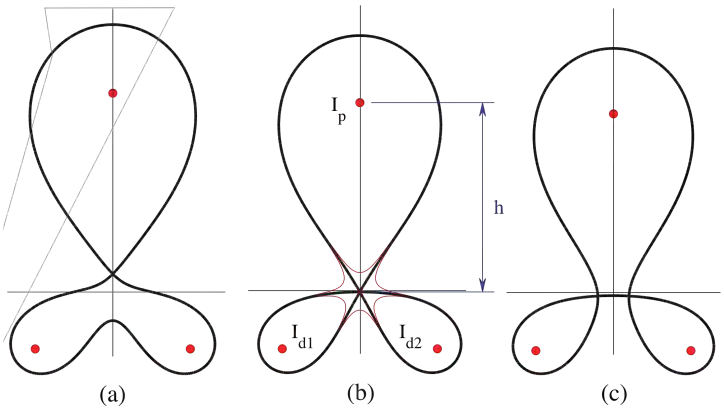

Fig. 2.1.16 *SF configurations in a straight tokamak model. The circles represent the current filaments (plasma, I_p, and divertor conductors, $I_{d1,2}$) and the bold black line is the separatrix.*

The second order null modifies the magnetic topology near the plasma boundary and is therefore expected to affect the plasma properties in the scrape-off layer (SOL). The magnetic shear at the edge where the pedestal lies is also modified, which may influence Edge Localized Modes (ELMs) activity in H-modes. Squeezing the flux tubes near the null point may also decouple the turbulence in the divertor legs and in the SOL and change the radial blob motion.

All three SF configurations have been created and controlled on the TCV tokamak, as shown in Fig. 2.1.17, demonstrating the feasibility of such plasmas. Although the CCD images in Fig. 2.1.17 are saturated, the visible emission qualitatively confirms the SF configurations reproduced by the magnetic reconstruction code.

The magnetic properties of the SF configurations are compared with those of the SN configuration using the magnetic measurements from the equilibria in Fig. 2.1.17.

For the SOL, an important parameter is the flux expansion. This quantity is related to the reduction of the poloidal magnetic field near the null point. The flux expansion influences the SOL thickness and the size of the radiating volume. Radial transport and possible filaments in the edge/SOL region, may also be influenced.

For a given flux surface, the flux expansion is defined as the ratio $\psi_{\exp} = \dfrac{\Delta}{R - R_{sep}}$, where Δ is the minimum distance between the X-point and the considered magnetic field line, and $R - R_{sep}$ is the distance between the same field line and the separatrix at the outer mid-plane.

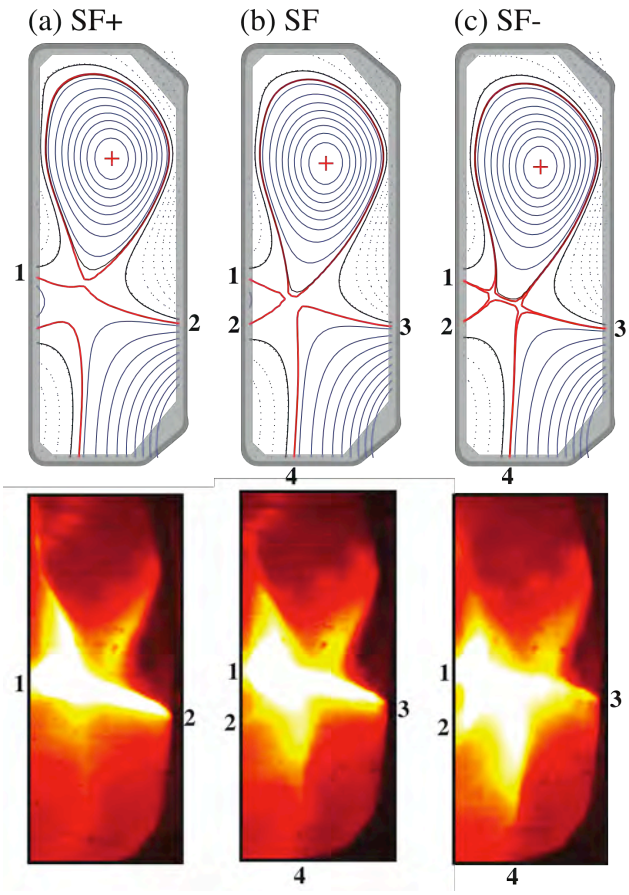

Fig. 2.1.17 *Equilibrium reconstructions and images from the tangential visible CCD camera for the SF configurations.*

In Fig. 2.1.18, the flux expansion for the SF configurations and for the SN configuration is plotted as a function of the distance $R - R_{sep}$. The connection length from the equatorial plane to the point closest to the X-point (CLx) is also shown. The connection length determines the residence time of a particle in the SOL and therefore affects the radioactive losses and the thermal power to the divertor plates (the thickness of the SOL at the outer mid-plane is typically ~2cm). The SF configuration has a flux expansion near the separatrix (near SOL) and a connection length over two times larger than that for the equivalent SN. The SF+ and the SF- have similar values of flux expansion and connection length, with values that fall between the values computed for the SF configuration and the SN configuration.

The safety factor profile (q) and the magnetic shear $s = \frac{\rho_{vol}}{q}\frac{dq}{d\rho_{vol}}$ are computed using the CHEASE code and are also shown in Fig. 2.1.18.

The LCFS used to compute these quantities ($\rho_{vol} = 1$) is just inside the separatrix to avoid the singularity of q and s at the null point.

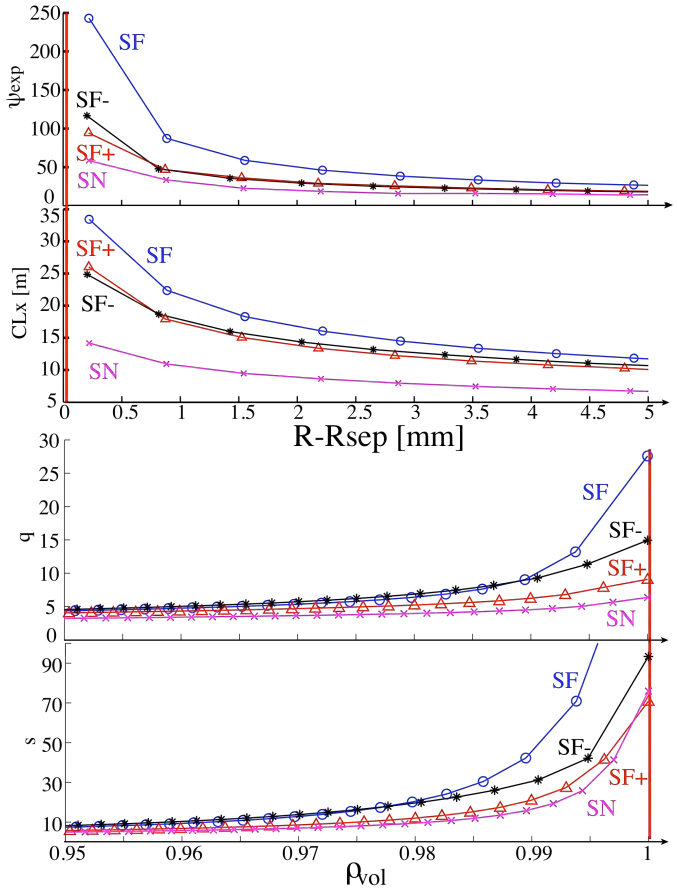

Fig. 2.1.18 *Flux expansion, connection length, q-profile and magnetic shear for the three SF configurations and an SN configuration.*

The SF configuration has a larger magnetic shear than the SN configuration. This difference is large for $\rho_{vol} > 0.96$. The SF+ and the SF- configurations also exhibit larger magnetic shear compared to the SN configuration. In the case of the SF- configuration, the presence of a double null in the separatrix results in a large volume where the poloidal magnetic field is small.

Note that the profiles of the SF- are very similar to the SF up to $\rho_{vol} \sim 0.985$ but then become closer to the SF+ and the SN. This may lead to differences in the MHD stability limits in between the SF+ and SF-, which will be investigated in the future.

The MHD stability limits of the SF configuration were computed and compared to those of a SN configuration. It was found that the SF configuration does not degrade edge MHD stability and that the current driven kink modes of medium *n* are predicted to be more stable compared to the SN configuration.

Starting from these theoretical results, an experimental campaign on TCV was undertaken to verify the accessibility of the H-mode with SF configurations. In Fig. 2.1.19, the electron plasma density n_e, the H_α and the C_{III} radiations and the soft-X radiation is plotted for an ohmic plasma discharge. During this experiment, the plasma configuration is modified; starting from a limited plasma, a SN configuration is created at *t=0.31*s and finally at *t=0.62*s the SF+ configuration is achieved. In spite of the small input power (I_P*=300*kA, P_{in}*~400*kW), an ELMy H-mode regime is observed in both the SN configuration and the SF configuration. More experiments are planned to investigate the H-mode accessibility and the pedestal stability in H-mode SF configurations.

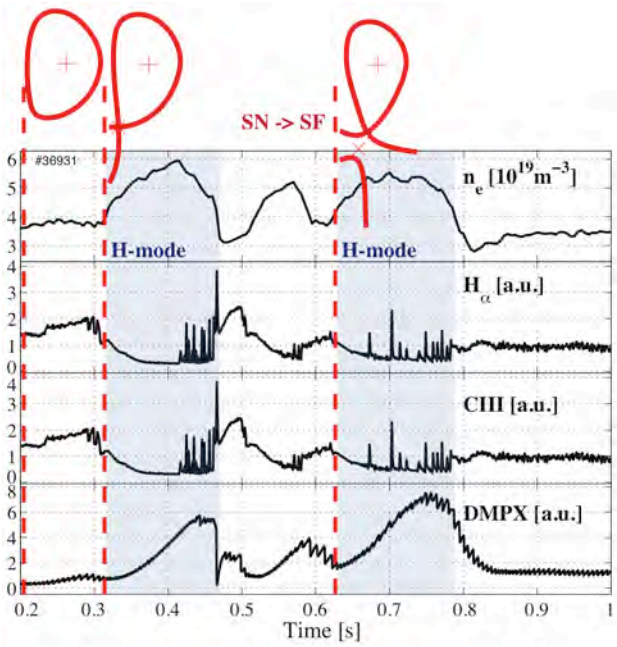

Fig. 2.1.19 *Electron plasma density (n_e), H_α, C_{III} and soft-X radiation (DMPX signal) during an H-mode in SN and SF configurations.*

2.1.8 Plasma start-up experiments

Plasma Start-Up Magnetic Analysis

A model based on a set of magnetic measurements combined with the circuit equation for the vacuum vessel has been developed to derive the magnetic configuration inside the vacuum vessel at the breakdown time. From this model, the position of the minima of the magnetic field and other important parameters have been computed (Fig. 2.1.20). In particular, the length of the open magnetic field lines from one solid surface to another has been computed (connection length). From the H-alpha detectors and from the frames from a tangential visible camera installed on TCV we verified that the ionization phase is localized in the region where the connection length is maximum.

Figure 2.1.21(a) shows the predicted radiated power in the visible range based on the magnetic reconstruction. We assume that the intensity of the radiation is only proportional to the connection length. In Fig. 2.1.21(b) the light measured with a tangential visible camera is shown for comparison. The good agreement validates the start-up model used for these scenarios.

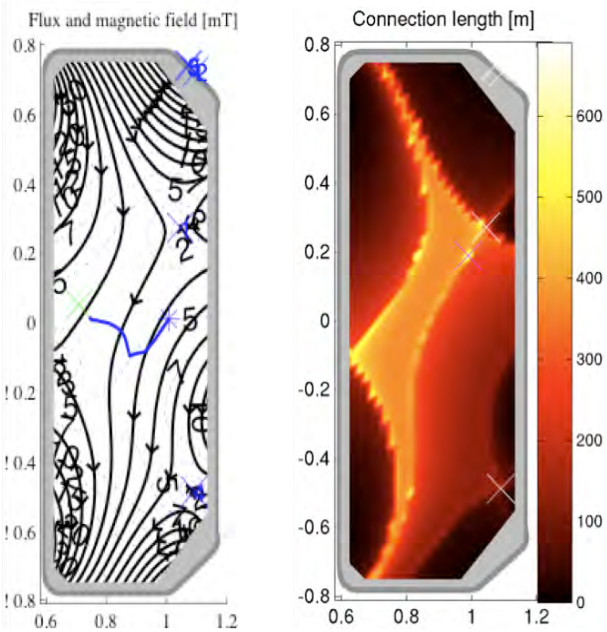

Fig. 2.1.20 *Magnetic field map and connection length at the breakdown time.*

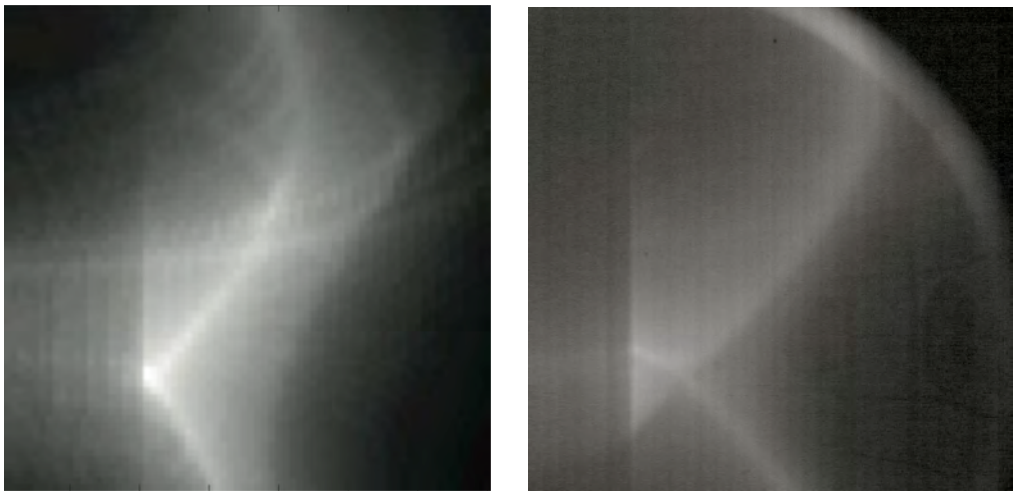

(a) **(b)**

Fig. 2.1.21 *Radiated power in the visible range as predicted from the magnetic reconstruction (a) and measured from the tangential visible camera (b).*

The ionization phase is followed by a ramp-up phase. The magnetic topology changes from an open-field line configuration to an MHD equilibrium with nested magnetic surfaces. The plasma current rises during this phase, giving an important contribution to the poloidal magnetic field.

To describe the ramp-up phase, a different model is used, based on a single-filament representation of the plasma current, in which the two main parameters are the position of the plasma filament the plasma current. The system is solved using the Nelder-Mead method. The solution is shown in Fig. 2.1.20 for a typical TCV start-up. The blue lines represent the evolution of the plasma current just after the ionization phase.

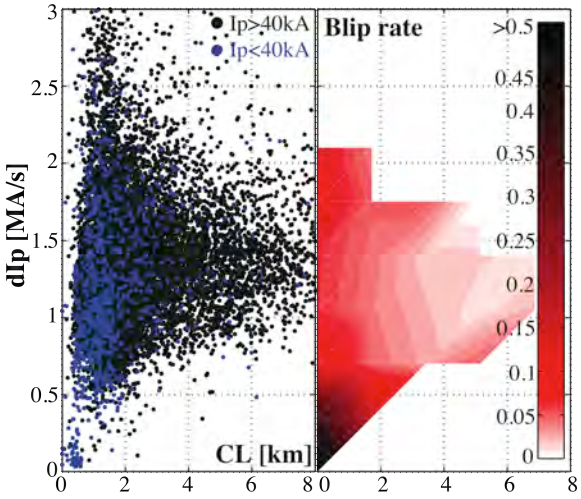

Fig. 2.1.22 *Left: plasma current derivative and connection length for 20000 considered TCV start-ups. The blue points are blips (Ip<40kA) and the black points are good start-ups (Ip>40kA). Right: blip rate distribution as a function of the connection length and the plasma current derivative.*

Statistical analysis of the start-up phase

A statistical analysis of the start-up parameters based on 20000 shots has been used to characterize the ionization and the rump-up phase in TCV. An interesting result is related to the role of the connection length, which has to be maximized to increase the probability to succeed in the plasma creation (Fig. 2.1.22).

ECH assisted breakdown

Preliminary experiments to investigate the ionization phase using second harmonic heating (ECH-X2) have been carried out in TCV (Fig. 2.1.23). A scan of the main parameters (absorbed power, voltage, poloidal and toroidal angle of the launchers) has been useful to characterize the breakdown with ECH. More experiments are necessary to complete the analysis.

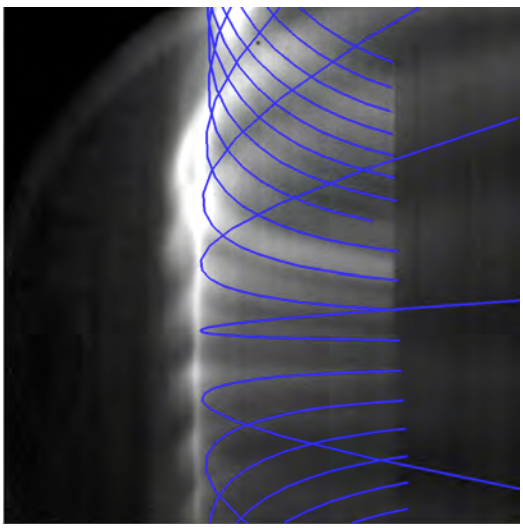

Fig. 2.1.23 *Ionization using ECH in a simple poloidal magnetic configuration (pure vertical field). The blue lines represent the considered magnetic field line at the deposition location.*

2.1.9 Exploration of new shapes and plasma configurations: doublets

A doublet configuration has a non-conventional plasma cross-section, characterised by an internal separatrix that divides the plasma in two separate confinement regions (Fig. 2.1.24).

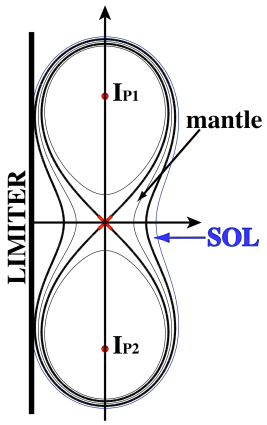

Fig. 2.1.24 *Doublet plasma configuration*

The doublet configuration has several potential advantages: it has an intrinsic reversed magnetic shear zone with beneficial effects on the energy confinement; the vertical instability growth rate is much lower than for a conventional plasma with the same overall elongation; one of the two plasmas could be used to control the particle content and the power exhaust of the other, especially for fusion reaction products and impurity removal. From a more fundamental point of view, studying the doublet configuration can also help us understand the role of the separatrix in advanced scenarios (H-mode), the physics of the Edge Localized Modes (ELMs) and the physics of magnetic reconnection.

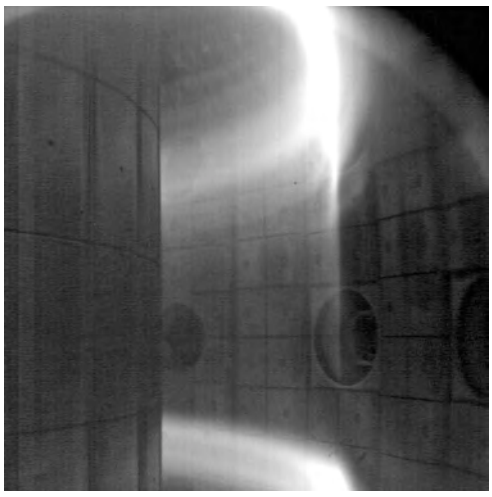

Fig. 2.1.25 Frame from tangential visible camera during a double breakdown.

The most promising way to create a doublet on TCV consists in initiating two plasmas at two different vertical positions, then allowing these two plasmas to grow until their reconnect. Therefore, the double breakdown is the first goal that needs to

be achieved. The magnetic configuration at the breakdown time has two null points where the two plasmas should grow simultaneously. To synchronize the ionization phase and the early ramp-up phase, two ECH-X2 waves are injected close to the position of the two null points. Fig. 2.1.25 shows an example of a double breakdown obtained with ECH on TCV.

2.1.10 Plasma edge characterisation and modelling

Most of the edge physics work on TCV in 2009 was concentrated on imaging diagnostic observations. A fast IR camera, of the type already installed on TCV, was obtained on loan from the MAST (UK) group. This permitted the simultaneous observation of the TCV vessel floor and central column that, with the use of camera sub sampling, is fast enough to determine the ELM power deposition evolution on each surface. The goal was to characterise the ratio of the energy deposition between the strike points for a range of plasma conditions and field directions, which is of great interest to ITER in the context of the mitigation of the effect of large power ELMs. A fast imaging visible camera was installed on TCV with an efficient relay optics to look for fast changing edge phenomena.

Edge Physics with IR

SOL Characterisation

The goal of the IR observations was to characterise the power in the Scrape Off Layer (SOL) for forward and reversed main magnetic field. Power leaving the plasma follows the non-closed field lines outside the LCFS onto the machine tiles that heat leaving a temperature pattern that the IR cameras observe. X3 ECRH into H-mode plasmas was used to generate high power ELMs in Single-Null Lower (SNL) diverted discharges whose thermal footprint is measured. The power folding lengths, heat fluxes and total heat loads were simultaneously measured for the outer and inner divertor strike points together with the heat deposition time-scale differences. With the high ELM power load in ITER, strong asymmetries in the ELM power deposition will strongly influence the divertor heat load design. These measurements were made possible by the loan of a second IR camera from the MAST group at Culham (UK) from July to September 2009. The CRPP camera observed the TCV floor through a modified IR relay optic that can now accommodate IR passband filters and the MAST camera observed the TCV central column tiles. The MAST camera's detector is more sensitive to longer IR wavelengths so the passband filters were designed to better match the two cameras sensitivities.

Following a large number of experimental sessions over which the plasma current and toroidal magnetic field directions were separately reversed, a large database of deposition parameters is being constructed for ECH heated and Ohmically heated discharges. One of the missing aspects of edge physics work on TCV was the lack of data on eventual divertor heat load imbalances, which this dataset will surely address.

Filamentary heat deposition

Filaments in the thermal footprint on the strike point have been observed on TCV and other machines. If sufficiently strong, these have the potential of stimulating a redesign of the ITER upper divertor dump plates as the power deposition near the

secondary X-point at the top of the vessel may be too high for components that were not previously thought to be submitted to large heat loads. The study of the power in these filaments was performed in Single-Null Upper (SNU) plasmas where the secondary strike point is on the floor tiles and thus in the field of view of the TCV IR camera. By operating in reversed toroidal magnetic field we simulated the situation of greatest interest to ITER. This study benefited from the use of floor tiles with a thin surface layer that is not in good thermal contact with the rest of the tile. As the layer heats faster than would the tile bulk, the IR camera is able to observe heat deposition powers that would not have heated the tile bulk sufficiently.

Visible filamentary structures in the TCV edge

A sector on the TCV tokamak is equipped with ports that are designed for near tangential view of the plasma (see Fig. 2.1.26a). A tangentially aligned camera could result in almost perpendicular to the magnetic field view, which could allow us to resolve the radial structure of the observed light distribution (at least at a certain poloidal cross section).

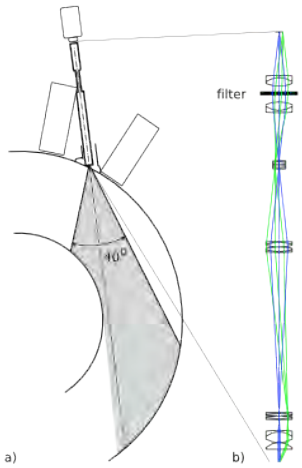

Fig. 2.1.26 *FastCam set-up and optics. A telecentric lens produces an intermediate image field of view of 40 degrees and a magnification of 1:60*

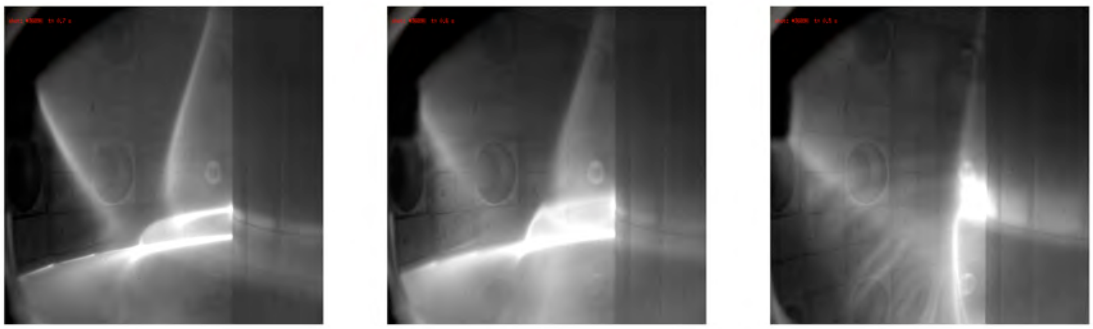

Fig. 2.1.27 *Example of the fast camera showing selected images from the time evolution in a snowflake diverted plasma. The time difference between the images is 100 ms. The relay telecentric optics preserves the camera resolution and provides images with a large depth of field.*

The optics is shown in Fig. 2.1.26b. In the first section the plasma is imaged into a relay tube. Telecentric imaging has the advantage of the possible inclusion of an interference filter in the optical path permitting the selection of a particular spectral

feature (the rays must be close to parallel at the filter). A second section relays the intermediate image to the sensor. The optical system has an f-number of ~4 and is 0.8m long that is considerably more light efficient than the fibre optic relay optics installed in 2008.

Observation of edge filaments

The coherent filamentary structures measured usually by Langmuir probes in the edge of several fusion plasma experiments are considered to be the main ingredients of radial intermittent anomalous transport. An attempt was made at TCV to observe these filaments from their visible light emission using a fast framing CMOS camera (in this case the Photron APX-RS) capable 1024x1024 pixel resolution at 3000 fps, 512x512 at 10 000 fps and in minimum sub array mode at 250000 fps (128x16 pixels). This camera is extremely sensitive (up to 6400 ASA) and can be operated at very low integration times (down to 1 micro second). The sensor is a 10-bit CMOS single sensor with a quantum efficiency of 50% at 527nm and includes a 2GB on-board memory that allows a recording time of 0.7 s at 3000 fps for full frame images.

The first images obtained show clearly field aligned structures at the plasma edge. During the snowflake formation these structures were suppressed.

To enhance the filament contrast in the images a background subtraction technique was employed, an example of which is shown in Fig. 2.1.28. This system will be used to measure the number and strength of the filamentary structures in the edge of L and H-mode plasma regimes. The DMV valve injection port is also in the direct field of view of the fast camera and there is some evidence that the contrast (emissivity) of the filaments may be enhanced by increasing the neutral gas density of the plasma edge in view.

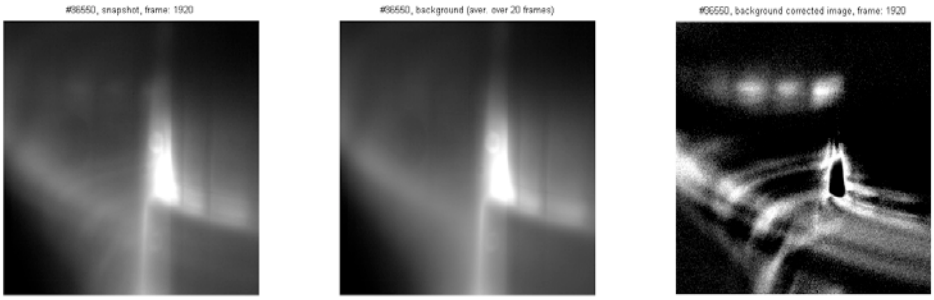

Fig. 2.1.28 *Background subtraction. From the left: the original image, a background image and the background corrected images, respectively. The filaments are clearly extracted as the toroidal features in the image although artifacts are still present.*

2.2 Theory and numerical simulation

Theory and numerical modeling activities cover the following main areas of research: first principle based simulations of turbulence, MHD analysis of tokamaks, application of RF waves, and investigations of 3D magnetic confinement configurations. In addition, the CRPP has made contributions to the Integrated Tokamak Modelling Task Force.

2.2.1 Physics underlying anomalous transport

Global gyrokinetic simulations (ORB5 code)

Towards consistent, long time scale simulations of turbulent induced transport

In order to simulate turbulence at transport timescales, the systems under consideration have to reach a steady state in a statistical sense on a long enough timescale. Both the effects of collisions (even though the core of fusion plasmas is weakly collisional) and of profile evolution under the action of power sources have to be taken into account.

The development of collision operators following Langevin's approach (random velocity kicks) have first been studied in simple test problems, among which the simulation of collisional effects on the Landau damping of electron plasma waves. These test problems have in particular enabled to analyze the issue of weight spreading resulting from these Langevin algorithms, leading to increased numerical noise. Possible noise reduction schemes have been considered. In a second phase, the collision algorithms have been implemented into the gyrokinetic code ORB5 for modeling both electron-ion, as well as both electron and ion self-collisions (ion-ion, electron-electron). The conservation properties of the algorithms have been tested. The code has been benchmarked against neoclassical transport theory, the Fokker-Planck code CQL3D and gyrokinetic codes (GENE, GT5D) for the study of collisional effects on linear micro-instability growth rates. Preliminary nonlinear runs for studying the effects of collisions on turbulence have been performed.

Computer resources available through DECI (DEISA Extreme Computing Initiative) have been used for an ITG size scaling (ρ^* scan) exercise in steady state. It has been demonstrated, using an entropy diagnostic, that the noise control operator is sufficient to ensure a statistically steady-state. An additional heating operator has been implemented in ORB5 which allows simulations with a specified input power, and more closely models the situation in a real tokamak. By running long ITG simulations of a moderate-sized plasma, we were able to demonstrate the relaxation of the radial temperature profile to a quasi-steady state, with net-zero input power.

Effects of an applied shear poloidal rotation on ITG turbulence

An investigation of the effects of poloidal rotation shear on ITG turbulence has been performed using the ORB5 code. Very little variation in steady-state flux was seen when flows with zero shearing rate were applied. A strong linear stabilization was found when sheared flows were specified, but nonlinear simulations indicated that the complete suppression of steady state flux was only seen at higher values of the applied ExB shearing rate. There appears to be a fairly wide range of shear flow states where the system undergoes subcritical turbulence. The suppression of flux versus shearing rate seems to be best fitted by a function of the square of the shearing rate, with the flux going to zero when the shearing rate is comparable to the zero-shear linear growth rate of the ITG mode (Fig. 2.2.1). Avalanche propagation depends on the sign of the flow shear, and for strongly sheared configurations the individual bursts traverse the full radial system extent. There is a tendency for the flux profile to shift inwards when the avalanches propagate inwards, and vice-versa, which cannot be explained in terms of local plasma stability. We intend to study these possible non-local effects in later work.

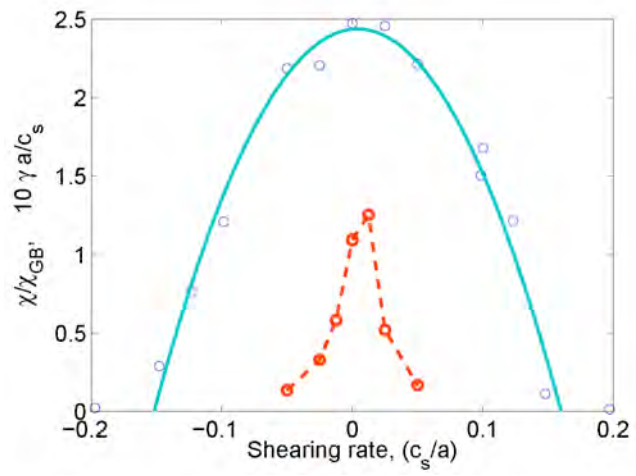

Fig. 2.2.1 *ITG turbulence induced heat diffusivity (blue) and linear growth rate (red) versus shearing rate of an applied ExB flow. There is a large range of shearing rate values for which the system is nonlinearly unstable but linearly stable.*

Homogeneous poloidal rotation shear is able to completely suppress flux at temperature gradients well above the Dimits' limit. We performed linear simulations where the sign of the background flow shear changes at mid radius, with various temperature gradients and shear flow levels (Figure 2.2.2). This can be seen as an investigation of the stability of the zone boundary. A Dimits' shift is recovered as maximal temperature gradient where a stable zone boundary exists.

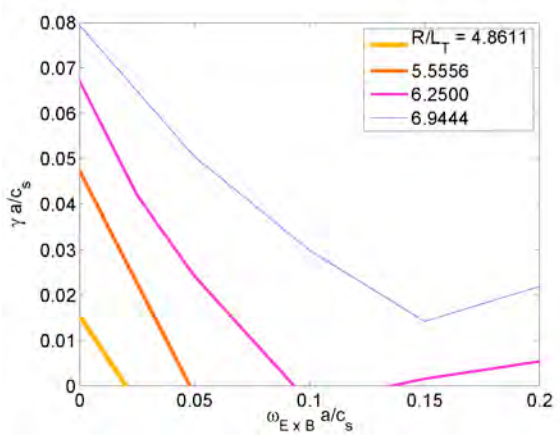

Fig. 2.2.2 *Linear ITG growth rate versus shearing rate of an applied ExB flow for various values of the ion temperature normalized gradient R/L_T. There is a gradient value beyond which complete stabilization cannot be reached. This value appears to be comparable to the nonlinear upshifted (so-called "Dimits' shift") critical temperature gradient.*

Effects of non-adiabatic trapped electron response on the development of turbulence have been studied. Nonlinear Trapped electron Mode (TEM) simulations at the Cyclone size have been performed for various ratios of the electron and ion temperature gradients, and with and without zonal flows. The zonal flows lead to a

significant reduction of TEM turbulent transport, but not as dramatic suppression as seen in ITG turbulence.

Numerical developments in ORB5

Final tests have been successfully achieved of the new interface between the ORB5 code and CHEASE, which provides axisymmetric MHD equilibria. In addition, the algorithm for the Fourier space Poisson solver, which allowed a massive speedup of ORB5 for large systems, was generalized to 3D geometries, opening up the possibility of its use in gyrokinetic codes for stellarators.

The ORB5 code was tested for its parallel scalability on an IBM BG/P up to 32768 processors in the frame of a DEISA Extreme computing initiative and on the Cray XT-5 "Monte Rosa" platform at the Swiss Centre for Supercomputing (CSCS). Both strong and weak scaling cases show excellent results, with speedup factors close to optimal and parallel efficiency close to 100% (Fig. 2.2.3). In addition, the ORB5 code was successfully ported to the HPC-FF "JUROPA" platform in Jülich. In preparation for the benchmarking effort, the computational performance of the ORB5 code's different components has been examined. For very large plasmas, a parallel transpose operation has been determined to be the computationally most demanding part of the code for parallel scalability.

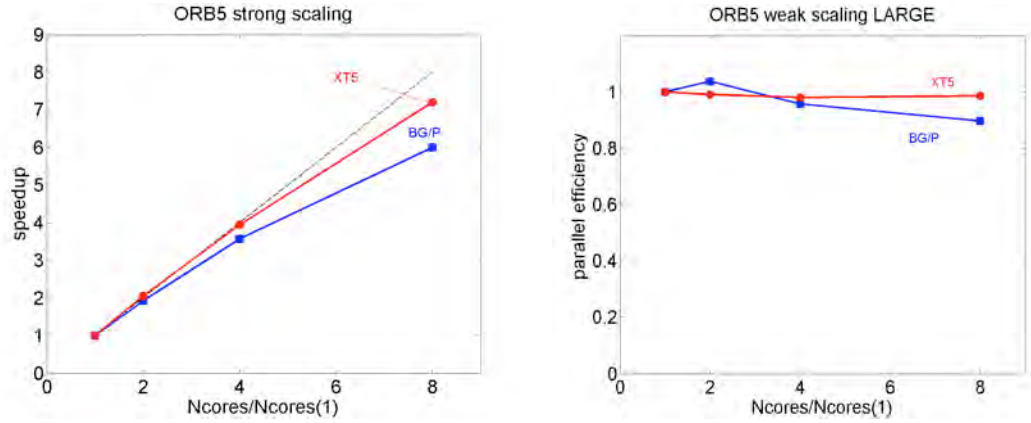

Fig. 2.2.3 *Strong (left) and weak (right) scaling tests of the ORB5 code, on a BG/P from 4096 to 32768 processors, and on a XT5 from 1024 to 8192 processors.*

Grid-based gyrokinetic simulations

Development of the global GENE code

The effort on extending the Eulerian code GENE from a local flux-tube to a global geometry has been pursued. This project is an ongoing collaboration between the CRPP and the group of F. Jenko at IPP Garching. The simulation volume considered in the current version of the global GENE code consists of a toroidal annulus covering a major fraction of the plasma core of a tokamak. A field-aligned coordinate system ensures a natural and thus optimum representation of the quasi-two dimensional fluctuations related to the microturbulence. The model accounts for the radial variation of temperature and density profiles, as well as of the magnetic geometry. The periodic boundary conditions used in standard flux-tube simulations become inappropriate in conjunction with the radial variation of

profiles, so that radial boundary conditions needed to be reconsidered. Various combinations of radial boundary conditions and particle/heat sources are currently being tested, which will enable profiles to evolve freely within the simulation system towards a quasi-steady state consistent with the microturbulent transport. The global code has also been interfaced with the MHD equilibrium code CHEASE, thus enabling to carry out simulations of realistic tokamak geometries. The code has already been extensively benchmarked in the linear ion temperature gradient (ITG), trapped electrom mode (TEM), and kinetic-ballooning regimes. Detailed comparisons with the global gyrokinetic ORB5 code, in particular carrying out non-linear ITG simulations, have shown very good agreement.

Study of electron internal transport barriers in TCV

Gyrokinetic simulations of conditions relevant to TCV electron-internal transport barriers (eITB) have been carried out using the local flux-tube version of GENE. The effort was focused towards identifying conditions consistent with experimental observations where heat and particle fluxes of the different species are simultaneously reduced. First simulations with the global GENE code for eITB conditions have also been carried out.

Investigation of alternative Eulerian schemes

Further efforts have been made towards developing a robust semi-Lagrangian scheme for solving the gyrokinetic equation. Contrary to standard Eulerian schemes based on the method of lines approach (i.e. separate discretization of space and time) and explicit time integration, semi-Lagrangian algorithms have the potential advantage of not being limited by a CFL condition, thus allowing for larger time steps. Alternatives to the three time level scheme currently implemented in the semi- Lagrangian code in straight slab geometry have been developed and applied to the 1-dimensional Vlasov-Poisson and 2-dimensional Kelvin-Helmholtz test problems, which separately address the parallel and perpendicular dynamics in the gyrokinetic equation. Three time level schemes, also called leap-frog, suffer from even and odd time steps drifting apart. These even and odd time series may be coupled together by periodic time averaging, which however leads to undesired numerical damping.

Implementation of collisions

An algorithm for implementing Coulomb collisions in the semi-Lagrangian code, based on time splitting and finite elements, has been derived. In a first stage, pitch angle scattering, represented by the Lorentz operator, has been implemented and tested. The implementation of the linearized Landau self-collision operator is currently underway. In view of carrying out simulations for which collisional effects are important but nonetheless not dominant over the advection dynamics, the choice of velocity variables for the Eulerian representation of the distribution is dictated by the latter. The collision operators have thus been discretized in the velocity variables (v_par, v_perp) instead of spherical coordinates, which would represent the natural choice with respect to purely collisional dynamics. The numerical effects of this non-ideal coordinate system have been investigated. This effort on developing a collisional module for Eulerian codes also integrates in the ongoing collaboration with the CASC (Center for Apllied Scientific Computation), funded by LLNL, for developing a Vlasov-type code applying Adaptive Mesh Refinement (AMR) techniques.

Turbulent transport of fast ions

Previous studies on the micro-turbulence driven transport of energetic ions have been extended by introducing a velocity space dependent diffusivity. The analysis has been focused on the ITER steady-state scenario, a candidate for long term burning plasma operation. The results of Fig. 2.2.4 clearly indicate that electrostatic fast ion diffusivities above 0.1 m^2/s, a value sufficiently high to cause significant redistribution, are observed over a wide energy range for alpha particles. Similar conclusions can be drawn for the electromagnetic component of the fast ion transport.

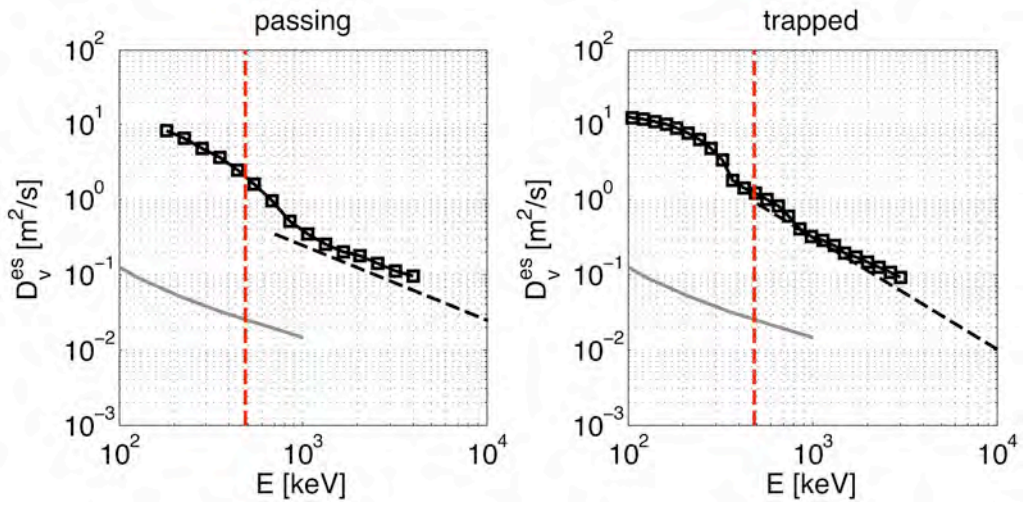

Fig. 2.2.4 *Electrostatic diffusivity, as a function of energy, of passing (left) and trapped (right) alpha particles in the ITER steady state scenario. The red dashed lines indicate the critical energy of alpha particles, the gray solid line the expected neoclassical diffusivity.*

A scenario with lower gradients has also been simulated, leading to reduced background ion heat conductivity and fast ion diffusivity. It has thus been demonstrated that neoclassical models are not sufficient for describing fast ion transport, whose anomalous component can be one order of magnitude larger than classical predictions. Also, anomalous transport of energetic ions is expected to show a poloidal dependence, with stronger transport on the low field side of the tokamak. Future analysis will be carried out to validate these conclusions and to model the expected anomalous diffusion of energetic ions in present day tokamaks.

Studies of ECH/ECCD for scenario control

Electron transport and current profile modeling

We have participated in the study of possibly only using ECH/ECCD in ITER to perform the various scenarios. It was shown that it might be sufficient for the standard scenario, i.e. scenario 2, since the main requirements concern bulk heating. However, for hybrid and advanced scenarios, even 70MW of ECCD would not be sufficient. The EC system is most appropriate when used in combination with a system like NBI which can drive bulk current.

Neoclassical tearing modes (NTM)

The conditions for tearing mode triggering and stabilization in TCV have been investigated, in particular related to the influence of current drive and heating on the classical Δ' term. Using TCV *q* profiles, a detailed study of the results obtained using a code solving the cylindrical equation and the code PEST-III, solving the toroidal Δ', has been performed. It was shown that the influence of local current drive might be either destabilizing or stabilizing, depending on several parameters. The high sensitivity now requires detailed experiments to be able to better understand the effective dependencies.

Particle transport modeling

A well-defined method based on a quasi-linear model has been developed for predicting particle transport. It was used with GS2 linear results and compared with TCV data. A comprehensive understanding has been drawn which has the potential of explaining the main trends seen experimentally. A paper has been submitted with more details. We have also defined a useful average mode frequency, which allows determining if the plasma is dominated by Ion Temperature Gradient (ITG) or Trapped Electron Modes (TEM). Since the former tend to sustain an inward pinch and the latter an outward pinch, this helps to understand if more peaked or flat profile are expected.

2.2.2 RF waves

Alfvén and ICRF waves in 2D and 3D configurations

The bi-Maxwellian distribution function that has been implemented in the warm dielectric tensor model of the LEMan code computes more accurately the impact of energetic particles on electromagnetic wave propagation and absorption. Applications to a JET-like equilibrium in the low frequency Alfvén range show a shift in the frequency of a TAE (Toroidal Alfvén Eigenmode). In the Ion Cyclotron Range of Frequencies (ICRH) frequency domain, the hot particle contribution is damped by interactions with the parallel electric field over a much larger extent than the thermal population, yielding a wave structure closer, in a two-ion species scenario, to the cold model.

The latest updates in the full-wave code LEMan allow to compute wave fields and power deposition in the ICRF using the exact value of the parallel wave vector (with an iterative method), in contrast to the widely used n/R approximation. A second improvement is the direct computation of the parallel and perpendicular wave vectors using the electrostatic potential gradient. These are the forms used by the single particle Monte Carlo code VENUS for computing the kicks in velocity space due to wave-particle interactions. Thus no approximations of the wave vectors or dispersion relation have to be used.

Comparisons with experimental results have also been performed with the LEMan code. A TAE with n=3 is driven by the new set of Alfvén antennas in JET during shot #77788. Good agreement has been obtained between the experimentally determined frequency and damping and the simulation undertaken with LEMan for cases where the equilibrium was close to be up-down symmetric.

For validation of the code package VMEC-LEMan-VENUS, benchmarking efforts have been started against the code SELFO form KTH, Stockholm. Preliminary

results in simple circular geometry are very encouraging. First ICRF heating computations show the emergence of asymmetric and ear-shaped distribution functions, which are characteristic for ICRF and result in anisotropic pressure and currents due to Ion Cyclotron Current Drive (ICCD).

2.2.3 Operational limits

MHD Stability and Kinetic effects

There has been much interest in recent years in reverse shear and hybrid scenarios. For the latter, the extended region of small or vanishing magnetic shear is susceptible to interchange, quasi-interchange or infernal mode instability when respectively q<1, q=1or q>1 in the low shear region. An MHD eigenvalue equation has been developed that encompasses all three cases. This has enabled analytical derivation of the mode structure, the growth rates and stability criteria of these important instabilities. Simple stability criteria now exist for the global oscillations, dubbed q>1 sawteeth, which are observed in TCV. The analysis is also relevant for the long-lived modes observed in the spherical tokamak MAST, and the MHD activity observed in JET during hybrid and advanced scenarios. Furthermore, a dispersion relation for infernal-fishbones (with q not necessarily equal to unity) has been derived. Of particular interest will be to investigate the numerous kinetic modes that exist simultaneously close to one magnetic surface.

Sawtooth behaviour and internal ideal stability

The sawtooth control mechanism in plasmas employing off-axis toroidally propagating ion cyclotron resonance waves in tokamaks is being investigated. The radial drift excursion of energetic passing ions distributed asymmetrically in the velocity parallel to the magnetic field is found to determine stability when the rational q=1 surface resides within a narrow region centred about the shifted fundamental cyclotron resonance. Analytical and full numerical calculations of the internal kink mode with the simulated JET ICRH distribution function demonstrate ideal instability when the deposition of the resonating ions is very close to the q=1 radius. Such is the sensitivity to the location of deposition, and the magnitude of the effect, that this fast ion mechanism, i.e. non-MHD mechanism, dominates over the previously assumed classical mechanism relating to the change in the magnetic shear due to the fast ions, and the resulting effect on MHD stability. Furthermore, unlike the classical sawtooth control mechanism, the fast ion mechanism derived here is independent of the plasma drag, which is expected to limit the current drive efficiency of the proposed ICRF system for ITER. In order to distinguish between the two mechanisms, and test the prospects of sawtooth control in ITER using ICCD, experiments at JET using minority He3 have been undertaken. Figure 2.2.5 shows the sawtooth period for two contrasting pulses, one with RF waves propagating counter to the plasma current (76189, -90 phasing), and one with RF waves progating in the direction of the plasma current (76190, +90 phasing). Compared with this is the simulated fast ion potential energy, also plotted with respect to the difference between the H3e resonance position and the measured smoothed average of the inversion radius. It is clear that the simulations recover the narrow region for which the sawteeth are sensitive to the RF deposition.

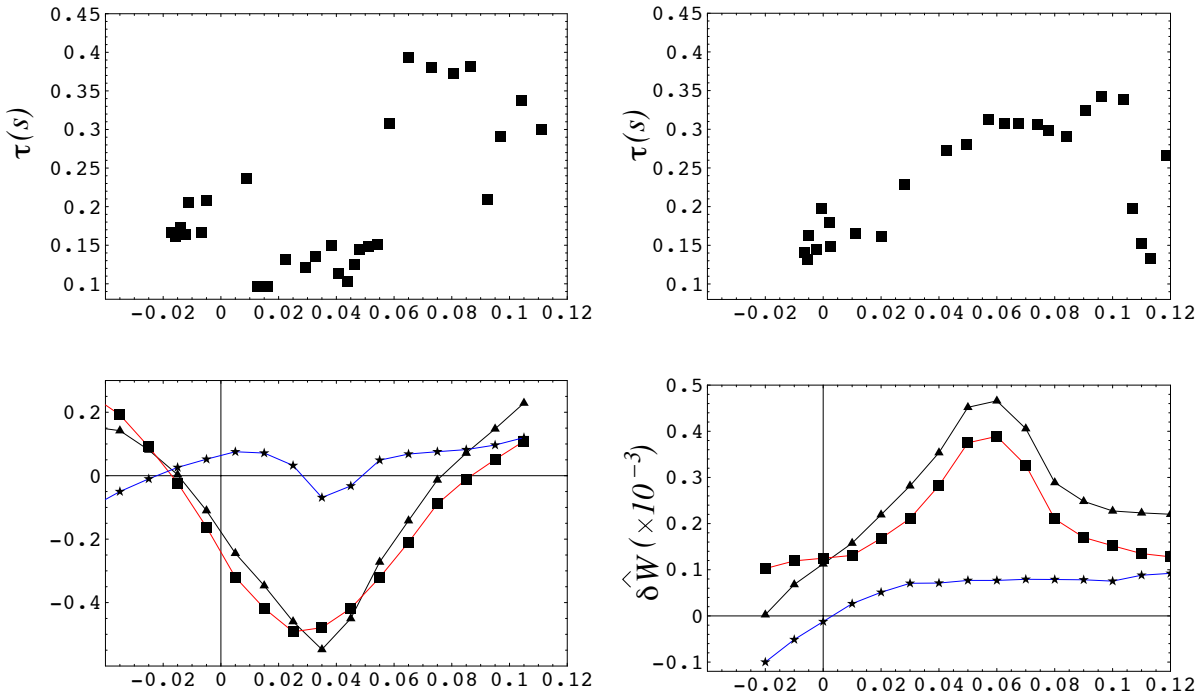

Fig. 2.2.5 *Showing (a) and (c) the sawtooth period for respectively pulses 76189 (-90 phasing) and 76190 (+90 phasing) plotted with respect to the difference between the smoothed average of the sawtooth inversion minor radius and the He3 resonance minor radius. Shown in (b) and (d) are corresponding ICRH fast ion contributions to the potential energy.*

MHD equilibria and stability computations of TCV plasmas

Ideal MHD stability studies have been performed with the KINX code of various configurations of the TCV tokamak in a range of shapes characterized by varying separately the upper and lower triangularities. Configurations that are compatible with the TCV vacuum vessel ports and LFS tiles have been identified and the corresponding edge stability diagrams have been produced. The general conclusion that negative triangularity is destabilizing the pedestal region has been confirmed. The edge kink/ballooning mode stability is mainly determined by the negative lower triangularity: the second stability access in the pedestal region is eliminated. This could lead to different types of ELMs triggered by high-n ballooning modes at relatively low values of pressure gradient and current density in the pedestal.

In support of the design of stable negative triangularity H-mode configurations in the frame of the TCV upgrade, an optimization of the plasma position and shape was performed. The plasma elongation 1.4 corresponds to a reasonable growth rate of vertical instability of about ~700 1/s when the presence of ports is neglected (a factor of 2 larger with axisymmetric openings in the place of ports). In series of equilibria with negative lower triangularity and varying upper triangularity, the n=0 growth rates are in the range 400-700 1/s (700-1000 1/s with 2D openings) with the minimum attained for zero upper triangularity. A series of n=0 mode stability calculations with the resistive TCV wall (the KINX-NW code) under plasma profile variations showed that growth rate values for negative triangularity equilibria are much less sensitive to the pedestal profiles than for standard D-shaped plasmas. In contrast to the positive triangularity case, the plasma displacement pattern for

negative triangularity equilibria significantly changes in the low current density region near the edge compared to the displacement corresponding to the equilibrium with reference H-mode profiles.

Studies of TCV snowflake configurations have also been performed. The flexibility of the TCV magnetic system for creating equilibria with different locations of the second order null point and positions of plasma in the vacuum chamber was demonstrated. For comparison, single null (SN) free boundary equilibria with an x-point in the place of the second order null were computed using the same set of control points (reconstructed boundary for the TCV snowflake shot #36151). The edge stability calculations with the KINX code showed an enhancement of the limiting pedestal poloidal beta values compared to standard SN divertor plasma especially in a combination with increased upper triangularity.

A study of the axisymmetric stability of plasma configurations related to doublet formation scenarios in the TCV tokamak has been performed. Axisymmetric stability calculations of two plasma columns inside an ideally conducting wall with the TCV vacuum vessel shape showed that the plasma columns interaction is essential in determining the value of ideal MHD growth rate. The plasma columns displaced in opposite directions correspond to the largest growth rate value (approximately twice as high as compared to the case of single axis plasma). The interaction is stronger for flatter current density profiles, which leads to further destabilization of the two column configuration, unlike the single plasma column case for which flatter current profiles lead to a stabilization of axisymmetric modes. On the other hand, the second unstable mode (plasma columns displaced vertically in the same direction) becomes more stable with flatter current density and stronger column interaction.

Equilibrium and stability of zero current configurations

Axisymmetric MHD stability calculations with the unstructured grid MHD_N0 code provided an additional insight into the modeling of zero current equilibria relevant for tokamak AC operation. In particular, zero current equilibria stable against n = 0 ideal modes with a conducting wall at finite distance from the plasma boundary were found in the class described by a linear Grad-Shafranov equation.

2.2.4 Optimization of 3D configurations

Optimization of quasi-isodynamic stellarator configurations

For the quasi-isodynamic stellarator with zero dipole secondary current (number of periods N=6, aspect ratio A=35) with averaged $<\beta>=0.2$, the boundary magnetic surface has been found using the optimizer. The configuration features an elaborated structure within each field period and favorable confinement properties: almost zero dipole secondary current, small effective ripple, good collisionless long-time confinement of alpha-particles, stable Mercier and resistive ballooning modes. However, the study of global mode stability has revealed a strong ballooning type internal instability even for $<\beta>=0.1$. An alternative possibility to diminish the dipole secondary current is to increase the aspect ratio. As a result, an N=18, A=90 configuration with very good neoclassical properties and high $<\beta>\sim0.2$ has been found.

Neoclassical transport in 3D stellarators

Good agreement between different code results has been obtained for general axisymmetric equilibria in arbitrary collisionality regimes and under LHD experimental conditions with model temperature and density profiles. A qualitative agreement with measured bootstrap current dependence on the value of collisionality has been observed. To evaluate the bootstrap current in nonaxisymmetric toroidal plasmas quantitatively, a delta-f Monte Carlo method is incorporated into the moment approach. From the drift-kinetic equation with the pitch-angle scattering collision operator, the bootstrap current and neoclassical conductivity coefficients are calculated. The neoclassical viscosity is evaluated from these two mono-energetic transport coefficients. Numerical results obtained by the delta-f Monte Carlo method for a model heliotron are in reasonable agreement with asymptotic formula and with the results obtained by the variational principle.

Drift stabilized ballooning modes in stellarators

The BECOOL finite element ballooning solver has been modified to treat thermal and fast ion diamagnetic drift correction effects using a perturbative technique. In our opinion, the developed model provides a more accurate description of the stability properties of the LHD Heliotron compared with ideal MHD (or other purely fluid anisotropic pressure schemes). This model has indeed demonstrated that the LHD heliotron is stable to ballooning instabilities for all values of beta including the experimentally achieved beta~5%. The applicability of the theory is shown to be valid when the fast to thermal ion density does not exceed 2%-3%.

Free-boundary, 3D, anisotropic pressure, stellarator equilibria

A diagnostic that determines the error in charge conservation has been developed for the ANIMEC code. For simplicity, this measure was determined in the Boozer coordinate frame which may have clouded the assessment of the error due to the introduction of coordinate transformation inaccuracies.

2.2.5 Tokamak discharge simulation

All activities in that area have been focused on ITER studies and are therefore reported in Chpater 4, section 4.7.

2.2.6 Integrated Tokamak Modelling (ITM)

The codes CHEASE, CAXE and KINX have been updated for the new versions of the ITM database structure. They are also being integrated into the KEPLER workflow environment.

The interface between TCV data, machine description and the ITM database is also being developed.

We have participated in the development of the sawteeth and NTM modules to be in particular coupled to the transport solver. The Consistent Physical Object (CPO) structure for the sawteeth has been included in version 4.07a of the data structure and the Fortran coupling to the database has been tested. It is being included into

the KEPLER workflow. The NTM module continues to be developed. The first routines which link the modules to the database have been tested.

As part of the Integrated Modeling Project on turbulence, we added the capability of reading equilibrium objects in ITM format to the gyrokinetic code ORB5. In addition, a standard circular concentric equilibrium file was produced, appropriate for basic benchmarking across the gyrokinetic and gyrofluid codes, using the CHEASE equilibrium code. Simple testing was performed to check the correct functioning of the ORB5 code with this equilibrium input.

In addition, the interpolation/extrapolation routines using cubic spline with tension have been re-written as a module in Fortran 90 and including all the various options, in particular for boundary conditions (2^{nd} , 1^{st} derivatives or function values given at edges, or periodic boundary conditions) or for extrapolation options. This new module and library has been proposed to the ITM as the standard interpolation tool. It is very useful both in numerical codes and for experimental data analyses.

2.3 Operation of a specialised basic plasma physics device, TORPEX

The activities of the Basic Plasma Physics group at CRPP continue to be focused on fundamental aspects of the physics of fluctuations and turbulence, and related transport phenomena in toroidal magnetized plasmas. In parallel with their fundamental nature, such studies can have an impact on the understanding of phenomena that play a very important practical role in the functioning of a magnetic fusion reactor, in particular in one of the most critical areas, the edge region.

The experiments are conducted on the TORPEX (TORoidal Plasma Experiment) device, characterized by low plasma densities and temperatures, allowing high-resolution measurements of plasma parameters and wave fields throughout the plasma cross-section. Plasmas are confined by a toroidal magnetic field up to BT=0.1T, and a vertical field, up to Bv~0.01T, corresponding to a simple magnetic configuration with open field lines terminating on the vessel wall. This configuration incorporates the main ingredients for drift and interchange wave instabilities and turbulence, namely pressure gradients and magnetic field line curvature. Highly reproducible plasma discharges of different gases (Argon, Hydrogen, Helium, and Neon) with density and electron temperature in the range ne~10^{16}-$10^{17}$$m^{-3}$ and Te~2-10eV are driven for more than 3s by microwaves at f=2.45GHz (P<50kW), in the electron cyclotron (EC) range of frequencies.

In 2009, the activities of the group included the study of the propagation of plasma filaments (blobs), the investigation of the interaction between suprathermal ions and electrostatic drift-interchange turbulence, the identification of a critical gradient for the stability of interchange modes, the development of plasma and turbulence imaging techniques using fast cameras, the refinement of probe design and data analysis, the development of a three-dimensional simulation of the plasma turbulence in TORPEX, and a number of technical improvements, as detailed below.

2.3.1 Propagation of plasma filaments in TORPEX

Magnetically confined plasma particles can efficiently be transported across the magnetic field in the form of filaments or blobs. These are magnetic-field-aligned structures of increased plasma density and temperature compared to the background plasma. The study of blobs and the resultant intermittent convective transport is a very active research area within plasma physics. This not only because blobs are believed to dominate the transport across the scrape-off-layer of fusion devices and possibly lead to serious wall erosion, impurity and recycling problems for future fusion reactors, but also because they seem to be a universal phenomenon found irrespective of the details of the magnetic geometries, devices and parameters.

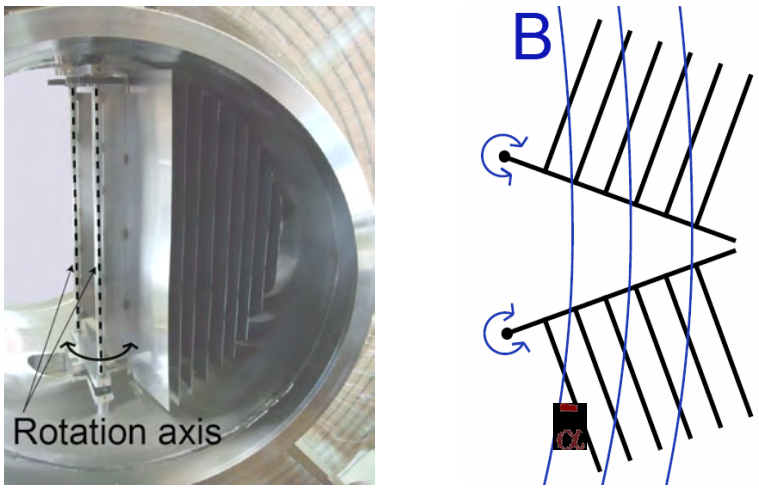

Fig. 2.3.1 *Left: Limiter à configuration variable. The view is along the toroidal direction. The angle between magnetic field lines and limiter can be varied by rotating the limiter around the vertical axis. Right: Shown is a sketch of the limiter (top view).*

TORPEX with its good diagnostic access and flexibility is an ideal experiment for the study of blob-dynamics and transport. Experiments in TORPEX have shed light on the formation mechanism of blobs. More recently, the cross-field motion of detached blobs has been investigated in a case where a plane steel limiter is inserted into the TORPEX vacuum vessel.

This year, after finalizing the study of the cross-field motion of blobs in this standard setup, we have increased the complexity of the system by varying the angle between magnetic field lines and limiter. This was achieved by a specially designed tiltable plate limiter, which, according to theoretical predictions, should influence the velocity of blobs (the limiter is shown in Fig. 2.3.1).

Experimental results are presented in Fig. 2.3.2. We are showing snapshots of the average dynamics that lead to a blob ejection, at a time of 96 microseconds before the blob is detected at the trigger location (black dot). The four frames correspond to cases with different angles between magnetic field lines and limiter. At some point, a positive structure of the mode radially elongates and forms the blob. The frames in Fig. 2.3.2 correspond to a time just before this happens. The fact that all four frames are almost identical indirectly shows that blob velocities are not significantly influenced by the angle between magnetic field lines and limiter.

Whether these results are disproving the theoretical prediction in general or if they are limited to our specific setup is still being explored.

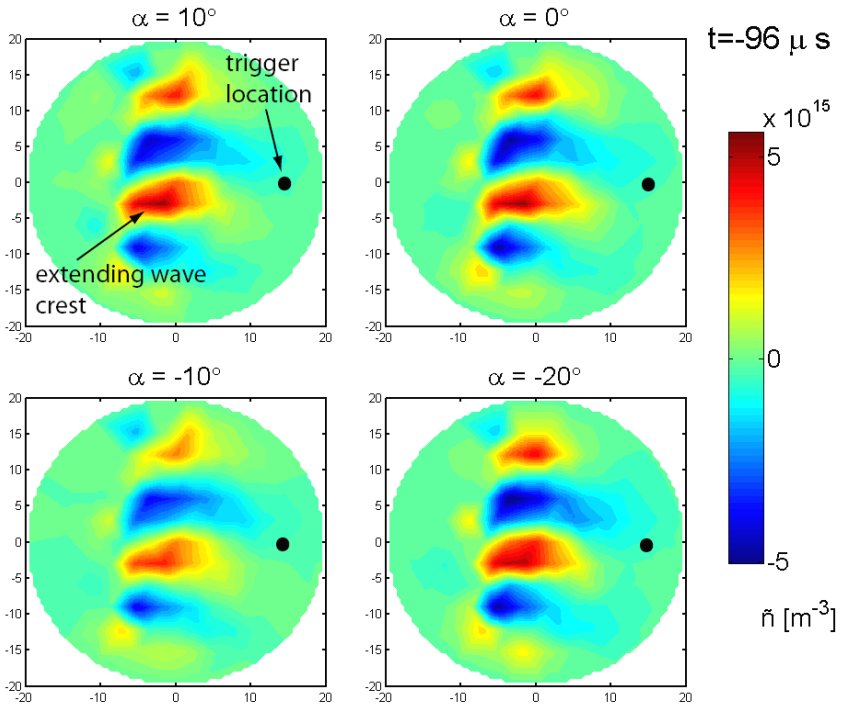

Fig. 2.3.2 *Average density fluctuations at a time of 96 microseconds before the blob is detected at the trigger location (indicated by a black dot). The blob forms from the central positive wave crest. The different frames correspond to cases with different angles between magnetic field lines and limiter. Theory predicts a slowing down of the blob for negative angles, and an acceleration for positive values.*

2.3.2 Triple probe studies

A considerable effort has been devoted this year to a detailed study of Langmuir probes, especially the triple probe. This probe provides in principle the time history of electron temperature, density and plasma potential. These quantities are not only needed for a more detailed study of blob dynamics, but also for the TORPEX turbulence code validation project.

Several difficulties with the triple probe have been encountered. An example is the issue of phase errors: The triple probe technique relies on the condition that all three probe tips see the same plasma parameters. However, for obvious reasons, the tips cannot be placed at exactly the same location, such that gradients in the plasma can violate this assumption. This problem can be solved by the use of a five tip probe, which allows one to average out phase errors by combining measurements of the different tips (Fig. 2.3.3). Preliminary results with this probe indicate that temperature fluctuations are much weaker than fluctuations in density. Further, temperature and density fluctuations appear to be in phase. The latter would justify the commonly used approach to use floating potential measurements to evaluate the time averaged ExB particle flux. In Fig. 2.3.3, we show an example of the frequency spectrum of the particle flux measured with the triple probe. Two modes can be clearly identified. They both contribute significantly to the radial transport of particles.

Other difficulties related to the triple probe are still being investigated. One is the experimental determination of the minimal tip size, such that Bohm's theory is still valid. Another one is the evaluation of the appropriate spacing between tips, such that shadowing effects are avoided. Finally, some more sophisticated electronics development is ongoing to limit the capacitive effects and to increase the bandwidth of the measurements.

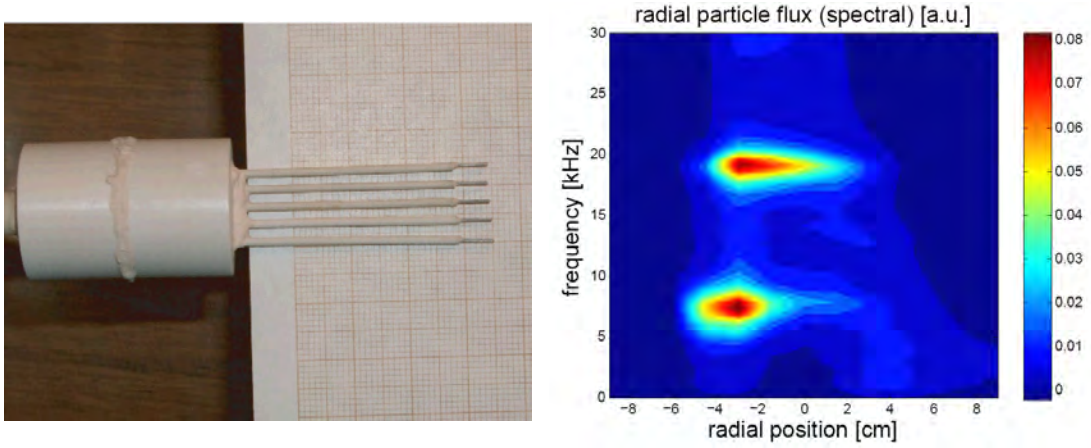

Fig. 2.3.3 *Left: Photograph of the five tip probe in TORPEX. Left: Plot of the evaluated (spectral) radial particle flux, as a function of radial position and frequency.*

2.3.3 Fast ions physics

In the past year, we continued to investigate the interaction between highly energetic ions and small-scale (drift wave-like) turbulence in TORPEX plasmas. This is an open problem in fusion plasmas, aspects of which can be addressed on TORPEX in a relatively simple experimental environment with easy access for diagnostics and well established plasma scenarios with drift-interchange instabilities and/or fully developed turbulence.

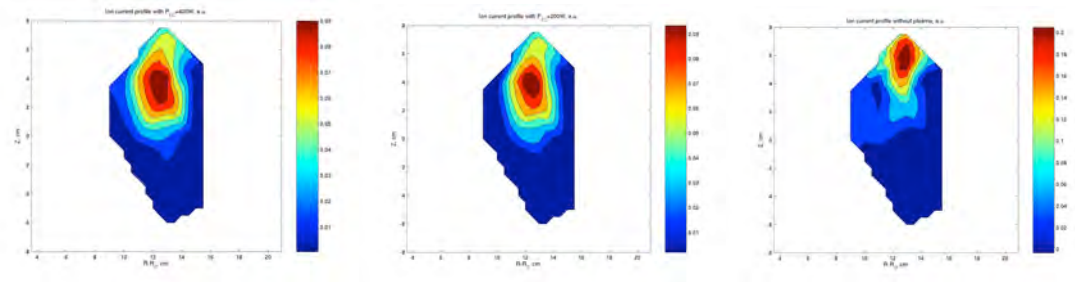

Fig. 2.3.4 *Fast ion current profiles: (a) for magnetron power of 400W, (b) 200W, (c) without plasma.*

Experiments with the fast ion source and detector were first conducted without plasma but with different configurations of magnetic fields. Next, in the well-characterized interchange-dominated plasma scenario, measurements of the fast ion current density profiles were performed in the presence of plasma in two main poloidal regions: a blob region, which is characterized by the propagation of

nonlinear structures of higher pressure than the local background plasma, with 300eV and 600eV of fast ion energy, and a mode region, where the fluctuation spectra are dominated by coherent oscillations, using the 300eV fast ions. The fast ion current profile was measured with the detector using synchronous detection to increase the signal to noise ratio. The experiments showed that with respect to the beam propagation in vacuum, in the plasma the fast ion current profile is more spread and vertically elongated (along axis Z). Moreover, the maximum of current profiles slightly moves down (Fig. 2.3.4).

A considerable effort has been devoted to develop a theoretical framework to help interpreting this experimental data. Using the single particle equation of motion a Matlab based numerical model was developed, which accounts for the realistic magnetic field and for the fast ion collisions with background plasma ions. A homogeneous, constant in time electric field can also be introduced. A second model, developed on a C++ platform, incorporates the effects of a turbulent electrical field, calculated using a two-fluid code based on the Braginskii equations. This electric field has a realistic structure, but its fluctuation levels are approximately two times higher than measured.

These models were used to interpret the experimental data. The Matlab based simulation qualitatively describes the fast ion beam behavior with different magnetic configurations in the absence of plasma. The experiments without any magnetic field and without plasma were used to calibrate the model, in particular to find a good estimate of the source angular distribution. Under the influence of the toroidal magnetic field the fast ion beam deviates in the direction of the ion toroidal drift and shrinks because of gyromotion. The addition of a weak vertical magnetic field component has negligible effect on the width of the profile and only slightly changes the poloidal position of the profile maximum. This simple single-particle Matlab model without turbulent field cannot explain the fast ion current density profiles in the presence of plasma: the collisions with background plasma ions have a negligible effect on the profiles and a static homogeneous electric field can only change the profile maximum position, but does not affect the profile width. The collisions with neutrals cannot explain the experimental profiles in the presence of plasma because the neutral pressure remains practically the same with or without plasma and because the fast ion mean free path for this pressure is around 1m, which is much longer than the toroidal path of the fast ions. The only remaining factor that can affect the profiles in the presence of plasma is a turbulent electric field. The C++ based simulation, which includes the turbulent electric field, was used to describe the experimental profiles in the presence of plasma. First, it was shown that the elongated fast ion current density profiles can be explained by the spread in the fast ion velocity distribution function. The shapes of the experimental profiles are in a qualitative agreement with the simulations. The increase in radial FWHM with respect to the case without plasma predicted by the simulation are in agreement with experimental observations.

2.3.4 Gas puffing and fast imaging of structures

Several methods to characterize the turbulence and turbulent structures naturally occurring in TORPEX plasmas are deployed at present. Local measurements of the fluctuation frequency and wave number spectra are used to identify the relevant dispersion relation, hence the nature of the underlying instability. Local time series yield the statistical properties of the fluctuations. These can be expressed in terms of Probability Density Functions (PDFs), which, along with the related moments, contain some indication on the physics of the fluctuations and turbulence. However, such local description does not contain direct information on the impact

of turbulence upon the plasma transport and confinement; neither does it univocally constrain the theoretical models adopted to simulate the turbulence evolution. To complete it, a full spatiotemporal imaging of turbulence with adequate spatial and temporal resolution, performed without perturbing the plasma, can provide significant insight into the nature of turbulence in magnetized plasmas. Fast framing cameras are one of the most recent diagnostics to monitor light emission from magnetically confined plasmas and are now commonly used to study turbulence in plasmas.

Recently, a Photron Ultima APS-RX framing camera has been acquired at CRPP for fast imaging of plasma turbulence in TORPEX plasmas, Fig. 2.3.5. This camera is equipped with a 10Bit CMOS monochrome sensor with 1024x1024 pixels which provides extreme light sensitivity up to 6400 ASA in the visible range. At the full chip resolution (1024x1024 pixels) the framing rate can be varied in the range 50fps-3kfps, which is appropriate for the monitoring of average visible light profiles during a TORPEX discharge. At reduced chip size (down to 16x128 pixels) the framing rate can be increased up to 250kfps, fluctuation and turbulence measurements of visible light emission from the plasma. The camera allows the acquisition of 1s of data at full chip size and 3fps and 4.2s of data at maximum frame rate.

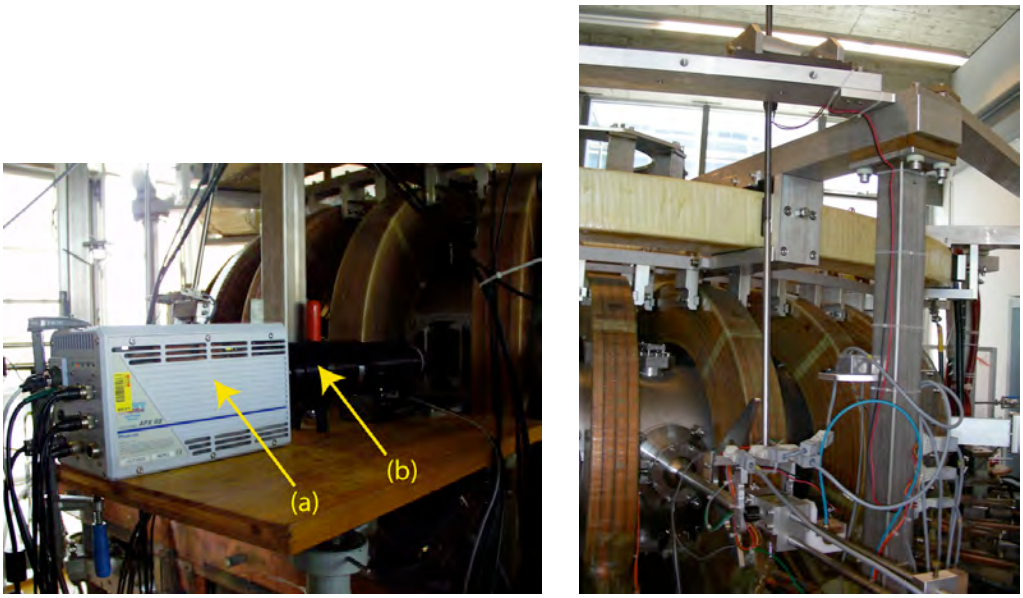

Fig. 2.3.5 *(a) The Ultima APS-RX fast framing camera and (b) the Lambert fast gated intensifier under test on TORPEX.(c) the GPI system installed onto a 2D movable system.*

The first attempts to interpret the light fluctuations with the plasma density fluctuations were only partially successful due to the low level of emitted light. To overcome these problems two major improvements of the system were considered: 1) the development of a gas puffing system; 2) the use of a fast-gated image intensifier.

A prototype GPI system, including a fast piezoelectric valve and ceramic tube having a 200μm nozzle, was already tested in 2008 in TORPEX plasmas. In 2009, the design was improved in order to install the injector onto a 2D movable system (see Fig. 2.3.4(c)). Preliminary tests of the new system reveal a problem in the gas injection pipeline, which fails after few discharges probably due to small debris of ceramic glue detaching from the junction between the ceramic tubing and the

stainless steel tubing. This led to a slightly changed design in which the ceramic tubing is directly brazed to the stainless steel tubing thus avoiding the use of ceramic glue. The system is presently under construction and will be tested in the first part of next year.

To increase the intensity of plasma radiation two Image Intensifier Units (IIUs) have been tested. These units are typically able to amplify the incoming light by a factor of 1000 in the visible range. In Fig. 2.3.5(b), we show the Lambert IIU under test on TORPEX. This enables the fast camera to image the TORPEX plasma with its maximum frame rate, 250 kframe per second, without the need for gas puffing. At this acquisition rate, the exposure time for imaging each frame is about 4μs, which is same as the time resolution of the probe data acquisition system. With the IIU it is possible to decrease the exposure time down to 1.3 μsec. A second IIU, produced by Hamamatsu, is presently under test.

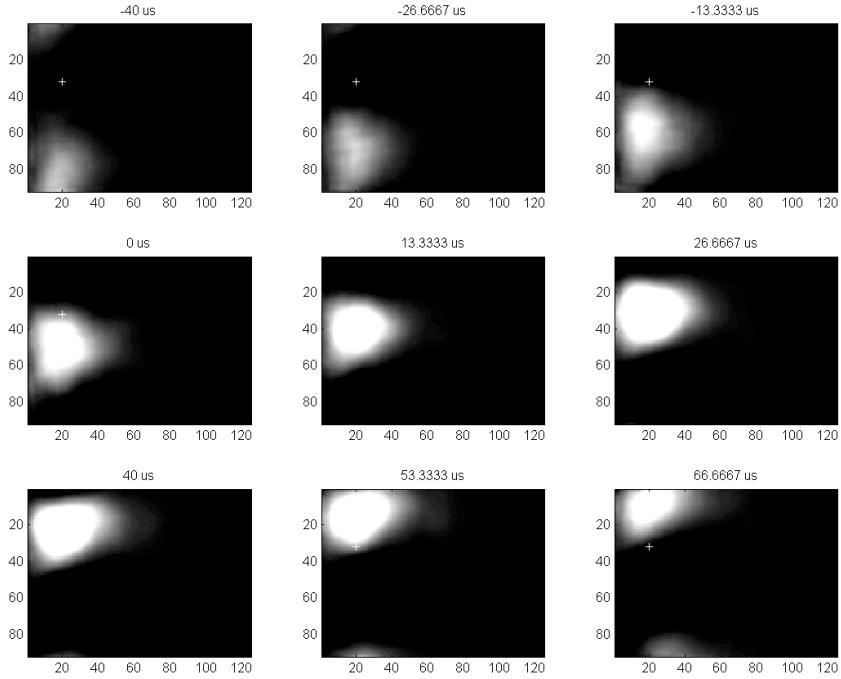

Fig. 2.3.6 *Conditionally sampled data of visible light emitted from the plasma, acquired with the fast camera and the Hamamatsu image intensifier unit. The propagating structures are associated with an interchange mode which is convected by the ExB flow.*

In Fig. 2.3.6, we show conditionally sampled images of visible light emitted from the plasma, acquired with the fast camera and the Hamamatsu image intensifier unit. The data are taken at 30 kframes per second in a hydrogen plasma, which is dominated by an interchange mode propagating with the ExB flow. The visible light structures of Fig. 2.3.6 are associated with this mode and are clearly resolved by the camera data.

2.3.5 Observation of a critical pressure gradient for the stability of interchange modes

The existence of a critical pressure gradient for the stabilization of interchange modes in simple magnetized toroidal plasmas was predicted theoretically and demonstrated experimentally in TORPEX plasmas. We focused on neon plasmas, characterized by the presence of a coherent interchange mode. The critical gradient is reached during a scan of the neutral gas pressure p_n. Around the p_n critical value, a small increase in the neutral gas pressure triggers a transition in the plasma behavior.

The plasma pressure pe and the normalized pressure gradient $|Lp|^{-1}$ radial profiles (see Fig. 2.3.7) show that for the case at higher neutral pressure, the p_e profile is locally broadened and flattened in the Low Field Side region (5 r 15cm), while on the High Field Side the profile doesn't change. In quantitative terms, the normalized pressure gradient $|Lp|^{-1}$ is reduced by a factor of four at r=11 cm (from $|Lp|^{-1}\cong 13m^{-1}$ to $|Lp|^{-1}\cong 3m^{-1}$). This latter measured value is close to the linear theory estimation obtained by solving a two-dimensional Braginskii drift-reduced equations system describing typical TORPEX plasmas (the black dashed line in Fig. 2.3.7).

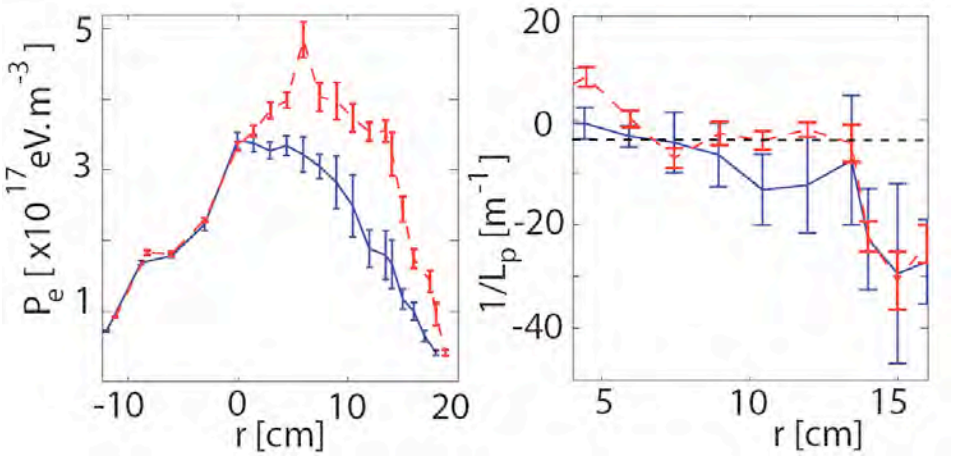

Fig. 2.3.7 *Radial profiles of the plasma pressure p_e (left side) and the normalized pressure gradient $Lp^{-1}=\nabla p_e/p_e$ (right side) for $p_n=1.2x10^{-3}$mbar (solid, blue) and $p_n=1.4x10$-3mbar (dashed, red). The black dashed line represents the critical value estimated from linear theory*

Together with the time-averaged profiles, the properties of the fluctuations are strongly affected by a small increase in the neutral pressure. In particular, the coherent features of the fluctuations spectrum display an abrupt change. The rms of the density fluctuations $\tilde{n}_e$ in the range Δf=[3.4,8] kHz normalized over the entire spectrum has been estimated for both neutral gas pressures and over the entire plasma cross section (see Fig. 2.3.8a–b)). For the higher pressure a strong reduction of the fluctuations amplitude is observed. Moreover, the spatial extent of the fluctuations, which are concentrated only at the very edge in the LFS region, is reduced. The power spectral densities estimated at r=10.5cm and r=14cm (z=0cm) reveal the interchange mode at 5.8kHz for the lower pressure. When the critical neutral gas pressure is exceeded, the mode at r=10.5cm is not detected anymore. An interchange mode is still visible at r=14cm, but with an amplitude reduced by

two orders of magnitude (Fig. 2.3.8c)). We can therefore conclude that the interchange mode observed at lower neutral gas densities has been locally stabilized.

The observed transition is relatively robust, since it can occur at a different critical neutral gas pressure for different rf power levels and/or vertical magnetic field values and it has also been observed in argon plasmas.

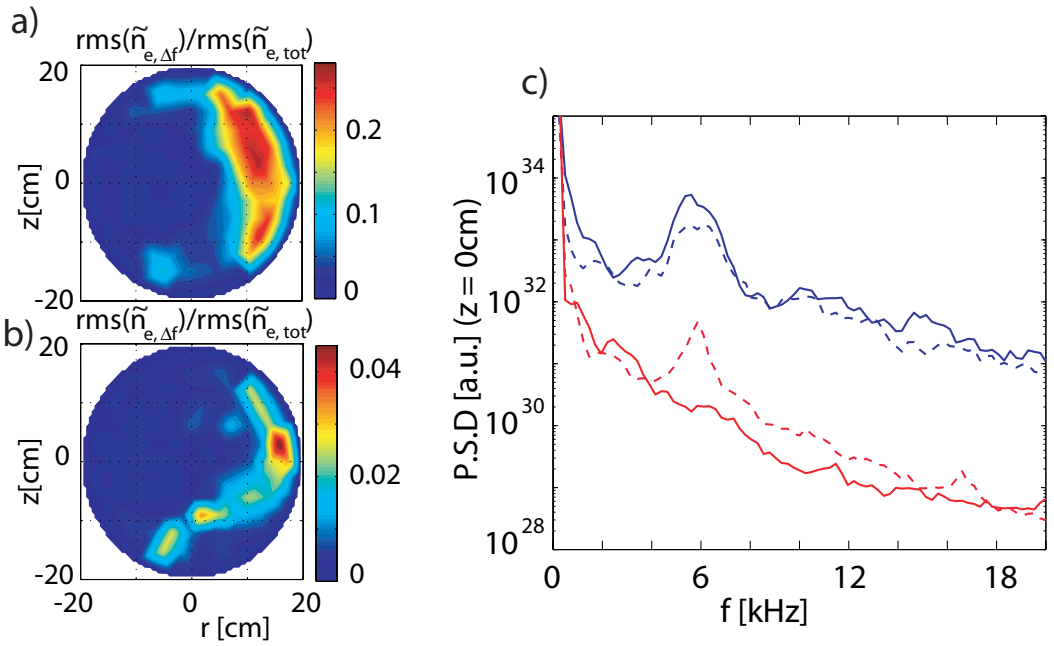

Fig. 2.3.8 *2D profile of the rms $\tilde{n}_e$ in the range Δf=[3.4,8]kHz normalized over the entire spectrum for a) p_n=1.2x10^{-3}mbar and b) pn=1.4x10^{-3}mbar and c) Power spectral densities for Isat measured at r=10.5cm (solid) and r=14cm (dashed) for the lower pressure (blue) and the higher pressure (red).*

2.3.5 Development of a 3D code

In 2009, progress has been made in the development of the code to simulate the TORPEX device and on the interpretation of the simulation results via direct comparisons with experimental results. Focusing on the computational aspect, the study of the two dimensional dynamics has been completed in the course of the year. In 2008, a three-dimensional code had been implemented to follow the TORPEX plasma dynamics. The fluid equations had been first solved in a flux tube geometry that follows the magnetic flux tube that wraps around TORPEX. The analysis of the simulation results has been completed in 2009. The most interesting findings from the three-dimensional flux tube simulation are observed at high parallel resistivity, where a fully three-dimensional plasma dynamics is observed, with the plasma decoupled from the dynamics at the sheath edge (Fig. 2.3.9). The threshold condition to access this new turbulence regime has been evaluated analytically, in good agreement with the simulation results. In 2009, the code development project has been completed with the implementation of a simulation code able to represent the global TORPEX geometry, overcoming the assumptions of the flux-tube geometry. The analysis of the results of this comprehensive code has shown that three turbulent regimes are present in the simulation. The first turbulence regime is dominated by the ideal interchange instability; this was the

turbulent regime studied in the course of the two-dimensional investigations. The second regime is dominated by the resistive interchange mode, which is a global instability driven by curvature and pressure gradient, that requires resistivity. The third turbulence regime, which occurs only for very steep plasma profile, is characterized by the drift wave dynamics. Finally, a specific effort aimed at a better understanding and definition of the plasma boundary conditions at the plasma has been started in the context of a newly launched PhD project.

The second research avenue focused on the comparison between experiment and simulations. TORPEX constitutes the ideal environment to perform a plasma turbulence code validation project: the magnetic geometry is relatively simple and, contrary to typical fusion devices, the diagnostics provide the full picture of the plasma dynamics that can be compared with the simulation results. The validation project started by considering the turbulence regime easier to simulate: the one dominated by interchange dynamics characterized by low confinement properties. For this scenario, a long two-dimensional simulation has been performed to provide the time series and the statics necessary for a quantitative comparison with TORPEX data. The comparison has been performed across a broad range of experimental measurements, starting from the analysis of quantities that are directly measured in TORPEX (e.g., ion saturation measurements), to quantities that require a sophisticated statistical treatment to be obtained from the direct experimental data (e.g., particle flux). For the purpose of code validation, the turbulence analysis techniques that had been developed to study TORPEX plasmas (e.g., structure analysis) have been applied to the simulation data.

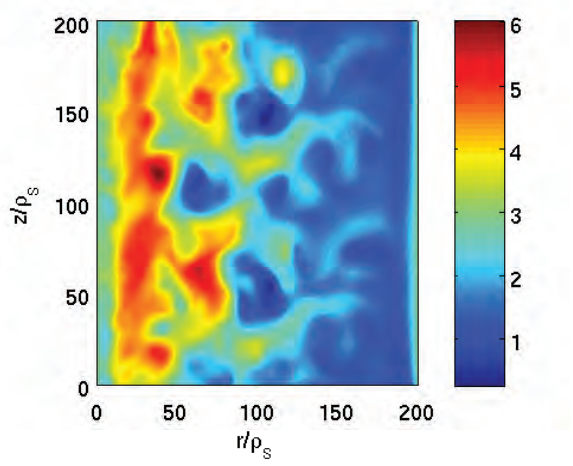

Fig. 2.3.9 *Typical snapshot of the electrostatic potential from the TORPEX global turbulence simulations. The ideal interchange is driving the present simulation, which is characterized by a two returns of the field line in the poloidal plane.*

2.3.6 Technical achievements

Active optical diagnostic for turbulence measurements

So far, turbulence studies in TORPEX have been conducted mainly using Langmuir probes and therefore focusing on the electron behavior, but without information on the ions and their velocity. A significant step forward in diagnosing plasma turbulence is the extension of the passive optical imaging system, described above, towards active optical methods, in particular Laser Induced Fluorescence (LIF). The

Laser Induced Fluorescence (LIF) technique aims at measuring the ion velocity distribution function in the plasma f(v). LIF performs a fully non-perturbative measurement, as the plasma dynamics is totally decoupled from the ion quantum levels. With an efficient LIF system, it will be possible not only to open new areas of research on TORPEX, but also to improve the understanding of phenomena that are already being studied, such as blob creation and propagation mechanisms or the relative importance and the role of instabilities (drift and interchange waves) in different plasma conditions.

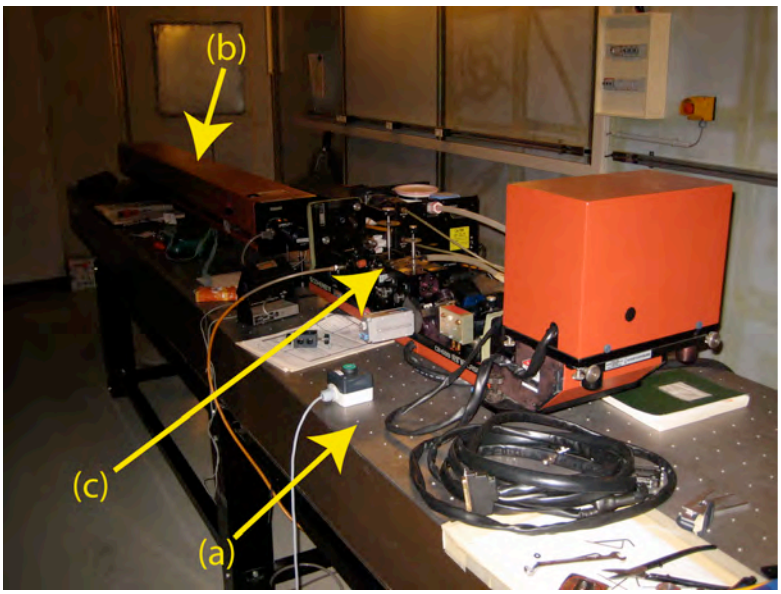

Fig. 2.3.10 *A view of the TORPEX laser system for LIF. Shown are (a) the optical table, (b) the Argon pump laser, and (c) the dye laser.*

In year 2009, we have started the development of the relevant hardware and related infrastructure for LIF (the laser itself, the laser room, the necessary relay optics, etc.). TORPEX is presently equipped with an Argon laser, whose output beam has a wavelength of 514nm and an output power of almost 10W. This laser is used to pump the dye (Rhodamine 6G) of the second laser. This dye laser has a narrow bandwidth, its wavelength output can vary between 550 and 650nm, with a power peak around 580 nm and its output power can reach about 800mW. The present setup is shown in Fig. 2.3.10. In 2009, the safety system for the lasers has been developed. The remote control system is presently under development. The laser injection system, together with the relevant optics, is presently under design. The detection volume is defined by the intersection of the laser beam and the detection area, and should ideally be moveable to cover a large part of the poloidal cross section. For the detection, we will first use a photomultiplier tube, while on the longer term, to complement the LIF system, the fast framing camera and possibly the fast gated intensifier, described above, will be used to detect the fluorescence signal from the plasma.

Larger fast ion source development

TORPEX is presently equipped by a miniaturized Li6+ ion source, which produces fast ions with energies in the range 100eV-1keV. The source is used with a gridded energy analyzer for the study of the interaction of plasma turbulence with supra-thermal ions. In 2009, in the framework of a European collaboration under the auspices of the European Fusion Development Agreement we have developed a

larger version of the Li6+ ion source. The new prototype consists of an Aluminosilicate emitter, encased into a vacuum and plasma safe BN casing, and includes a two-grid system to accelerate the ions. This new source will be soon tested in a plasma environment on TORPEX and, if successful, will be ready to be used on other devices, including in configurations characterized by closed field lines and rotational transform.

2.4 Materials research

The main objective of the Fusion Technology Materials (FTM) group of the CRPP is to investigate the effects of the damage produced by irradiation in a variety of materials, in particular candidate structural materials for plasma facing (first wall, divertor) and breeding blanket components of the future fusion reactors but also pure metals and model alloys. This group is located at the Paul Scherrer Institute (PSI) in Villigen.

The main R&D activities of the FTM group include the development and characterization of advanced metallic materials for fusion power reactors, in particular oxide dispersion strengthened (ODS) reduced activation ferritic (RAF) steels and reduced activation tungsten-base materials, modelling of radiation damage and radiation effects, qualification of metallic materials for the International Thermonuclear Experimental Reactor (ITER), and small specimen test technology for the future International Fusion Materials Irradiation Facility (IFMIF). The scientific approach adopted by the FTM group to understand the fundamentals of radiation damage in metals and alloys is based on investigating the structure/mechanics relationships at different length scales (micro-, meso-, and macroscopical). A range of experimental and numerical tools is used to reach these objectives. For simulating experimentally the effects of 14MeV neutrons, that will be the product, together with 3.5MeV helium nuclei, of the envisaged fusion reactions between deuterium and tritium nuclei, the FTM group is involved in proton/neutron irradiations performed in the target of the Swiss Spallation Neutron Source (SINQ) as well as in neutron irradiations performed in reactors in Belgium, the Netherlands and Hungary.

2.4.1 Emerging technologies

Development of material science and advanced materials for DEMO

Irradiation experiments

The definitive shutdown of the PIREX facility took place on December 22, 2003. Decommissioning of the PIREX facility was started in March 2004 and achieved in September 2006. A number of specimens of various materials have been irradiated in SINQ for two years in 2004-2005. The cooling phase of the specimens took place in 2006. Post-irradiation experiments should be performed in 2009/2010 within the EFDA Task TW6-TTMS-001/D4. A new irradiation campaign was started in April 2007 and achieved in December 2008. The cooling phase of the specimens is in progress.

Development of ODS ferritic steels

Recent activities have been focused on the ODS RAF steel Fe-14Cr-2W-0.3Ti-$0.3Y_2O_3$ (in weight percent), which was prepared by mechanically alloying pre-alloyed Fe-14Cr-2W-0.3Ti powder particles, having a mean size around 50μm, with $0.3Y_2O_3$ powder particles (20-30nm in size), and compacting the mixed powder by hot isostatic pressing (HIPping). Mechanical alloying was performed in an attritor, in a hydrogen atmosphere, at 300rpm for 42 hours. The mixed powder was then canned in a stainless steel container, degassed at temperatures up to 450 C for 24 hours in a vacuum of 10^{-2}mbar, and compacted by HIPping at 1150 C for 4 hours under a pressure of 200MPa. (1) It was attempted to improve the Charpy impact behaviour of the material by applying a variety of thermal-mechanical treatments, such as hot pressing or hot rolling, and heat treatments. Indeed, just after HIPping the material exhibits a very high ductile-to-brittle transition temperature (DBTT) of about 160 C and a low upper shelf energy (USE) of about 3.1J. A much better Charpy impact behaviour, with a DBTT of about 10 C and an USE of about 4.2J, was obtained by compacting the mixed powder by hot extrusion, instead of HIPping, and applying a hot rolling at 700 C (yielding an amount of deformation of about 50%) followed by a heat treatment at 1050 C for 1 hour (Table 2.4.1). (2) An ingot of about 1kg of the Fe-14Cr-2W-0.3Ti-$0.3Y_2O_3$ ODS RAF steel has been manufactured using the procedure described just above. (3) A batch of about 500 grams of the Fe-14Cr-2W-0.3Ti-$0.3Y_2O_3$ ODS RAF steel powder has been prepared from elemental powders and sent to the CEA (France) for compaction by hot extrusion using a cylindrical shape die. (4) Small ingots of the Fe-14Cr-2W-0.3Ti-$0.3Y_2O_3$ ODS RAF steel have been prepared by mechanically alloying Fe, Cr, W and Ti elemental powder particles either with $0.3Y_2O_3$ powder particles or $0.5Fe_2Y$ powder particles and compaction of the mixed powders by HIPping. They have been sent to Oxford University (England) for analysis of the nanoclusters by atom probe tomography and transmission electron microscopy (TEM).

Material	HIPped	HIPped + hot pressed + annealed at 850°C for 1 hour	HIPped + hot rolled + annealed at 850°C for 1 hour	Hot extruded + hot rolled + annealed at 1050°C for 1 hour
DBTT [°C]	160	63	63	10
USE [J]	3.1	4.5	2.8	4.2

Table 2.4.1 *Effects of various thermal-mechanical treatments on the Charpy impact behaviour of the Fe-14Cr-2W-0.3Ti-$0.3Y_2O_3$ ODS RAF steel prepared using a pre-alloyed powder.*

Development of tungsten-base materials

Recent activities have been focused on the development of W-$2Y_2O_3$ and W-2Y materials and W-(0.3-0.9-1.7)TiC materials (in weight percent) by dry mechanical alloying and hot isostatic pressing (HIPping) with the aim of obtaining materials with improved properties with respect to those prepared by dry mechanical alloying and sintering. On the one hand, elemental powder particles of pure W (99.9%), with sizes in the range of 1-5μm, were mechanically alloyed either with pure 2Y (99.99%) powder particles, with sizes below 40μm, or with $2Y_2O_3$ particles with sizes in the range of 20-40nm. Mechanical alloying was performed in a planetary ball mill at 350rpm for 15 hours in an argon atmosphere. The mixed powders were then canned in stainless steel containers, degassed at temperatures up to 450 C for 24 hours in a vacuum of 10^{-5}mbar, and compacted by HIPping at 1300 C for 3 hours under a pressure of 200MPa. Much higher density values of 97.4 and 97.5% were obtained by compacting the W-$2Y_2O_3$ and W-2Y materials by HIPping,

instead of sintering, respectively. The microhardness of W-2Y_2O_3 and W-2Y materials was found equal to 1460$HV_{0.2}$ and 1800$HV_{0.2}$, respectively. Microstructural investigation of the W-2Y material showed that it contains Y_2O_3 particles that form during HIPping, have various shapes and are located at the grain boundaries and inside the grains. The mean grain size is equal to about 30nm and the mean particle size to about 2-3nm. Residual porosity was also observed. On the other hand, elemental powder particles of pure W (99.9%), with sizes in the range of 1-5μm, were first mixed and secondly mechanically alloyed with pure (0.3-0.9-1.7)TiC (99.5%) powder particles with a size of about 40nm. Mixing was performed in a planetary ball mill at 150rpm for 1 hour in an argon atmosphere, while mechanical alloying was performed in the same planetary ball mill at 300rpm for 10 hours in an argon atmosphere. The mixed powders were then canned in stainless steel containers, degassed at temperatures up to 750 C for 24 hours in a vacuum of 10^{-5}mbar, and compacted by HIPping at 1350 C for 3 hours under a pressure of 200MPa. Some powders were also submitted to a 2nd HIPping at 1500 C for 3 hours under a pressure of 200MPa. The density (Fig. 2.4.1) and microhardness of the W-TiC materials were observed to increase with the TiC content. It was also observed that the 2nd HIPping yields a slight increase in the density of the W-TiC materials (Fig. 2.4.1) and a slight decrease of the microhardness. However, as it also yields an increase in the grain size, due to the higher HIPping temperature being used, it should be avoided. The maximum density was found equal to 95% for W-1.7TiC after the 2nd HIPping, while the maximum microhardness was found equal to 1203$HV_{0.2}$ for W-1.7TiC after the 1st HIPping. Microstructural investigation of the W-(0.9-1.7)TiC materials revealed the presence of a bimodal grain size distribution in all the materials, before and after the 2nd HIPping, with mean grain sizes in the range of 30-60nm and 145-170nm. Residual porosity was also observed.

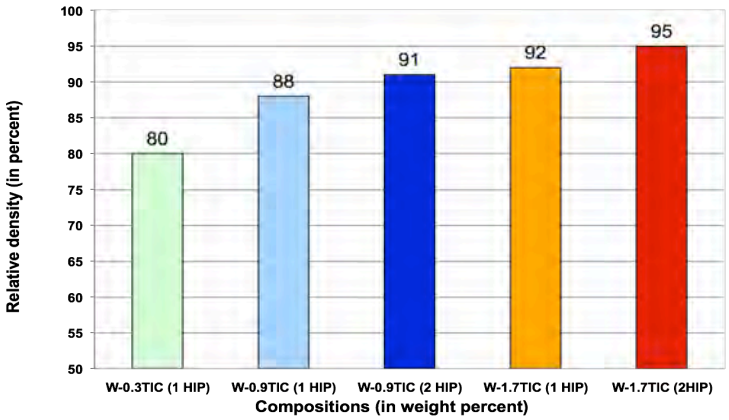

Fig. 2.4.1 *Relative density of the various W-TiC compacted materials, as measured after the 1st and 2nd HIPping experiments.*

Pure tungsten and tungsten-base materials exhibit a low ductility and a low fracture toughness at all temperatures associated with a high DBTT value. This is due to the fact that the plasticity of body centred cubic (bcc) metals is governed at low and intermediate temperatures by the mobility of the screw ½a_o<111> dislocations. Indeed, the non-planar core structure of screw dislocations, as opposed to the planar core configuration of edge dislocations, makes them difficult to move in the lattice without costly (in terms of energy) constriction onto one of the {110} glide planes. It has been postulated long ago and confirmed later by molecular dynamics (MD) simulations that the core should have a 3-fold symmetry, developing onto three conjugate {110} planes around the <111> dislocation line. This development might lead to either a symmetrical configuration, giving rise to a 6-fold

symmetry, or to a degenerate configuration, which is asymmetrical. In addition, depending on the exact location of the dislocation in the lattice, it is either relatively easy or hard to move it with an external shear stress, thus resulting in the naming of easy core or hard core, respectively. This is critical to understand hardening due to irradiation-induced damage, as dislocations progress only when their screw parts can start to move. However, there are still only a few experimental TEM observations supporting these theoretical descriptions. Therefore, the possibility to distinguish by TEM the various screw dislocation cores in tungsten was explored. Figure 2.4.2 shows four possible screw dislocation cores. Corresponding TEM image simulations revealed that in bright field TEM imaging mode the symmetrical core can be distinguished from the asymmetrical one.

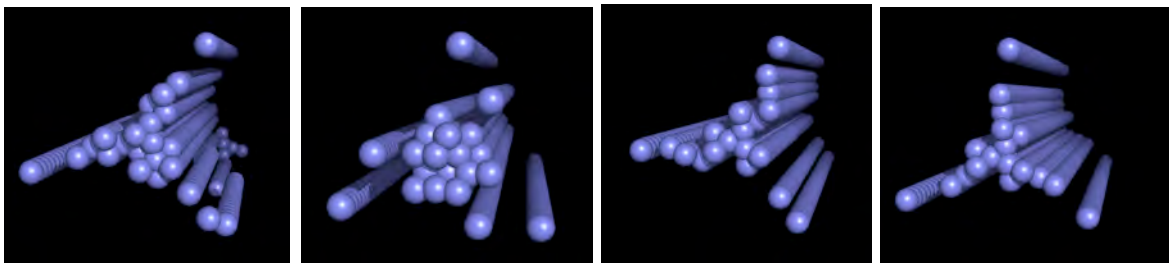

Fig. 2.4.2 *Atomistic description of possible screw dislocation cores, viewed end-on, in tungsten. From left to right: easy symmetrical, easy degenerate, hard symmetrical and hard degenerate configurations.*

Materials modelling

Assessment of plasticity mechanisms in Fe and Fe-Cr alloys

The complexity of the structure of Reduced Activation Ferritic-Martensitic (RAFM) steels limits the identification of the microscopic phenomena underlying their mechanical properties using e.g. multiscale simulation methods. Hence, many simulation works are focused on the base phases of these materials, such as pure Fe and Fe-Cr alloys. Although the presence of Cr in these materials reduces swelling and creep due to irradiation, it results in hardening and loss of ductility. Simulation works have however shown that in the collisional stage of the atomic displacement cascade the influence of Cr is insignificant. Then, in the post-cascade stage, the Cr atoms in interstitial positions, in the form of single interstitials or clusters, lead to a local increase in the average composition of the alloy. The Cr atoms in substitutional positions may also segregate in the form of α' phase as a result from ageing at high temperatures. All these can lead to the formation of Cr clusters and precipitates with various Fe/Cr ratios, which can act as obstacles to moving dislocations. It results in a degradation of the mechanical properties, whose extent has never been quantified. Therefore, this work was aimed at performing Molecular Dynamics (MD) simulations of an edge dislocation moving towards a Cr precipitate using the MOLDY code. The MD sample consisted of a $14\times25\times20nm^3$ simulation box containing an edge ½ a<111>{110} dislocation in the <112> direction and a 2nm Cr precipitate located in the dislocation slip plane, 7nm away from the dislocation. The Cr/Fe ratio in the Cr precipitate was 0.2, 0.4, 0.6, 0.8 or 1.0. Periodic boundary conditions were applied along the dislocation line and dislocation glide directions. In order to model the deformation mode the shear stress resulting from an applied imposed strain rate was calculated at each time step of one femtosecond from the internal force of atoms in the upper region of the sample. The strain rates used for the calculations were 10^6, 10^7 and $3\times10^7 s^{-1}$. An

annealing was performed for two picoseconds prior to the straining, in order to stabilize the temperature. Three interatomic potentials, namely the Ackland et al. potential (2004) for the Fe-Fe interactions and the Olsson et al. potentials (2005) for the Fe-Cr and Cr-Cr interactions, were used. The stress-strain responses of the interaction between the edge dislocation and a 1.0Cr/Fe ratio precipitate at different temperatures are plotted in Fig. 2.4.3(a). It shows that a temperature rise softens the dislocation-Cr precipitate interaction, a trend that was also observed in simulations of the interaction of an edge dislocation with a 2nm void or a 2nm He bubble. Close views of the dislocation-Cr precipitate interaction and the dislocation-void interaction are shown in Figs. 2.4.3(b-c) and 2.4.3(d-e), respectively. It can be seen that there is some repulsion between the edge dislocation and the Cr precipitate. The central segment of the dislocation is thus the last part penetrating into the Cr precipitate. In the case of the void, conversely, there is a strong attraction of the edge dislocation by the void and the central part of the dislocation sinks into the void with a strong drop in stress. This is explained by the fact that any surface or interface in materials responds to the close proximity of a dislocation by a so-called image force, describing the fact that this force is equivalent to the presence of a mirror dislocation of opposite sign on the other side of the surface or interface. In particular, when an edge dislocation moves towards a second phase with a larger elastic modulus than the one of the matrix, the image force is repulsive. This is what happens in the case of a Cr precipitate in a matrix made of Fe, as the shear modulus of Fe is 76GPa and the one of Cr is 136GPa for the selected interatomic potentials. On the contrary, when an edge dislocation moves towards a second phase with a lower elastic modulus than the one of the matrix or towards a free surface, the image force is attractive, as what was observed in the case of the dislocation-void interaction.

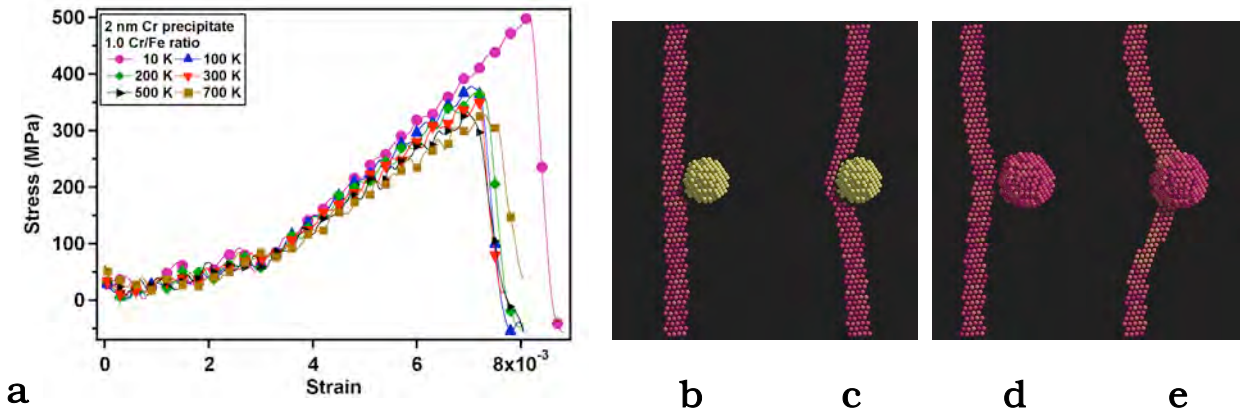

Fig. 2.4.3 *(a) Stress-strain response of the interaction between an edge $1/2a_o$<111> dislocation in pure Fe and a 2nm Cr precipitate with a 1.0Cr/Fe ratio. Interaction of the moving edge dislocation with (b, c) a 2nm Cr precipitate with a 1.0Cr/Fe ratio, and (d, e) a 2nm void, showing repulsion and attraction between them, respectively, due to the elastic constants mismatch between the two phases.*

JANNuS: Ion implantation induced damage effect in Fe and Fe-Cr alloys

Single beam irradiation/implantation experiments were conducted in the JANNuS facility on specimens of ultra high purity (UHP) Fe, Fe-5Cr, Fe-10Cr and Fe-14Cr, at room temperature and liquid Nitrogen temperature to 1dpa. In addition, a dual beam (Fe+He) experiment, first of its kind in the world, was performed on UHP Fe specimens at room temperature. The experiment was successful and showed that the presence of helium dramatically increases the density of irradiation-induced

dislocation loops (Fig. 2.4.4). This indicates that helium stabilizes the self-interstitial atoms, thus providing indirectly more vacancies for cavity nucleation, so validating the results of previous modelling activities.

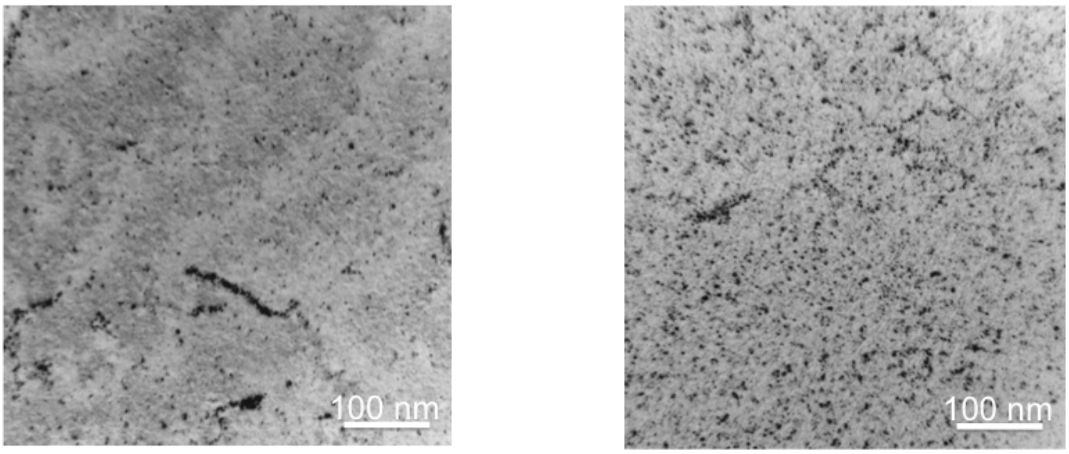

Fig. 2.4.4 *TEM images of the microstructure of UHP Fe irradiated/implanted with (left) 500keV Fe ions to 1dpa at room temperature, and (right) 500keV Fe ions to 1dpa and 10keV He ions to 0.1at.%He at room temperature.*

2.4.2 EFDA Technology Tasks

Tasks Long Term

TW2-TTMS-004b deliverable 3 : Development and testing of coatings to improve the corrosion resistance vs Pb17Li at T>450 C

Corrosion experiments of the reduced activation ferritic/martensitic (RAFM) steel EUROFER with W and Cr coatings have been pursued up to exposure times of 10'000 hours. Up to this exposure time, the thickness of Physical Vapor Depositions (PVD) W coatings was found more or less unchanged. This confirms our earlier finding that PVD-W coatings seem to offer a much better barrier protection against corrosion by flowing Pb-17Li at 550 C than Galvanic (GAL)-Cr and Plasma Spraying (PS)-W coatings (Fig. 2.4.5).

The corrosion rate measured for bare EUROFER 97 specimens seems to correlate quite well with the value of 27μm/year calculated for a Pb-17Li flow rate of 1cm/s from the corrosion rate of 400μm/year that was measured for bare EUROFER 97 specimens exposed to Pb-17Li flowing at 550 C and 22cm/s in the PICOLO loop [W. Krauss et al., Final report on the EFDA task TW6-TTMS-003/D03, (2008)]. The final report has been issued in August 2009.

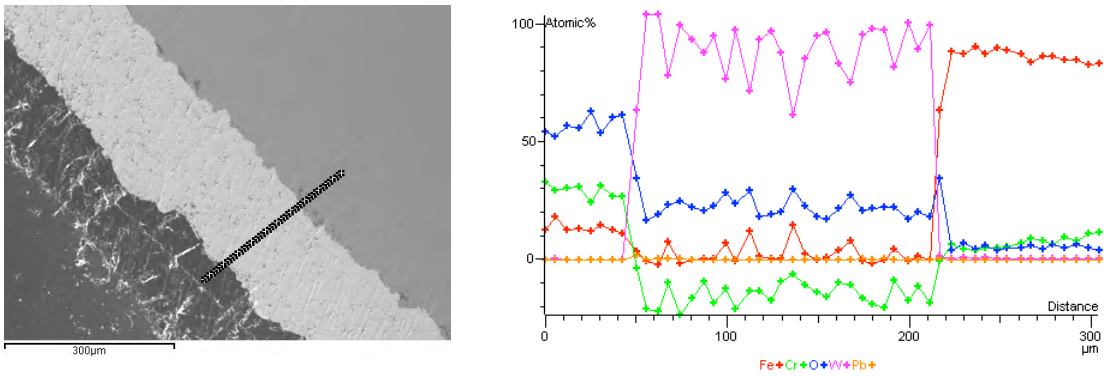

Fig. 2.4.5 *(Left) Scanning electron microscopy (SEM) image of a PS-W specimen, exposed to PbLi flowing at 550 C and 1cm/s for 10'000 hours, and (right) corresponding line scan chemical analysis. The substrate is located on the right-side hand in both pictures.*

TW3-TTMS-005 deliverable 2 : Investigation of irradiated fracture mechanics samples by indentation/punch tests

This Task has been re-defined in 2008 in agreement with the F4E Leadership. It was previously entitled: 'Investigation (tensile and Charpy testing) of PHT and PWHT to improve the design limits and to define the acceptable temperature range'. Ball and Vickers microhardness tests were carried out on undeformed and pre-deformed specimens of the EUROFER 97 RAFM steel. In the latter case, standard tensile specimens were deformed up to various plastic deformation levels. Then, they were sectioned perpendicularly to the deformation axis and the surfaces were well polished and readied for micro-indentation tests. Finite element simulations of ball microhardness tests were also performed using the constitutive behaviour of the pre-deformed material. The finite element and mechanical test results are currently being analyzed in a self-consistent manner in order to extract reliable information on the respective effects of the yield stress level and strain-hardening capacity from the shape of the indentation curves.

TW5-TTMS-005/D10 : Support in development of design rules for structural materials with low ductility

Compression test experiments were performed on specimens of Fe-Cr model alloys and of two types of RAFM steels, namely T91 and EUROFER 97. The compression tests were carried out at room temperature on small cylinders, 3mm in diameter and 5.5mm in length. Four model alloys with different Cr contents, ranging from 2.36 to 11.62wt.%, were investigated. Some specimens were irradiated in the BR2 reactor at SCK-CEN (Belgium) at 300 C to 0.6dpa. The plastic flow properties, represented by the true stress-strain curves, were determined for both unirradiated and irradiated specimens. The radiation hardening determined from the compression tests was found to be in good agreement with previous data obtained from tensile tests. The strain-hardening capacity after irradiation of all materials was found to be positive, in other words, the flow stress was found to increase with strain beyond the yield stress. However, for all the irradiated materials the strain-hardening rate was found to be lower than that of the unirradiated materials. No strong effect of the Cr content on the radiation hardening of the model alloys was evidenced, but just a relatively shallow minimum around 8-9wt.%. Finite element

simulations of small ball punch tests were used to assess the plastic flow properties of RAFM steels. In the past, a calibration between the yield load derived from the ball punch force-deflection curve and the yield stress derived from the tensile tests was established. However, this calibration suffers from the drawback of being, to some extent, dependent on the post-yield behaviour. Since the post-yield behaviour of the irradiated materials is in principle not known, this induces uncertainty in the assessment of the radiation hardening. Based on a careful analysis of the punch test deformation behaviour, using well validated finite element simulations, a new parameter was then proposed, which correlates with the yield stress and was shown to be much less dependent on the post-yield behaviour, being thus more suited for post-irradiation examination studies. A very good estimation of the strain-hardening capacity of the materials after irradiation could also be done in considering the slope of the ball punch curves at a deflection larger than 0.2mm.

TW6-TTMS-001/D4 : PIE SINQ irradiation

The irradiation rig containing specimens of the EUROFER 97 RAFM steel and the ODS EUROFER material, which had been irradiated in the SINQ facility in 2004/2005, has been transported to the Hot Laboratory of the PSI in Spring 2007. Unfortunately, due to a lack of technical manpower at the PSI, the irradiated specimens have been extracted from the rig only in spring 2008. Depending on the availability of the hot cells at the PSI, Charpy impact testing of irradiated specimens should be performed at the end of 2009, while tensile testing and TEM observations of irradiated specimens should be performed in 2010.

TW6-TTMA-002/D10 : Development of W-TiC and W-Y_2O_3 alloys

W-(0.3-1.0-2.0)Y_2O_3 and W-(0.3-1.0-2.0)Y materials (in weight percent) have been manufactured by conventional powder metallurgy methods including dry mechanical alloying of pure W (99.9%) powder particles, with sizes in the range of 1-5μm, either with pure (0.3-1.0-2.0)Y (99.99%) powder particles, with sizes below 40μm, or with (0.3-1.0-2.0)Y_2O_3 powder particles with sizes in the range of 20-40nm. Mechanical alloying was performed in a planetary ball mill, in an argon atmosphere, using a jar and grinding media made of WC-Co and a ball-to-powder ratio of 10:1. Powders were first mixed for 1 hour using a speed of 150rpm. The mixed powders were then mechanically alloyed for various times up to 30 hours using a speed of 350rpm. The powders were cold compacted in air using a pressure in the range of 150-250MPa. Then, the green compacts were sintered either in a vacuum of 10^{-3}mbar or in an argon atmosphere, by applying a heating rate of 300 C/h followed by an isothermal annealing at 1800 C for 4 hours, and using finally a cooling rate of 500 C/h. Some of the specimens were sintered for a second time at 2000 C instead of 1800 C. The mechanical alloying time was optimized by means of X-ray diffractometry and SEM analyses of the particles. It was found that it should not exceed 15 hours, in order to obtain small and homogeneous particle sizes and crystallite sizes and to avoid important oxygen contamination as well as contamination by the jar and the balls, leading to the formation of WC impurities. The density and microhardness of the sintered specimens were found to increase with the Y_2O_3 or Y content. The highest density of about 88% was obtained for the W-2Y material, while the highest microhardness of 1790$HV_{0.2}$ was measured for the W-2Y_2O_3 material. Scanning Electron Microscope (SEM) observations revealed that sintering occurred, at least partially, from the liquid phase, the amount of the corresponding dense regions increasing with the Y_2O_3 or Y content (Fig. 2.4.6).

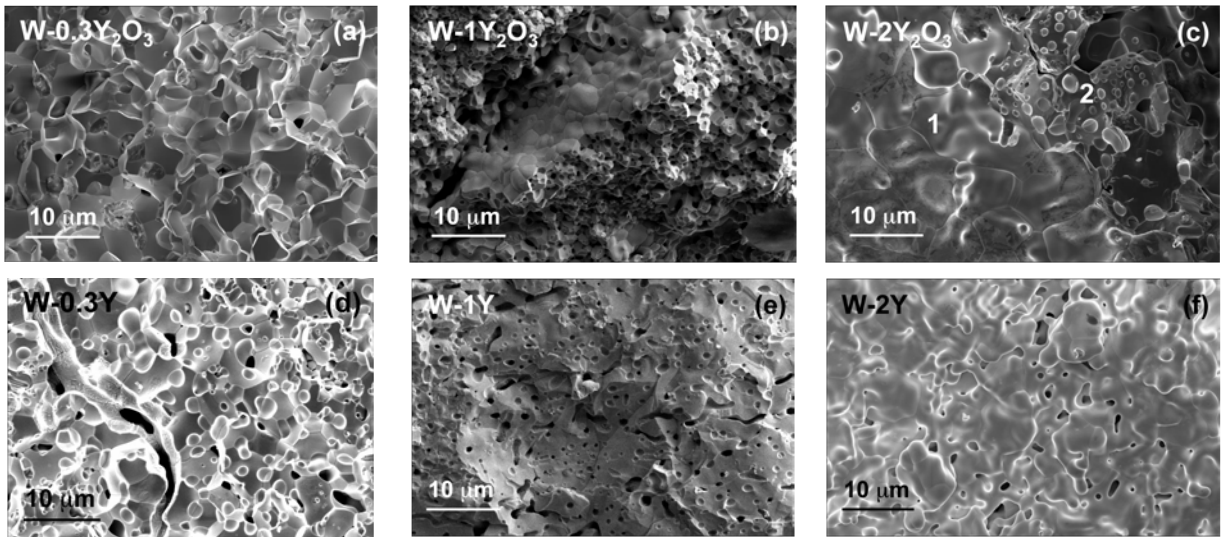

Fig. 2.4.6 *Secondary electron SEM images of the microstructure of the a) W-0.3Y_2O_3 , b) W-1Y, c) W-2Y_2O_3, d) W-0.3Y, (e) W-1Y, and (f) W-2Y materials sintered at 1800 C in vacuum. Area 1 refers to a region of the material that was successfully sintered from the liquid phase, while area 2 refers to a region that was not successfully sintered and remained porous.*

Tasks Next Step

TW4-TVM-CUSSPIT : Testing of irradiated CuCrZr/SS joints produced under different blanket manufacturing conditions

CuCrZr/SS joints, where CuCrZr refers to a precipitation strengthened Cu-base alloy and SS to the 316LN austenitic stainless steel, are part of the current ITER design. Their final applicability in ITER will depend on their mechanical properties before and after neutron irradiation, with respect to those of the base materials. This work is aimed at investigating the effects of two different heat treatments on the mechanical properties (joint strength, fracture toughness) of unirradiated and neutron-irradiated CuCrZr/SS joints and base materials. The work is being performed by three partners: SCK-CEN (Belgium) is responsible for the neutron irradiations, VTT Manufacturing Technology (Finland) is in charge of testing the joints, and CRPP is in charge of measuring the fracture toughness of the CuCrZr base material. Two series of six specimens of the CuCrZr base material, having withstood two different heat treatments, have been irradiated with neutrons at SCK/CEN to three different doses of 0.001, 0.01 and 0.1dpa. The irradiated specimens have been then delivered to Risøe National Laboratory (Denmark). In a further step, they were unfortunately shipped by error to the VTT laboratories in Finland. They were finally shipped from Finland to the PSI in September 2008. The specimens will be tested at the end of 2009 by means of Charpy impact tests.

*2.4.3 Broader approach activities**

IFMIF-EVEDA: Design of a test module for in-situ creep-fatigue tests to be performed in the IFMIF facility and construction of a mock-up of the test module

The creep-fatigue test module (CFTM) for IFMIF will consist of three testing machines deforming independently a creep-fatigue specimen. A preliminary design of the whole CFTM has been made as well as a detailed design of a single deformation machine (Fig. 2.4.7). The specimen will be part of an elongated assembly made of two bars in which a helium coolant will flow. The specimen will constitute the central part of it and the bars will serve as loading elements and pipes for cooling the specimen. The heat will be deposited by gamma heating. Sleeves of tungsten will be inserted close to the specimen and serve to generate the required power. The temperature control will be achieved in varying the helium mass flow. First results of thermo-dynamical calculations showed that it should be possible to reach specimen temperatures as high as 470 C in decreasing the helium flow rate to 0.08g/s. This should be enough to cope with accelerator power shutdowns lasting up to about 10 minutes.

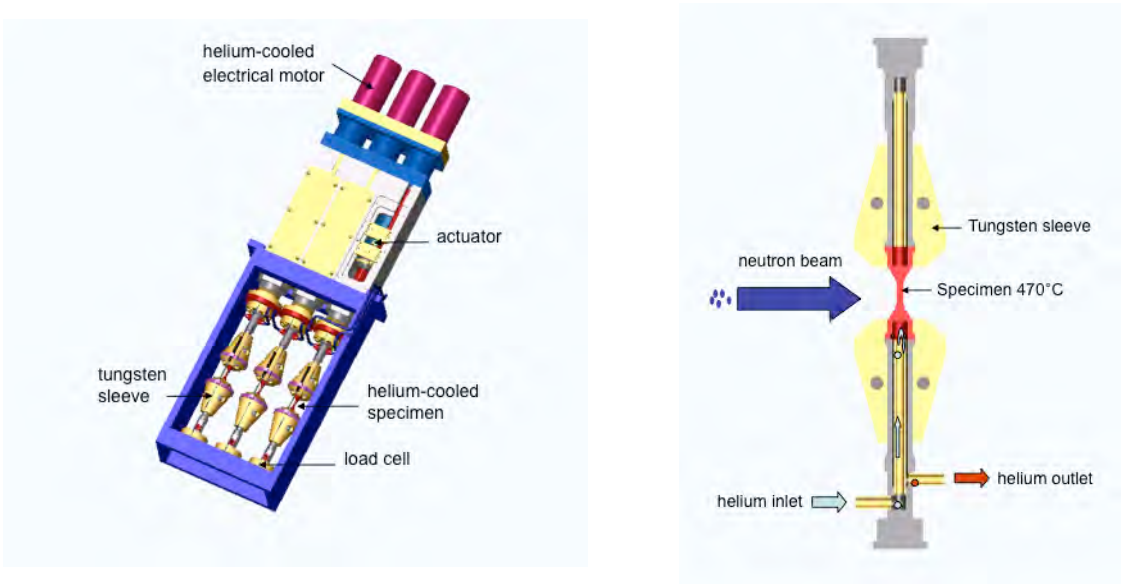

Fig. 2.4.7 *(Left) Preliminary design of the whole CFTM for IFMIF. (Right) Schematics of the central part of a single deformation machine.*

IFERC: Contribution to the definition of irradiation matrices for IFMIF by means of development of new methods for testing and analysing subsized specimens

Recent activities were focused on characterizing a so-called 'degraded' (cold rolled) plate of the EUROFER 97 RAFM steel, from which the evolution of the fracture properties are going to be evaluated. Before preparing fracture specimens from the cold-rolled plate, it is necessary to know precisely the work-hardened state of the plate. Therefore, Vickers microhardness tests were first carried out at different locations inside the plate, in order to estimate the amount of cold working and to

* Work not belonging to the EURATOM Association's work programme.

evaluate the homogeneity of the deformation induced by cold working. From the microhardness data one estimated to have pre-deformed the plate by a few percents of equivalent plastic strain. Micro-pillars were machined from the as-received plate using the focused ion beam technique and tested using a flat indenter mounted on a microindenter, in order to better assess the plastic flow properties of the degraded plate. Two types of micro-pillars were prepared, namely parallelepiped and cylindrical ones, as shown in Fig. 2.4.8. Some true stress-strain curves obtained with those micro-pillars are plotted in Fig. 2.4.9 along with a reference tensile curve of the EUROFER 97 RAFM steel in the as-received condition. Despite some discrepancies between the curves of the micro-pillars, intrinsic to this type of ultra small specimens, the results are quite representative of the plastic flow curve determined with standard tensile specimens. Micro-pillars are currently being machined from the degraded plate using the focused ion beam technique.

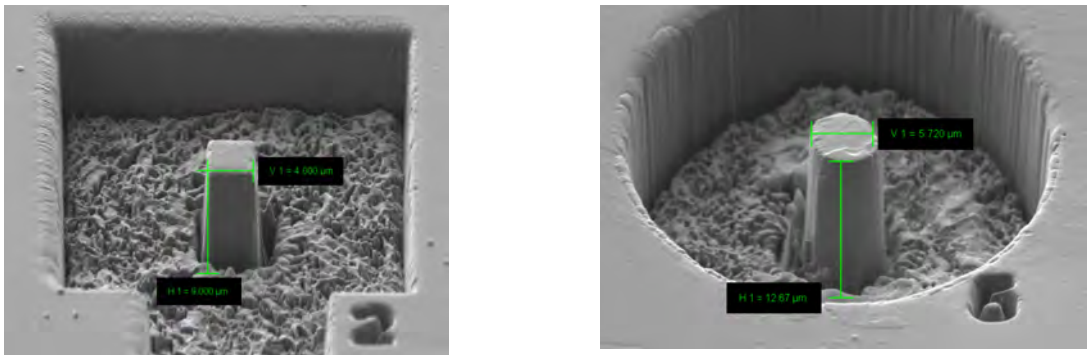

Fig. 2.4.8 *Two types of micro-pillars prepared from the EUROFER 97 RAFM steel.*

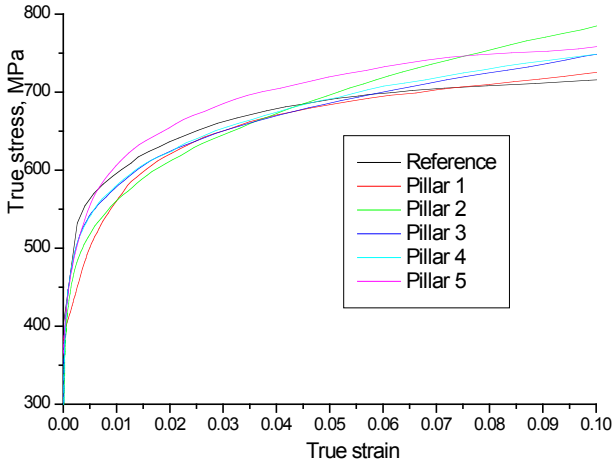

Fig. 2.4.9 *True stress-strain curves obtained for the EUROFER 97 RAFM steel using either micro-pillars or a standard tensile specimen.*

2.4.4 Supporting research

Modelling of the fracture toughness-temperature curve of the EUROFER 97 RAFM steel in the ductile-to-brittle transition region

Fractographic observations were performed on compact tension (C(T)) specimens of the F82H and EUROFER 97 RAFM steels at various temperatures, namely -196 C, -100 C and -120 C. The goal was to check whether crack initiators could be

identified on fracture surfaces. At -196 C fracture surfaces of both steels were found to exhibit typical quasi-cleavage features of RAFM steels, i.e., small facets linked by tear ridges. While not quantified in detail, the size of the small facets appears smaller in EUROFER 97, of the order of 1-3μm, than in F82H where many facets larger than 10μm were observed. We recall here that the prior austenite grain (PAG) size is about 10μm in EUROFER 97 and 80μm in F82H. As a consequence, the lath packs and lath blocks are also smaller in EUROFER 97 than in F82H, leading to corresponding smaller facets. However, the fracture toughness difference between the two steels at -196 C is about 25MPa, indicating that neither the PAG size nor the lath size seems to play a role in the macroscopic toughness. In order to identify the crack initiators in EUROFER 97, observations were performed on both C(T) and notched tensile specimens, as shown in Fig. 2.4.10. On the left hand side of Fig. 2.4.10 (left), the red star corresponds to the convergence point of the river pattern, which indicates the initiation point of the macro-crack. Note that the red star is located within the so-called process zone, where the stress reaches a maximum very close to the crack tip. On the right hand side of Fig. 2.4.10 (left), a close-up view of the areas under the red star is shown. However, no specific features, such as broken carbides or some decohesion between an inclusion and the matrix could be identified in these areas. In the case of the notched tensile specimen, as shown in Fig. 2.4.10 (right), the fracture seems to have been initiated in the large hole observed in the middle of the specimen, which is the position of the maximum stress. Even though the initiators could not be identified, an estimate of the size of the unstable micro-crack was done, based upon a nominal critical fracture stress of 2000MPa (calibrated previously within the framework of a local approach for cleavage fracture). It was found that the micro-crack length must be of the order of 0.5μm to 2μm to be consistent with the critical fracture stress.

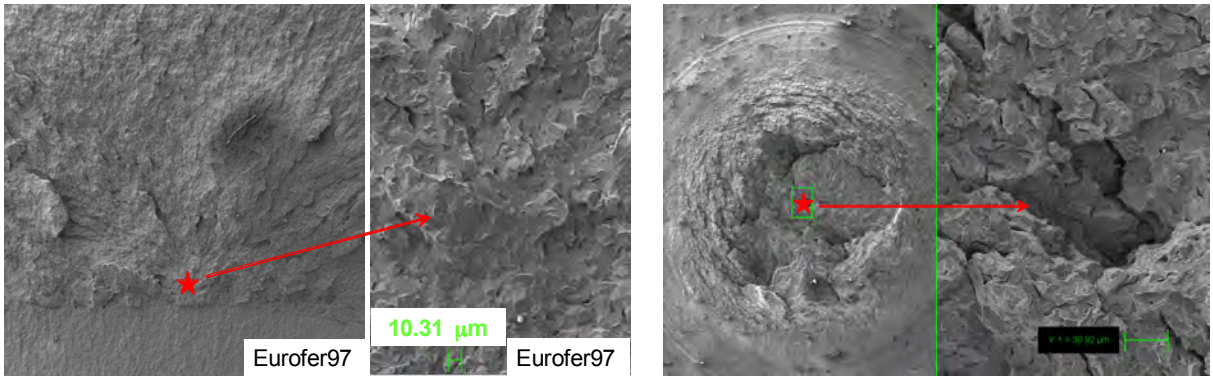

Fig. 2.4.10 *Fracture surfaces of (left) a C(T) specimen of EUROFER 97 tested at -100 C, and (right) a notched tensile specimen of EUROFER 97 tested at -100 C.*

2.5 Superconductivity

The activities of the Superconductivity section have expanded in the last period. SULTAN has been busy with the test of ITER and JT60 conductor samples. The R&D activities includes thermal-hydraulics experiment and code, joints development, feeder design, ac loss, inter-strand resistance and, outside Fusion, design studies with ESRF (Grenoble) and HZB (Berlin).

The preparation work for the European Dipole (EDIPO) test facility at CRPP has progressed in 2009 with procurement of large items, refurbishment work in the hall and pre-assembly activities. The delivery of the main dipole winding from F4E has

been once more delayed. The overall schedule of the EDIPO project has been updated with deadline for commissioning in 2011.

ITER studies are reported in Chapter 4, section 4.5 and technical developments in Chapter 3, Section 3.6.

2.5.1 Testing of prototype conductors for JT-60SA

Two samples with prototype conductors for JT-60SA Tokakmak were tested in SULTAN test facility. The samples are “hair pin” type, i.e. there was no bottom joint.

The Helium pressure drop was measured in the samples by means of capillary over a distance of 2 m. The helium flow was closed first in both legs, and the outlet valve of the right leg was open in steps. Each step was held for a few minutes till a steady state of pressure and Helium mass flow rate was reached (Fig. 2.5.1, left).

Stability runs were performed after electromagnetic cycling loading at the end of test campaign. The capacitor bank with 10 connected capacitors produced half-sinusoidal pulses with 130 ms duration. The test was performed at various combinations of the SULTAN background field and set temperatures of the sample (Fig. 2.5.1, right).

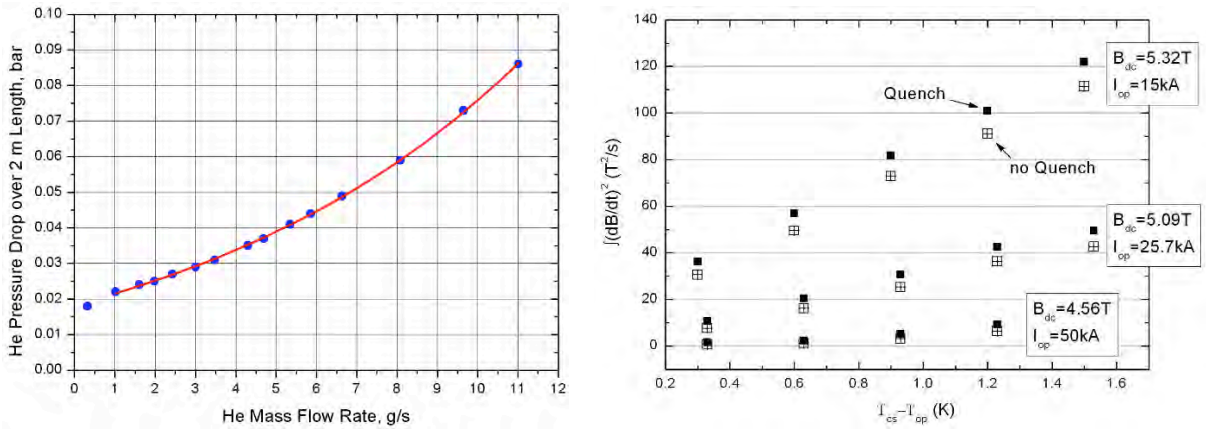

Fig. 2.5.1 *Results of the pressure drop measurement (left) and stability test (right)*

The ENEA JT-60 sample with NbTi conductor was manufactured and instrumented at CRPP. This sample was tested for pressure drop, DC performance, AC loss and stability.

The DC tests consisted mainly of the T_{cs} (current-sharing temperature) runs, and a few I_c (critical current) runs were performed. The T_{cs} runs were performed at various combinations of SULTAN background field (from 4T to 6.5T) and conductor operating current (from 17kA to 30kA). Also, the influence of field gradient on conductor performance was studied. Upon the DC tests the electromagnetic cycling loading was applied at 7.5T background field and 17.5kA operating current (170 cycles), and the T_{cs} run at 5.09T and 25.7kA current was repeated to check a change of conductor performance (Fig. 2.5.2, left).

AC-loss measurements were performed prior any electromagnetic load and after DC measurements and electromagnetic cycling. The AC-loss measurement was

performed without transport current and with transport current of 25.7kA as well. After electromagnetic cycling, both conductors showed practically identical AC losses independently of transport current at frequencies below 0.3Hz (Fig. 2.5.2, right).

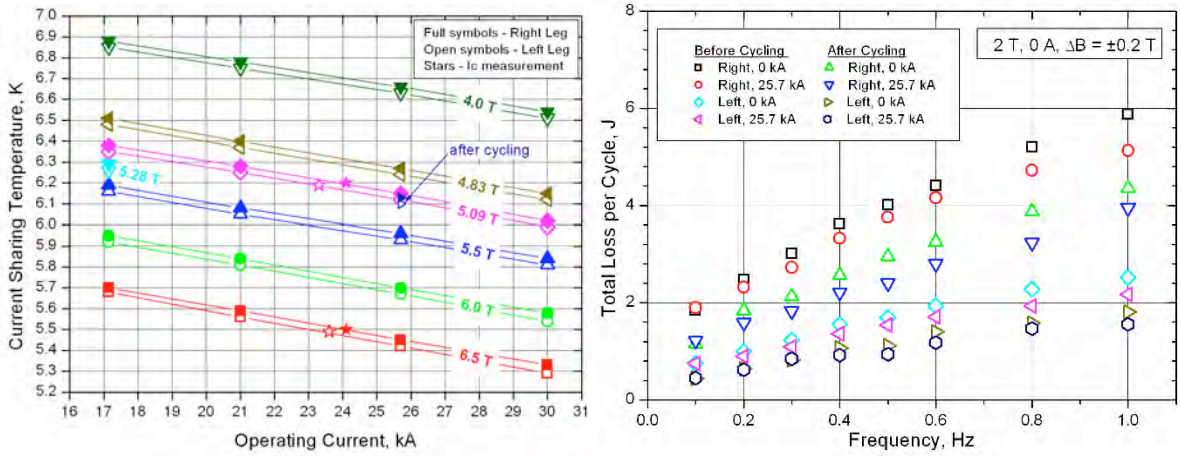

Fig. 2.5.2 *Results of the DC tests (left) and AC loss measurements (right)*

The CEA JT-60 sample (TFJS1) with NbTi conductor was manufactured and instrumented at CEA, the bottom joint (prototype) provided an electrical connection between square (right leg) and round (left leg) shaped conductors. This sample was tested for DC performance, AC loss and stability.

The DC tests consisted mainly of the T_{cs} runs, and a few I_c runs were performed. The T_{cs} runs were conducted at various combinations of SULTAN background field and conductor operating current (Fig. 2.5.3, left). Upon the DC tests the electromagnetic cycling loading was applied at 8T background field and 17kA operating current (200 cycles), and some points of T_{cs} and I_c runs were checked for a change of conductor performance. No change of conductor performance was observed after cycling loading.

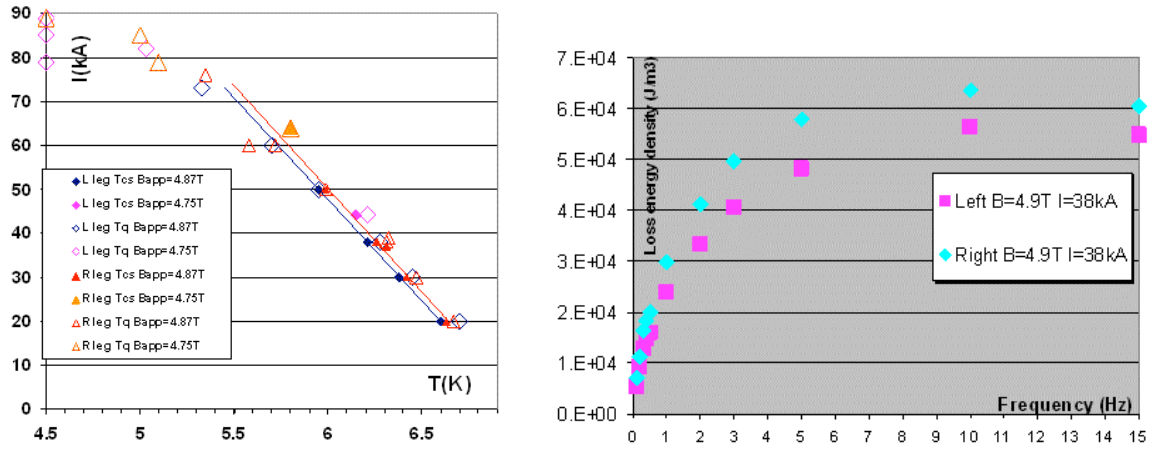

Fig. 2.5.3 *Results of the DC tests (left) and final AC loss measurements (right)*

AC-loss measurements were performed prior any electromagnetic load and after DC measurements and electromagnetic cycling in wide range of pulsing field frequencies (0.05 – 15Hz). The AC-loss measurement was performed with and

without transport current at 0T field, and they were repeated with transport current of 38kA and field of 4.9T as well. The two conductors showed the difference in AC losses due to the different shape of the conductors (Fig. 2.5.3 right).

Stability runs were performed before electromagnetic cycling loading and some points were checked at the end of test campaign. The capacitor bank with 10 connected capacitors produced the full-sinusoidal pulse with 130ms duration. The test was performed at various combinations of the SULTAN background field, transport current and set temperatures of the sample.

The EDIPO joint sample was designed, fabricated and tested at CRPP. Fig. 2.5.4 shows the layout of the sample with its instrumentation.

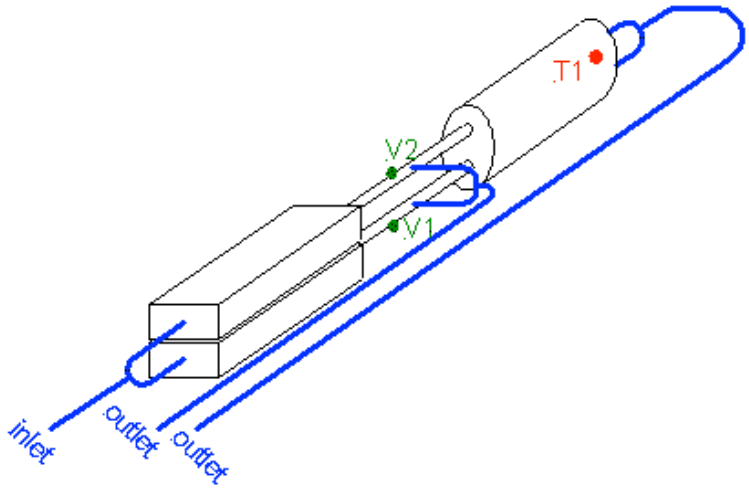

Fig. 2.5.4 *Layout of the EDIPO joint sample and its instrumentation*

The EDIPO joint sample was tested for pressure drop, resistance measurement at various currents and for heating of the joint with active and passive cooling modes. The results of pressure drop measurements are is shown in Fig. 2.5.5 left.

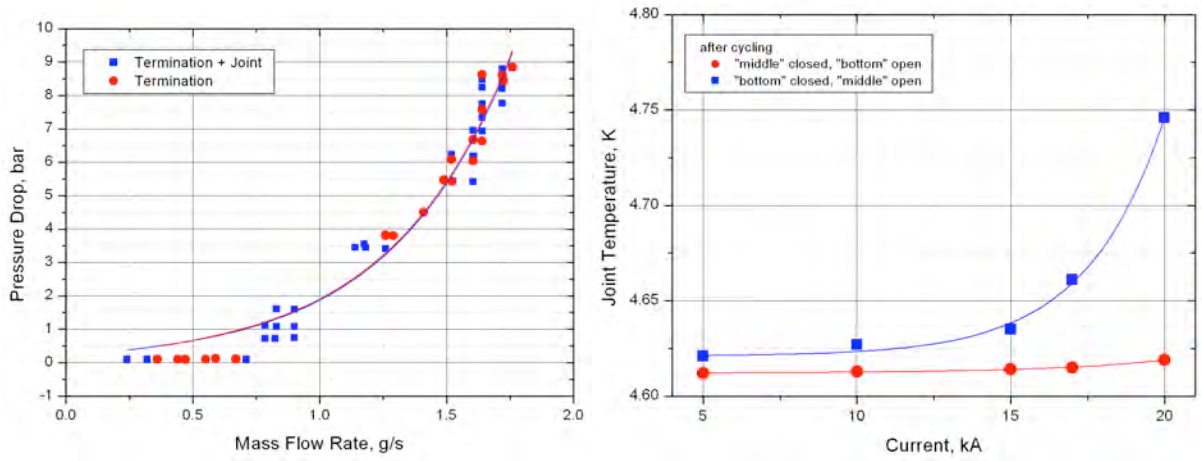

Fig. 2.5.5 *The results of pressure drop measurement (left) and heating of the joint (right) depending on active or passive cooling manner*

The resistance of the EDIPO joint was measured before charging by the current and after 100 charging/discharging cycles by 20kA current. The resistance did not change with the cycling and stays 1.2nΩ at operating current of 17kA.

The temperature of the EDIPO joint was watched along the resistance measurement at T1 thermometer. The temperature of the joint did not change behaviour with charging/discharging cycles by 20kA current, but was dependent on the cooling mode, i.e. active or passive cooling of the joint (Fig. 2.5.5 right).

2.5.2 Preparation of EDIPO test facility

The order for the *Vacuum Vessel* (including all flanges, the support structure of the cold mass) has been placed in spring 2009. The delivery and acceptance has been made in August 2009. The order for the copper thermal shield has been placed at the same time and the delivery was in September 2009. Using a new type of pre-assembled, multi-layer, super-insulation, the segmented thermal shield has been prepared and assembled in the vacuum vessel in November 2009. The big steel frame for personnel access and support of the outer iron shield was delivered and assembled at the end of October, see Fig. 2.5.6.

The order for the new helium transfer lines from the refrigerator to the vacuum vessel, including the valve boxes, has been delayed due to the public call for tender procedure. Eventually the order was signed in August 2009 and the delivery of the components is expected in February 2010. Other cryogenic components (sub-cooler) have been manufactured in the workshop.

The secondary coil of the new 100kA *Transformer and Sample Holder* has been delivered in April 2009. All components for the transformer – sample holder are now ready for assembly. The schedule for final assembly work is delayed due to the manpower priorities. A test of a left section of the cable-in-conduit conductor of the secondary coil is planned in January 2010. The sample assembly is in progress.

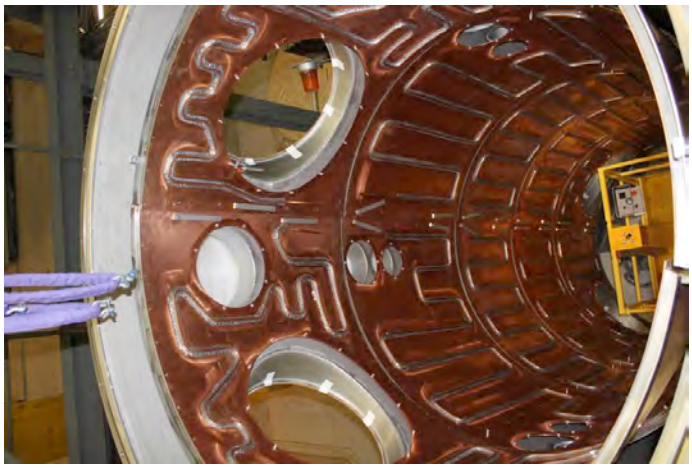

Fig. 2.5.6 *The pink steel frame for EDIPO, erected beside SULTAN, left, and the thermal shield with superinsulation assembled in the vacuum vessel*

The main *18kA, ±10V Power Supply* was delivered by Danfysik in September 2009 The EDIPO energy extraction switches, part of the *quench protection system*, were

procured by CRPP in January 2009 and integrated in the Danfysik power supply. The installation and commissioning of the power supply was carried out in November 2009. Commissioning of the switches is delayed due to the replacement of few control cards.

The *±300A, ±40V Power Supply* for the transformer, including the quench protection, was delivered by Danfysik in May 2009. The commissioning was done by using it to power the existing superconducting transformer of SULTAN.

The manufacture of the 17kA *High-Temperature-Superconductor Current Leads* is in progress. The soldered stacks of HTS tape have been delivered in October 2008. The other parts to assemble the HTS module are ready for assembly. Taking advantage of the large delay in the overall schedule, the manufacture of the leads includes now a prototype step, to validate the assembly procedure, and a low voltage / high current test in the EDIPO vacuum vessel using a short circuit in early 2010.

The EDIPO performance limits during current ramp-up have been analyzed with a model including the cryogenic system and the DC winding, i.e. all 14 double layers (DL) wound with cable-in-conduit conductors (CICC). The CryoSoft™ suite of codes was used, i.e. one code THEA for each DL, the code FLOWER for the cryogenic system and the new code SUPERMAGNET to launch, schedule communication and terminate execution of the above 15 processes in parallel.

The figure of merit is the minimum temperature margin in the DC winding $T_{Mmin}=\min(T_{CS}-T)$ where T_{CS} is the current sharing temperature and T the conductor temperature, see Fig. 2.5.7. At the design value of the longitudinal strain in the Nb_3Sn filaments inside the CICC (ε=-0.65 %) T_{Mmin} is within acceptable limits (>2K) and almost constant in the range of current ramp rates provided by the power converter (0-50A/s). The latter result highlights a problem in case of major superconductor degradation, e.g. T_{Mmin}=0.5K at ε=-0.85 %. The simultaneous simulation of all 14 double layers is an advantage for the assessment of the performance limits as it is unknown *a priori* where and when T_{Mmin} occurs.

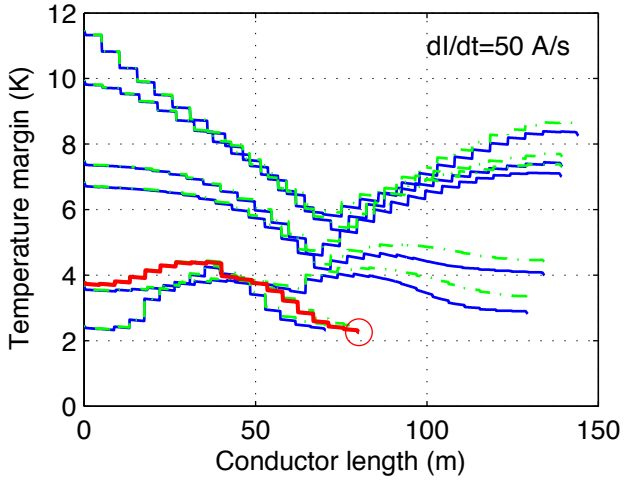

Fig. 2.5.7 *Distribution of the temperature margin along the conductor length in all 14 double layers (blue: DL1-DL7, green: DL8-DL14). In this example T_{Mmin} occurs at the outlet of DL2 (red).*

*2.5.3 High temperature superconductors**

In October 2009, the work on the project *"Use of HTS for High Magnetic Field Generation"*, funded by the Swiss National Science Foundation, has been started. In the framework of this project, a high temperature superconductor insert coil will be designed, manufactured and tested. The insert coil will be used to enhance the magnetic field of 12T generated by a Nb_3Sn laboratory magnet.

In collaboration with the Helmholtz Zentrum Berlin, a pair of 20kA high temperature superconductor (HTS) current leads will be designed and manufactured by CRPP. The current leads will be used to supply a current of 20kA to the Superconducting Hybrid Magnet System to be installed at the Helmholtz Zentrum Berlin. Very recently the interfaces between the high temperature superconductor current leads and the cryostat have been defined.

CRPP and WEKA AG (Bäretswil) intend to develop high temperature superconductor current leads for currents above 10kA. CRPP and WEKA requested funding for this project (project title: *Hoch-Tc-Supraleiter Stromzuführungen für supraleitende Magnete*) by the "Förderagentur für Innovation KTI". The experts of KTI asked for a revised request to be submitted before the end of December 2009. The main goal of the project is the standardization of the current lead design to a degree, which allows the industrial manufacture of high current HTS current leads.

Due to the lack of funds, EFDA did not endorse the R&D program proposed by a group of Associations since 2008. In 2009, HTS was initially not even quoted in the EFDA Work Program. On the initiative of Associations, a request of expression of interest (Task WP09-SCF01) was launched by EFDA in April 2009. The objective of this task is to prepare in 2009 a plan of activities for a three years program (2010-2012) devoted to the use of coated conductors and MgB_2 for future fusion magnets. At the kick-off meeting, held on July 6, 2009 in Garching, EFDA and the interested Associations agreed that the goal of the first three years period of the HTS task is the manufacture and test of a straight cable made of $YBa_2Cu_3O_7$ (Y-123) or $REBa_2Cu_3O_7$ (RE-123, RE: rare earth element) coated conductors, which can be scaled up to ITER-relevant currents. For the MgB_2, the target of the first three years period is the manufacture and test of a small demonstration coil. The specific role of CRPP will be to coordinate the "*Elaboration of a project for the preparation and execution of the qualification tests*". The manufacture of the straight RE-123 scalable cable and the MgB_2 demonstrator coil will be coordinated by the Forschungszentrum Karlsruhe.

The following two targets of the three years program have been agreed by EFDA and the Associations:

- Manufacture of a straight scalable RE-123 cable, which has to be tested under 3kA in a magnetic field of 6T at an operation temperature of at least 50K.
- Manufacture of MgB_2 demonstrator coil with 3 windings and an inner diameter of 500mm to be tested at 3kA in a magnetic field of 6T and an operation temperature of 4.5K. The costs of the MgB_2 conductor shall not exceed the commercial values of NbTi for the same length.

The feasibility of HTS current leads for SULTAN has been studied. Due to the stray field at the location of the current leads, it is prohibitive to operate the HTS current leads at 74K (shield temperature). The supply of 50K helium from the refrigerator is in principle possible but requires expensive modifications of cold box, ports and

* Some the activities do not belong to the Association Work Programme

transfer lines. Considering the large financial demand for the replacement of the SULTAN current leads and the lack of support from EFDA, the design of the SULTAN HTS current leads will not continue to the engineering level.

*2.5.4 Design study of a magnet for ESRF**

The European Synchrotron Radiation Facility (ESRF) located in Grenoble provides radiation in the X-rays range by means of a 6GeV storage ring. Thirty beam lines are available for external users. One of these beam lines (ID08) is devoted to the study of the electric and magnetic properties of the matter by using the X-ray Magnetic Dichroism technique. This technique is based on measurements of the X-ray absorption spectra of the sample during the application of a magnetic field, which can be perpendicular or parallel to the beam axis. In order to improve the characteristics of the present magnet system, it has been decided to upgrade the dichroism station with a new superconducting magnet able to generate a magnetic field in both directions, i.e. parallel and perpendicular to the beam.

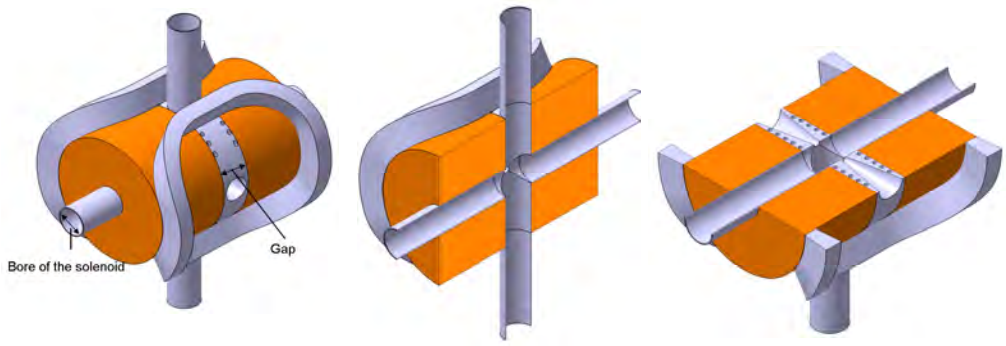

Fig. 2.5.8 *Magnet system, Option2.*

Two different conceptual options are studied. The first consists in using a split solenoid in NbTi for the main field and a pair of NbTi racetrack coils nested inside the solenoid for the perpendicular field. The second option foresees a split solenoid with both NbTi and Nb_3Sn grades for the main field and a pair of NbTi saddle shape coils outside the solenoid for the perpendicular field. The study has been focused only on this last solution (Fig. 2.5.8), since the first option does not satisfy the field requirements.

Initially, the goal was to design a superconducting magnet able to reach 7T in the direction parallel to the X-ray and 2T in the perpendicular direction. However, by accepting the use of the Nb_3Sn (option 2) the requirements have been upgraded to 9T and 4T, respectively. A high sweeping rate, 0-Bmax within 1 minute, is also foreseen.

The main characteristics (size, current density, field and temperature margins) of the magnet are defined by means of Finite Element electromagnetic models run iteratively. In the chosen configurations, the temperature margin is larger than 3K for the Nb_3Sn grade and over 1.5K for the NbTi one. These large margins together with heat removal computations guarantee that the requirement of fast charge (60s to full field) is also achievable with good confidence, provided that low ac loss strands are taken. The main drawback of the system is the large inductance that

* Work not belonging to the Euratom Association Programme

leads to the necessity of a large, non-standard power supply to achieve the 60s charge time. A mechanical structure is also conceptually designed in order to support the coils system against the electromagnetic loads.

*2.5.5 Superconducting Outsert for the HZB Hybrid Magnet**

The Hybrid magnet to be installed in the HZB in Berlin is a solenoid composed by a resistive insert and a superconducting outsert. The outsert is composed of three grades, High Field (HF), Medium Field (MF) and Low Field (LF), all made of layer wound CICC in Nb_3Sn. There are 18 layers in total. The assembly, devoted to neutron scattering experiments, is designed to generate up to 30T in the center of the solenoid.

CRPP reviewed the design of the SuperConducting outsert of the Hybrid (SCH) magnet to assess margins of improvement in the original design, aiming to an enhancement of the efficiency / reliability of the system and to a possible reduction of the costs. The following aspects are investigated:

- Grading scheme: a modification of the grading scheme is proposed to raise the minimum temperature margin up to 2K maintaining the maximum hot spot temperature (computed with the adiabatic criterion) below 250K. It is suggested also to increase the conductor insulation thickness in all layers and to use thicker ground insulation. Finite Element (FE) models are developed with the ANSYS code in order to study the magnetic and mechanical behaviours of the winding and compare them to the initial design. Stress and deformations in the winding pack are below the allowable limits in all the proposed configurations. The temperature margins satisfies the design criterion and the hot spot temperature computed by considering an adiabatic discharge is below 190K, guaranteeing large safety margin in case of a quench.
- Pre-compression structure: the necessity of a pre-compression structure to prevent through-thickness tension in the conductor insulation due to the large axial electromagnetic forces (what would lead to de-bonding and failure) is outlined. A pre-compression structure is also proposed. The pre-loading can be achieved with a structure of segmented steel tie plates with 70% inner coverage. The pre-loading force is created by bolts and transmitted to the winding pack through glass-epoxy structure.
- Current leads: a list of available options for the current leads design is suggested. The advantages and disadvantages of Cu and HTS current leads are highlighted and several cooling options are proposed. The use of binary current leads, characterized by a superconducting part and a Cu one, is suggested as optimal solution due to the reduction of the refrigeration power necessary to cool the current leads.
- Thermo-hydraulic analyses: the cooling of the system is studied in many respects.

The original cooling configuration, consisting in the full parallel of the 18 channels, is compared to other cooling configurations, such as the series or a mixed configuration, focusing on the cooling efficiency (heat removal capability, residence time), design simplification and/or drawbacks. The cool down time as a function of the available refrigeration power is studied in detail for each configuration. The friction factor used in the analyses is derived by experimental measurements performed at CRPP on a HF cable.

* Work not belonging to the Euratom Association Programme

The parallel configuration ensures the smallest pressure drop and a fast cool down. On the other hand, the residence time of He is the longest due to the low mass flow rate in the longest channel. As a compromise, a mixed configuration is proposed, consisting of series of three groups of channels in parallel. This has the advantage to guarantee a high mass flow rate, by keeping the pressure drop at an acceptable level. The total heat removal capability is higher than in the parallel layout and the residence time much lower.

2.5.6 AC loss vs. aspect ratio

The loss in rectangular superconducting cables is strictly depending on their aspect ratio, which has an impact on the area crossed by the field variation and consequently on the coupling current between strands. The relation between AC loss and aspect ratio is studied with reference to the test of three Cable in Conduit Conductor (CICC) short samples. The first sample consists of a NbTi cable designed by CEA and ENEA for the JT60 tokamak, the second of a Nb_3Sn cable for the HZB hybrid magnet. The last sample is an ITER TF CICC (called "EUTF alternate") compacted and enclosed in a square jacket. All samples are composed of two legs assembled with the same conductor and differing only in the orientation with respect to the external variable field. In the JT60 and ITER samples, the cable of one leg is rotated by 90°, while in the HZB sample by 45° with respect to the other leg. The AC loss is measured in the SULTAN test facility with a gas flow calorimetric method. A sample length of 39cm is exposed to a sinusoidal field having an amplitude of ±0.2T or ±0.3T, depending on the conductor specifications, and variable frequency in the range 0.1-0.8Hz. A background field of 2T perpendicular both to the sinusoidal field and to the sample axis is also applied. The AC loss is assessed by measuring the variation of the He enthalpy, assuming the metal enthalpy negligible. The AC loss per cycle as a function of the frequency measured in each conductor is shown in Fig. 2.5.9.

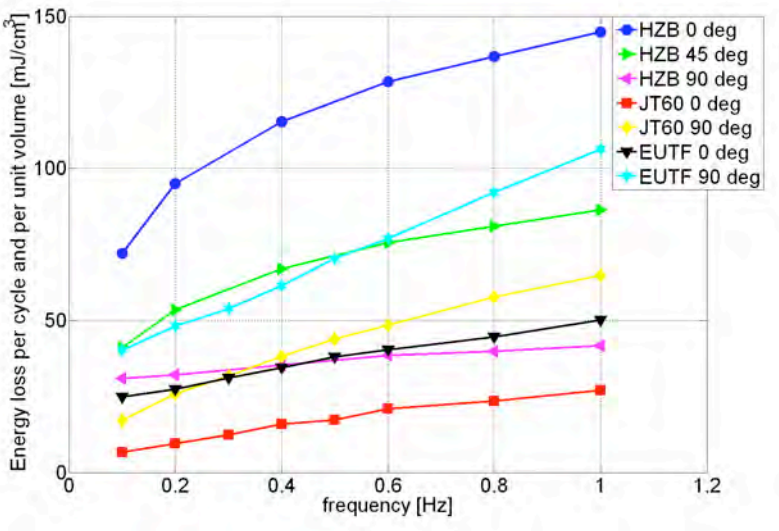

Fig. 2.5.9 *AC loss per cycle and per unit volume as a function of the frequency for the HZB, the JT60 and the EUTF conductors.*

In the attempt to find a relationship between loss and aspect ratio, the results are then fit with an expression based on an analytical formula deduced by means of a theoretical approach and already proposed in the literature.

The experimental data suggest that the theoretical relation does not satisfactorily represent the behaviour of cables with different characteristics, such as superconducting material, coating, layout, twist pitch, that have a relevant impact on the loss. As a matter of fact, the theoretical law is derived from an anisotropic but continuous model, which does not take into account the changes in the transverse resistivity due for example to the presence of Cu strands or to variable twist pitch.

*2.6 Industrial process plasmas**

The general situation at the CRPP has strongly influenced the R&D activities of the industrial plasma group. The number of projects and in particular the manpower remained nearly unchanged compared to the preceding year.

Obtaining high deposition rates is an important issue in industries applying plasma coating. New high deposition rate plasma sources have to be developed and, as the results from the last year suggest, novel plasma reactor design and process development are necessary before introduction in industry. Therefore the group will continue to work on these very important topics within a CTI project with Sulzer-Metco and a CTI project with Helyssen and TetraPak.

During this year a new CTI project in collaboration with OC Oerlikon Solar started with the aim of developing a novel capacitively coupled RF plasma reactor type with high deposition rate and very homogeneous film thickness for application in solar cell industry.

Discharge physics is still a key issue in the world of industrial plasmas. Fundamental studies to understand breakdown and discharges are still a necessity. One of the main problems for high deposition rate plasma sources where high AC/DC power is applied is the occurrence of arcing and parasitic discharges. These phenomena can damage or destroy the plasma source and therefore hinder a successful introduction into industrial production lines. Arcing starts to be a limiting factor in several plasma applications, thus triggering intense research and development.

Research and development of Electrical Discharge Machining (EDM) is another important point in the research of the industrial plasma group. For the current running CTI project, grouped around inspire SA at the ETHZ, dry EDM is the focus of research. Dry EDM could have many advantages with respect to conventional EDM, however it is far away from being introduced on industrial level. Further projects with RUAG Aerospace on robust electrical transfer systems for solar array drive mechanism slip ring assembly on spacecraft is on the way to be started if the last administration difficulty is removed by the end of 2009.

The diversification of the R&D activities such as with COMET SA on the breakdown phenomena is ongoing and long-term topics have been initiated. To summarize a particular weight is given to discharge physics, arcing under various conditions and the development of novel high deposition rate plasma sources and its processing procedures. During the year meetings and discussions with various industries on

* Work not belonging to the EURATOM Association's work programme.

other new plasma processing issues have been made and will give new R&D topics and interesting science for the industrial plasma group of the CRPP in future. Furthermore the industrial plasma group ensured the education of a large fraction of Master Project and Advanced Laboratory (TP IV) students at the CRPP.

2.6.1 Thin and thick film coating using liquid and gaseous precursors with low pressure plasma spraying (LPPS) equipment

Conventional plasma spraying provides rapid coating due to the high enthalpy of the plasma jet. Metal and also ceramic powder material can be melted and deposited in the form of splats which produce thick and porous coatings. In the previous project, we showed that it is possible to deposit thin and dense layers from liquid or gaseous precursors at very high deposition rates using conventional plasma spraying equipment operated at low pressure. With this approach it is possible to combine the conventional thermal spray coating with the newly-developed thin film deposition using the same equipment to obtain multilayer deposits with special functionalities and properties.

Most of the work done during the reporting period was focused on processing of possible future applications and on investigations exploring the limits of the novel process and the necessary equipment. The following applications have been considered to be interesting for future industrial use: deposition of SiO_x, deposition of carbon containing layers, of metals and metallic oxides and as well as for surface transformation such as processing of zirconium oxide for decorative purposes.

The efforts focused in particular on the basics of the deposition of SiO_x using the injection of Hexamethyldisiloxane (HMDSO) and oxygen. As plasma diagnostics, emission spectroscopy and mass spectroscopy have been used, whereas (Fourier Transform Infrared (FTIR) absorption spectroscopy, interferometry and corrosion tests have been applied for ex-situ characterisation of the thin SiO_x layers. Main results are very high deposition rates exceeding 40nm/s, with good film quality compared to other deposition techniques as measured by FTIR absorption spectroscopy. The test on the corrosion behaviour of SiO_x-covered iron samples showed that the coating cracks and therefore is losing its barrier protection.

These results lead to the problem of heat management during the plasma-substrate interaction. Intensive investigation concerning the heat transfer due to the intense plasmas jet have been performed, in particular for typical substrates such as metal and glass substrates. The plasma jet inducing large temperature gradients is one of the reasons giving rise to broken glass substrates, a problem to be solved in future. Furthermore it was found that the gas flow in the reactor chamber strongly influences the process and plasma chemistry. In addition the impinging fast plasma jet (velocity about 400m/s) leads to a stagnation flow on the substrates and in turn leads to coating thickness inhomogeities in the presence of small obstacles on the substrate. It was found that these results might also apply to other high deposition rate plasma sources under development. This findings are important for optimizing high deposition rate thin film coatings using the plasma torch equipment
As a result of the encouraging overall advance of the previous and current project, Sulzer decided to finance additionally the replacement of the present oil-containing primary pump by a more suitable dry pump (screw pump from Busch SA) in order to increase the versatility of the installation at the CRPP. With this change, new applications can be envisioned in the near future. Furthermore, funding of a effusion cell for the evaporation of metals has been attributed to develop of metal-containing films such as pure metal or metal oxide films.

2.6.2 Arcing and parasitic discharges in RF plasma reactors

In the frame of the (Competence Center Energy and Mobility (CCEM) project “Cost efficient thin film photovoltaics for future electricity generation” funded by Swisselectric, the arcing and the appearance of parasitic discharges in high power RF plasmas have been investigated.

The need for more powerful and larger area reactors for plasma-enhanced chemical vapour deposition brings current designs to their limits. Parasitic plasmas and arcing become more common and can damage or even destroy these reactors. A better understanding of these phenomena is crucial for the development of new reactor generations. In a very large area reactor many types of arcs and parasitic plasmas can coexist, possibly influencing or causing each other. Since such a reactor is a very complex system, it is difficult to develop simple models explaining the cause of the damage observed in industry. After listing rough subgroups of arcing damage, the first step has been to try and reproduce these discharges in a small research reactor, with a simlified geometry. This procedure will then allow us to isolate the underlying fundamental physical principles. Once the types of discharges behind the arcs and parasitic plasmas are known, methods to prevent damage to the reactor can be developed. A short term solution would be to find real-time diagnostics to detect damaging arcs during operation. It is important to note that to be of use for the industry, such diagnostics have to be relatively cheap and easy to implement.

During 2009 in particular the breakdown in small gaps with irregular features have been investigated. RF breakdown has been extensively studied in parallel plate configurations. However, in capacitively-coupled reactors for plasma-enhanced chemical vapour deposition, there are areas in the reactor where small gaps are used between RF electrode and ground that are meant to prevent RF breakdown – predominantly in the showerhead. These gaps can be, as a first approximation, considered as parallel plates with holes and/or elevations, and are supposed to be narrow enough to prevent a glow discharge, but wide enough to prevent metal-vapour arcing between the electrodes. These gaps have been shown to be vulnerable to damaging parasitic discharges when the reactor is used at higher powers and therefore higher RF voltages. In the last year we investigated the behaviour of breakdown in these non-parallel surfaces. A typical experimental setup consisted in a flat cylindrical RF electrode, and separated from it by a gap of 4mm a ground electrode with a 5mm deep cylindrical hole, such that the distance between the bottom of the hole and the RF electrode was 9 mm. The diameter of the electrodes was 90 mm, and they were separated by Perspex-rings. Figure 1 shows some results of experiments with different hole radii. Each of the curves represents the breakdown RF voltage (peak-to-peak) versus pressure. It can be easily seen that the breakdown curves for all the hole-diameters fall between the two extrema of no hole (i.e. parallel plates with a 4mm gap) and a hole the size of the electrode (i.e. parallel plates with a 9mm gap). Furthermore, as the diameter of the holes increases from 4mm to 60mm, the curves steadily approach the limit of the case of two 9mm parallel plates.

Future work will focus on further analyzing the data, and creating a fluid-simulation model of the breakdown in a finite elements solver.

With the present test bed reactor we have a very versatile tool for testing various geometries in view of arcing and parasitic discharges.

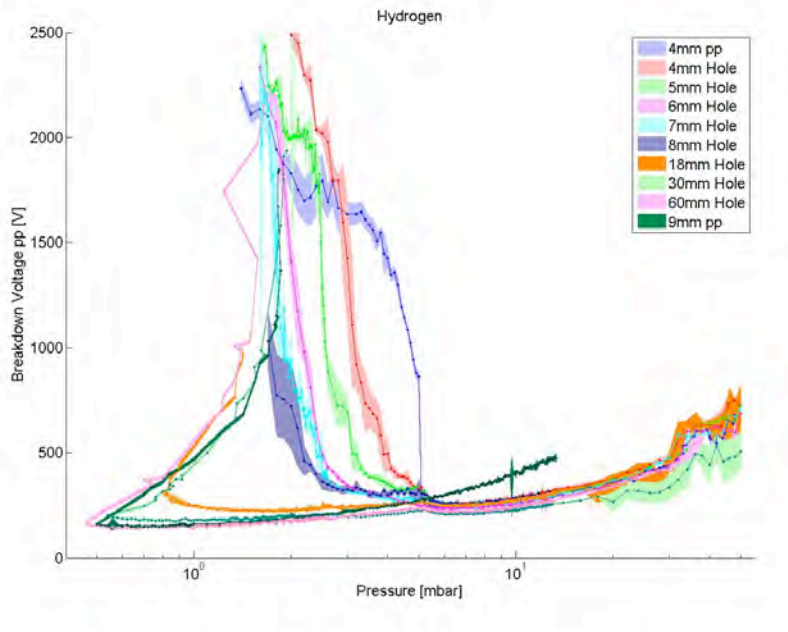

Fig. 2.6.1 *Breakdown curves for different hole sizes in Hydrogen. The lines labeled "4mm pp" and "9mm pp" represent no hole and a hole size equal to the electrode diameter, respectively.*

2.6.3 A new low ion energy bombardment PECVD reactor for the deposition of thin film silicon for solar cell applications

The scientific objective is to investigate a new electrode configuration for radio-frequency (RF) plasma dissociation of gas for thin film deposition, where the novel aspect is to suppress the ion bombardment of the growing film. The fundamental aim is to protect the sensitive atomic arrangement of the film surface from the destructive bombardment of high-energy ions in the plasma. Ion bombardment with ions accelerated over a certain threshold voltage creates defects in the deposited bulk material and damages sensitive interfaces and, hence, deteriorates the material quality and interface performance. However, to increase the deposition rate, and thereby the equipment throughput, higher RF power levels become necessary. Consequently, in the standard parallel plate configuration, high deposition rate at high power results in poorer module performance.

At the start of the project during 2009 the existing KAI reactor has been redesigned and modified to house an additional plate electrode with different holes and at a variable gap distance from the RF showerhead electrode. Parameter scans in pressure, RF power and gap distance are being performed to study their influence on plasma ignition. Argon, hydrogen, and mixtures have been used to study their different breakdown behaviours. First diagnostics include RF electrode voltage, RF power, Langmuir probes and emission spectroscopy .

The new reactor design led to technical complications of coupling of the RF power into the reactor. The reason is the additional grid close to the front of the RF electrode which changes drastically the capacitance of the RF electrode assembly. Consequently, there is a higher RF current for a given RF electrode voltage and reactor power. This reactive current also flows in the stripline which is connected in series with the reactor, where it causes power loss due to ohmic heating by the skin currents. Stripline heating and power loss restrict the power level delivered to the

reactor and thereby limit the RF electrode voltage below the threshold for igniting a plasma in hydrogen.

A high quality, (i.e. without breakdown and parasitic discharges), completely solid stripline design was necessary for operation. Furthermore different possiblities for efficient matching of the RF generator and the novel plasma reactor have been elaborated. With these measures, stable and full-area argon and hydrogen plasmas at 13 and 40 MHz have been obtained. Single Langmuir probe scans showed good lateral uniformity of argon plasma density.

Numerical simulations of the gas flow dynamics, and of the electric field configuration at the perforated electrode have been started.

2.6.4 Optimization of the plasma-enhanced chemical vapour (PECVD) process for the deposition of SiO_x barrier coatings on polymers.

One of the best known barrier coatings is by far SiOx. SiOx coatings are in particular used in the packaging industry as an oxygen barrier. One way to produce SiOx coatings is the so-called PECVD, plasma-enhanced chemical vapour deposition, where a suitable organosilicon is decomposed, and fragments attached on the polymer film surface react with oxygen atoms to form SiO_x layers. During SiO_x deposition, production of fine sized powder is a great disadvantage of the process. Powder leads to damage in the equipment but might also be a potential health risk. Powder production is also a sign that the process could have much higher deposition rate since much of the available monomer is transformed into fine-sized SiO_x powder instead of being used for the coating.

In the present project the basics of the SiO_x powder formation is investigated in order to understand better the different mechanisms and processes leading to powder formation,

Different organosilicon plasmas with various amounts of oxygen admixture have been investigated. The analysis is performed with time resolved in-situ Fourier Transform Infrared (FTIR) Absorption Spectroscopy in the spectral range between 4000-600 cm^{-1}. The following plasma and particle diagnostics are presently installed on the capacitively-coupled RF reactor: optical emission spectroscopy, far-infrared absorption spectroscopy (FTIR), laser extinction measurement (which can be extended to laser scattering if necessary) and the typical electrical measurements, as used on capacitively coupled RF reactors (bias voltage, RF voltage).

All the experiments and results obtained lead to the main conclusion that a high dissociation rate of the monomers is necessary to strongly reduce the powder formation in these reactive organosilicon plasmas used for SiO_x barrier coating in packaging industry. This result also lead to new ways in the development of future plasma sources, which must attain much higher degrees of dissociation than the commonly used capacitively- or inductively-coupled RF plasma discharges.

Since SiN films also attract considerable attention in the packaging industry the plasma chemistry of SiN film production using organosilicons has been started. Therefore in the following HMDSN plasmas diluted with N_2 or NH_3 have been studied. FTIR spectroscopy of the obtained film and in-situ FTIR absorption spectroscopy of the plasmas have been performed in order to determine the film and plasma composition respectively. Detailed investigations for different gas

admixtures of N_2 and NH_3, different RF power and gas pressures have been made. In all these cases, no powder formation at all in these processing plasmas has been observed. Furthermore it was observed that the films as well as the plasma are still very rich in carbon. The strong carbon contamination in the films as well as of the plasma results from the CH_3, a dominant part of the HMDSN molecule. Not astonishingly it turned out that the obtained coatings on the polymer were of bad quality and therefore not of great interest for the present industrial applications. These results reflect well the importance of the choice of the monomer to produce SiN films. In silane (SiH_4) plasmas diluted with N_2 or NH_3 SiN films are easily produced, however in the presence of large powder formation. The contrary was, as mentioned above, observed in HMDSN diluted N_2 orNH_3 plasmas. Therefore silane (a relatively cheap gas) would be a much more interesting monomer. However, due to its spontaneous flammability it is considered as a dangerous gas which will unfortunately not easyly find application in industry. The present first indication of particle formation in HMDSO/O_2 plasma is new with respect to powder formation and these investigations will help to understand the plasma chemistry in important plasma applications.

2.6.5 Plasma diagnostics for dry electrical discharge machining (EDM)

Electrical Discharge Machining (EDM) is a widely-used machining technique. The process consists in successively removing small volumes of workpiece material, molten or vaporized during a discharge. The sparks are usually created in a flowing dielectric, generally water or oil. The liquid dielectric plays a crucial role for the electrode cooling and for the material removal: it increases the removing force on the molten metal when the plasma collapses, then it solidifies the molten metal into small particles, and finally it flushes them away.

During 2009 the CTI project in collaboration with Charmilles-Agie Technologies SA, Inspire AG at the ETHZ, Balzer Technik and Carbagas, a project concerning DRY Electrical Machining has been started (Fig. 2.6.2). In Dry EDM the oil or water dielectric is replaced by air or some reactive or inert gases. The first experiments indicate that Dry EDM is quite a difficult process and its industrialization is still far from being achieved.

In dry electrical machining a very small gap between the electrodes is necessary to ensure electrical breakdown. The precise control of the very small electrode gap avoiding deleterious short circuits is one of the main challenges in dry electrical machining. Larger electrode gap necessitates higher working voltage, beyond the voltages available from commercial EDM generators. A simple RC pulse circuit with voltages up to several hundreds of volts and current pulses of a few tens of amperes during about 100ns has been used to investigate the on-going plasma physics in dry electrical machining. Fast voltage and current probes have been used to characterize electrically the discharges. Time-averaged emission spectroscopy was used to study the spark used in dry electrical machining. These investigations revealed that as in the conventional EDM a cold (<1eV) dense metal plasma exists. Compared to the EDM in oil or water no large continuum emission, but only line radiation from the electrode material was observed. At very high electrode voltages uncontrollable discharges probably due to oxidizing reactions in the air could be observed. Therefore inert gas protection of the working area during machining might be the way to go in future dry electrical machining.

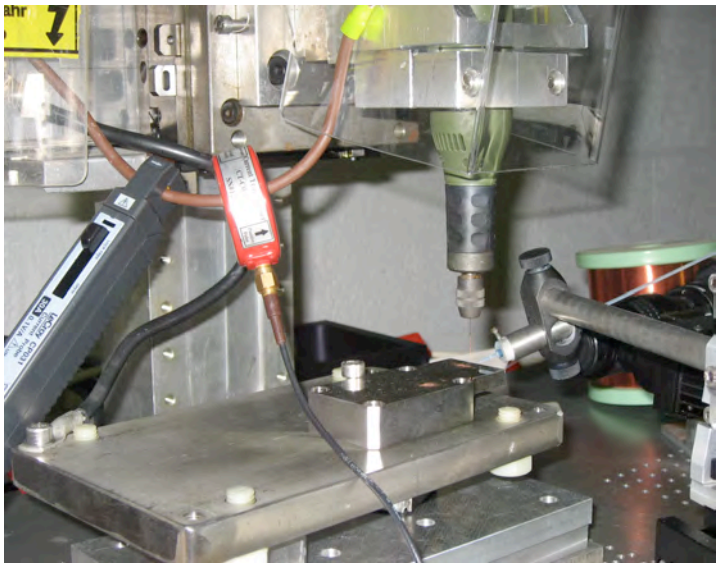

Fig. 2.6.2 *Test bed for Dry Electrical Discharge Machining (DryEDM)*

2.6.6 Very fast SiO_x barrier deposition on polymers by plasma-enhanced chemical vapour (PECVD) process with a helicon plasma source

The principal objectives of the present project is to increase the deposition rate in the PECVD process producing SiO_x barrier coatings by using the novel high density Helyssen source and to optimize the use of monomers while keeping excellent barrier characteristics of the coating. The use of plasma deposition on polymer films for the formation of barrier layers was shown to be very efficient in terms of the quality of coating. But until now, this technique suffers from its relatively low deposition rate compared to competitive processes such as electron beam reactive evaporation or reactive evaporation. High deposition rates of SiO_x for barrier application can probably only be achieved if the monomer is dissociated as much as possible (see above). In this case powder production is also strongly reduced. To achieve high dissociation degrees new more powerful plasma sources must be applied. The main goal of this project is to design and to test a novel planar RF plasma source developed by Helyssen S.a.r.l. A large part of the physical concepts and capabilities of this source is still only theoretical and has to be concretized by basic experiments at the CRPP. On the basis of this research, a semi-industrial version of a RF planar source will then be implemented on a roll-to-roll equipment located at Tetra Pak.

The CTI project started on September 1st at the CRPP and in a first part a tubular RF source (Fig. 2.6.3) shall be used in order to test if sufficient oxygen barrier effects can be achieved at very high deposition rates. In parallel to these investigations Helyssen is developing a novel planar RF antenna for application in the semi-industrial device at Tetrapak. The planar Helicon source is a new innovative development from Helyssen and is based on the principle of the bird-cage coil used in the tubular antenna. The foreseen planar RF source will be able to coat large substrates in the modified roll-to-roll device. Also in this case high deposition rates and good barrier coatings are demanded. During this phase of the project the CRPP is responsible for the plasma diagnostics and the interpretation of the obtained results. Tetrapak will transform the existing semi-industrial device and perform the tests of the planar antenna. Material characterization will be made by TetraPak whereas the CRPP will assist for plasma physics related problems.

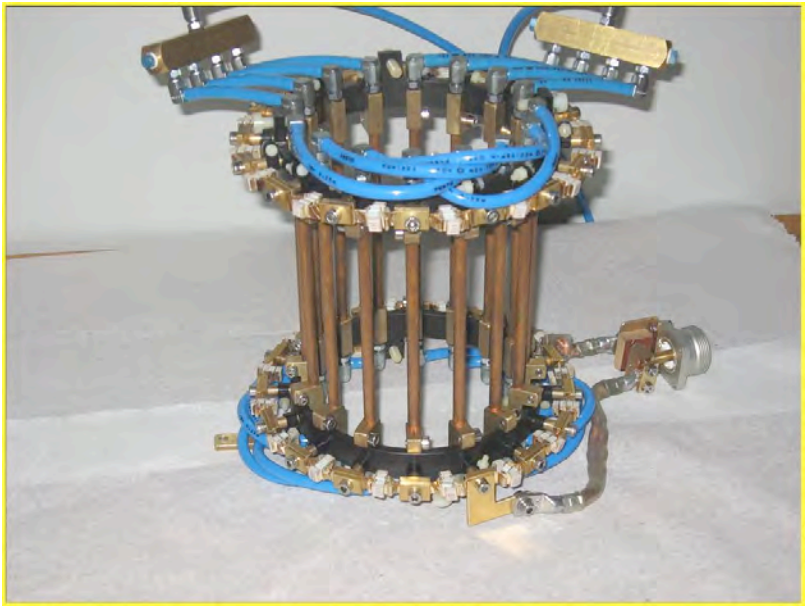

Fig. 2.6.3 *A 10 cm diameter RF antenna for helicon plasma source as designed by Helyssen S.a.r.l.*

2.6.7 European FP7 project: Plasmaero

On October 1st 2009 the FP7 project PLASMAERO was officially started and will last three years. The consortium is composed of 12 partners from 8 countries (Arttic (F), ONERA (F), CNRS (F), EPFL (CH), CIRA (I), Technische Universitaet Darmstadt (D), University of Nottingham (GB), NLR (NL), University of South Hampton (GB), TRINITI (RU), SNECMA (F) and IMP (PL)). It gathers the key players from the plasma and aerodynamic scientific community of Europe.

The design of tomorrow's aircraft will be oriented by the need to have more environmentally friendly aircraft. To move forward towards this objective, it is necessary to study breakthrough and emerging technologies going beyond the limitations of the aircraft's fixed structure and to use efficient actuators to optimize the flow over the airfoil. Plasmaero (Fig. 2.6.4) seeks to demonstrate how surface and arc discharges plasma actuators can be used to influence and control aircraft flows.

The objectives of the present European project which is coordinated by ONERA(F) are:

- Understand, model and classify, through experimental and numerical studies, the most relevant physical characteristics of surface and jet plasma actuators capable of influencing airflow.
- Perform comparative experimental tests & numerical studies of different actuator configurations to select the most promising for further development.
- Demonstrate through wind tunnel experiments the ability of plasma devices to significantly improve aircraft aerodynamics in terms of lift, lift/drag and high lift noise in representative airflow conditions (take- off, cruise and landing).
- Demonstrate the ease of use and installation of these actuators in a reduced size flight platform.

- Provide exhaustive recommendations on future work to be performed in order to implement this technology in the next generation of aircraft programmes.

Fig. 2.6.4 *European FP7 project PLASMAERO*

The CRPP participates together with the Laboratoire de Thermique Appliquée et de Turbomachines (LTT) and the Laboratoire d'Ingénierie Numérique (LIN) of the Energy Institute (ISE) from the Faculty of Engineering (STI) in this programme. In addition the CRPP is leader of the work package on "plasma devices, investigation, development and improvement" and task leader for "Shock/Boundary layer interaction".

2.6.8 Arc Phenomena in Space Environment and Equipment (Project RETS)

Arc phenomena are one of the oldest topics in plasma physics. Arcing is again a key issue in the application of plasmas in industry and also in space environment and space equipment. Modern satellites, in particular transmission satellites are being equipped with larger and larger power systems. Since the weight aspect is very important the dimensions of the conducting paths, for instance in slide rings, are small. Unfortunately several incidents showed that arcs producing short circuits of the power system can dangerous for the satellite. Arcing also starts to be the limiting factor in several other applications of plasmas, thus triggering intense research and development on this topic.

In the present work for the space agency ESA in collaboration with RUAG Aerospace in Nyon and the Haute Ecole d'Ingénierie et de Gestion du Canton de Vaud (HEIG/VD-IESE) laboratory, the necessary fundamentals of arcing shall be established and be applied to space equipment in order to reduce or suppress arcing in space environment.

The aim of the tasks of the CRPP is to conduct arc ignition, propagation and stability experiments in space environment and to define and conduct elementary experiments. It is foreseen to make elementary testing with micro wires in gaseous and vacuum environments. Electrical simulations will be conducted by the HEIG/VD-IESE laboratory based in Switzerland. The aim of this part of the project is to establish a simulation model for each elementary component composing a powering system for the satellite. In order to perform these tasks the Industrial Plasma group of the CRPP has test equipment allowing operation in ambient air and down to a pressure of 10^{-8} mbar which can be applied for the purpose of the present project. The equipment can use different gas atmospheres, gas pressures and gas flows which can be obtained using different gases such as noble gases but also certain reactive gases. The test facilities proposed at the present time consist of a part of the slip ring connected to a high power DC power supply. The connecting wire will initially be a moving thin tungsten wire connected to the arc ignition

circuit. The fast destruction of the thin tungsten wire can lead to a metal plasma and the resulting metal vapour can in turn trigger an arc discharge between the power line conductors. Preliminary experiments have been made at the CRPP and first results are presented in Fig. 2.6.5. The project is expected to start in 2010.

Fig. 2.6.5 *Tungsten micro wire explosion obtained on the atmospheric test bed*

2.6.9 Helyssen SARL, a start-up company in the CRPP

Helyssen SARL, a start-up company, has used for several years a test bed at the laboratories of the industrial plasma group to evaluate the performances of different novel antennae for high deposition rate sources. The magnets and the necessary equipment for benchmarking and infrastructure have been lent to Helyssen SARL by the CRPP. This also includes equipment for plasma diagnostics and know-how in order to quantify the performance of high power RF plasma sources.

In collaboration with Tetra Pak Romont and the CRPP a CTI project has been started to investigate the application of the Helicon RF Plasma source developed by Helyssen SARL in the packaging industry.

2.6.10 Future and future projects

Preliminary experiments on breakdown conditioning and breakdown mechanism have been performed in a small UHV device. Small Rogowski-shape electrodes have been investigated concerning the small gap breakdown in collaboration with Comet SA at Flamatt. These investigations shall be continued in the next year and a collaboration with the CERN (S.Calatroni) is foreseen.

During the last year numerous discussions with interested industries have been made resulting in many small experiments and tests which have been performed on the various plasma reactors at the CRPP.

3 TECHNICAL ACHIEVEMENTS

3.1 TCV operation

TCV operation restarted on the 10th of March, 2009, after replacement of the excitation transformer for the motor generator which broke in 2008. Operation was interrupted by two incidents related to damages in diagnostic windows due to uncontrolled micro-wave launching, reported in details in Section 3.2 and a planned venting of the torus in June to upgrade some diagnostics. All these interruptions were limited to less than two weeks. Scientific operation until end of November consisted of about 200 sessions (half days).

3.2 TCV ECH systems

The X2 system for TCV has operated successfully with 5 gyrotrons during 2009. A decision not to repair of the oldest gyrotron magnet at the factory was taken. It is not necessary to have 6 X2 gyrotrons, at present, and the cost of repair is being weighed against future investments in upgrades of the overall EC system. The decision can be reconsidered at a later date. One of the 5 X2 gyrotrons is providing only ~1/2 nominal power due to low beam current. It is foreseen to replace this gyrotron with the one in the non-working magnet to make more power available in 2010. This changeover and re-calibration is expected to take 2 weeks during a scheduled shutdown and will provide an excellent training opportunity for new gyrotron operators. It is planned to use free-space beam measurements with phase reconstruction to aid in the alignment of the associated Matching Optics Unit (MOU) – measurements lacking during previous alignments.

The full X3 system was planned to be used heavily during 2009 for experimental investigation of the quasi-stationary, high performance ELM-free regime, but a window fault, in June, limited the total available power to ~1MW (2 gyrotrons). This power level is not sufficient to enter this regime; instead, other X3-dependant physics experiments have been given priority.

3.2.1 ECH security

The window and mirror of the Phase Contrast Interferometer (PCI) system were damaged during an experiment in April, due to excess refraction of 1.5MW of X3 EC power, leading to a vacuum leak. The protection system used during EC operations had been reviewed and upgraded by the TCV operations team in view of avoiding this type of event, but the X3 part of the system was not functional at the time of the incident. A new window was ordered and the mirror repaired. These were re-installed and the X3-protection detection circuitry is now functional.

The regulated high voltage power supplies (RHVPS) of the TCV EC system can be used as backup power supply for the ITER 170GHz gyrotron test facility sited in an adjacent building. During use of this system in 2008 with the ITER gyrotron, it was found that several of the free-wheeling diodes of the power supply were damaged. A security system is in place to switch the trip protection and computer control between the two installations. The switching box was mechanically damaged at

some point and repaired. Subsequently, tests were performed in the autumn 2009 to investigate the diode problem. Following these tests, the TCV vertical ECE window – directly above 2 X2 launchers – was broken due to an error in programming of the launcher angles compounded with an error in re-cabling of the fibre optic security at the RHVPS.

A concerted effort has been made to improve the protection concept from EC waves as more windows, in more vulnerable places relative to the EC injection, are continually being installed on the machine to accommodate novel diagnostics which can no longer be placed elsewhere due to port occupation. Nevertheless, a more systematic procedural method is required. To this end, TCV now *requires* an 'ECRH standard shot' to test the full functionality of the entire security chain from torus to power supply before the start of any operational day needing EC power. Both the Physicist-in-charge and Gyrotron-operator-in-charge take joint responsibility to carry out this procedure.

3.2.2 ECH Real-time control

One gyrotron and their associated launchers were successfully used for real-time feedback control of the sawtooth period and for control of the x-ray emission profile (amplitude and shape).

Experiments of feedback control of the polarization of ECH waves by rotating polarizers in a transmission line have continued to be carried out in collaboration with NIFS-Japan. A series of algorithms were developed both for the control of the polarization state and for the maximization of ECH absorption (or a simulation thereof). Both variants were successfully tested in a low-power set-up, and the latter has been applied successfully to the Large Helical Device (LHD). This collaboration fits well with a task launched by EFDA for experimental investigation of real-time control of EC polarization on European machines. CRPP is the coordinator of this work. Fast polarizers for one X2 transmission line have been purchased and are being integrated into the TCV hardware and control system. The algorithms used on LHD will be directly applicable to TCV.

3.3 Diagnostics

3.3.1 Diagnostic Neutral Beam Injector (DNBI)

The hydrogen diagnostic neutral beam (H+ fraction 85%) is used on TCV for active Charge exchange Recombination Spectroscopy (CXRS) measurement of the plasma ion temperature, impurity (carbon) density, toroidal and poloidal CVI ion velocity. A series of dedicated experiments with deuterium beam was performed to study the fast ion confinement and orbit losses at low plasma current.

The Computer Automated Measurement And Control (CAMAC) based local control system, with timing and other beam parameters pre-set by the Java routines originally delivered with the Diagnostic Neutral Beam (DNBI) in 2001, was completely replaced in June 2009 by a system based on industrial PCI cards from National Instruments Corporation and LabView. All input-output for control-measurement circuits of DNBI power supplies and electronics were adapted to the NI standards. The new control system has improved the integration of the DNBI

diagnostic in the TCV control system and has increased the beam availability up to >95%. The beam was used for approx. 800 plasma discharges, typically with a beam energy of 45-49keV and ion current of 2.3-2.8A (see Fig. 3.3.1).

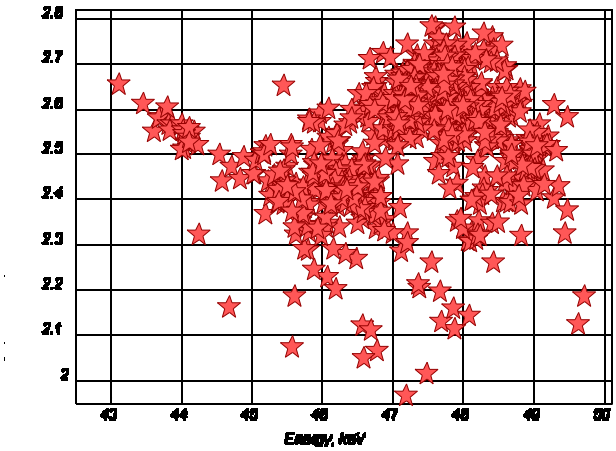

Fig. 3.3.1 *Beam ion current vs. beam energy during the 2009 campaign*

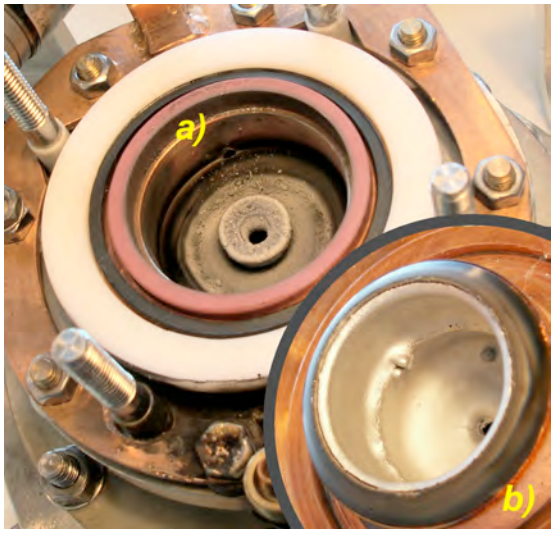

Fig. 3.3.2 *Arc discharge channel of the DNBI plasma source: a) – channel with floating electrode; b) – cathode.*

The intensive use of the DNBI with the arc-discharge plasma source since October 2006 and source inspections in December 2008 and October 2009 were used to evaluate the robustness of key elements of the arc-discharge channel (Fig. 3.3.2). The integral resource time for arc discharge cathode, anode and channel washers expected to be in the range of 3000-5000sec (2000-3000 shots in the tokamak plasma). The delivery and replacement of a replacement arc discharge plasma source is planed in December 2009 – beginning of 2010 in a contract with Budker Institute (Novosibirsk, Russia). In this way CXRS, that has become a strongly requested diagnostic on TCV, should be available for all experiments through 2010.

3.3.2 Tangential X-ray detector array

A new 6-detector, tangential X-ray diagnostic was designed and built in collaboration with RRC-Kurchatov Institute (Moscow, Russian Federation). The goal of the diagnostic is to investigate the dynamics of suprathermal electron generation, with special emphasis on fast transient events. The diagnostic assembly can be rotated in two directions, using motorised drives coupled to vacuum bellows (see Fig. 3.3.3), enabling observation along a wide range of directions in the vast majority of TCV plasma discharges.

The diagnostic was nominally completed at the end of 2008 but the amplifier electronics were found to be defective upon initial testing. The electronics assembly was shipped to Moscow for repair in December 2008 and returned to the CRPP in March 2009. Operation of the diagnostic began at the start of the 2009 TCV campaign. Initial data have been collected on suprathermal emission associated with the periodic sawtooth instability. The magnetic reconnection event causing the end of the cycle, i.e., the sawtooth crash, is accompanied by electron acceleration along the separatrix of the magnetic island, which in turn results in hard X-ray

bremsstrahlung emission. Systematic scans of the orientation of the diagnostic head are being performed to fully characterise and commission the system.

Fig. 3.3.3 *View of the X-ray diagnostic head from inside the vessel. The system is rotated to a typical near-tangential viewing direction.*

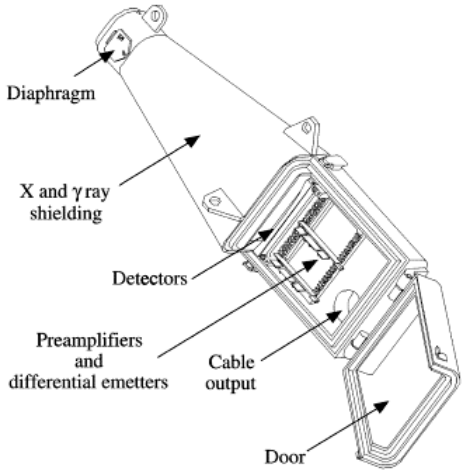

Fig. 3.3.4 *Hard X-ray camera on loan from CEA.*

3.3.3 Hard X-ray camera

A 21-chord CdTe-detector hard X-ray (HXR) camera (see Fig. 3.3.4), used on TCV during several separate periods between 1999 and 2005 on loan from CEA-Cadarache, has returned once again to TCV at the end of 2008 and is due to remain until the end of 2009 and possibly beyond. The camera is employed as a spectroscopic system, with energy resolution ~8keV in the 10-200keV range and is used to diagnose the suprathermal electron population generated by electron cyclotron heating and current drive. The instrument is employed both as a survey diagnostic and for dedicated studies of suprathermal electron dynamics in the presence of both second and third harmonic EC heating.

CEA personnel visited the CRPP at the beginning of 2009 to recalibrate the instrument *in situ*. After realignment and testing, the diagnostic has been operational since the beginning of EC operations in the current experimental campaign.

3.3.4 Hard X-ray tomography

A spectroscopic hard X-ray tomography diagnostic is being designed for TCV. This system is envisioned to comprise up to 4 cameras, of typically 20 detectors each, distributed around the poloidal plane to provide information for tomographic inversion. The primary goal is to study, for the first time, the full 2D distribution of bremsstrahlung emission and compare its poloidal dependence with theoretical predictions. One port assembly, including a rotational degree of freedom to turn the observation fan from poloidal to toroidal, has been fabricated and a second one is currently under construction. Two Beryllium vacuum windows have been procured and one already installed on TCV. In parallel, we have procured and thoroughly tested sample room-temperature solid-state detectors from leading manufacturers.

A fast (50-MHz bandwidth) prototype charge preamplifier was developed at the CRPP and is now being tested *in situ* on the vessel with one of the detectors. A choice of detector type and size together with a final design of the electronics will follow from these tests and lead to installation of the first full camera assembly in 2010.

3.3.5 Tangential phase contrast imaging

A laser imaging apparatus has been installed on TCV to study core density fluctuations with very high spatial localisation, (down to 1% of the minor radius), thanks to a tangential viewing arrangement. The diagnostic is expected to access an extremely broad spectrum of turbulence, with wave numbers ranging from 0.9 to 60 cm^{-1} thus covering both electron and ion microinstability scale lengths (ITG, TEM and ETG modes). All components have been procured and the system awaits final alignment and initial testing. The loss of a ZnSe vacuum window to a misdirected high-power microwave beam put the project on hold for several months in 2009, compounding the delay caused by the transition between a graduating PhD student and his successor. A new window has been procured and installed and the diagnostic is expected to become operational by early 2010.

3.3.6 FIR Polarimeter

A new far-infrared (FIR) polarimeter diagnostic began operating on the TCV in 2009. It operates at λ=432.5μm and uses a dual cavity far-infrared laser optically pumped by a CO_2 laser which is shown on the left side of the Fig. 3.3.5. For the measurement of Faraday rotation angles, this diagnostic uses a technique in which the polarisation of the probing beam is modulated. For this purpose, the cavity lengths of the FIR lasers are detuned to create a beat frequency of 750kHz that is equal to the difference in the frequencies of two cavities. The FIR Polarimeter has to provide the measurements of the magnetic field distribution and hence the current density in the TCV plasmas.

The installation of the diagnostic was completed in March of 2009. Then the calibration of the system was carried out and the results confirmed that the diagnostic works as expected.

The experiments with plasma showed that the changes in the magnitudes of the Faraday rotation angles, measured by the Polarimeter, correspond to the appropriate changes in the magnitudes of the currents and densities. However, the noise level and the fluctuations of the signal necessitated an improved system performance in order to achieve a sufficient resolution for its use as a diagnostic of plasma phenomena.

A number of steps for the diagnostic improvement have been undertaken. The amplifiers for the detectors were modified, adding gain and replacing the existing cables with the shielded ones. Also, an additional array of the focusing lenses was installed so that the detectors and part of the electronics, could be moved as far out of the magnetic field as possible (the assembly of the detectors and lenses above the coils can be seen on the right picture of Fig. 3.3.5). Since the stability of the beat frequency has an effect on the accuracy of the measurements, an improvement of the automatic adjustment of the CO_2-FIR laser system was also found.

First results of the upgraded FIR Polarimeter are expected in the early 2010.

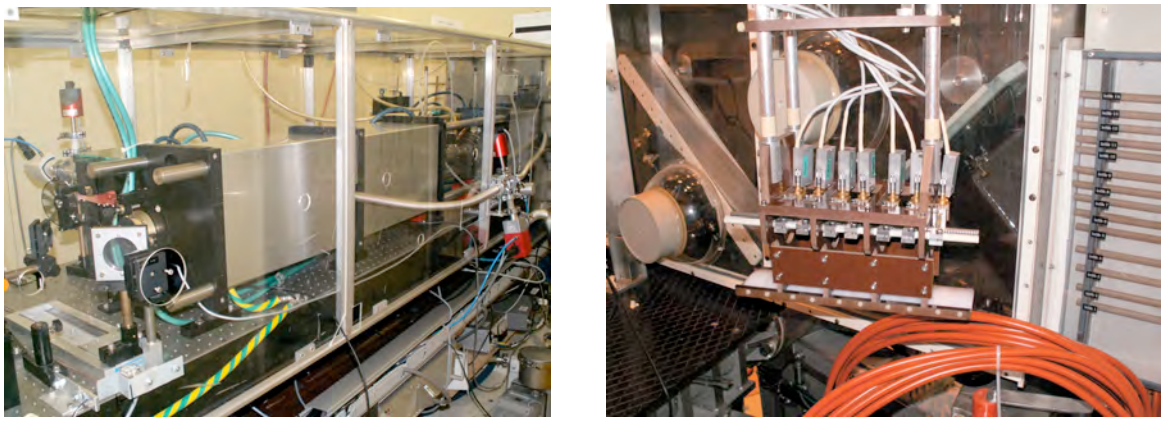

Fig. 3.3.5 *CO_2 laser used for the optical pumping of three FIR laser cavities of the FIR Polarimeter (left) and the assembly of the wave guide detectors and lenses placed above the coils of the TCV (right).*

3.3.7 Lower Hybrid Parametric Instability antenna

A loop antenna is installed in the torus of TCV for the detection and monitoring of waves (in the 0.1-1GHz range) from the lower hybrid parametric instability (LHPI) expected to occur during the injection of O-SX-B mode-converted electron Bernstein waves (EBW). The initial data acquired in piggyback experiments demonstrate the need for a spectrum analyser of higher time resolution. A device with sweep time down to 1ms has been installed and the diagnostic is now ready for EBW experiments in the somewhat transient high-density TCV H-modes.

3.3.8 EC stray power detection system

In TCV, the electron cyclotron (EC) safety system is based on the detection of the EC stray power with microwave detectors. This system has also been used as a diagnostic of the coupling efficiency, particularly useful in electron Bernstein wave (EBW) experiments where the O-SX-B mode conversion coefficient strongly depends on the plasma edge conditions and on the injection angles. In the present state, the microwave detectors can not provide an exhaustive protection of the TCV vessel due to the limited number of detectors and the larger number of vulnerable components. Some EC power injection configurations with large toroidal angles are thus, at present, not permitted.

A new EC stray power detection system using low-cost pyroelectric infrared (IR) sensors is being designed, to cover all sensitive installations on TCV. A test IR sensor was mounted on an integrator circuit, with a 1mm-thick teflon slab in front of the pyroelectric element to filter out the IR radiation and detect only the microwave power. Tests with different modulated microwave sources show that the prototype has a 2.5V/W sensitivity at 1kHz with a 2ms electronic time constant. The IR sensor prototype, (without teflon filter), was installed on TCV adjacent to a standard microwave detector for comparison. The signal of both detectors behave similarly, showing a peak one order of magnitude higher than the average signal when the EC power coupling is lost (Fig. 3.3.6). IR sensors are thus sensitive and fast enough to detect sudden high level of EC stray power and to trip off the gyrotrons.

To make a safety system out of these detectors, 20-40 systems must be built and, due to the large range of applications, a threshold system with a 1000x range is required. In the final system, each detector will be compared to an individual threshold and, should any detector exceed this threshold, all the gyrotron power will be cut within 1ms.

From the calculation side, ray tracing codes are being implemented for shot to shot operation on TCV such that the operators will receive a warning if the codes indicate any significant power not absorbed by the plasma is likely to hit a sensitive part of TCV. Most of the damage events recorded on TCV were due to an uncontrolled increase in the plasma density causing the ECH power to be deflected away from the plasma. To take this into account, the interferometer fringe count trace, proportional to the line integrated density, will be equipped with lower and higher threshold traces that will be a function of time in the plasma discharge. Again, should these limits be exceeded, the microwave power will be cut. To monitor and debug this system, the raw traces from the detectors will be recorded so that the element causing the ECH power trip can be recorded.

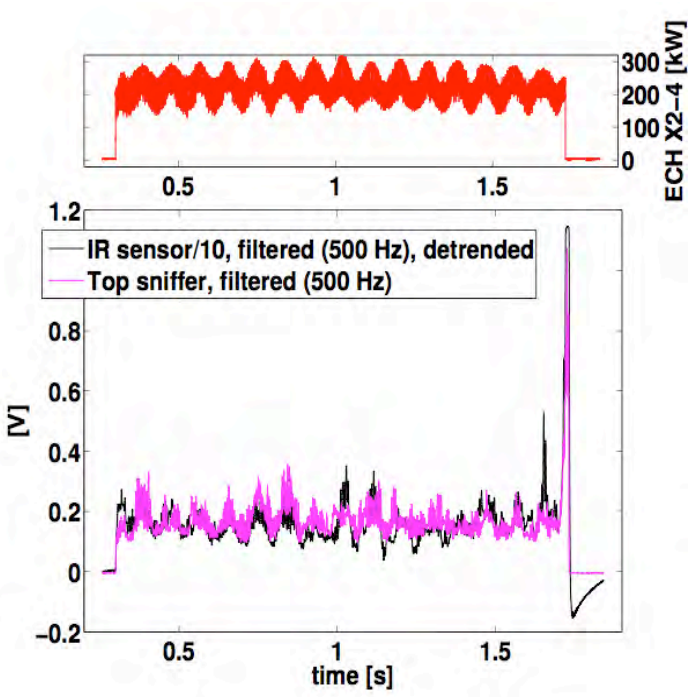

Fig. 3.3.6 *Traces of the modulated EC power (top), the microwave detector (bottom, pink) and the IR sensor (bottom, black). At the end of the discharge, the power coupling is lost and both stray power detectors exhibit a signal peak one order of magnitude higher than the average signal, which can be used to trip off the ECH power (#37084).*

3.3.9 Disruption Mitigation Valve

The Disruption Mitigation Valve (DMV) is a gas injection system based on a solenoidal valve, a bell-shaped nozzle and a skimmer. It serves two main purposes:

1. Deliver minor amounts of gaseous impurities in short, repetitive pulses for impurity studies.
2. Produce massive gas puff in one single pulse to provoke plasma disruption.

For transport studies, a valve with an orifice diameter 0.8 mm is used with backing gas pressures up to 70 bar. In this case, pulses as short as 300 us could be produced with 10^{19} atoms/pulse. On the other hand, for massive gas injection, the valve's orifice is 1.6 mm and the backing pressure 25 bar, in which case the pulses contain up to $8x10^{19}$ molecules depending on the gas type (D2, He, Ne, Ar). In 2009 the commissioning of the system was completed. The main area of exploitation will be impurity studies. However, it is foreseen that it may also be an essential tool for research connected to ELM filaments and fast ion physics by using injected gas to enhance the neutral particle density and thus the filament luminosity.

3.3.10 CXRS diagnostics and momentum transport studies on TCV

The second part of this year was principally focused on the transfer to a new PhD student of the CXRS diagnostic in TCV and the related analysis tools as well as to the main theoretical models describing plasma rotation and momentum transport.
During the last TCV opening, the alignment between the toroidal and poloidal system was performed in order to reconstruct the observations chords for both systems and to compare them to the old alignment values (Fig. 3.3.7).

Moreover, complementary experiments with reversed toroidal magnetic field were performed in TCV in order to complete a previous density scan in ohmic diverted plasmas.

Support was given during experiments performed to determine whether the up-down asymmetry of the magnetic configuration, producing a radial toroidal momentum flux, affects the toroidal rotation gradient in the outer region of TCV plasmas as theoretically predicted. Preliminary results show a variation in the toroidal velocity gradient for reversed plasmas shapes, which is in agreement with this prediction.

The CCD detector system of the CXRS was re-examined in 2009 following the assignment of EFDA support for an upgrade to faster readout systems. In recent years new CCD detectors have been developed that feature on-chip gain. Since a large proportion of the noise in CCD systems is due to the primary amplifier on the CCD chip, additional gain before this amplifier can dramatically improve the signal to noise. For radial electric field measurements, it is essential to simultaneously measure the poloidal and toroidal rotation components so at least 2 detectors are required. With the increased sensitivity, it is hoped to be able to resolve changes in the plasma rotation on times scales of 2ms (compared to typically 20ms at the present time) and/or to improve the signal to noise by a factor over 7, thus extending the operational range of the CXRS system to higher plasma densities.

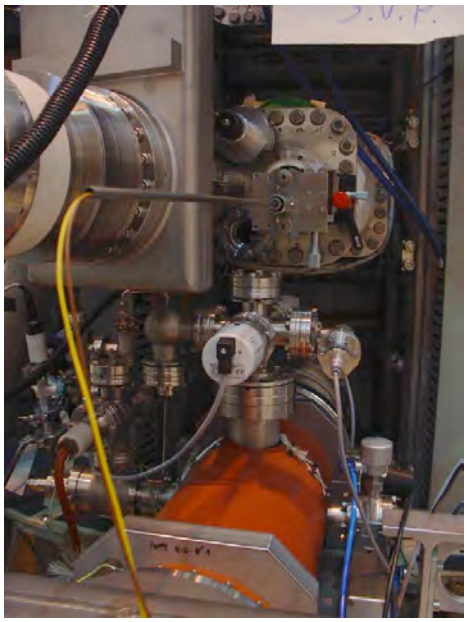

Fig. 3.3.7 *Photograph of the observation port next to the DNB injection duct (on the left of the image). The light source was introduced in the TCV chamber, at atmospheric pressure, in order to verify the alignment of the horizontal and vertical CXRS systems without the presence of somebody inside the machine vessel.*

3.3.11 Vertical ECE

Following the failure of the vertical ECE observation window due to misdirected high power ECH, a ceramic element was installed that should be considerably more robust. The transmission line to take ECE radiation to the analyser is proceeding at a relatively slow pace due to staffing limitations. All the components have, however, already been procured and tested.

3.3.12 Foil Bolometers

The foil bolometer array was one of the first multichord diagnostics on TCV. It relies on measuring the temperature change on a foil that sees the plasma directly and is therefore sensitive to all emitted energy including the emitted particle flux. Following calibration problems, all 5 cameras, consisting of 7 bolometer arrays, was dismounted from TCV and installed in a customised calibration chamber. The sensitivity and étendue of all the cameras, together with their control and analogue electronics, will be verified and upgraded before re-installation on TCV at the end of 2009 or early 2010.

3.3.13 AXUV Bolometers

The 7 dual camera bolometer array continues to cause operational problems. Although the electronics and data acquisition systems function well, the diodes appear to suffer from rapid changes in sensitivity making tomographic inversion of the detected radiation impossible. The detectors were replaced in 2008 by radiation hardened modules, but soon showed problematic behaviour.

Following extensive TCV experimentation, all the cameras have been dismounted from TCV. Examination of the AXUV diodes confirmed the previous assumption that some of the diodes had been severely damaged may have been the cause of their sensitivity degradation. In collaboration with KFK, it is intended to install

separate shutters on each array in each camera. There are serious space constrains to install the shutters and a conceptual study is ongoing. The most promising solution to date is a piezoelectric mover (this requires only a single electrical vacuum feed through). After re-installation on TCV, it is intended to keep one array shielded from the TCV plasma except for periodic comparison with the second array in each camera. By limiting plasma exposure and closing all the shutters during boronisation and glow discharge cleaning, it is hoped to use the AXUV bolometer array only when required and thus extend its operational lifetime. This diagnostic is invaluable in the analysis of the energy balance of short timescale events such as ELMs and breakdown/disruption studies.

3.3.14 Digital camera system

MultiCam is a multi camera system composed of four PCO Pixelfly visible cameras. The light coming from the plasma through a relay optics is distributed to the cameras by a series of beam splitters. In front of each camera a filter can be placed. This way each camera observes a specific part of the visible spectrum in the very same volume of the plasma.

3.3.15 Fast Camera

A fast (3000fps) 1024x1024 CMOS camera was mounted on TCV to monitor the DMV system described in 3.3.9 and to look at the possibly filamentary ELM structure from light emission in the plasma edge. In 2009, the initial fibre optic coupling was replaced by a relay optics that features both a higher throughput and considerably reduced optical distortion. The system will be upgraded at the end of 2009 with a new window on an upper tangential port to better observe the plasma edge for the fast ELM structure.

In order to increase the time resolution, the camera can declare a smaller region of interest whose frame rate can approach 100'000fps. To obtain sufficient signal on the detector surface, a mircrochannel plate preamplifier is being tested with the fast camera.

3.3.16 IR Camera

During 2009, TCV was able to borrow second fast IR camera in collaboration with the MAST group from Culham, UK. Using the CRPP and MAST cameras, simultaneous views of the central column and floor strike points were possible during ELM events. Although the analysis is still far from complete, the goal was to characterise the ratio of the energy deposition between the strike points for a range of plasma conditions and field directions which is of great interest to ITER in their effort to mitigate the effect of large power ELMs.

Figure 3.3.8 resumes the position of the two cameras and some examples of the acquired data.

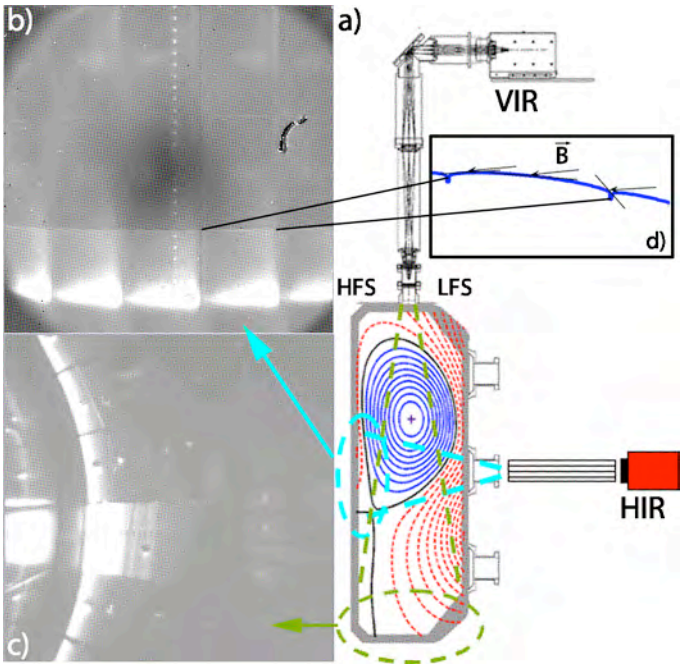

Fig. 3.3.8 *This figure showing the IR camera position and two views of the strike points on the central column and the Vessel floor. (See following text)*

a) Vertical cross-section of TCV showing the location of both IR systems and the magnetic geometry of a typical diverted SNL discharge. The hot regions in the camera images are the zones where the strike points (drawn in black) intersect the vessel's graphite tiles at the bottom and central column of the machine.

b) IR image from the HIR system (on loan from the MAST group). The triangular temperature pattern is a consequence of the tiles rounded shape - as the toroidally symmetric magnetic field intersects the rounded tiles, it will have a higher incident angle near its right edge facing the magnetic field than the centre or left hand side, where the intersection angle is smaller (see d). The vertical line of small bright dots near the image centre correspond to the central column Langmuir probe positions.

c) IR image from the VIR system. The heat deposition zone can be seen as a circular ring, with the not-cleaned tiles just below the centre emitting significantly more radiation than the others. Reflections of the radiation from the vessel floor tiles can be seen on the central column (left hand side), as well as tile holding screws and the floor Langmuir probes (e.g. above the screw of the central uncleaned tile). The bright stripe over the probes and the screw corresponds to an ELM filament, of which a smaller, more narrow example can be seen to the left of the screw.

d) Magnified schematic of a central column tile, showing the variation in tile surface-magnetic field line intercept angles.

3.3.17 Thomson real time control system

A real time control algorithm was developed for the Thomson scattering system. It is based on a Simulink template which is readily implemented into the TCV real time control system. It provides an algorithm to trigger the Thomson scattering diagnostic on repetitive MHD modes such as ELMs and sawteeth. This became

necessary for the measurement of the edge pedestal properties in a H-mode discharge with low ELM frequency, where the probability of coincidence of a Thomson laser pulse measurement at an ELM event is low. The aim is therefore to improve the probability of measuring the pedestal evolution during an ELM event which can, for example, give insight in the maximum pressure gradient and bootstrap current fraction closely before the ELM crash. These measurements would provide precious information in the attempt to model ideal MHD stability of the H-mode pedestal.

3.4 TCV control and acquisition

3.4.1 Acquisition changes

Following the introduction of new, SCSI based, controllers for our legacy CAMAC acquisition, all but a couple of the ~18 crates have now been updated. Together with the introduction of Linux based data hosting machines, the acquisition time of almost a whole TCV data cycle is now completed in less than 2 minutes from the end of the plasma discharge. New acquisition is now entirely accomplished using EtherNet linked acquisition modules that also fall within this time.

The remaining major challenge is to migrate as much of the TCV control and data storage away from our rather old VMS machines to UNIX machines such that preliminary data analysis following the shot acquisition can be completed within 3 minutes of the discharge termination. Our UNIX-based tape backup system has also been migrated to a compatible environment and the result should be a decrease of almost an order of magnitude in the data access time to stored data. It should be recalled that this speed is required for TCV to be technically capable of firing a discharge every 10 minutes that the power supply systems were designed for.

3.4.2 Real time control

A new distributed, multi-channel real time control system is currently being integrated and tested on TCV. This provides the ability to obtain real time information from several diagnostics, such as soft x-ray, photodiodes as well as magnetic coils and loops to control the whole TCV actuator set including the coil current power supplies, gas valves and microwave heating systems (launcher angles and power). The system consists of real time nodes linked by a real time network. Each node in the network may consist of differing combinations of data acquisition cards (acquiring up to around 200 signals), analogue & digital output cards and computers. The network enables data to be shared between the nodes in real time and is based on Reflective Memory technology. This provides a memory area which is shared between each node in the Reflective Memory network. When one node writes to an address inside the shared memory, the data is transferred around the network and appears at the same memory address inside the other nodes.

The real time control system is being designed to be simple to program and set up, yet extremely powerful. The algorithms for the control are entirely developed and tested inside a Simulink template of the whole control system. They can be tested against models of the system response and using data acquired from previous plasma shots. Simulink, together with the real time workshop embedded coder

automatically generates the real time code from the Simulink model for each node on the network. Plasma shape control as well as profile, current and instability control are all planned to be implemented on the new control system. Additionally, the control system will trigger diagnostic systems in response to interesting events occuring within the plasma. For example, the Thomson measurements of the plasma temperature and density profile requires a laser pulse which will be triggered by the control system when a diagnostic detects an event, for example an edge localised mode (ELM). In this way, the event can be more closely analysed and studied, potentially leading to a deeper physics understanding of the processes involved in such an event.

3.5 TCV upgrades

3.5.1 Introduction

We expect TCV to continue playing an important role in the future international fusion research effort. This includes testing novel concepts, contributing to answering the many physics questions, which regularly arise as the ITER project grapples with concerns old and new, as well as training new generations of fusion scientists. The upgrade studies which are underway aim at extending the operational domain of TCV towards increased ITER relevance, as well as for fundamental physics studies. In terms of physics parameters in particular, they thrive towards achieving higher normalised pressure β_N, a wider range of accessible temperature ratios (T_i/T_e) and lower collisionality, as will prevail in a reactor. This implies enhancements of the heating systems as well as improvements in plasma control, notably ELM control. One of the hallmarks of the TCV device is its unmatched configurational flexibility, with the possibility of exploring new plasma shapes and divertor configurations. The planned upgrades therefore should not only improve our ability to investigate the physics of standard (ITER-like) configurations, but also of unconventional plasmas. Both negative triangularity plasmas and highly elongated plasmas in L-mode have up to twice the confinement time of their conventional counterparts, but could so far not be produced in H-mode or indeed (for high elongations) produced with auxiliary heating. Therefore a lot remains to be learnt from TCV when equipped with the full range of enhancements currently under study.

These enhancement aim at:

- **Improving MHD control.** TCV has already demonstrated the vast potential of controlling MHD by local ECH and ECCD in low density plasmas (e.g. local magnetic shear control for sawtooth control and for controlling eITB's). At higher densities no such tools are available. The one type of instability which has most hindered progress in H-modes in TCV are the ELMs. This is partly due to their irreproducibility, partly to their often large size (leading to a loss of plasma position control) and in some cases due to density control in the absence of ELMs. We therefore think that it is essential to provide TCV with effective ways to mitigate or suppress ELMs, whilst controlling heat and particle flux through the edge transport barrier. This is the main goal of an integrated saddle coil system currently under design. The system will also be able to produce error fields and compensate for existing error fields and will be integrated with the vertical control system.

- **Enhancing the capability of heating high density plasmas and achieving higher normalised plasma pressures**. Heating at higher density than has been possible so far may be achieved by a power increase of the 3rd harmonic EC system (X3) or a neutral beam heating system or a combination of both. In ELMy H-modes the highest normalised pressures correspond to β_N=1.9 with 1.5 MW of X3 power. In order to attain the β limit (β_N~3) an extra 2MW should be available, assuming a power degradation exponent of -0.5. Since some of the plasmas would be of negative triangularity with divertor strike zones at the low field side, an improvement of the LFS inner wall power handling capability will be necessary.

- **Increasing the ion to electron temperature ratio (T_i/T_e) by directly heating the ions**. Currently, ECH plasmas have Ti/Te in the range 0.1-0.5 typically, which is clearly outside the ITER relevant range. This is due to the inherently weak electron-ion coupling in small devices. For bringing this ratio to near unity the implementation of an NBI system is under investigation. An NBI system would also be a versatile tool for studying energetic particle physics.

3.5.2 Saddle coil system

The upgrade project for TCV includes the installation of a set of saddle coils, namely the saddle coil system (SCS), to allow ELM control, error field correction and vertical control. Other experimental applications, like Resistive Wall Mode (RWM) control and mode rotation, are also in view.

Motivations

ELM control

Edge localized modes (ELM), related to the high confinement regime (H-mode), lead to a degradation of the plasma confinement and a release of energetic particles towards the vessel walls. Scaling the current experimental data to ITER predicts that the power flux related to ELMs will cause an intolerable erosion and heat load on the plasma facing components. Experiments on DIII-D, JET and MAST have demonstrated that the application of resonant magnetic perturbation (RMP) is able to mitigate or suppress ELMs while keeping sufficient confinement properties. The current explanation of this phenomenon is based on the overlap of the magnetic islands created by the RMP that generates an ergodic zone in the plasma edge, itself increasing the outward transport and thereby limiting the pedestal gradients to values below the instability limits. This description is, however, still incomplete as the weak effect of RMP on the pedestal electron temperature remains unexplained. The limits of the process, in terms of operation domain, are not yet accurately known, DIII-D being up to now the only Tokamak where a complete suppression of ELMs has successfully been obtained. In addition, experiments in different Tokamaks reveal opposite results for similar conditions, for example RMP can trigger ELMs during ELM-free phases in NSTX and COMPASS. With that respect, TCV (Tokamak à Configuration Variable) unique plasma shaping and positioning capability could extend the range of accessible magnetic perturbation modes for a given RMP coil system geometry and contribute to a clearer description of the conditions required for ELM suppression.

Error field correction

Error fields are another aspect of toroidally asymmetric magnetic fields. They are created by construction tolerances in tokamak coil positions and shapes. These fields, dominated by low values of the toroidal mode number, induce plasma braking and locked modes, themselves responsible for disruptions. Their effects can be corrected by applying an asymmetric field in opposite phase, as provided by a SCS. Measurements have shown that these fields are non negligible on TCV and that their correction could be beneficial to the operation of the machine.

Vertical control

Vertical control is required to stabilize the highly unstable vertical position of the plasma. It is obtained by applying an axisymmetric radial magnetic field. The growth rate of vertical modes is such that the vertical control coils need to be located inside the Tokamak vessel to avoid screening of the control field. TCV already has a vertical control system, namely the internal fast coils. Due to the lack of free space inside the vessel and to the required number of feedthroughs, it would be difficult to have both a new SCS and the actual fast coil systems coexisting in the machine. Therefore, the fast coil system must be removed and the SCS must be designed to provide the vertical control functionality.

Rotation control

Generally, stationary asymmetric magnetic fields result in a toroidal plasma braking, as observed in the case of strong error fields. For higher toroidal harmonics, perturbation fields can also lead to counter-current toroidal acceleration, as reported recently on DIII-D. This effect could be of particular interest for TCV, since no NBI source is present to produce external momentum source.
Tearing modes are regularly present in tokamaks. In TCV, their frequency is typically in the range of 5 kHz. A SCS powered with a high bandwidth source could, taking into account the vessel screening, open a field of research on the interaction of these modes with rotating perturbations, especially on the question of stability and phase locking of the modes.

RWM correction

Resistive wall modes are ideal MHD instabilities that are not stabilized by the vessel wall because their growth is slower than the resistive time of the vessel. A SCS covering a sufficient portion of the wall could be used as a way to actively reproduce the wall screening on slower time scales, following the smart shell principle demonstrated on RFX.

Physics driven design

Coil system topology

A large variety of geometrical arrangements have been qualified, including ex-vessel and in-vessel coils. The ex-vessel solution was discarded due to a large distance from the plasma and the screening of the conducting vessel for AC operation, both implying an excessively large coil current. For the in-vessel option, given the toroidal periodicity of TCV and the large variation in the plasma shape and position, a set of 3 rows of 8 coils is envisaged. This coil configuration was shown to produce the adequate edge magnetic ergodization and to offer the required flexibility for an experimental approach of the ELM control and mitigation method using saddle coils. For internal coils, the space between the vessel and the protection tiles must be increased to accommodate the coils. A total distance of 4 cm between the surface of the tiles and the vessel has been chosen as a trade-off between the space required for the coils, the decrease of plasma minor radius (0.8cm in this case) and the passive stabilization provided by the vessel.

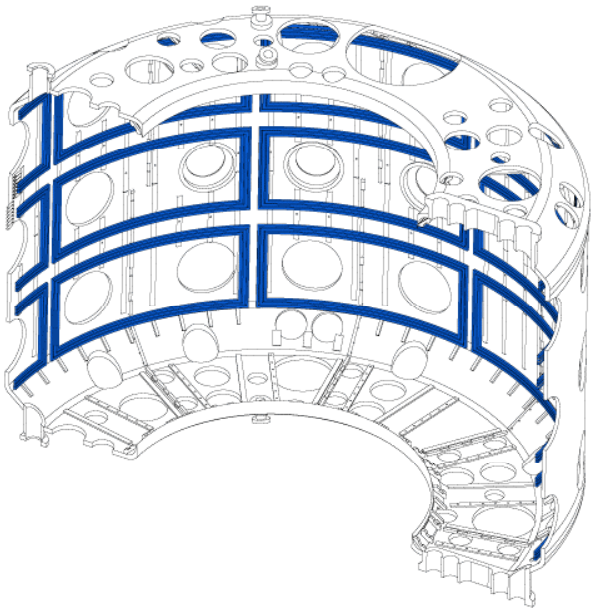

Fig. 3.5.1 *Saddle Coil System (SCS) for TCV.*

Spectral characterization

The magnetic perturbation created by a SCS can be characterized in terms of space spectrum, applying a Fourier transform along both poloidal and toroidal dimensions on each flux surface of interest. The spectrum of the magnetic field perturbation is a function of the coil locations and relative coil currents. Due to the small number of coils and to their identical geometry, spectral degeneracy occurs, consequently limiting the number of controlled simultaneous modes provided by the SCS. A simple theory, based on the combination of the real-space Fourier transform of a the perturbation due to a single coil and the current-space Fourier transform of the current distribution of a set of equivalent coils, is used to entirely characterize the spectral limitations of a SCS. In the case of TCV, 5 orthogonal classes of n are available {0; 1; 2; 3; 4}, with main degenerate pairs {0; 8}, {1; 7}, {2; 6} and {3; 5}. For classes n=1, n=2 and n=3, the 3 coil rows allow a maximum of 3

simultaneous targets per class, while for classes n=0 and n=4, only 1 target per class is allowed (with simultaneous spectrum optimization if independent power supplies are used). The toroidal periodicity results in maximal gains for each row as follows: g({0;4})=8, g({1;3})=4.3 and g({2})=5.6, where g is the gain of a perturbation amplitude for 8 coils with respect to the amplitude given by a single coil. For class 3, the degeneracy between n=3 and n=5 and the small spectral distance between these modes implies a non negligible effect of n=5 modes when working in n=3 configurations.

Current requirements

Experimental values provided by DIII-D and JET and island overlap calculations indicate that ELM control would require 4kAt on TCV. For vertical stabilisation, currents of the order of 5kAt are required to provide a control equivalent to the actual fast coil system. Experimental measurement of error field on TCV have lead to the conclusion that 3kAt would be required for its correction.

Inductance and response function calculation

Due to the presence of the vessel wall close to the SCS, the apparent self and mutual inductance of the coils are a function of the coil current frequency. To quantify the frequency dependence, the wall is assumed to be equivalent to a number of saddle-shaped filaments similar to the coils. The self and mutual inductances are then calculated for each element in the SCS – wall system. The electrical behaviour of the system is finally obtained by solving the linear voltage and current equations. Knowing this behaviour, the apparent self and mutual inductances can be deduced.

In terms of power supply design, it is more convenient to obtain an approximate response function of the SCS – wall system. As the equations describing this system are equivalent to a Linear Time-Invariant (LTI) model, the LTI standard tools can be used to extract the dominant features of the SCS and return the response function relating the input voltage to the output current as a function of frequency.

Screening calculation

In AC operation, the magnetic field produced by the SCS is partly screened by the magnetic field produced by the image currents induced in the vessel wall. The apparent inductance calculation described above also returns the wall currents, which can then be used to calculate the effective magnetic field on the coil axis. The results show that for a distance of 2 cm between the wall and the coils, only 20% of the magnetic perturbation remains at saturation (above 5kHz).

Force calculation

The magnetic forces created by magnetic fields perpendicular to the coil current are assessed using a worst case approach. The magnetic sources considered in this study include the whole set of TCV's coils, all powered at their nominal currents, a family of plasma current density, the vessel currents at disruption and the SCS itself. The fields are added up in absolute value at each coil location. The current flowing in the SCS is taken as the 12 kAt given by the combination of the three experimental applications added to the worst case disruption induced current,

assuming a closed loop SCS. This yields a maximal toroidal force of 40kN/m, radial force of 52kN/m and vertical force of 40kN/m.

Optimal current distribution

When a SCS is fed with independent power supplies, the effectiveness of the created perturbation may be enhanced by a fine-tuning of the relative distribution of currents in the coils. We have developed a method of optimization of the currents of generic radial field coil systems based on Lagrange multipliers, working in real current space. This method is not limited to evenly spaced identical coil systems and makes simultaneous multi-mode optimization possible. It would therefore work even if one of the coils becomes unavailable. Using a Lagrange method allows us to distinguish between constraints to satisfy exactly – e.g. the corrected error field – and optimization of cost functions – e.g. the minimization of core islands in the case of ELM mitigation. The Lagrange method is an efficient way to minimize parasitic modes and current requirements while imposing the amplitude and phase of a number of target modes. Applying this optimal current method to a number of study cases has revealed that independent coil powering represents a real benefit for the experiments.

Power source requirements

Each experimental application described above requires different values of the toroidal wave number of the perturbation created by the SCS. Vertical control requires n=0, error field correction n=1 and ELM control n>1. The other applications would also require a range of values of n. Therefore, independent power supplies are required for each coil in the system. In addition, using independent power supplies is the only way to optimize the perturbation spectrum as described in the previous section.

In terms of required bandwidth, the lower limit is given by the principle of equivalence to the actual vertical control system. This system is able to deliver 6kAt in 250μs. Following these characteristics, mode rotation would be limited to 1kHz, which is below the average mode frequencies observed in TCV (approximately 5kHz). Higher bandwidth could therefore be desired, as long as the additional complexity remains tractable.

Current requirements have been described above and add up to approximately 12kAt. Other coil electrical characteristics, like inductance or frequency response are available.

Technical design

Power supplies

24 independent fast power supplies are proposed as the final design. The previous idea of decoupling fast and slow power supplies, keeping only one fast power supply feeding all the coils in serial connection (n = 0 for vertical control) , has been abandoned due to the loss of experimental prospect and the technical complexity it would imply.

The preliminary design is based on 24 inverters supplied by a common DC source. The inverters would be based on Insulated Gate Bipolar Transistor (IGBT)

semiconductors. Metal-Oxide-Semiconductor Field-Effect (MOSFET) based inverters are also under investigation.

The number of turns in each coil is determined by the optimal current/voltage ratio, the optimization being based on the price of IGBT semiconductors. A market study has shown that from 10 turns and above, the price of the IGBTs stayed constant, while increasing rapidly under 10 turns. 25 turns are recommended for an IGBT based power supply in order to avoid parallel connection of semiconductors. This aspect has a strong impact on the mechanical design of the coils, since the turns must be packed together if more than 3 turns are used.

A power supply pre-design using the technology described above is now available.

Winding design

Tokamak environment has a strong impact on the choices leading the design of the coils. The coils must not deteriorate the quality of the vacuum established in the vessel, the coil turns must be insulated and this insulation must resist large changes of temperature as well as plasma activation and radiowave radiation. The coils must be able to withstand large forces while being as radially flat as possible to minimize the loss of plasma radius. Finally, putting the coil in a steel casing is forbidden since screening must be avoided. Different choices of material and insulation methods have been advanced, but no final choice has been made yet.

The mechanical design of the coils is driven by two main constraints: the resistance to thermal and magnetic forces and the minimization of space occupation. A “sandwich” design has been proposed. It consists in superposing flat coil turns in the radial direction, therefore combining several advantages: both connections are in the same radial plan as the coil, each turn covers the same surface, a variety of insulation types can be chosen between turns and the mechanical rigidity is good. However, the final decision regarding the mechanical design has not been taken yet.

Feedthroughs

A feedthrough design allowing the passage of 4 electric lines per porthole has been proposed. This design is able to withstand radial and vertical mechanical shocks. The number of available portholes is sufficient to connect all the coils.

In-vessel routing

A routing plan of the in-vessel connection lines has been drawn. No major difficulties have appeared in the process.

Coil mounting support

A preliminary design of coil mounting support has been proposed. This design accounts for the available mounting points on the inner wall of the vessel. It is now being analyzed with respect to the magnetic forces and thermal stresses.

3.5.3 Neutral beam heating for TCV

There are four ports currently available, allowing access for suitably narrow neutral beams. Two of the ports have a 15cm circular aperture and allow access at angles of ±11.5 degrees, corresponding to a tangency radius R_{tan} of ±23cm. One of these ports is currently occupied by the TCV diagnostic neutral beam. The two other ports are more tangential with R_{tan}=40 and 63cm, for duct diameters of 12 and 10cm respectively. A precise assessment of the power that can be transmitted through these ports requires a fairly detailed duct design in collaboration with a prospective supplier. This has been deferred to a later stage in the feasibility study. Options requiring a cut in the vessel for better tangential access, as considered last year, have been excluded as technically unfeasible.

Orbit confinement calculations have been made for these geometries. The results are little changed from those presented last year. Shine through and tile heating restricts operating densities to above about $4\times10^{19}m^{-3}$ for R_{tan} of 23cm and R_{tan}=40cm and an injection energy of 20keV. For R_{tan}=63cm the incidence angle on the tiles is small and the minimum density below $2\times10^{19}m^{-3}$. Orbit losses provide a lower plasma current limit, which in co-injection at a beam energy of 20keV is about 250kA for R_{tan}=23cm and R_{tan}=40cm and about 100kA for R_{tan}=63cm. Counter-injection is always worse. Heating efficiencies for R_{tan}=23cm and R_{tan}=63cm are shown in Fig. 3.5.2.

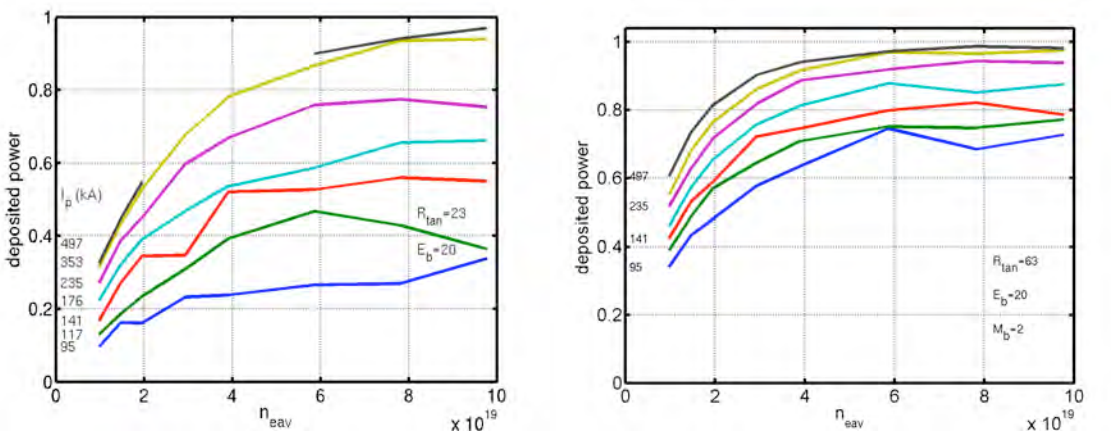

Fig. 3.5.2 *Monte-Carlo calculations of heat deposition for a range of densities from 1 to $10\times10^{19}m^{-3}$ and plasma currents from 95 to 497kA, assuming typical monotonic density, temperature and current profiles. The Deuterium NBI energy was assumed to be 20keV. Left: for a tangency radius R_{tan}=23cm. Right: R_{tan}=63cm.*

At the low densities typical for eITB experiments ($10^{19}m^{-3}$), slowing down times are of the order of 0.1s. In the absence of other losses, this would lead to extremely high fast ion pressures and beam driven currents, even with only 0.5MW injected. This means that ion heating matching the level of ECH (1-3MW) in these experiments is impossible, however it opens up the possibility of a range of fusion-relevant energetic particle physics investigations, since fast particle induced instabilities would certainly be encountered. At high densities too, fast ion fractions are significant, without however precluding ion heating. ASTRA simulations taking an achieved 1.5MW X3 ECH ELMy H-mode plasma with $T_i/T_e\cong0.5$ as a target, suggest that for 1.5MW ECH and 1MW NBI, $T_i/T_e\cong1$ can be achieved.

3.6 Superconductivity

On January 12th 2009, the engine of the main compressor of the SULTAN cryo-plant failed. Post mortem investigations found that the reason for the failure was some short circuit inside the winding of the stator. The likely reason for the short is mechanical friction, which occurs at the start up of the engine, when "kick currents" over 1kA induce shacking of the winding in the region where the main leads of each phase are soldered to the windings of each slot. After 25 years of operation and several hundred start-ups an internal short in the winding led to an over-current in one phase, which destroyed the connection box of the engine, see Fig. 3.6.1. No short to ground was observed. The control system shut down with the "over-heating" notice.

The company Meier, also responsible for the maintenance of the engine, was trusted with the repair. The engine was removed from the helium compressor on January 16th and transported to Regensdorf. The full winding was cut away and replaced by a new electric winding. The repaired engine was delivered to CRPP on March 4th 2009. The refrigerator was re-started on March 7th. The test operation in SULTAN was resumed on March 12th after re-cooling the facility. The interruption of the test operation lasted overall 8 weeks.

Fig. 3.6.1 *Damage of the electrical engine due to over-current in one phase, January 09*

In July 2009, a new ±40V, ±300A power supply of the superconducting transformer (current source for the SULTAN sample) was put in operation to replace the old one (±10V, ±300A). It is a constant current regulated Buck converter with IBGTs in H bridge configuration. The PS is equipped with 20 bits, thermally controlled DAC to generate precise reference voltage for current regulation (linear ramps, triangular cycles and sinusoids). This last option allows substantially increasing the cyclic loading rate in the sample, a factor of two has been already achieved, corresponding to over 50 cycles/hour 0-68kA, see Fig. 3.6.2, using a maximum voltage of about 18V. Further efforts are ongoing to investigate the limits of the system, the main restriction on the cycling rate being given by the quench detection system (QDS), where the rejection of the inductive component of the voltage works reasonably well

during smooth voltage variations but fails during fast transients. The sinusoidal excitation guarantees the absence of voltage discontinuities and simplifies the rejection of the inductive component. However, the absolute amplitude of the voltage from the QDS now exceeds the range of the data acquisition modules. A partition of the voltage signals will enable the future exploration of higher current rates, at the price of reduced accuracy of the QDS.

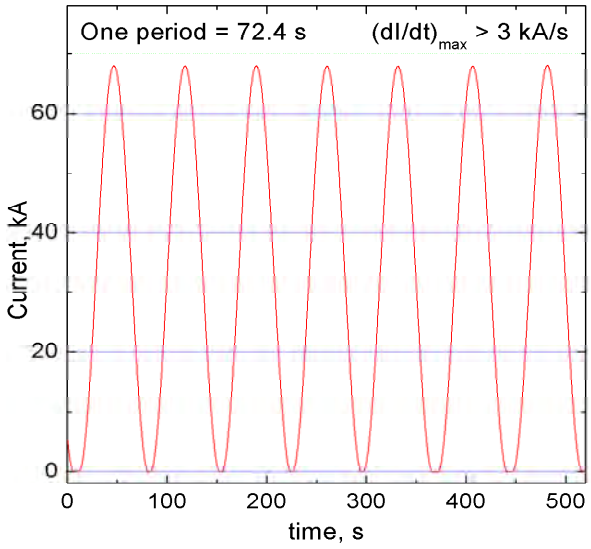

Fig. 3.6.2 *Current in the SULTAN sample at cyclic loading. 0-68kA-0 with the new power supply for the primary winding*

3.7 Gyrotron for Dynamic Nuclear Polarization Enhanced Magic Angle Spinning Nuclear Magnetic Resonance Spectroscopy[1]

During 2009 the activity in this project has evolved from the design phase to the construction phase of the frequency-tunable gyrotron system. Within the frame of the 'Requip' funding, consisting in a combination of funds from SNSF, EPFL and FSB, all the contracts with industries have been placed for the purchase of the scientific equipment designed by CRPP.

Since March 2009 the activity on the 'CRPP side' is carried out by a post-doc funded by 'Sinergia', who is responsible for the design finalization, contract follow-up, construction, testing and system integration of the gyrotron system. All internal elements of the gyrotron are presently designed and a significant number of meetings with the gyrotron manufacturer (Thomson Electron Devices, France) have been carried out in order to properly address all the complex technological issues associated with the gyrotron manufacturing. Figure 3.6.3 shows the designed gyrotron assembly inserted into the 9.7T He-free superconducting magnet.

[1] Work not belonging to the EURATOM Association's work programme.

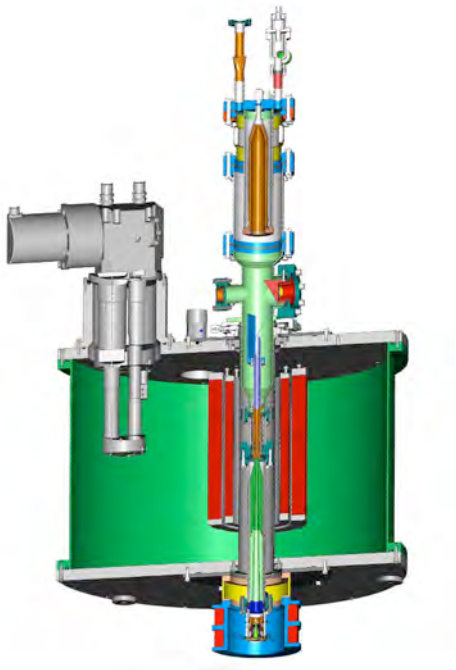

Fig. 3.7.1 *Layout of the designed gyrotron mounted inside the 9.7T He-free superconducting magnet.*

Auxiliary systems such as HV power supplies, RF diagnostic systems for characterizing the RF spectral properties and the spatial mode distribution of the radiated RF beam have been presently procured and characterized. An important effort, which includes a significant contribution of the CRPP services, is devoted to the preparation of the laboratory in which the tests and characterization will be carried out. The design of the gyrotron control and protection system as well as different additional diagnostics is ongoing. It is expected to have the gyrotron system fully characterized at CRPP by mid 2010.

In parallel to this activity, and in collaboration with the second post-doc also funded by the 'Sinergia' grant, the first integration of the gyrotron system on a NMR spectrometer for performing a preliminary DNP-NMR experiments is foreseen at the Institute of Condensed Matter Physics (IPMC) on a 14T NMR spectrometer with a sweep coil. The "gyrotron-DNP" research activities are discussed in weekly meetings with all members from CRPP, IPMC and the Laboratory of Biomolecular Magnetic Resonance (LRMB) active in this research field. The global DNP activity, which includes "Dissolution-DNP", "Gyrotron-DNP" and "Photo-excited triplet state DNP", is coordinated within the Swiss DNP Initiative (http://sdnpi.epfl.ch/)

4 ACTIVITIES IN SUPPORT OF ITER

4.1 Introduction

In this section we assemble a large fraction of the work performed by the CRPP in 2009 for the ITER project, which has assumed an increasing importance over the last few years. Since most of the research programme of CRPP is linked to fusion development in general, and therefore to ITER in particular, the distinctions are sometimes artificial and work for ITER still appears throughout the report. However, we have identified those areas in which the work carried out is clearly in direct support of the project.

4.2 ITER 170GHz/2MW Coaxial Cavity Gyrotron

4.2.1 Summary of the activities

After the First prototype 2MW/170GHz/CW Coaxial gyrotron testing period, which ended in October 2008, the tube was shipped back to TED for an opening and an inspection before a refurbishment, as was contractually foreseen.

The initial plan was to replace a minimum of subassemblies, with a minimum of redesign, the main change consisting in replacing the launcher to install a promising version developed at FZK, (and tested in the mean time).

The inspection of the tube revealed unexpected damages in the gun region as well as in the cavity-launcher region. It is presently believed that some of these damages may be related to voltage stand-off problems which seem to be associated to the existence of magnetic and electric field configurations, in the gun region, allowing to potentially trap secondary electrons.

On the other hand, no damages was seen on the following elements, which were potentially critical such as the collector (tested at 2MW/10s), body-collector insulator, water loads, beam tunnel and DC breaks.

4.2.2 Identification of the cause of the damages

The observed problems sources are not clearly identified. Nevertheless, some studies have been carried out and have permitted to outline some guidelines for the improvement of the tube behaviour.

- A more detailed computation of the electron beam properties allowed the determination of its properties more accurately. In particular, the beam spread is higher than expected and could explain the lower than expected rf output power.
- The existence of magnetic potential wells and of possibly trapped particles has been deeply investigated. It appears that regions of the cathode and the coaxial insert where damages have been observed intercept magnetic field lines, which guide trapped particles. Although the underlying physical phenomena need more investigations, they are potential candidates to

explain the poor voltage-standoff properties of the tube. To corroborate this hypothesis, voltage standoff tests were made in a potential wells free magnetic field configuration. The improvement of the standoff properties was spectacular.

4.2.3 Refurbishment

Because of the numerous problems encountered during the operation of the tube, and confirmed by the opening and expertise, it was decided to activate most of the options of the refurbishment, but also to allow a higher level of redesign.

- The electron gun was completely redesigned at CRPP, with the additional criteria:
  - Improvement of the electron beam characteristics (spread)
  - Decrease of the electric fields on the different anodes
  - Suppression of any magnetic potential well
  - Suppression of the possibility to have trapped trajectories

- In order to suppress potential parasitic rf oscillations close to the electron cyclotron frequency, the beam tunnel was redesigned by KIT (see further) to include corrugations in the copper rings, to make the shape conical, and to increase its length.

- The launcher and internal mirror system have been significantly improved.

4.2.4 Short pulse experiments at KIT

In parallel to the CW tube development, the short pulse (1ms) experiments at FZK have continued and allowed testing some of the proposed solutions:

- The corrugated bean tunnel concept was validated on 2 gyrotrons (the pre-prototype, and the multi-frequency tube). The rf parasitic oscillations have almost disappeared.
- The improved version of the launcher was successfully tested, leading to a Gaussian content of the order of 95%.
- A gun, similar to the one proposed for the refurbishment, will be tested soon.

The result of these modifications is a record output power of 2.2MW corresponding to a 30% efficiency (without single stage depressed collector).

4.2.5 Prospects

A contract for the refurbishment has been signed between F4E and Thales on July 2009. The refurbished tube is expected to arrive in Lausanne for tests by end of June 2010, leaving 4-6 months of experiments before the 1MW/cylindrical – 2MW/coaxial decision point.

A maquette of the refurbished gun will be delivered in February 2010. It has been designed to be flexible, in order to validate the proposed gun design, but also to give the possibility to make deeper studies of the potential wells, the trapped particles, and their influence on the voltage stand-off properties.

4.2.6 Gaussian content estimates

In parallel to the 170GHz/2MW development, a PhD student (Sudheer Jawla) is finishing his thesis. He developed a formalism to estimate the lowest order mode content (Gaussian content) of a coherent microwave beam satisfying the paraxial approximation.

The presently generally adopted method to estimate the Gaussian content is to find a set of beam parameters (beam waist, beam waist position, misalignment, etc..) which will maximize the projection of the reconstructed filed pattern (amplitude and phase) on the lowest order mode.

The method developed here considers a mode mix of MxN modes with unknown power coefficients. The beam parameters are then optimized to minimize the error between the reconstructed field and the one given by the mode mix. The Gaussian content is then the (0,0) coefficient of the matrix.

It was shown that the original method can be inaccurate and may lead to wrong results especially for the cases of rf beams with low Gaussian content. As an example, the theoretical Gaussian content of the first prototype output beam was initially estimated to 76%. The new method gives only 50%.

The applicability of the new method to actual experimental data (i.e. with noisy signal and a dynamic of the order of 15dB) is presently under investigation. Initial considerations show that the dynamic should be significantly increased to allow a good estimation of the output beam Gaussian content.

4.3 The ITER gyrotron test stand at CRPP

In 2009, the test facility has not been used for gyrotron testing purposes since, as mentioned in the section above, the prototype has been returned to factory for investigation and improvement. This period has been mainly dedicated to the installation and tests on-site of the Main High Voltage Power Supply (MHVPS) as described below in more details.

4.3.1 MHVPS

This power supply will be connected to the gyrotron cathode and will be able to operate in continuous mode (DC) in order to comply with the development of the CW ITER gyrotrons. CRPP is responsible to follow the procurement contract passed with the industry (OCEM, Italy). This task implied to review regularly the design choices proposed by the industry, to ensure the on-site integration, to follow the acceptance tests and to participate to the progress meetings foreseen in the framework of the contract agreement.

During the last quarter of 2008, the MHVPS equipment has been integrally installed at the factory in order to demonstrate the design compliance with the specification requirements. The factory acceptance tests were passed successfully in the third week of December. Only minor points necessitated an on-site improvement prior to shipment to CRPP.

January 2009 has been dedicated to the dismounting and to the transport from Bologna to CRPP. The Swiss company, Friderici, has been selected to ensure the transport, the unloading and the installation of the transformers at their final places in the basement of the CRPP laboratory hosting the ITER gyrotron test stand. The pictures below are presenting part of this complicated task, which took place beginning of February.

Fig. 4.3.1 *Unloading of one of the transformer (19 tons).*

Fig. 4.3.2 *Unloading through the trap door into the basement.*

Following the transformers installation, during one month, the company in charge installed the rest of the equipment: 128 power modules, AC distribution cells and the 5MW/20sec resistive dummy load to be used during the final tests on-site.

Fig. 4.3.3 *Front view of the 128 power modules placed in an isolated frame and cooled down with demineralised water.*

Fig. 4.3.4 *AC 20 kV cells, including the start-up system limiting the transformer inrush current to the nominal value.*

The factory tests took place in two sessions: first week of April and the second of May 2009. All the tests specified have been passed successfully. During the two sessions, several modifications required have been brought by OCEM to the installation to be fully compatible with the HV standards. The characteristics reported below are showing few output results recorded during the tests applied to the MHVPS equipment on-site.

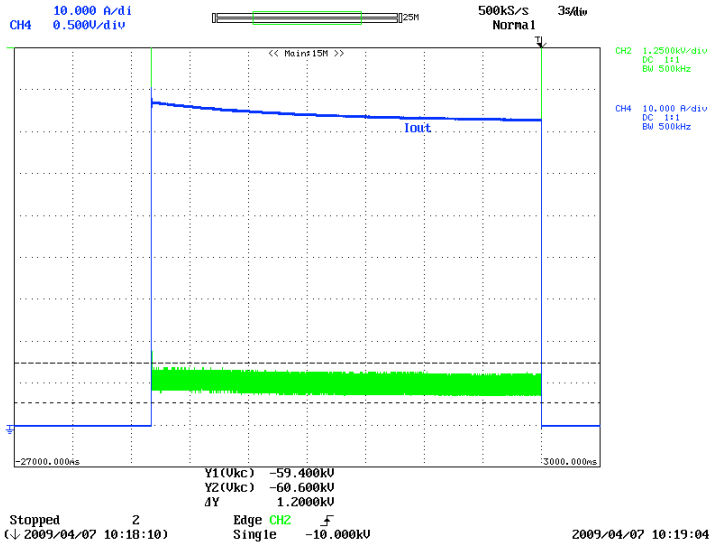

Fig. 4.3.5 *20 sec pulse on dummy load:*
Blue trace: Output current, 10A/div, decreasing along the pulse since the dummy load is warming up
Green Trace: Zoom on the voltage flat-top @ -60 kV, showing that the output voltage is well inside the accuracy bandwidth (+/- 600V) marketed by the two cursors

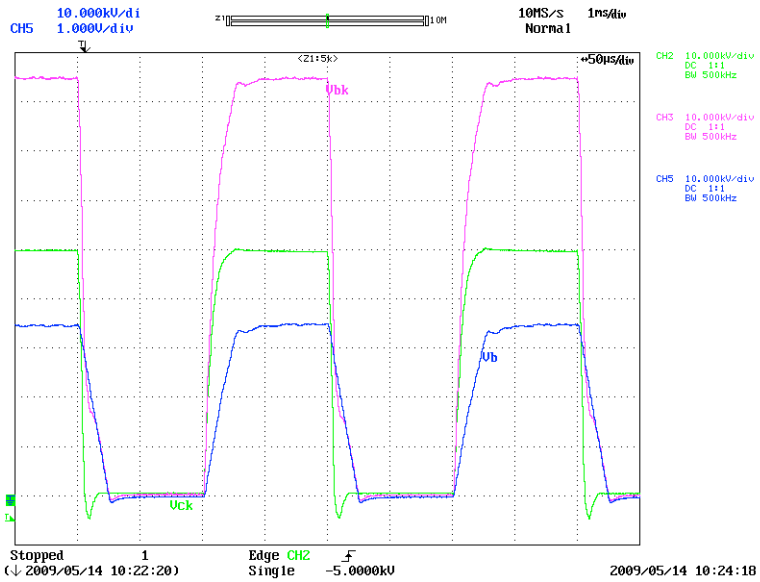

Fig. 4.3.6 *Modulation at 5 kHz:*
Green trace: MHVPS output voltage, 10 kV/div
Blue trace: BPS output voltage, 10 kV/div
Magenta trace: Equivalent beam voltage which should be applied to the gyrotron, 10kV/div

CRPP team contributed from the beginning to the installation of the AC cables and cable trays, as well as to the primary water distribution required to cool down the HV room, where, more than 100kW can be dissipated at full operation rate. Then, the integration of the power supply control into the test facility remote operation sequences has been performed and tested. During September, additional tests on the HV room cooling regulation have been performed in presence of OCEM engineers.

Presently and up to the end of the year, the new resources offered by this power supply will be implemented into the ITER gyrotron test facility control system. In addition, improvements of the test facility equipments in view of the next tests campaign of the 2MW EU gyrotron have been agreed and shall be implemented soon.

4.4 The ITER Upper Launcher for Electron Cyclotron Waves

The final report for the EFDA Task and Contract on the Upper launcher were submitted.

4.5 Superconductivity ITER studies

SULTAN tests

In the period of October 2008 – December 2009, the following test campaigns have been carried out:
TFKO2, ITER TF Korean conductor sample (October – November 2008)
RFTF2, ITER TF Russian conductor sample (November 2008)
USTF3, ITER TF American conductor sample (December 2008)
ENEA JT-60, prototype NbTi conductor for TJ-60SA Tokamak (March 2009)
EUTF3, ITER TF European conductor sample (March – April 2009)
EUTF4, ITER TF European conductor sample (April – May 2009)
USTF4, ITER TF American conductor sample (May 2009)
CNTF1, ITER TF Chinese conductor sample (June 2009)
SCH HF, AC loss investigations on rectangular CICC (June 2009)
Buoyancy 2, thermo-hydraulic experiments with ITER conductor (June 2009)
CEA JT-60 (TFJS1), prototype NbTi conductor for TJ-60SA Tokamak (July 2009)
EDIPO Joint, prototype terminal joint for EDIPO test facility (July 2009)
EUTF5, ITER TF European conductor sample (September – October 2009)
EUTF-Alt., alternative ITER TF rectangular conductor (started in October 2009)
JATF4, ITER TF Japanese conductor sample (November - December 2009)

4.5.1 The use of SULTAN for developing and testing ITER conductors

The main characteristics and test results for the ITER TF samples are listed in Table 4.5.1.

Sample Nickname	**KOTF2**	**RFTF2**	**USTF3**	**EUTF3**	**EUTF4**	**USTF4**	**CNTF1**	**EUTF5**
Country of Origin	Korea	Russian Federation	Unites States	Europe	Europe	United States	China	Europe
Conductor Nickname	RC48 / RC49	A / B	Baseline / Alternate	EAS / Alstom A	Luvata / OST	A / B	A / B	ENEA / NEXANS
Cable Layout	TF Opt.2	TF Opt.2	TF Opt.1/Alt	TF Opt.2	TF Opt.2	TF Opt.2	TF Opt.2	TF Opt.2
Nb_3Sn Strand	Internal Sn	Bronze	Internal Sn	Bronze / Intern. Sn	Internal Sn	Internal Sn	Internal Sn	Bronze
Load Cycles Number	700	707	650	1000	1000	600	950	1000
Intermediate Warm-up	Yes	Yes	No	Yes	Yes	No	Yes	Yes
Termination and Joint	Solder dipped	Solder dipped	Solder dipped	Solder dipped	Solder dipped	Solder filled	Solder dipped	Solder filled

Table 4.5.1 *ITER TF conductors measured in SULTAN from October 2008 to October 2009*

For three cases, RFTF2, USTF4 and CNTF1, the two conductor sections in the sample are identical and are just named A and B. In the other samples the two conductors are different either for strand type (KOTF2, EUTF3 and EUTF4) or for cable layout (USTF3) or for cabling company (EUTF5).

The ITER TF conductor has two designs, named Options 1 and 2. The main specifications are identical, e.g. outer CICC diameter, strand diameter, number of strands and cable pattern. In *Option 1* the void fraction is 33%, the jacket wall thickness is 1.6mm, the steel foils wrapped around the cables and sub-cables are 0.08mm and 0.05mm thick respectively, the central spiral is 7x9mm, the sequence of twist pitches is "short" (45/85/125/250/450mm) and the overall flow area is 444mm^2. In *Option 2*, the void fraction is 29%, the jacket wall thickness is 2.0mm, all the steel foils are 0.1mm thick, the central spiral is 8x10mm, the sequence of twist pitches is "long" (80/14/190/300/420 mm) and the overall flow area is 394mm^2.

A typical test campaign for ITER TF samples lasts three weeks including cool-down and warm-up, with a target of 1000 load cycles. An intermediate warm-up is done before the final test. The test program was reduced for USTF3 and USTF4, which are benchmark samples against the former USTF1 and USTF2.

All tested ITER TF samples were fabricated at CRPP including the heat treatment of the conductor, termination and joint preparation, mechanical assembly of the sample and its instrumentation. The heat treatment of the conductors was conducted in accordance to the schedule specified by the supplier, the witness strand barrels were heat treated together with the conductors. Figure 4.5.1 shows the conductor sections for samples CNF1 and EUTF3 assembled for heat treatment and ready to be inserted in the furnace.

Fig. 4.5.1 *CNTF1 and EUTF3 conductors assembled for heat treatment before insertion into the furnace*

The instrumentation of the each ITER TF sample was done in accordance to ITER IO specification (Fig. 4.5.2). Eight thermometers (T1, T3 and T2, T4) and six voltage pairs (VH1, VH3 and VH2, VH4) on each conductor in high field zone were used to define the current sharing temperature (T_{cs}) or for the critical current (I_c) measurements. Voltage pair V1V2 was used to define the joint resistance, and voltage taps V3 and V4 were intended to measure the resistance of the termination to transformer connection.

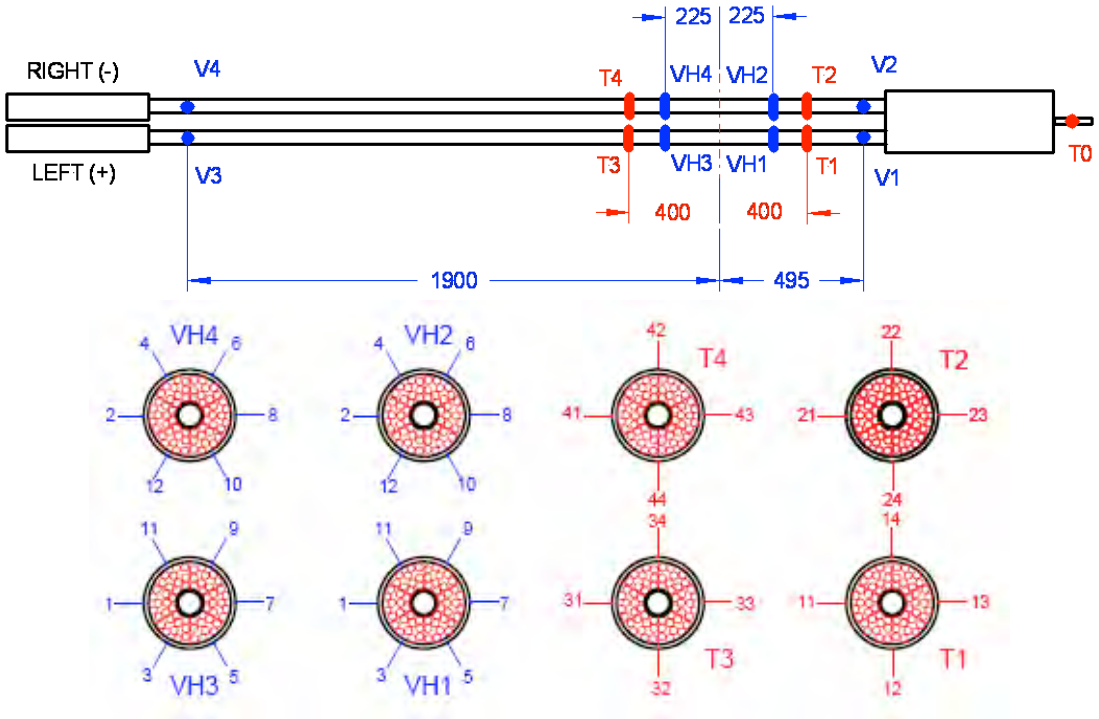

Fig. 4.5.2 *The typical instrumentation of the ITER TF sample. The joint "solder dipping" option has one common Helium inlet (shown in this figure) entering the joint box, the joint "solder filling" option has two individual Helium inlets for the each conductor*

For the terminations and joint of the tested samples the “solder dipping” and “solder filling” techniques have been used (see Table 5.2.1).

The “solder dipping” technique went trough the following preparation steps:
- Compaction of the termination/joint length
- Heat treatment of the conductor
- Opening of the jacket in termination/joint length
- Outer cable wrap removal and sub-wrap at the termination/joint
- Cr removal in HCl solution in ultrasonic bath at the termination/joint
- Dipping of the prepared termination/joint into the molten SnAg5
- Termination/joint assembly

The “solder filling” technique went trough the following preparation steps:
- Opening of the jacket in termination/joint length
- Outer cable wrap and sub-wrap removal at the termination/joint
- Cu sleeve assembly onto the termination/joint
- Compaction of the Cu sleeve
- Heat treatment of the conductor
- Solder feeling with use of siphon welded to the Cu sleeve
- Termination/joint assembly

The terminations and joints of the samples are shown in Fig. 4.5.3. The destructive investigations of the prepared ends of the conductors ready for the joint assembly are shown in Fig. 4.5.4.

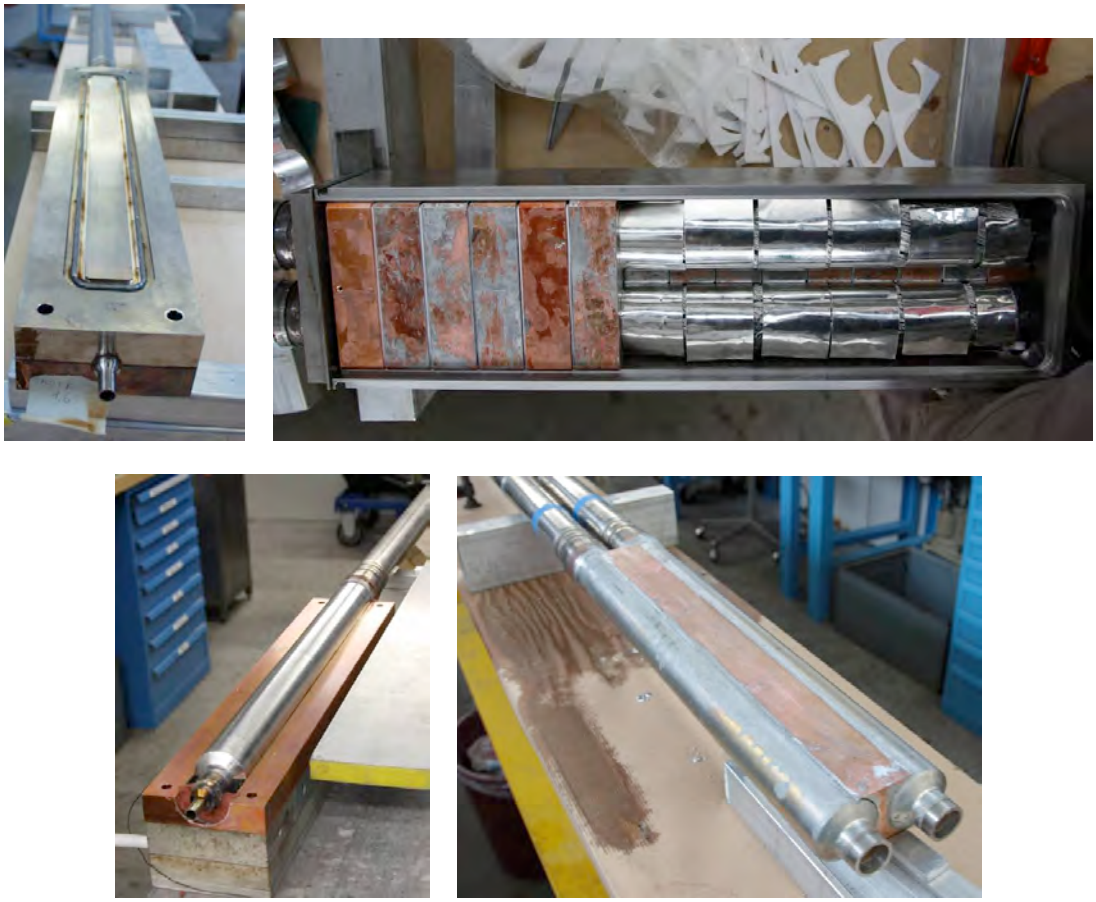

Fig. 4.5.3 *Termination (top, left) and joint (top, right) of the sample with use of “solder dipping” technique; termination (bottom, left) and joint (bottom, right) with use of “solder filling” technique*

The tests of the ITER TF samples consisted mainly of T_{cs} runs, repeated along the cycling loadings. A few I_c tests were performed in order to define the n-value of conductors. Also, AC loss measurement was conducted before any electromagnetic loading and repeated after the cycling loadings.

The results of T_{cs} runs along the cycling loadings and after intermediate warm-up/cool-down procedure for all ITER TF samples are reported in Fig. 4.5.5, and the results of AC loss measurements after cycling loadings for all ITER TF samples are summarized in Fig. 4.5.6.

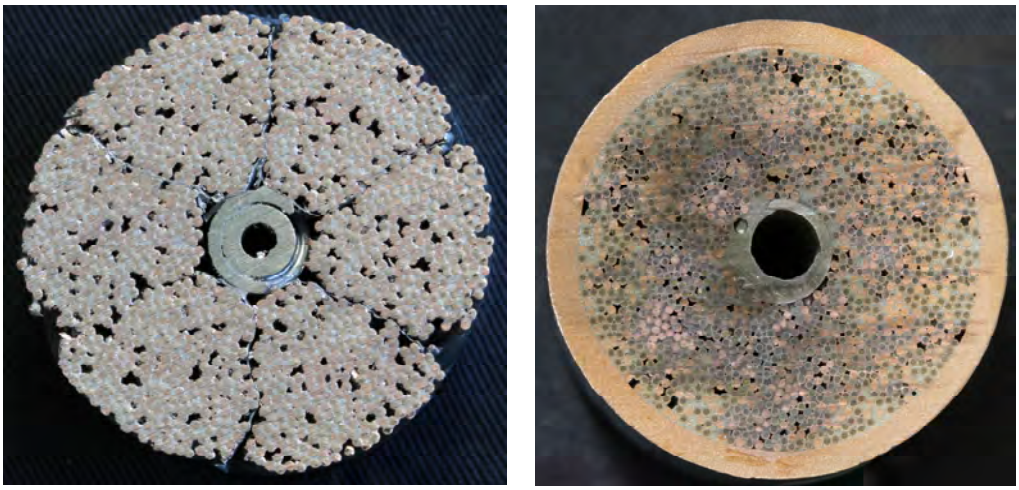

Fig. 4.5.4 *Destructive investigation of the "solder dipping" (left) and "solder filling" (right) techniques*

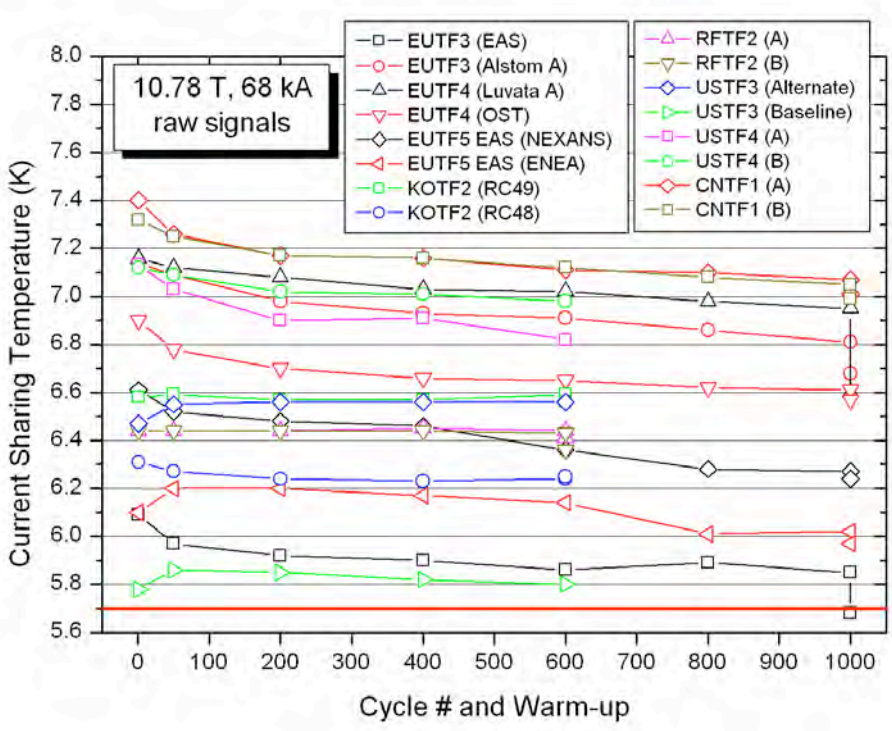

Fig. 4.5.5 *Summary of the Tcs measurements along the cycling loadings and after intermediate warm-up/cool-down procedure*

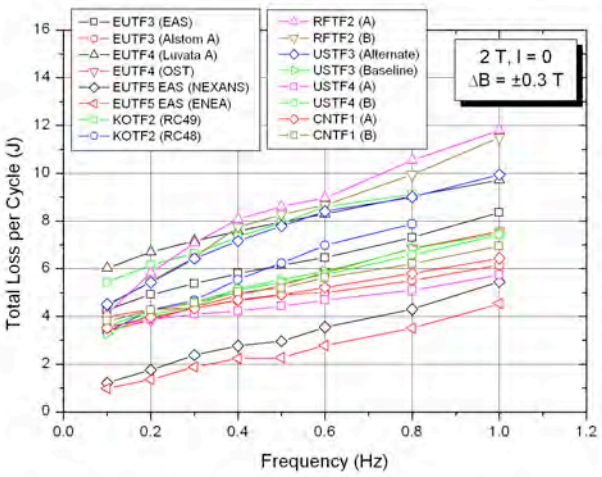

Fig. 4.5.6 *Summary of the AC loss measurement after cycling loadings*

The impact of the termination layout, "dipped" vs. "filled", on the behavior of the baseline V-I characteristic ("initial slope") is reviewed for the last eight ITER TF and EUTF-Alt samples in Fig. 4.5.7. The EU-Alt sample has no bottom joint (U-bent conductor in steel box). The first T_{cs} run is analyzed for each sample and the voltages sensed in the six voltage pairs distributed over the conductor circumference are assessed at 10, 20 and 30kA. The voltages may be either positive or negative. The algebraic average of the six voltages and the average of their absolute values are also computed. The accuracy of the assessment is estimated 0.1μV. The "error bars" represent the spread of the six voltage pairs in each leg.

From Fig. 4.5.7 it can be recognized that the range of voltages measured on the "solder filled" sample (US4 and EU5) and those measured on the "solder dipped" samples overlap. The left leg of US4 (solder filled) shows the lowest initial slope among the 8 samples (even if they are still comparable with the EU samples and US3), but the right legs of US4 and EU5 show early voltages larger than the average of all solder dipped samples.

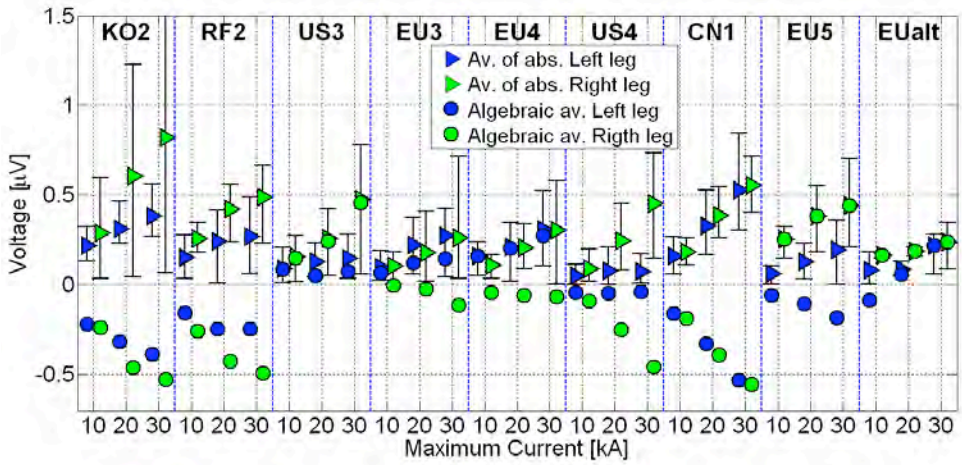

Fig. 4.5.7 *Summary of the voltages sensed at 10, 20 and 30kA in the last 8ITER TF and EUTF-alt. samples. The circles represent the algebraic average of the voltages from the 6 six stars, while the triangles represent the average of their absolute values. The samples US4 and EU5 have solder filled terminations. The sample EUalt has no bottom joint (U-bent conductor in steel box).*

4.5.2 Thermal-hydraulic experiment on buoyancy

In order to understand the thermo-hydraulic behaviour of the helium flow in the dual-channel cable-in-conduit conductor (CICC) for the ITER toroidal-field coils in detail, ITER IO requested EPFL/CRPP to conduct a series of experiments in the SULTAN test facility on a dedicated sample made according to the final Option II conductor design. With helium flowing downward through the conductor, as expected during ITER operation in parts of the TF coils, the sample was heated by eddy-current losses induced in the strands by an applied AC magnetic field as well as by foil heaters mounted on the outside of the conductor jacket.

The thermo-hydraulic measurements on an ITER TF conductor of the final design confirmed the observations on similar conductors: helium flowing in the bundle region mixes with helium in the central channel over a characteristic distance of 35 to 60cm. At the expected heat deposition levels (per unit length) the temperature differences between the two regions and thus helium-density differences remain small and no gravity-driven flow reversal arises in the bundle region.

The measured ΔT at the jacket surface, relative to the 1D expectation, scales well with the heat deposition per unit length and the mass flow rate. It is therefore possible to predict local maximum temperatures from known or expected heat deposition profiles and the mass flow rate. ΔT remains well below 40mK for the conditions expected in ITER (dP/dz<3W/m, dm/dt > 8g/s).

The pressure drop as a function of the overall mass flow rate was measured accurately and may serve as a reference for this final-design cable (Fig. 4.5.8, left).

In addition to the measurements and the empirical evaluation, an attempt to find the most fitting two-channel-flow model was made. The combination of empirical formulae proposed in the ITER Design Description Document for the friction factor in the central channel and 0.66 times that proposed by Katheder for the bundle friction factor describes the pressure drop as well as the measured flow velocities best.

The heat transfer coefficient of the two-channel model calculated with a convective heat transfer correlation and the coefficient derived from the experimentally observed temperature profiles agree to within 20%, which is quite good considering the simplifying assumptions.

Heat pulses generated by small resistors in the central channel created regions of helium with a temperature elevated by a few mK. The helium 'marked' in this way drifted with the flow of the helium in the channel to several temperature sensors downstream where the small temperature pulse was observed with a delay from which the helium flow velocity could be accurately calculated (time-of-flight method). Figure 4.5.8 shows on the right the experimentally observed velocities as well as approximations with best-fitting parameters of the two channel flow model in CICCs.

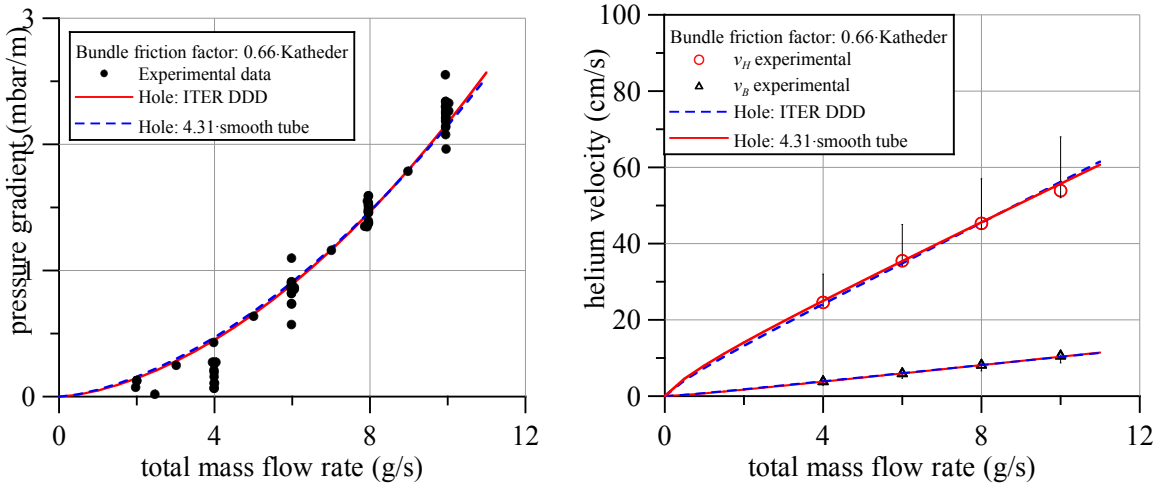

Fig. 4.5.8 *Pressured drop per unit length and helium velocity in the Option II ITER TF conductor sample measured and calculated using final correlations for the bundle and central-channel friction factor.*

4.5.3 Inter-strand resistance and contact resistance distribution in ITER conductor termination

The current uniformity among the strands in large cabled conductors is affected mostly by the contact resistance distribution and the interstrand resistance in the electrical terminations. While the contact resistance distribution between the strands and the copper of the termination affects the current distribution among the strands, the resistance between the strands in the termination (inter-strand resistance) has an effect on the re-distribution of the current from the most to the less loaded strands.

The contact resistance distribution of an ITER conductor termination is measured in the JORDI (JOint Resistance DIstribution) facility at CRPP. The sample is prepared starting from a section of Nb_3Sn Cable in Conduit Conductor (CICC) and the joint is assembled following the procedure ("solder dipped") used for most of the ITER qualification samples tested in the SULTAN facility. The cable is opened into 150 groups of strands ("elements") and each element is connected to low temperature shunt resistors which split the current from a 10kA power supply. The voltage drop is sensed between each element and the contact surface of the joint made equi-potential by a superconducting soldering alloy. The resistance of each channel is deduced from the measured voltage drop.

The results of the measurements are reported in Fig. 4.5.9. The resistance distribution measured under imposed current uniformity can be used to infer the current distribution in normal operation, namely under imposed voltage. In particular, the ratio between the average and the maximum value of the channel resistance is equal to 1.36. Translated in terms of current, in cabled conductors using the analyzed type of joint, the maximum current overload that could be expected in a channel is 36% of the average current. From the picture it can be deduced that inside the 4_{th} stages (indicated with the letters A-F) the current is highly homogeneous, while the wraps hinder the distribution of the current among the petals.

The same sample is then removed from the JORDI test facility and adjusted to measure the inter-strand resistance. While in JORDI the voltage drop between each

current carrying element and the equipotential surface is measured, in the "interstrand resistance" measurement the voltage drop between two strands and the corresponding resistance are assessed. Two strands at the time are fed with a current of the order of 100A, the voltage between the selected strands is sensed and the equivalent resistance deduced.

The resistance between strands in not adjacent petals (4^{th} stages) is the highest, in the range 8.5-9.2nΩ. The resistance between strands in adjacent petals is in the range 7.9-8.4nΩ, while that between strands in the same petal is in the range 6.6-6.7nΩ. Therefore, the presence of the internal wraps slightly enhances the resistance between strands in different petals, as noticed also in the contact resistance distribution experiment.

The values found in these experiments can be used as reference for future simulations in order to investigate and simulate the current distribution in ITER conductors.

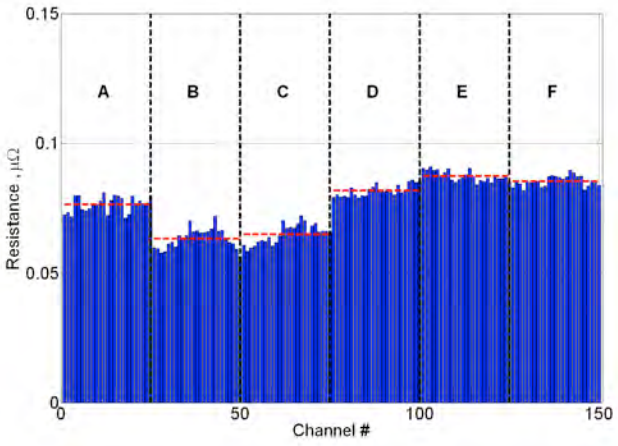

Fig. 4.5.9 *Contact resistance distribution results. The petals (4^{th} stages) are labeled with the letters A-F. The horizontal dotted lines represent the average resistance in each sub-cable.*

4.5.10 ITER busbar design

A design study for the conductor of the busbars feeder system of ITER has been carried out under the ITER CT 09/4100000526 contract. Two different conductor layouts have been developed, one for the TF, PF and CS circuits, called MB, and one for the CC circuits, called CB (see Fig. 4.5.10). The cable in conduit conductor technology has been selected for both layouts to profit from the cryogenics circuits already present for the ITER magnets and NbTi superconducting material (suggested by ITER-IO) has been considered a good option for the operation conditions of these components.

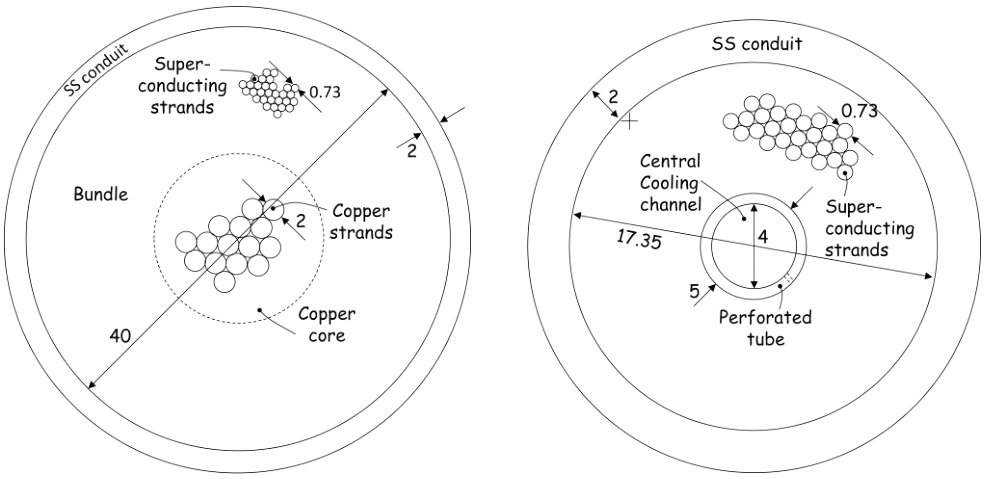

Fig. 4.5.10 *Conductor layouts, on the left side the main busbar (MB) design and on the right side the corrector busbar (CB) design.*

Several analyses have been carried out to optimize and validate the design. The estimate of the superconducting material cross sections has been made with the critical surface parameterization given by ITER-IO. The first estimate of the copper cross section has been calculated with simple adiabatic assumptions. A detailed campaign of thermo-hydraulic analysis has been carried out to simulate the behavior of the conductor during a quench (i.e. the transition of a superconductor into normal conduction followed by a thermal run away) to optimize the cross sections and the protection parameters (i.e. voltage threshold). A second campaign of simulations has been carried out to optimize the hydraulic impedance of the conductor to meet the requirements on pressure drop. These calculations led to a fine tuning of the total helium cross section and void fraction for the MB conductor and to the additional implementation of a central cooling channel for the CB conductor. Finally, a careful analysis of the conductors during the expected operating conditions has been carried out to validate the design, see Fig. 4.5.11. For this purpose static and dynamic losses have been estimated both in the conductor and in the splices. An external review committee has approved the design at the end of November 2009.

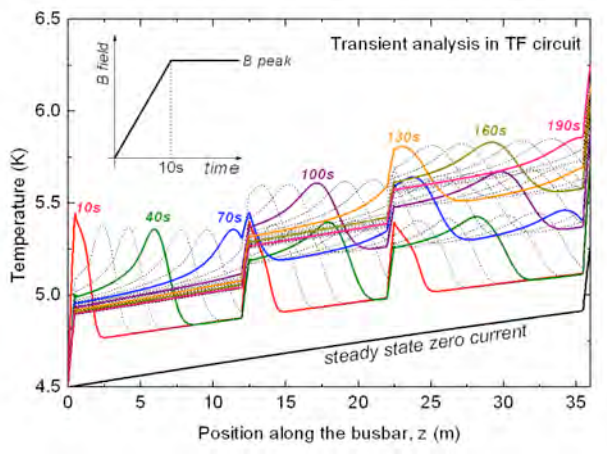

Fig. 4.5.11 *Example of the simulation of the conductor during the operation conditions.*

4.5.4 Thermal-hydraulic code development

The increasing importance gained by the superconducting magnet system in the frame of the ITER project has required a more and more detailed analysis by means of computational tools with different degrees of complexity and various targets. In this way the design of superconducting magnets has been not only assisted but it could be also verified during the preparatory R&D phase. The SuperMagnet™ suite, created by CryoSoft, collects different computer codes, which in turn simulate separate aspects of the operation of a superconducting magnet. The SuperMagnet™ external environment provides the *glue* among these tools, managing the coupling between different codes, providing the correct data exchange between every running process.

In order to extend the modeling capability of SuperMagnet™ (with already existing tools for cable 1D electric and thermal-hydraulic analysis and external cryogenic circuit and electric network simulations) a new tool has been prototyped and tested, HEATER, devoted to pure heat conduction in winding packs and structures. In the HEATER module the conduction equation

$$\rho c_p(T)\frac{\partial T(x,y,z)}{\partial t} - \nabla\cdot\left(k(T)\nabla T(x,y,z)\right) = Q(x,y,z) \qquad (1)$$

where T is the temperature, k is the material thermal conductivity and Q the external heat source, is solved in the selected domain. The discretization is performed with finite element meshes defined by means of implemented routines (e.g. the pancake wound coil, see below) or provided to the code via external files containing the node coordinates, the element boundaries and the element material. The conduction matrix is built considering the material properties provided in the mesh definition and recalculated at each computation step to account for temperature dependent properties. Boundary conditions, temperature and/or heat loads can be imposed to model coupling with warmer structures or perform stand-alone HEATER runs.

Inside the HEATER module, the coupling with other external processes is performed by defining a specific node or line as “external”. This means that boundary conditions for the heat conduction equation will be provided by SuperMagnet™ after inquiring the corresponding process.

An example of the application of the new HEATER module is shown in Fig. 4.5.12. Here an ITER CS-like single pancake is modeled with a circle in square stainless steel jacket with an outer dimension of 42mm and an insulation layer of 0.2 mm thickness. As boundary conditions the pancake is adiabatic and the temperature on the third turn is set to 9.5K whereas elsewhere it is set to 4.5K. It can be seen how the heat propagates not only in the longitudinal direction thanks to the jacket elements but also in the radial direction through the jacket and insulation layers.

Since the target of the SuperMagnet™ suite is the simulation of a real ITER magnet system, which includes up to hundreds of conductors, a study was performed to assess the limits of the SuperMagnet™-operating system interaction with increasing number of simulated components. From the observed trend, the performance scales quite linearly until an upper hardware dependent limit is reached where the available memory does not allow anymore addressing properly all the required data.

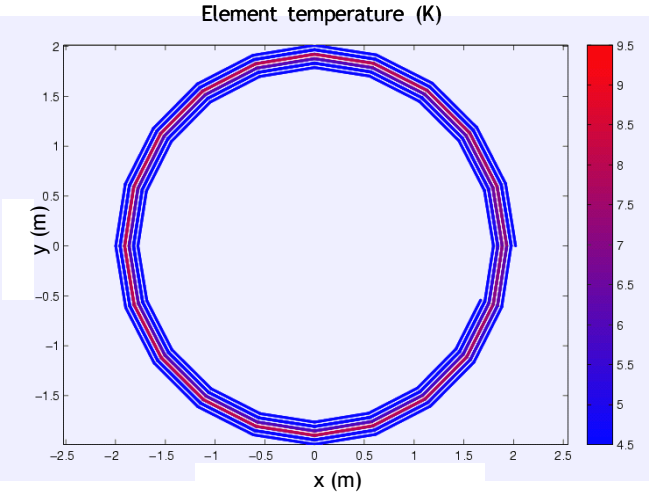

Fig. 4.5.12 *Heater: Temperature distribution in the CS-like pancake*

4.6 The development of the ITER magnetics diagnostic

During 2009, the ITERMAG Consortium Agreement was finalised between CRPP, CEA, CIEMAT and Consorzio RFX. Signature took place in April.

Negotiations between Fusion for Energy and three of the ITERMAG Associates (CRPP, CEA, RFX) took place concerning an F4E Grant "GRT-012" on prototyping and especially calibrating ex-vessel sensors. A number of iterations of the Proposal submitted at the end of September 2008 were developed to reach a final version in Spring 2009. The Draft Grant Agreement is currently being perfected and might still be signed in 2009. Supporting activities included the development of a Quality Manual for the Consortium.

In September 2009 a larger F4E Grant was announced as Call "GRT-047" and a Proposal was developed between the ITERMAG Consortium, SCKCEN and CCFE. This Proposal was submitted in November and is being evaluated at the time of writing.

4.7 ITER discharge simulation

4.7.1 Operation of ITER in the hybrid scenario

The ITER hybrid mode of operation which aims at operating the plasma for a long plasma burn time (>1000s) with sufficient fusion gain (Q>5) has been studied using the combined DINA-CH/CRONOS full tokamak discharge simulator. The plasma is operated at lower plasma current and averge electron density compared with the fully inductive ITER operation scenario 2 to provide the poloidal flux for a long flat-top. In the past experiments targeting the hybrid mode operation, improved plasma confinement above ELMy H-mode confinement has been achieved. The safety factor (q) profile is maintained above 1.0 by virtue of the existence of a self-regulating mechanism which prevents the central q value from being decreased below 1.0. The onset of sawteeth crashes is usually avoided and a low magnetic shear appears to be favourable for stabilizing MHD instabilities.

In this simulation study, we have focused on the operational possibility of obtaining a flat q profile at the beginning of the flat-top phase and sustaining it as long as possible by combining various non-inductively driven current sources. The plasma current ramp-up scenario for ITER hybrid mode operation is generated by tailoring the initial part of the inductive 15MA ELMy H-mode ITER operation as shown in figure 1. The total plasma current is ramped up to 12MA and the average electron density is assumed to be linearly ramped up along with the total plasma current. The electron density at the separatrix is assumed to be 35% of the central value. The pedestal top is assumed to be at 95% of the square root of the normalized toroidal flux (ρ_{tor}). The plasma starts with a large bore, a(t=1.6s)=1.6m. It then experiences a transition to a diverted SNL configuration at about 20s. At the beginning of the flat-top phase, 33MW of NBI and 20MW of ICRH are applied to trigger an L-H mode transition and to initiate the plasma burn. The energy confinement improvement observed in the experiments targeting hybrid mode operation is taken into account using a confinement enhancement factor for the H-mode scaling, H_{98}=1.2.

The full tokamak discharge simulation results are shown in Fig. 4.7.2. The non-inductively driven current was produced by the application of NBI and the bootstrap current fraction evolved in response to the plasma heating and density evolution. The alpha particle self-heating power is slightly over 70MW during the flat-top phase, indicating that the fusion gain Q is about 6~7. The plasma poloidal beta (β_p) is increased by the application of the main H&CD up to about 0.85 and the internal inductance (l_i) is maintained around 0.75 during the flat-top phase. The central q value was slightly above 1.0 at the start of flat-top phase (SOF), avoiding an early onset of sawtooth crashes during the current ramp-up phase. At t=200s of this simulation, the electron temperature at the centre and pedestal top were about 25.5keV and 3.14keV, respectively. The normalized plasma beta ($\beta_N=\beta aB_T/I_p$) was slightly over 2.0. The central q value was 0.94 and Q was about 6.75. All the CS coil currents evolve far away from the coil current limits due to the reduced volt-second consumption during the current ramp-up phase. However, a violation of the PF1 coil current limit was identified after the plasma configuration is fully diverted at 20s. The PF1 coil current is increased above its limit due to the reduction of volt-second consumption caused by the confinement improvement in the hybrid mode operation. In the simulation with the assumption of L-mode confinement and peaked heat conductivity profile shape (these assumptions were chosen based on JET plasma current ramp-up experiments), the violation of PF1 coil current limit was easily avoided while more poloidal flux was consumed as shown in Fig. 4.7.3. As an active method of avoiding this violation, modifying the evolution of the PF coil currents has shown its potential (see figure 3), although the vertical stability of the plasma is slightly deteriorated.

Based on the reference hybrid mode operation simulation, the effect of different heating and current drive (H&CD) schemes on the evolution of the safety factor profile has been studied. Slightly off-axis ECH&ECCD and/or far off-axis LHH&LHCD were/was added to the main H&CD scheme, starting from 110s. Application of 20MW of additional EC through the upper launchers mainly modified the plasma current density profile at the centre by adding a slightly off-axis current in which its maximum is localized inside ρ_{tor}=0.2. Application of 20MW of additional LH provides a localized far off-axis current in which its maximum is localized around ρ_{tor}=0.8. The evolution of the central q value and the q profiles at t=200s are compared in Fig. 4.7.4. The slightly off-axis EC driven current was effective in modifying the central q value, while the far off-axis LHCD had a small and delayed influence on the central q profile. When the far off-axis LHCD was applied, q values were increased around the deposition location. Although the contribution of the far off-axis LHCD over a longer time scale has not been investigated, it appears less

effective for an active control of q profile during the flat-top phase, in which the plasma current is high. Application of both ECCD and LHCD, in which half of the power is stepped up at 160s, showed combined contributions at different locations.

[Collaboration with: Kurchatov Inst., Moscow, RU; TRINITI Inst., RU; CEA Cadarache, F]

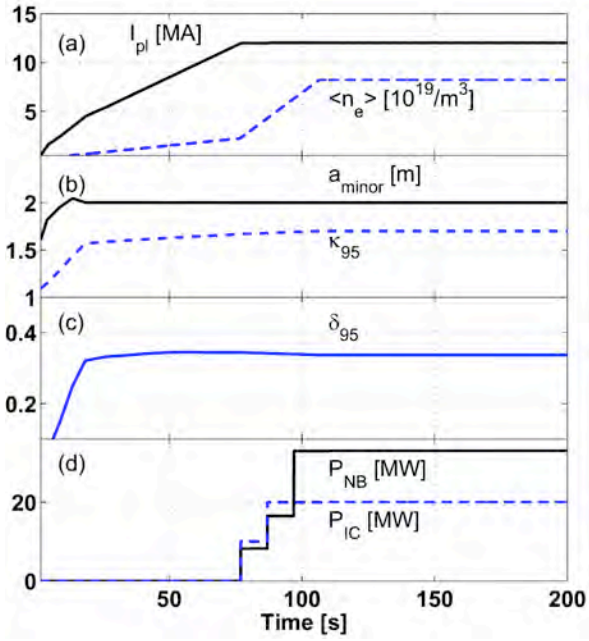

Fig. 4.7.1 *ITER 12MA hybrid mode operation scenario. (a) The total plasma current, average electron density, (b) minor radius, plasma elongation (c) plasma triangularity and (d) auxiliary H&CD powers are shown.*

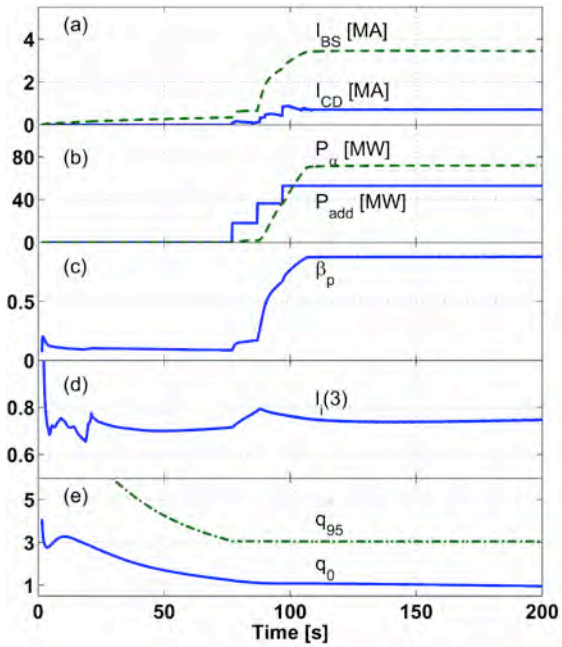

Fig. 4.7.2 *Time traces of (a) bootstrap and driven currents, (b) alpha particle and auxiliary heating powers, (c) plasma poloidal beta, (d) internal inductance and (e) safety factor values.*

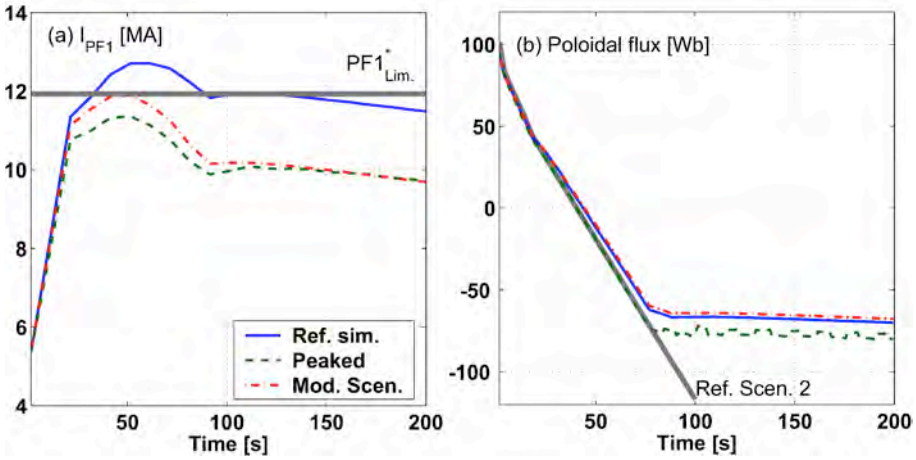

Fig. 4.7.3 *Time traces of (a) currents in PF1 coil and (b) poloidal fluxes. Three cases, reference simulation, with an assumed heat conductivity profile resulting in a peaked plasma temperature profile shape and with modified pre-programmed coil current waveforms, are compared. The PF1 coil current limit ($PF1_{lim.}^{*}$) given in the recent ITER design review.*

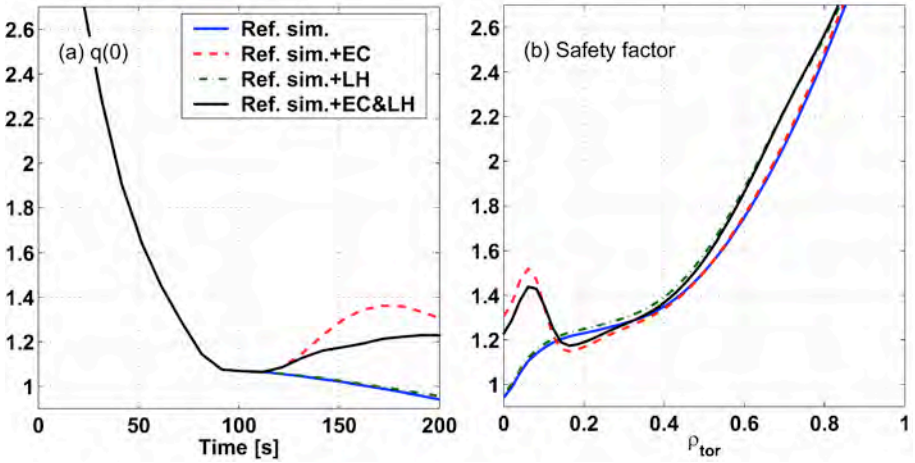

Fig. 4.7.4 *Time traces of (a) central safety factor values and (b) profiles at t=200s. Four cases are compared. Reference simulation, with additional 20MW of EC, with additional 20MW of LH and with both additional 20MW of EC and 20MW of LH.*

4.7.2 Active control of kinetic plasma profiles in ITER

The operation of ITER in steady-state and hybrid mode scenarios require an active real-time control of kinetic plasma profiles to achieve the advanced tokamak regimes for sustained operation. Experiments on this active plasma profile control have been conducted on several devices, including JET, Tore-Supra and DIII-D. A model based technique for integrated real-time kinetic plasma profile control, which appears to be the most promising technique, has been developed and demonstrated in JET experiments and simulations. In this technique, the response model of the plasma profiles to power changes of auxiliary heating and current drive (H&CD) systems is deduced from identification experiments and is then used to control the

plasma profiles. However, the range of applicability of this experimentally deduced plasma profile response model is still in question. This model might be not valid if the plasma state varies away from the reference state achieved in the identification experiments. Real-time update of the plasma profile response model would be the most plausible approach to resolving this difficulty. This is possible either by selecting an adequate plasma profile response model from an existing database or by identifying one in real-time. However, due to the cost of preparing a database of plasma profile response models, the latter will be more attractive if an adequate method for calculating the plasma profile response model in real-time without consuming too much computational time is provided.

Therefore we have developed a robust control technique using simplified plasma profiles response models. The response of the plasma profiles to power changes of auxiliary H&CD systems are modelled by simplifying the related physics to allow real-time update of them. The electron temperature profile response is modelled by simplifying the electron heat transport equation and the safety factor profile response is modelled by directly relating it to the changes of source current density profiles. The required changes of actuator powers are calculated using the singular value decomposition (SVD) technique, taking the saturation of the actuator powers into account. This control technique can be used for real-time active control of the plasma profiles, if a fast equilibrium reconstruction and source profile calculation methods are provided. In the CRONOS simulations with a control interval of 10 seconds, the electron temperature and safety factor profiles were well controlled either independently or simultaneously. In the simulation of the simultaneous control of plasma profiles (see Fig. 4.7.5 and 4.7.6), the control of the safety factor profile was started first at about 300s and then the control of the electron temperature was started at about 400s, to avoid a strong conflict between the two controls observed when starting them at the same time. The actuators for the control of the safety factor profile, EC, LH and NB, already reached their maximum powers at about 600s as shown in Fig. 4.7.6. However, the control of the electron temperature profile was still active with the IC power until the end of the simulation. The control of safety factor profile revealed that ITER will require additional auxiliary H&CD power to maintain the stationary flat safety factor profile for the hybrid mode operation.

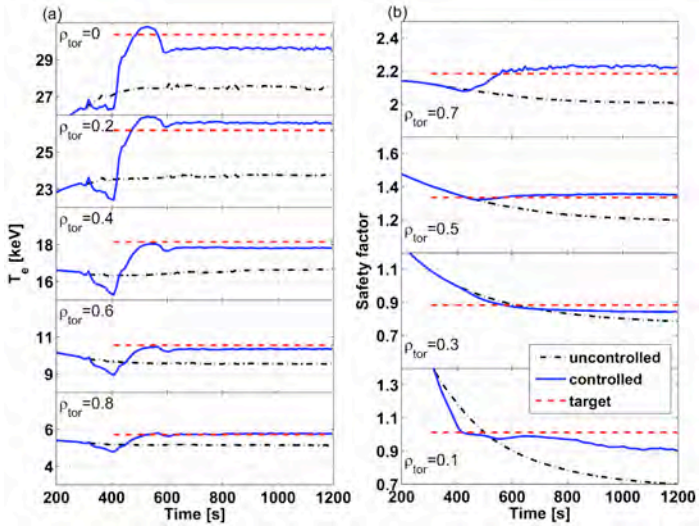

Fig. 4.7.5 *Time traces of (a) the electron temperatures at 5 radial control locations and (b) safety factor values at 4 radial control locations. Control of the electron temperature profile was started at about t=400s and control of the safety factor profile was started at about t=300s.*

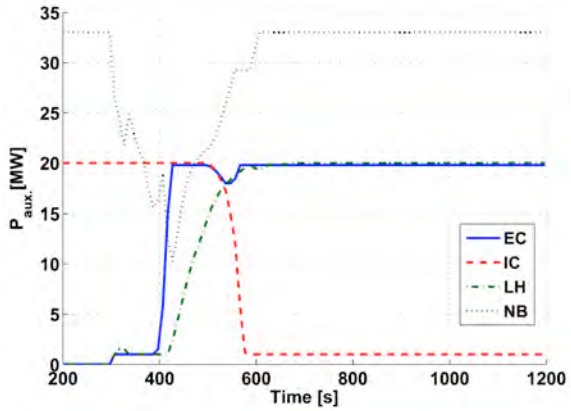

Fig. 4.7.6 *Time traces of auxiliary H&CD powers. Control of the electron temperature profile was started at about t = 400s and control of the safety factor profile was started at about t = 300s.*

4.8 Contributions to the ITPA

CRPP staff participates regularly in the ITPA activities.

4.9 Contributions to ITER committees

Professor M.Q. Tran has been a member of the EU deleguation to ITER STAC.

5 INTERNATIONAL AND NATIONAL COLLABORATIONS

5.1 Exploitation of the JET facilities

5.1.1 Edge physics studies

The work constitutes a contribution to the confidence building in the predictive ability of the biggest edge plasma fluid - Monte Carlo SOLPS code package for tokamak operation in both steady state and during transient events. The SOLPS code, which has been long used for predictions of ITER divertor design, has been applied to the time-dependent simulations of two JET ELMy H-mode cases with different sizes of Edge Localized Modes (ELMs) in terms of the energy expelled by event (~200kJ and ~0.7MJ, respectively). The pulse with lower expelled energy (~200kJ) has been exhaustively modelled in earlier works with another fluid-Monte Carlo code package EDGE2D/NIMBUS. Both the code-experiment benchmark and a comparison of the two world's major edge plasma code packages have been successfully performed last year. The work in 2009 has built on this exercise and in-out target power loads asymmetries have been studied. The second simulated pulse is - in terms of the expelled energy - close to the limit corresponding to the current maximum ELM energy which is though to be tolerable on ITER for acceptable divertor target lifetime. The solution of pre-ELM steady state has been obtained last year and, using an ad-hoc increase of diffusive particle and heat coefficients, the whole ELM cycle has been successfully modelled.

The code-experiment comparison was limited since experimentally measured ion fluxes of high quality have been available only for the lower ELM energy JET pulse and the heat fluxes only for the higher ELM energy pulse. For lower ELM energy case the radiated energy during the ELM is found in satisfactory agreement with experiment (by a factor of ~1.5 less in SOLPS). For the higher ELM energy pulse the SOLPS radiation is about order of magnitude lower than in the experiment. This is very likely due to the ablation or thermal decomposition of thick layers on the inboard target accumulating there as a consequence of the erosion migration processes often seen in carbon dominated, single null divertor tokamak operating with forward toroidal field. Such effects are not included in the SOLPS description of material erosion, which considers only physical and chemical sputtering. The SOLPS solution is in both cases characterized by an asymmetric radiation distribution favouring the inner target. In the lower ELM energy case the computed asymmetry is about twice stronger than the experiment (which is due to the very low temperature at the inner target). Conversely, in the high ELM energy pulse a very good agreement of in-out radiation asymmetry with experiment (~3) is found.

Even though the situation with radiation seems to be rather encouraging, the question of the in-out target power deposition asymmetry is more concerning. During the pre-ELM phase of JET discharges with forward B-field (as in both cases simulated in this work) more energy is deposited on the outer target and this asymmetry is observed to be reversed during the ELM. The experimentally observed in-out target power deposition ratio is ~1.7-2. Even though the pre-ELM power asymmetries in the SOLPS simulations of the JET pulses are more closely matched, strong disagreement is observed during the ELM when SOLPS predicts, like in the pre-ELM phase, more power at the outer target in both simulated cases (with in-out

ratio 0.22 and 0.45 for ~200kJ and ~700kJ ELMs, respectively). This discrepancy has been always seen as a general feature of the fluid codes.

A recent development has been the suggestion that the ELM, in convecting plasma from the pedestal to SOL regions, conserves the high toroidal rotation velocity known to characterise the H-mode pedestal on all devices. This hypothesis has been tested in a preliminary manner, and for the first time in this kind of simulation, by imposing a toroidal velocity inside the magnetic separatrix in the simulations and studying the radial transport of this toroidal momentum into the SOL. The parallel velocity has been imposed to the inner boundary of the simulation grid. When applied, for example, to the smaller TCV Type III ELM, the indications are that transfer of this rotation into the SOL can drive target asymmetries in the direction seen experimentally. The same trends of target power asymmetries, however less marked than in the TCV cases, were obtained with the toroidal rotation included in the simulation of the much more conductive JET ELM. It appears that these ELMs are too conductive for the free-streaming particle model with toroidal velocity to be applicable, and further work is required to fully understand this scenario.

5.1.2 Control of MHD instabilities

Experiments have been carried out under the JET-Task Force MHD to investigate the mechanism for sawtooth control using toroidally propagating ion cyclotron resonance heating (ICRH). By employing minority He3, the experiment proved the theoretical mechanism recently published in *Physical Review Letters*, and described in this report in Section 2.2.3. The success of this first experiment, led by CRPP personnel, led to two further sessions with the aim of again employing He3 minority ICRH, but in conjunction with moderate NBI power. The NBI ions played the role of alpha particles in ITER, and the trapped fraction of the NBI ions initially created monster sawteeth. Following this, the application of -90 phased ICRH with resonance close to the q=1 surface on the high field side, greatly reduced the sawtooth period. This was undertaken also in H-mode, and as a result, improves the prospect of sawtooth control via ICRH in ITER. Investigations are under way, in collaboration with the ITPA working group, into the ICRH power required in ITER to reduce the long sawtooth periods generated by trapped alpha particles.

5.1.3 Collaboration on Alfvén waves and fast particles studies

The study of Alfvén waves and their interaction with fast particles is an important topic in the JET programme. During the period covered in this report, JET has been in continuous operation until early April 2009, then entering a shutdown phase, with operation restarting in June 2009 until 23rd October 2009. During this period, our activities have mainly focused on the operation of the new Alfvén Eigenmodes Diagnostic system (KC1T), on the analysis of the data obtained during the 2007 and early 2009 experimental campaigns, and on the scientific preparation and control-room running of dedicated AE experimental sessions scheduled within the JET experimental programme.

Regarding the development of existing hardware, various matching units designed for the optimization of the antenna currents were successfully built, installed, tested and used for routine operation. Figure 5.1.1 shows the measured antenna currents obtained using various matching units. The TAE frequency range for usual combinations of the JET magnetic field and density is covered efficiently with high

antenna current operation. This results in improving the antenna-plasma coupling and in high signal-to-noise ratio when the excited modes are observed on the Mirnov coils. The engineering signals have been fully calibrated using a high-voltage *in situ* method, which has been found to be superior to the usual low-voltage remote approach. This has now finally resulted in the resolution of a long-standing discrepancy between the impedance measurements obtained via a network analyzer outside plasma operation, and those deduced form the voltage/current measurements during a JET pulse, which completely confirms the accuracy of the measurements performed with the new antenna system.

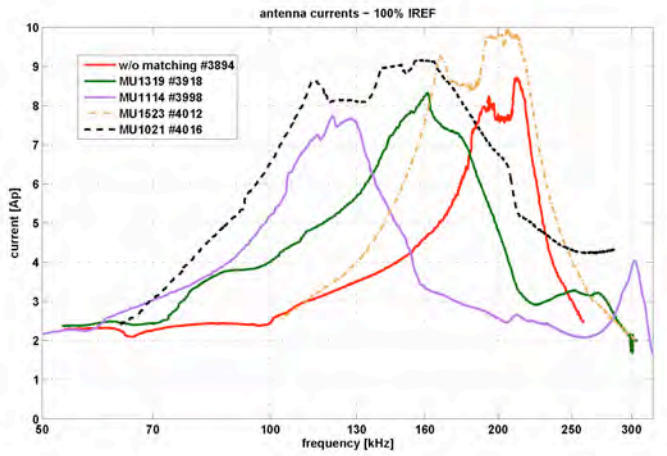

Fig. 5.1.1 *Comparison of the antenna currents obtained on vacuum shot with various matching units, optimized for different frequency ranges.*

In addition to the dedicated experimental sessions, measurements have been taken routinely (i.e. parasitically to the main JET experiments) of the frequency and damping rate of Toroidal Alfvén Eigenmodes (TAEs) with toroidal mode numbers (n) in the range $|n|<20$. This has been facilitated by the successful implementation of the *SparSpec* software as part of the real-time control software within the Alfvén Eigenmode Local Manager (AELM). This has allowed us to separate the measured (frequency-degenerated) multi-harmonic spectrum into its individual components, whose frequency separation is usually of the same order as their damping (i.e. their *line width* in frequency space). Before integrating it within the real-time signal server, we tested the new software on the bench by simulating operation using selected shots from the past and also ran it parasitically on a number of plasma shots. Several bugs were spotted and modifications had to be made. The *SparSpec* real-time detection software is now fully operational, and is routinely used during JET operation as it is a very robust mode detection and discrimination algorithm. Now, it is possible to target modes or sets of modes with specific toroidal mode numbers n and measure their damping rate as the plasma parameters evolve. An example of this use is shown in Figs 5.1.2 and 5.1.3: whereas in the spectrogram shown Fig. 5.1.2 we notice three distinct bands of TAEs, using *SparSpec* we recognize that the lower frequency band consists of three different modes, as shown in Fig. 5.1.3. A further example of the accuracy of the real-time implementation of SparSpec is shown in Fig. 5.1.4, where the real-time signals treated by the AELM are shown. In this example, the user of the system has selected to target modes with n=4-8, which is the set of candidate modes. As verified by the post-pulse analysis, the systems correctly finds and tracks n=4 TAEs at t=9.5s when the proper mode resonance identification criteria are fully met.

During the JET 2008/9 experimental campaigns, KC1T was operated in more than 700 JET discharges with each discharge providing tens of damping measurements of various toroidal mode numbers. Thus, a damping rate database is being built, which so far includes more than 10'000 damping measurements for different plasma configurations. This database will be used to systematically study the stability of AEs on JET by revealing possible dependencies on macroscopic plasma parameters and comparing the experimental findings to the theory predictions.

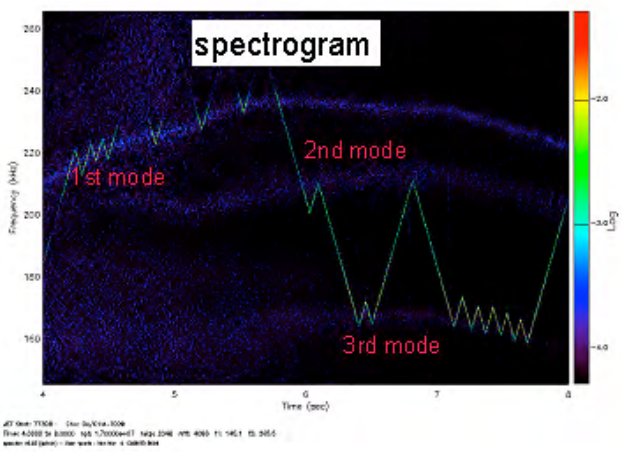

Fig. 5.1.2 *Spectrogram of the magnetic perturbation measured for the JET shot #77308: three different bands where modes are excited by the AE antennas are observed, but it is only with the SparSpec analysis shown in Fig. 5.1.3 that we can determine precisely the mode numbers.*

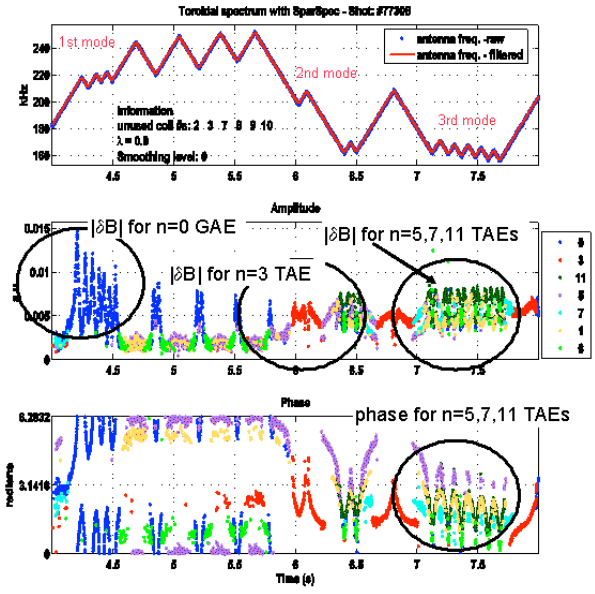

Fig. 5.1.3 *SparSpec analysis of the synchronously detected data corresponding to the spectrogram shown in Fig. 5.1.2: we find that three separate n=5, n=7 and n=11 coexist in the lowest frequency band around 160kHz.*

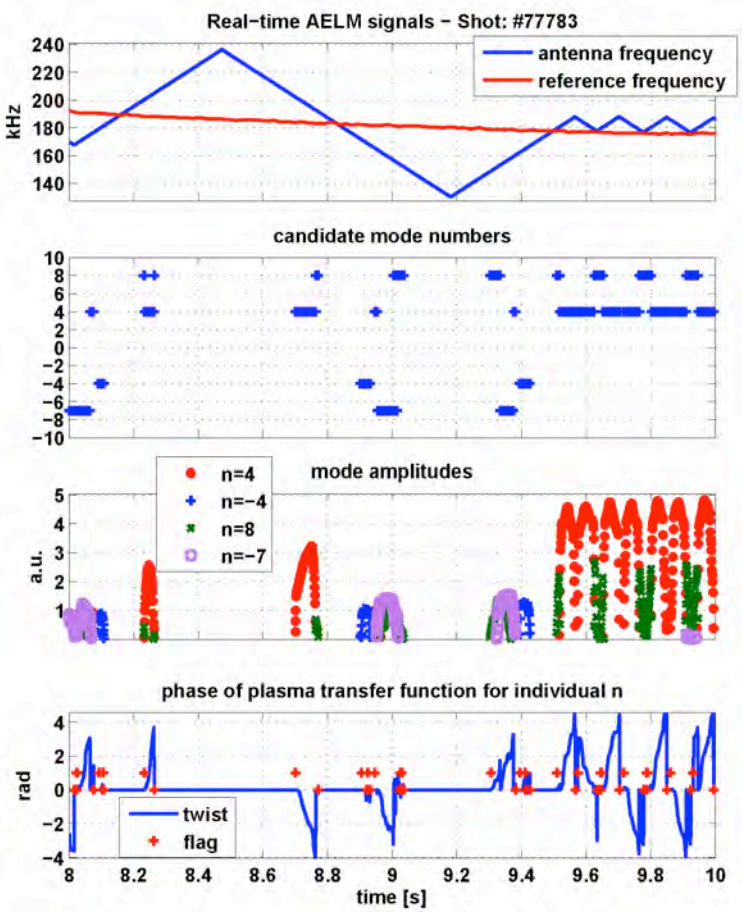

Fig. 5.1.4 *Comparison of the mode number decomposition obtained in real-time and post-pulse with the SparSpec code.*

Dedicated experimental sessions have been run to measure the dependence of the damping rate for medium-n TAEs on the edge shape parameters, such as the elongation and magnetic shear, keeping fixed profiles of the plasma density and temperature and of the core safety factor. It has been found that, consistently with the previous results for low-n modes, the damping rate of n=3-7 TAEs increases by almost a factor 3 when increasing the edge elongation (κ_{95}) from κ_{95}=1.25 (limiter phase) to κ_{95}=1.55 (X-point phase). Progress is being made on the analysis of this data, with the aim of preparing a full database for the damping rate of the individual n-components. In the framework of an ITPA-sponsored activity, a number of selected time points have been analysed in conjunction with the theoretical models provided by the LEMAN and LIGKA codes, resulting in the first direct benchmark and validation of these numerical tools for medium-n TAEs.

One such example is given in Fig. 5.1.5, where several damping measurements of n=3 TAEs have been obtained. In this JET discharge, the limiter plasma was subject to a very slow edge elongation increase over about 10s while the other background plasma parameters were stationary. The damping rates of n=3 TAEs were measured several times throughout this phase, allowing us to identify a clear increase as a function of the edge elongation. The damping rates γ/ω span the range from 0.3% at low values of edge elongation to 5% at high values of edge elongation. Moreover, the increase of the damping rate from 0.3% to 1% in the time interval t=4.5÷6s, when the edge elongation is constant, can be due to the effect of the decrease in q_0 from q_0=1.1 to q_0=0.87, combined with the increase in density. The frequencies and damping rates predicted for the n=3 TAEs with the LEMan

code, shown in Fig. 5.1.5, are in good agreement with the experimental measurements with the exception of the damping rate for the highest elongation.

Further dedicated experimental sessions have been run to assess the dependence of the damping rate of medium-n TAEs as function of the plasma effective mass A_{EFF} for n=3÷12 TAEs. This parameter is particularly important because it enters theoretical damping rate mechanisms depending on the ion Larmor radius. Similar experiments performed for low-n TAEs have conclusively demonstrated that only gyrokinetic codes can provide a good understanding of the damping rate for these modes, and effort is now ongoing to extend the ITPA benchmark exercise reported previously to these cases.

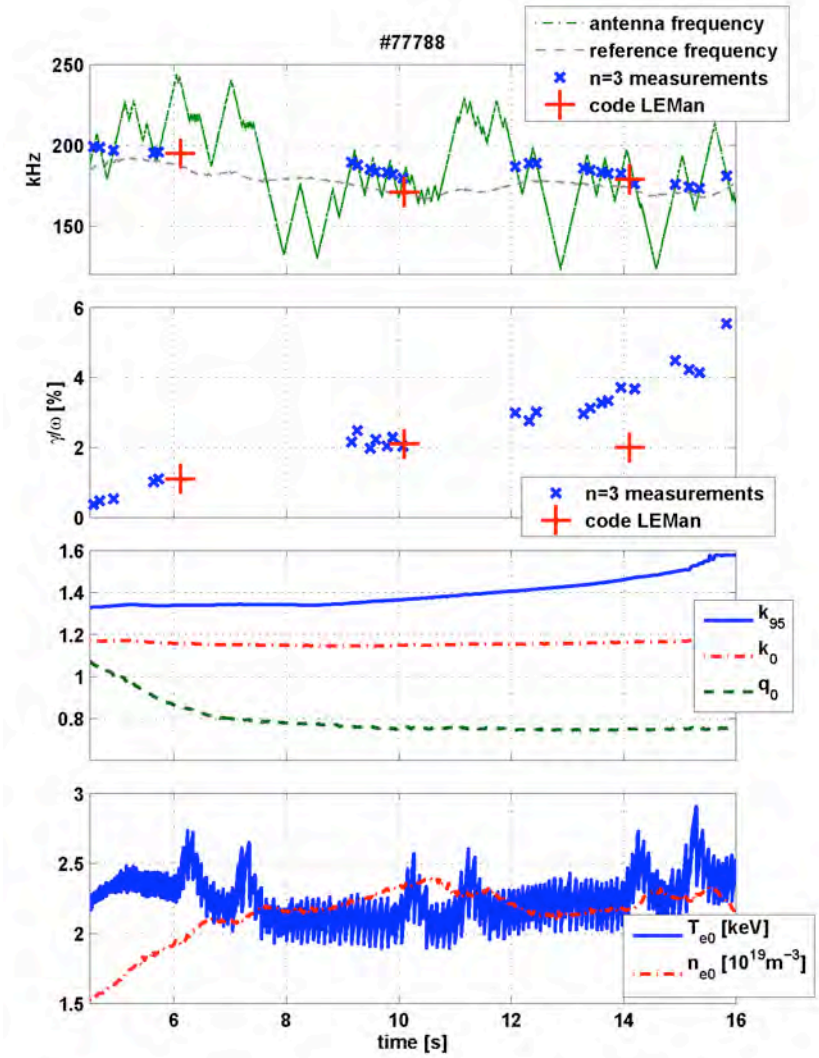

Fig. 5.1.5 *Overview of the main background plasma parameters for the JET shots #77788 where an n=3 TAE was detected and its evolution tracked in real-time; we also show the measured damping rate and frequency, and the results obtained with LEMan code.*

Operation of the new AE antennas in JET on a variety of ITER-relevant plasma regimes has allowed us to determine that the modes most likely to become unstable in ITER due to fast ion drive are those with toroidal mode numbers $|n|<15$, as in current JET experiments we do not see evidence of stable $|n|>15$ modes with small damping rate <0.1%, i.e. very close to the marginal stability limit. Some of these

experimental measurements are now being compared with theoretical predictions, so as to determine the main damping mechanisms.

5.1.4 General diagnostic support for JET operation

CRPP staff has been involved throughout 2009 in ensuring reliable operation of the low and high energy Neutral Particle Analyzers (NPA) diagnostics (KF1 and KR2). After minor repairs on both NPA diagnostics during March-April 2009, they were made again fully operational for the whole of the C27 campaign. In addition to the routine measurements of H/D fluxes from the low energy NPA and fast H tails in minority heating schemes from high energy NPA, the first measurements of neutral 4He and 3He escaping the plasma were done, via tuning the system for detection of single ionized ions produced by the stripping foil.

CRPP staff has also been involved in the routine operation and data analysis in support of JET operation for the temperature and density profiles provided by the LIDAR systems, and for the observations of MHD instabilities using the KC1M diagnostic system.

5.2 Collaborations on other fusion experiments

Other collaborations inlcuded:

- Stability Studies of ARIES Compact Stellarator Reactors - Collaboration with General Atomics, USA
- On the possible usage of the T-10 heavy ion beam for poloidal magnetic flux measurements - Collaboration with RRC Kurchatov, Russian Federation
- TCV and C-Mod collaboration on rotation inversion with density, MIT, USA
- Control of ECH polarization – Collaboration with National Institute of Fusion Science, Japan Contribution to JT60-SA [*]
- Reflectometry measurements on TEXTOR – Collaboration with FZJ, Jülich, Germany

An ongoing collaboration on reflectometry measurements exists between the TEXTOR and TCV devices. The TEXTOR tokamak features an advanced correlation reflectometry diagnostic, using two simultaneous frequencies and two launching antennae, one on the midplane and one at the top of the device. Four poloidally spaced receiving antennae are available at each location, and tunable receivers permit a variety of turbulence correlation measurements with both poloidal and radial spacing. Time delay detection can additionally provide information on the ExB flow. A Ph.D student has spent five weeks at TEXTOR in 2009 to carry out a measurement campaign of correlation lengths and flows in the edge barrier region of H-mode plasmas with an ergodic divertor. The results are promising and data analysis is currently underway. Further measurements are planned for early 2010 to complete the dataset

Design of a phase contrast imaging diagnostic for MAST – Collaboration with UKAEA, Culham Science Centre, UK
A phase contrast imaging diagnostic has been proposed for studying electron-scale turbulence in the MAST spherical tokamak. The CRPP is collaborating on this

[*] Part of Swiss Voluntary Contribution to Broader Approach. Not part of the Association workprogrammeme

project owing to its long-standing expertise in this technique. The collaboration has so far involved remote technical discussions, mediated by a CRPP member currently on site at Culham, and visits to MAST by CRPP personnel are expected in the future.

Participation of Switzerland to the Broader Approach (BA) through the JT60-SA project

In the context of the negotiation between EU and JA about ITER, it has been agreed that several projects relative to the fusion research will be integrated under the BA concept, in which both partners (EU and Japan) will collaborate in order to accelerate the development of fusion as a source of energy. Several EU countries participate to this project, and the Swiss government decided to support the ECRH part by supplying in kind the procurement of the High Voltage Power Supplies (HVPS) required to power the gyrotrons.
The contribution of CRPP as RO (Responsible Officer) for EU in the ECRH domain has been started in 2008. The continuation of this task in 2009 can be highlighted by the main points listed below:

- The participation of a CRPP representative to the TCM-4 (Technical Coordination meeting) at Naka (JA), in order to investigate both the mode of operation of the gyrotrons on JT60-U and the site characteristics where the Swiss power supplies will be installed.
- The kick-off of a collaboration with a Swiss industry well known in the domain of the HVPS allowing to study a supply topology for gyrotrons in the framework of JT60-SA and ITER. Then, the follow up of this task by participating to regular review meetings.
- The continuous exchange of information with the JAEA colleagues in view of the preparation of the specifications for the HVPS to be delivered by the Swiss company
- The reporting to F4E through the EU PL (Project Leader)

The future work will be oriented to the finalisation of the HVPS specifications and the preparation of the HVPS PA (Procurement Agreement) defining the rules applied to the Swiss in-kind contribution.

5.3 Plasma surface interactions in collaboration with the University of Basel

A modification of JET is presently being prepared for installation in 2009, to bring operational experience in steady and transient conditions with ITER-like first wall and divertor materials, geometry and plasma parameters. One aspect of this change is that the reflectivity of metallic components is significantly higher than that of carbon fibre composite. Reflectivity measurements of JET sample tiles have been performed at the Univ of Basel, and these data are used within a simplified model of the JET vessel to predict additional contributions to quantitative spectroscopic measurements of e.g. Bremsstrahlung and impurity influx. The model is also applied in actual ITER geometry for comparison

Rhodium is considered as one of the most promising materials for the first mirrors of diagnostic systems of ITER, due to its high reflectivity in the visible range and its low sputtering yield. It is thus envisaged to use rhodium coatings on polished metallic substrates. To ensure the reliability of these components in a nuclear fusion environment it is necessary to determine their chemical stability and in particular the reactivity of rhodium towards typical impurities in a tokamak such as oxygen. Indeed any change in the surface composition will affect the mirror reflectivity and in turn the signal measured by the diagnostic system. To investigate

this, annealing cycles were carried out (10 times for 5h at 200 C in air). No evolution of the total and the diffuse reflectivity are observed in the range of 250-2500nm. The optical observations did not reveal any modification or delamination of the layer. To investigate relevant ITER baking procedure, one sample deposited on molybdenum was annealed for 6h at 400 C in vacuum (1.10^{-4}Pa). The observations after this treatment were similar as previously described, i.e., no change of the reflectivity, no delamination and no surface modification.

5.4 Collaborations with other EURATOM Associations

Y. Andrew, JET, Abingdon, UK, *"Plasma rotation measurement comparison between JET and TCV plasmas"*

J-F. Artaud, V. Basiuk, Association EURATOM-CEA, France, *"Coupling of the DINA-CH and CRONOS codes to simulate the ITER hybrid scenario"*

K. Avramidis, Association Euratom Hellenic Republic, Greece, *"Studies of high-power gyrotrons for ITER"*

I. Chapman, UKAEA Fusion, UK, *"Sawtooth Stability with Fast Ions"*

A. dellaCorte, Association EURATOM-ENEA, Italy, *"Assembly and instrumentation of a ENEA-broader approach prototype conductor"*

D. Coster, IPP-Garching, Germany, *"SOLPS simulations of scrape-off layer in TCV and JET elmy-H discharges"*

C. Cianfarani, ENEA-Frascati, Italy, *"Development of low-temperature co-fired ceramic magnetic pick-up coils for the measurement of high-frequency instabilities in the FTU tokamak"*

J. Decker, Y. Peysson, CEA-Cadarache, France, *"Electron Bernstein Wave Heating and Current Drive in axisymmetric toroidal plasmas"*

T. Eich, IPP-Garching, Germany, *"Parallel transport dynamics of type-I ELMs in JET and comparison to PIC modelling"*

L.-G. Eriksson, CEA Cadarache, France, *"Ion cyclotron current drive, heating, and sawteeth"*

X. Garbet, Ph. Ghendrih, V. Grandgirard, G. Falchetto, Association EURATOM-CEA, France, *"Gyrokinetic global turbulence simulations"*

M. Hirsch, IPP-Greifswald, **E. Holzhauer,** University of Stuttgart, Germany, *"Loan of two homodyne single-frequency reflectometers and participation in reflectometer measurements and analysis on TCV"*

F. Jenko, T. Goerler, F. Merz, IPP-Garching, Germany, *"Development and application of the gyrokinetic code GENE"*

T. Johnson, EURATOM-VR Association, Stockholm Univ., Sweden *"Ion cyclotron current drive, heating, and sawteeth"*

A. Koenies, V. Kornilov, A. Mishchenko, S. Sorge, IPP Greifswald, Germany, **A. Bottino, A. Peeters**, IPP Garching, Germany, **R. Hatzky**, Rechenzentrum MPG Garching, Germany *"Linear and nonlinear gyrokinetic code developments and simulations"*

A. Krämer-Flecken, Forschungszentrum Jülich, Germany, *"Fluctuation studies by reflectometry on the TCV and TEXTOR tokamaks"*

P. Lauper, IPP-Garching, Germany, *"Damping rates of Alfvén Eigenmodes: theory-experiment comparison"*

H.P. Laqua, IPP Greifswald, Germany, *"Electron Bernstein Waves on TCV"*

E. Lazzaro, **M. Lontano**, **G. Grosso**, EURATOM-ENEA-CNR Association, Italy, *"Development of a linear plasma device for basic wave-particle interactions studies"*

M. Lewandowska, EURATOM-Poland Association, Un. Of Stectin, *"Hydraulic experiments and modeling of CICC"*

Y. Peysson, J. Decker, Association EURATOM-CEA, France, *"Quasilinear Fokker-Planck simulations and modelling of hard X-ray emission in TCV"*

A. Rodrigues, N. Cruz, C. Varandas, CFN Lisbon, Portugal, *"Advanced plasma control for TCV"*.

S. Shibaev, Association UKAEA Fusion, UK, *"Data acquisition for fast framing camera on TORPEX and TCV"*

G. Temmerman, UKAEA-MAST, UK, *"Inner-outer divertor power assymetries on TCV (using another fast IR camera we will borrow from MAST for our inner, as yet undiagnosed divertor) & Investigating the effect of optical filters on improving the S/N ratio for infrared divertor measurements"*

I. Tigelis, G. Latsas, Association Euratom Hellenic Republic, Greece, *"Instability calculations in the 170GHz coaxial-cavity-gyrotron beam-duct"*

J. Urban, IPP, Acad. Of Science of Czech Republic, Praha, CZ, *"Benchmarking of the AMR (Antenna Mode-Conversion Raytracing) and LUKE code for the TCV tokamak EBW experiments"*

G. Veres, M. Berta, B. Tal, S. Zoltenik, Association EURATOM-HAS, KFKI Reasearch Inst. For Particle & Nuclear Physics, Budapest, Hungary, *"Plasma imaging and tomography" and "Mitigation disruption studies, particle transport studies in the SOL, high temporal resolution radiation measurements for ELMs"*

C. Wahlberg, EURATOM-VR Association, Uppsala University, Sweden, *"MHD aspects of the sawtooth instability"*

P. Xanthopoulos, P. Helander, IPP-Greifswald, Germany, **F. Jenko**, IPP-Garching, Germany, *"Geometry interface for Stellarator turbulence"*

L. Zani, Association EURATOM-CEA, France, *"Test of a CEA-broader approach prototype conductor in SULTAN"*

5.5 Other international collaborations

H. Carfantan, Laboratoire d'Astrophysique de Toulouse - Tarbes, Université de Toulouse - CNRS, Toulouse, FR, *"Development of the Sparse Signal Representation method for real-time and post-pulse decomposition and analysis of a frequency-degenerate spectrum"*

P. Chattopadhyay, Inst. For Plasma Research, Bhat, Gandhinagar, India, *"Electron Bernstein Wave heating", "Correlation ECE turbulence measurements"*

G.A. Cooper, R.S. Peterson, Univ. of the South, Sewanee, TN, USA, *"3D finite element ballooning eigensolvers"*

C. Criginski, ESRF Grenoble, France, *"Design study of the superconducting magnet for X ray strectroscopy"*

D. Ernst, Plasma Science and Fusion Center, M.I.T., Cambridge, MA, USA, *"Implementation of a synthetic tangential phase contrast imaging diagnostic in the gyrokinetic code GS2 for TCV"*

R. Ganesh, J. Chowdury, Inst. For Plasma Research, Bhat, Gandhinagar, India, *"Effects of non-adiabatic electron dynamics in gyrokinetic simulations of microinstabilities"*

R. Gruber, EPF-Lausanne, Switzerland, **S.P. Hirshman**, ORNL, USA, **K.Y. Watanabe, H. Yamada, S. Okumara, Y. Narushima**, NIFS, Japan, **K. Yamazaki**, Nagoya Univ., Japan, *"3D anistropic pressure equilibrium and fluid magnetohydrodynamic stability"*

R.W. Harvey, A.P. Smirnov, E. Nelson-Melby, CompX, San Diego, CA, USA, *"Modelling of electron cyclotron wave propagation and electron cyclotron emission in TCV"*

W. Heidbrink, H. Boehmer, UC Irvine, USA, *"Sources for energetic ions for a simple magnetized torus"*

S.P. Hirshman, Oak Ridge National Laboratory, USA, *"Three-dimensional anisotropic pressure free boundary equilibria: the ANIMEC code"*

J. Hittinger, R. Berger, Lawrence Livermore National Laboratory, USA, **E. Valeo**, Princeton University, USA, and *"Development of numerical methods for Vlasov simulations"*

M.Yu. Isaev, Russian Research Centre Kurchatov Institute, Moscow, Russia *"Development of the VENUS-df Code for Bootstrap Current and Neoclassical Transport in Stellarators"*

M.Yu. Isaev, Kurchatov Inst. Moscow, Russia, **H. Maassberg, C. Beidler, J. Nuehrenberg, M. Schmidt, J. Geiger**, IPP-Greifswald, Germany, **A. Bergmann**, IPP Garching, Germany, *"Montecarlo-delta-f neoclassical transport in 3D systems"*

K. Kim, KBSI, South Korea,, "*Assembly and test of the Korean TF conductor qualification sample KOTF2*"

N. Kirneva, RRC Kurchatov Institute, Moscow, Russia, *"Investigation of turbulent tokamak plasma self-organization and influence of the tokamak cross-section geometry on the plasma-pressure self-consistant radial profile"*

S.Yu. Medvedev, A.A. Martynov, A.A. Ivanov, Yu.Yu. Poshekhonov, Keldysh Institute of Applied Mathematics, Moscow, Russia, **M.Yu. Isaev, V.D.Shafranov, A.A. Subbotin**, RRC Kurchatov Institute, Moscow, Russia, *"Equilibrium and Stability of 2D and 3D plasma configurations"*

M. Mikhailov, A. Subbotin, V.D. Shafranov, M.Yu. Isaev, M. Samitov, Russian Research Centre Kurchatov Institute, Moscow, Russia; J**. Nuehrenberg**, Max Planck Institut fuer Plasma Physik, Greifswald *"Optimisation of Advanced Stellarator Systems"*

J. Miller, ORNL, USA, *"Test of the US TF conductor qualification sample USTF3 and USTF4"*

N. Mitchell, ITER Organisation, *"Assembly of the US TF conductor qualification sample USTF4", "Development of a solder filled termination", "Preliminary development of a thermal-hydraulic code", "Design of the ITER superconducting bus bars" and "A buoyancy experiment on TF conductor Option2"*

G.R. Odette, Univ. California Santa Barbara (UCSB), Santa Barbara, CA, USA, *"Fracture mechanics and small specimen test technology"*

K. Okuno, JAEA, Japan, *"Assembly and test of the Japanese TF conductor qualification sample JATF4"*

A. Peeters, Y. Camenen, Warwick Univ., UK, *"Modelling of plasma rotation and momentum transport on the TCV tokamak"*

F. Poli, Warwick Univ., UK, *"Characterization of the linear and nonlinear spectral properties of plasma density fluctuations in the TORPEX device in a limited magnetic configuration"*

B. Rogers, Dartmouth College, USA, *"Theoretical characterization of turbulence in TORPEX plasmas"*.

P. Savrukhin, A. Sushkov, D. Kravtsov, RRC Kurchatov Institute, Moscow, Russian Federation, "*Design and fabrication of a tangential X-ray diagnostic for TCV*"

Dr. T.Shimozuma, National Institute of Fusion Science, Japan, *"Real-time control of ECH polarization"*

F. Skiff, Univ. of Iowa, USA, *"Basic wave-particle interactions and turbulence studies in TORPEX"*

P. Smeibidl, HZB, Berlin, Germany, *"Design and construction of a SC Cable-in-Conduit coil for a horizontal series-connected hybrid magnet system within the framework of the high field magnet project (HFM) at HZB"*

J. Snipes, R. Parker, M. Porkolab, J. Freidberg, J. Sears, **P. Woskov,** PFSC, MIT, USA, *"Fast particle physics, Alfven waves, and active MHD mode excitation on the Alcator C-Mod tokamak plasma"*

D. Tskhakaya, Innsbruck Univ., Austria, *"Comparison of SOLPS and PIC BIT-1 code simulations of the scrape-off layer in TCV and JET elmy-H mode discharges and TCV fast infrared measurements"*

A.D. Turnbull, General Atomics, San Diego, USA, *"Stability studies of ARIES stellarator configurations"*

K.Y. Watanabe, S. Okamura, Y. Narushima, H. Yamada, S. Sakakibara, National Institute for Fusion Science, Toki, Japan, *"MHD stability in LHD"*

Y. Wu, ASIPP, P.R. China, *"Assembly and test of the Chinese TF conductor qualification sample CNTF1"*

J. Yu, China Institute of Atomic Energy (CIAE), Beijing, P.R. China, *"Modelling of radiation damage and radiation effects"*

5.6 Other collaborations within Switzerland

E. Cadoni, University of Applied Sciences of Southern Switzerland, Canobbio, *"High strain rate tensile testing of the EUROFER 97 RAFM steel"*

Besides the activities in the field of plasma wall interaction with the University of Basel, of the socio-economics with the LASEN (EPFL) and CEPE (ETHZ), the CRPP also collaborates with the PSI in the field of materials under irradiation.

6 THE EDUCATIONAL ROLE OF THE CRPP

The CRPP plays a role in the education of undergraduate and postgraduate students, particularly in the Faculté des Sciences de Base (FSB) of the EPFL. Advanced education and training in fusion physics and technology and plasma physics topics is carried out as part of the research activities of the Association. Section 6.1 presents the 6 courses given to physics undergraduates and to engineering undergraduates. In their fourth and final year, physics undergraduates spend time with a research group at the EPFL, typically 12 hours per week for the whole year. During this period, they perform experimental or theoretical studies alongside research staff, discovering the differences between formal laboratory experiments and the "real" world of research. After successful completion of the first year of the Master Programmeme (4^{th} year of studies), physics students are required to complete a "master project" with a research group, lasting a full semester. This master project is written up and defended in front of external experts. The CRPP plays a role in all of these phases of an undergraduate's education, detailed in Sections 6.2 and 6.3.

As an academic institution, the CRPP supervises many Ph.D. theses, also in the frame of the Physics Section of the EPFL. 13 PhDs were awarded in 2009. At the end of 2009 we had 32 PhD students supervised by CRPP members of staff, in Lausanne and at the PSI site in Villigen. Their work is summarised in Section 6.4.

6.1 Undergraduate courses given by CRPP staff

S. Alberti, *Chargé de cours – "Plasma Physics I"*
This course is an introduction to plasma physics aimed at giving an overall view of the essential properties of a plasma and at presenting the approaches commonly used to describe its behaviour. We study single particle motion, the fluid description and the kinetic model. The relation between plasma physics and developing a thermonuclear reactor is presented and illustrated with examples.

N. Baluc - Profresseure titulaire, **J. Fikar, R. Schäublin** - Maître d'Enseignement et Recherche, **P. Spätig** - Maître d'Enseignement et Recherche: *"Fundamentals of radiation damage and effects"*
This 28-hours course is part of the EPFL's Minor in Space Technologies. The objective of this course is to provide a detailed description of fundamental interaction mechanisms between particles and matter, radiation damage and its characterization methods, and radiation effects with emphasis on the relationships between microstructure and mechanical properties. Various types of materials are being considered as well as various examples of applications related to nuclear, semi-conductor and aerospace industries.

A. Fasoli, Professor – *"Plasma physics II"*
One semester option course presented to 4th year Physics students, introducing the theory of hot plasmas via the foundations of kinetic and magnetohydrodynamic theories and using them to describe simple collective phenomena. Coulomb collisions and elementary transport theory are also treated. The students also learn to use various theoretical techniques like perturbation theory, complex analysis, integral transforms and solutions of differential equations.

A. Fasoli, Professor – *"General Physics II"*
This course completes the introduction to mechanics provided in the first semester with the basic concepts of statics, oscillations and special relativity. It also covers the whole of thermodynamics, from the introduction to heat, temperature and kinetic theory to the first and second principles, including entropy and thermal engines, ending with a treatment of transport and non-equilibrium phenomena in open systems.

A. Fasoli, Professor and **M.Q. Tran**, Professor - *"Nuclear fusion and plasma physics"*
The aim of this course is to provide a basic understanding of plasma physics concepts of fusion energy, and of the basic principles of fusion reactors, including the main technological aspects. This course was given within the frame of the Master in Nuclear Engineering.

J.B. Lister, *Maître d'Enseignement et Recherche (MER) – "Plasma Physics III"*
An introduction to controlled fusion, presented as a one semester option to 4th year Physics students. The course covers the basics of controlled fusion energy research. Inertial confinement is summarily treated and the course concentrates on magnetic confinement from the earliest linear experiments through to tokamaks and stellarators, leading to the open questions related to future large scale fusion experiments.

M.Q. Tran, *Professor - "General Physics III and IV"*
This course, given to the Mathematics Section, covers hydrostatic, hydrodynamics waves and electromagnetism (General Physics III) and quantum mechanics (General Physics IV).

L. Villard, *Professeur Titulaire – "Computational Physics I-II"*
Full year course given to students in their 2nd year in Physics. The course covers various time and space integration techniques for ordinary and partial differential equations, and is applied to various physics problems ranging from particle dynamics, hydrodynamical equilibrium, electromagnetism and waves. It includes a strong practical work aspect.

6.2 Undergraduate work performed at the CRPP

EPFL Master students (4th year)

During the Spring semester of 2009, CRPP staff members have supervised 9 students performing their Advanced Physics Laboratory work. During the Automn semester of 2009, we had 10 students, including 3 ERASMUS exchange students.

6.3 EPFL Master degrees awarded in 2009

Urs Amherd: *"Studies of suprathermal electrons on the TCV tokamak"*

Sébastien Boutinard Rouelle: *"Déposition en phase vapeur de couches de SiO_x par jet de plasma à basse pression: etude du procédé par spectroscopie d'émission optique"*

Alexandre Bovet: *"Anomalous diffusion of fast ions in the presence of fishbone instabilities in tokamaks"*

Alice Burckel: *"Fast ion transport in the TORPEX experiment"*

David Grange: *"First characterisation of the plasma during dry electrical discharge machining (Dry EDM)"*

Jérôme Guterl: *"Investigation of sheath effects on interchange modes in TORPEX plasmas"*

Francis Voutaz: *"Etude de l'influence des termes dominant le transport d'énergie électronique en fonciton de la forme dans des équilibres de TCV"*

6.4 Postgraduate studies

Postgraduate courses given in 2009

N. Baluc, D. Gavillet, R. Schäublin, Ph. Spätig: *"Effects of Radiation on Materials"*
This 28-hours course (2 credits) is part of the EPFL's doctoral programme in Materials Science and Engineering (MX-002). The course is given by three lecturers from the CRPP and one lecturer from the PSI (Dr. D. Gavillet). It is aimed at providing extensive information on the effects of irradiation (neutrons, protons, ions) on the structure, microstructure and mechanical properties of materials for nuclear installations. It is divided into five chapters: 1) introduction to radiation damage and radiation effects, 2) radiation damage and analysis tools, 3) radiation damage and fracture mechanics, 4) radiation effects on materials for fusion reactors, 5) radiation effects on materials for fission reactors.

Doctorate degrees awarded during 2009

Alessandro BORTOLON: *"Plasma rotation and momentum transport studies in the TCV Tokamak based on Charge Exchange Spectroscopy measurements"* (EPFL Thesis 4569(2009))
This thesis is devoted to the detailed and systematic study of plasma rotation in the Tokamak à Configuration Variable (TCV). In TCV, plasma rotation is measured by the Charge eXchange Recombination Spectroscopy diagnostic (CXRS). The spectroscopic signal comes from the perpendicular observation of a low power Diagnostic Neutral Beam Injector (DNBI), which applies a negligible torque to the plasma. Hence, the DNBI/CXRS pair is an effective tool for the experimental study of intrinsic tokamak plasma rotation. During this work, the pre existing toroidal observation view was complemented with two new systems, permitting the measurement of toroidal rotation, on inboard plasma radius, and poloidal rotation in the plasma periphery. The implementation of an automated wavelength calibration procedure, based on reference Neon spectra, permitted the first viable (toroidal and poloidal) rotation measurements of TCV, with uncertainties down to 1km/s. Using upgraded light collection optics and fibre optic transmission lines, simultaneous measurement of core and edge plasma was achieved, with a doubling of the radial resolution of the toroidal rotation measurement. The measurable range of plasma parameters was also extended to higher densities by the installation of

back illuminated CCD detectors. In the present configuration (CXRS09), the diagnostic is capable of routinely measuring toroidal and poloidal plasma rotations with a radial resolution of 1cm and a sample frequency of 10 20Hz, for average plasma densities of $0.8<n_{e,av}<8\ 10^{19}m^{-3}$.
The basic scenario of Ohmically heated discharges in limiter L-mode configuration was initially addressed. A large core toroidal rotation up to u_ϕ 50 km/s in the counter current direction is measured, reversing nearly exactly upon reversal of plasma current I_p. The toroidal rotation profile may be schematically divided into a core, a peripheral and an intermediate region. For q_e 3 (magnetic safety factor at the plasma edge) the core region velocity is relatively flat or slightly "bulged" in the co current direction inside the sawtooth inversion radius. In the peripheral region, the toroidal rotation is small with a monotonic intermediate region. The central rotation appears to be limited to approximately its value at the sawtooth inversion radius. Poloidal rotation u_θ 3 km/s, measured in Ohmic discharges, is only weakly dependent on plasma parameters but reverses with reversed magnetic field, with values and direction coherent iv with neoclassical predictions. Combining u_ϕ and u_θ measurements, the profile of the radial electric field E_r was estimated through the radial force balance equation. E_r down to 8 kV/m (inward directed) is found in the plasma bulk, and close to zero at the plasma edge.
A spontaneous reversal of the toroidal rotation profile is observed when the average density exceeds $n_{e,av}$ 4 $10^{19}m^{-3}$ at low q_e 3, with the plasma now rotating in the co current direction. The transition between the co and counter rotation regimes is studied dynamically using n_e and I_p ramps and with the application of Electro Cyclotron Heating (ECH). The rotation reversal is weakly sensitive to impurity concentration and positive plasma triangularity appears to be a key ingredient. Whilst a physical explanation has not been identified yet, dynamic u_ϕ reversal observations indicate that it results from a changed balance of radial non-diffusive fluxes of toroidal momentum.
The study was extended to the divertor magnetic configuration in which the plasma column rotates in the co current direction at low ne, and u_ϕ reverses at high ne, opposite from the limited configuration. The rotation profile may again be divided into three regions, although the rotation at the plasma periphery does not always remain close to zero but evolves with the plasma parameters. In particular, independently on the core rotation regime, peripheral u_ϕ decreases with n_e and I_p and is strongly sensitive to the ion B ∇B direction, suggesting a link with parallel fluxes in the Scrape-Off Layer (SOL). Combined measurements of CXRS and Mach probe indicate that in the plasma edge toroidal rotation matches the toroidal component of SOL flows. From the analysis of toroidal rotation in stationary and transient phases, a characterization of the momentum transport is presented. The resulting radial momentum diffusivity, of the order of χ_ϕ~ 0.1 $0.3m^2/s$, exceeds by 2 orders of magnitude the neoclassical estimation. A remarkable result is the existence of a "residual stress" component, which sustains a substantial stationary rotation gradient for null background rotation. Conversely, the analysis suggests a minor role for the convective (pinch) component, which is preliminarily confirmed by gyro-kinetic simulations including turbulent Coriolis convective pinch. Neoclassical predictions are in quantitative and qualitative disagreement with the experimental observations.
The effect of the sawtooth instability on the core rotation was addressed in a specific experimental scenario where the inter crash evolution of the core u_ϕ could be measured. The measurement required the development of a fast CXRS acquisition scheme based on a trigger constructed in real time from a Soft X-ray measurement. At the sawtooth crash the plasma core undergoes a strong acceleration in the co current direction (Δu_ϕ 9km/s in the experimental scenario), possibly related to a strong transient toroidal electric field.
The systematic and varied observations reported in this work extend the experimental knowledge of bulk plasma rotation in low confinement regimes. In

particular, the rotation reversal phenomena constitute an important test for momentum transport models of tokamak plasmas.

Emiliano FABLE: *"Experimental and theoretical study of particle transport in the TCV Tokamak"* (EPFL Thesis 4334(2009))
The problem of understanding several experimental features of stationary particle transport observed in different machines is undertaken in the quasi-linear gyrokinetic framework. Several parameters scan around typical parameters of the most exploited scenarios, i.e. L-modes, H-modes and eITBs, are studied by means of initial-value linear gyrokinetic simulations and the logarithmic density gradient at the null of the particle flux is evaluated with a quasi-linear rule that takes into account a full spectrum of pure toroidal modes. With respect to previous works, this study sheds some light on the interplay between the dominant turbulent instability and the background equilibrium parameters in characterizing the stationary density profile. The results obtained seem to reconcile apparently contradicting experimental results on the behavior of plasmas with Te of the order of Ti and varying collisionality (typically H-modes) and of plasmas with Te larger than Ti and varying magnetic shear (typically L-modes). In particular, it is found that when the TEM (Trapped Electron Mode) is the dominant instability the stationary logarithmic density gradient increases with increasing magnetic shear, with increasing collisionality (but in the latter case in a weak way), and with decreasing Te/Ti. On the other hand, when the ITG (Ion Temperature Gradient) mode is the dominant instability, the stationary logarithmic density gradient is found to decrease with increasing collisionality and to be not so sensitive on the magnetic shear. It also increases with increasing Te/Ti. When the two modes have similar importance, what is called a mixed (or transition) regime, the logarithmic density gradient seems to be maximal with respect to collisionality variations (in general with respect to the parameter that causes the variation of mode frequency). This result is also found to stay in preliminary non-linear calculations.

Barbora GULEJOVA: *"SOLPS modelling of ELMing H-mode"*, (EPFL thesis 4562(2009))
Numerical simulation of the tokamak scrape-off layer (SOL) is an essential tool for the prediction of the conditions to be expected in future fusion reactors such as the ITER project, now under construction in Southern France. One particularly important issue regards the estimation of the expected transient power loads on plasma-facing components (PFC) due to magnetohydrodynamic plasma relaxations, known as Edge Localised Modes (ELMs). These loads are a major cause of concern for ITER owing to the very severe restrictions on PFC lifetime (especially the divertor targets) that they will impose if their amplitude is not maintained below a given size. Even though SOL plasma modelling has reached a comparatively high level of sophistication (the ITER divertor is being designed in part with complex edge plasma codes), the majority of simulations are performed for steady state conditions, necessarily excluding the description of transient events.
This thesis explores the utility and validity of the fluid plasma, Monte-Carlo neutrals approach to SOL and divertor modelling in the presence of time dependent ELM phenomena. It aims to test the most complex tool of this type currently available, the fluid (B2.5)-neutral Monte-Carlo (EIRENE) code package SOLPS5, against a variety of ELM sizes in two very different tokamaks, TCV and JET. Although the SOLPS package has been the modelling tool of choice for ITER design, it has not yet been systematically used for the study of ELM transients. A key element throughout is rigorous benchmarking – seeking the best possible agreement between both experiment and simulation and between different codes for the same experiment, using as many different measurements as possible to constrain the model. Such benchmarking attempts are still, unfortunately,

comparatively rare on today's machines.
Fully time-dependent simulations (2-D plasma, 3-D neutrals) have been performed of four H-mode plasmas, two each on TCV and JET, covering Type III and Type I ELMs over a range of pedestal collisionality and energy expelled per ELM from ΔW_{ELM}~0.005→0.7 MJ. The high end of this limit corresponds to the current maximum ΔW_{ELM} which is thought to be tolerable on ITER for acceptable divertor target lifetime. The two tokamaks differ radically in size, input power and divertor geometry, but share carbon as the main PFC material. The SOLPS5 simulations have thus been performed with all carbon charge states included but do not feature activated poloidal drift terms.
The approach is first to seek the closest match to experimental upstream, pedestal/SOL and downstream target profiles during the inter-ELM phase. This is achieved through the specification of radially varying perpendicular particle and heat diffusivities and/or convective radial velocity in order to account for the different transport levels in the edge and SOL regions. Poloidal variation of these transport coefficients is also applied to distinguish between main chamber SOL and divertor regions. This is important in a device like TCV with rather unconventional divertor geometry. Similar reasoning applies even more to the ELM itself, which is known to burst into the SOL in the outboard, unfavourable curvature region and is thus extremely poloidally localized. This has also been accounted for especially in the attempts to simulate the TCV ELM events.
The complexity of the ELM instability continues to prevent a complete theoretical description of the evolution of transport during the event. In SOLPS5, the simplest and currently only method by which the ELM can be simulated is to increase the anomalous transport coefficients used to simulate the pre-ELM state during a brief interval corresponding to the ELM duration, such that the total energy expelled during this time is compatible with that measured experimentally. In the case of TCV Type III ELM, where reasonable upstream and downstream data are available and for which the largest number of sensitivity studies have been performed in this thesis with SOLPS, agreement is good in the pre-ELM phase and reasonable, but less satisfactory during the ELM. This ELM is a largely convective event in terms of pedestal temperature collapse and is, by virtue of its low ΔW_{ELM}, the "least kinetic" of the four events studied. Nevertheless, comparison of the SOLPS5 simulation results at the divertor target with those from dedicated Particle-in-Cell kinetic transport code calculations for the same ELM, demonstrate that kinetic effects are important and must be properly accounted for (by appropriate adjustment of kinetic coefficients in the fluid simulations). This presumably becomes even more important as the ELM size increases, but can only be tested to the extent that the appropriate experimental data is available. As a consequence, the tentative conclusion from the work presented here is that the use of SOLPS in a predictive sense for ITER would at best provide indicative results.
In addition to the code-experiment benchmark, a code-code comparison has also been performed, checking SOLPS5 against published and well known time dependent Type I ELM simulations obtained with the dedicated JET code suite EDGE2D-Nimbus. A benchmark of this complexity has not previously been attempted and has been reassuringly somewhat successful, albeit with some unresolved discrepancies.
A key feature of ELM boundary physics occupying much current research are the energy deposition asymmetries observed at the targets, which favour the inner target during the ELM for forward toroidal field direction and which appear to reverse when the field direction is inverted. These trends are opposite to the behaviour seen in inter-ELM phases, behaviour which is conventionally understood to result from toroidal geometry and the contribution of poloidal drift physics. Added complexity comes from magnetic geometry, a prominent feature of the TCV-JET comparisons described in this thesis, the results of which seem to influence the simulation results (which do not include drift effects).
A recent development has been the suggestion that the ELM, in convecting plasma

from pedestal to SOL regions, carries with it memory of the high toroidal rotation velocity known to characterise the H-mode pedestal on all devices. This hypothesis has been tested here in a preliminary manner, and for the first time in this kind of simulation, by imposing a toroidal velocity inside the magnetic separatrix in the simulations and studying the radial transport of this toroidal momentum into the SOL. Applied in the first instance to the TCV Type III ELM, the indications are that transfer of this rotation into the SOL can drive target asymmetries in the direction seen experimentally, though there are significant negative consequences for the resulting target profiles in other parameters for which a potential resolution would require protracted further study which has not been possible here.

Sébastien JOLLIET: *"Gyrokinetic Particle-In-Cell Global Simulations of Ion-Temperature-Gradient and Collisionless-Trapped-Electron-Mode Turbulence in Tokamaks"* (EPFL Thesis 4326(2009))

Microturbulence is one of the most active fields of research in plasma physics because it is believed to be responsible for anomalous transport. Therefore, understanding and predicting plasma turbulence is extremely important for the performance of future fusion devices such as ITER. This phenomenon is studied with the help of the gyrokinetic theory, which, through an appropriate ordering, eliminates the gyro-angle dependence in the Vlasov-Poisson system. Then, such problems are tackled numerically with the help of gyrokinetic codes.The main goal of this thesis was to develop the gyrokinetic Particle-In-Cell (PIC) global code ORB5, which originally aimed at studying Ion-Temperature-Gradient (ITG) electrosatic turbulence in Tokamak geometry. The PIC approach usually suffers from statistical noise, which unavoidably degrades the qualiy of the simulation. In the first part of this work, the code has been greatly optimized by writing the equations with the straight-field-line angle and applying a Fourier field-aligned filter. The overall result of the optimization is that for a given accuracy, the CPU time has been decreased by a factor two thousand, the total memory has been decreased by a factor ten and the numerical noise has been reduced by a factor two hundred. In addition, the scaling of the code with respect to plasma size is presently optimal, suggesting that ORB5 could compute heat transport for future fusion devices such as ITER. The second part of this thesis presents the validation of the code with numerical convergence tests, linear (including dispersion relations) and nonlinear benchmarks. Furthermore, the code has been applied to important issues in gyrokinetic theory. It is shown for the first time that a 5D global delta-f PIC code can achieve a thermodynamic steady state on the condition that some dissipation is present. This is a fundamental result as the main criticism against delta-f PIC codes is their inability to deal with long time simulations. Next, the role of the parallel nonlinearity is studied and it is demonstrated in this work that this term has no real influence on turbulence, provided the numerical noise is sufficiently low. This result should put an end to the controversy that recently occurred, in which gyrokinetic simulations using different numerical approaches yielded contradictory results. Finally, thanks to the optimization of the code, the gyrokinetic model has been extended to include the kinetic response of trapped-electrons, in place to the usual adiabatic (Boltzmann) approximation. For the first time, global TEM nonlinear simulations are presented, and the role of the zonal flow on heat transport is shown to be less important compared to the ITG case, confirming previous studies performed with local codes. This study will help in acquiring some knowledge on the less-known TEM turbulence (as compared to ITG). In conclusion, this thesis is one of the main steps of the development of ORB5, which is now a state-of-the-art gyrokinetic code for collisionless ITG and TEM turbulence, and has brought several contributions to the understanding of these phenomena.

Sun Hee Kim: *"Full tokamak discharge simulation and kinetic plasma profile control for ITER"*, (EPFL Thesis 4500(2009))
Understanding non-linearly coupled physics between plasma transport and free-boundary equilibrium evolution is essential to operating future tokamak devices, such as ITER and DEMO, in the advanced tokamak operation regimes. To study the non-linearly coupled physics, we need a simulation tool which can self-consistently calculate all the main plasma physics, taking the operational constraints into account. As the main part of this thesis work, we have developed a full tokamak discharge simulator by combining a non-linear free-boundary plasma equilibrium evolution code, DINA-CH, and an advanced transport modelling code, CRONOS. This tokamak discharge simulator has been used to study the feasibility of ITER operation scenarios and several specific issues related to ITER operation. ITER operation scenario 2 has been simulated as a demonstration of the capabilities of the combined simulator, as well as being a design study in itself. The capacity of lower hybrid (LH) for saving the poloidal flux and increasing the safety margins in operating PF coils has been studied. ITER hybrid mode operation has been studied focusing on the capability of operating the plasma with a stationary flat safety factor (q) profile.
In parallel, DINA-CH has been used to study dynamic responses of the free-boundary plasma equilibrium to either external voltage perturbations or internal plasma disturbances using a non-linear free-boundary plasma equilibrium evolution code, DINA-CH. Firstly, the opposite plasma behaviour observed in the magnetic triggering of ELMs between TCV and ASDEX Upgrade has been investigated. Secondly, plasma dynamic responses to strong disturbances anticipated in ITER are examined to study the capability of the feedback control system in rejecting the disturbances.
One of the very challenging issues in ITER, the active control of kinetic plasma profiles, has also been studied. We have developed a robust control technique that simplifies the active real-time control of several kinetic plasma profiles in ITER. The response of the plasma profiles to power changes of auxiliary H&CD systems is modelled. To allow real-time update of the plasma profile response model, the related physics are simplified with several assumptions. The electron temperature profile response is modelled by simplifying the electron heat transport equation and the q profile response is modelled by directly relating it to the changes of source current density profiles. The required actuator power changes are calculated using the singular value decomposition (SVD) technique, taking the saturation of the actuator powers into account. The potential of this control technique has been shown by applying it to simulations of the ITER hybrid mode operation.

Bin LONG: *"Liquid lead-bismuth embrittlement effects on unirradiated and irradiated Ferritic/Martensitic steels for nuclear applications"* (EPFL Thesis 4355(2009))
In liquid metal spallation targets such as the MEGAPIE (the megawatt pilot experiment) target and the future ADS (accelerator driven system) spallation targets, which utilize liquid lead-bismuth eutectic (LBE) as the target material, liquid metal embrittlement (LME) effects on the target structural materials are considered as one of the critical issues that determine the lifetime of the targets. However, nowadays, the LBE embrittlement effects are not yet well understood, particularly under irradiation conditions.
The aim of this work was: (a) to investigate the effects of LBE embrittlement on the mechanical properties of ferritic-martensitic (FM) steels (candidate materials for applications in spallation targets) in various states, and (b) to study the mechanisms of LBE embrittlement effects on the mechanical properties of FM steels.
These two goals have been reached by studying LBE embrittlement effects on the mechanical properties of the T91 FM steel in various conditions: (i) the standard

normalized and tempered condition, (ii) hardened by tempering at lower temperatures, and (iii) after irradiation under high energy proton and spallation neutron mixed spectrum. Mechanical tests such as slow-strain-rate tensile (SSRT) tests and 3-point bending tests have been performed to characterize the mechanical properties of the T91 FM steel and to determine the effects of LBE embrittlement on these mechanical properties. Microstructural analyses such as transition electron microscopy (TEM) and scanning electron mirocopy (SEM) observations have been conducted to obtain the microstructural information needed for understanding the embrittlement mechanisms.
The present results indicate that a great attention should be paid to application of FM steels in liquid LBE, since the mechanical properties of FM steels, such as the ductility and the fracture toughness, can be substantially degraded by LBE embrittlement effects, particularly under irradiation conditions as the LBE embrittlement are enhanced by irradiation-induced hardening. Fundamentally, the observations made in this work suggest that the mechanism responsible for liquid LBE-induced embrittlement effects on FM steels can be essentially interpreted by using the adsorption-induced reduction in cohesion of atomic bonds model combined with the KTC criterion for brittle cleavage fracture.

Mikhail MASLOV: *"Particle transport in JET and TCV H-mode plasmas"* (EPFL Thesis 4450(2009))
The work was dedicated to the investigation of so-called 'particle pinch' phenomena in tokamak plasmas. This effect was observed from the beginning of tokamak history, but early explanations (such as the neoclassical Ware pinch) proved unable to explain the wide variety of observed behaviour. This motivated detailed studies for understanding the underlying processes and for being able to provide guidance as to what kind of density profile to expect in ITER. The work was carried out by collecting experimental data from 2 different tokamaks (JET and TCV), analyzing them and testing linear gyrokinetic simulation results against the experimental observations.
The first part of the thesis describes the resolution of a discrepancy between two main diagnostics on JET for density measurements. A problem in the LIDAR processing code was solved and the discrepancy decreased significantly. This work resulted in reprocessing of all JET LIDAR data collected during 2000-2004 and benefited all subsequent papers using JET LIDAR data from 2006 onwards. Another part of the diagnostic work was dedicated to the technique of far infrared interferometer data inversion (to obtain density profiles from line integrated measurements). A new method was developed and implemented for experimental data analysis part of this thesis.
The second chapter of the thesis is dedicated to the experimental data analysis. A significant density profile database was created on the basis of JET experiments from the 2006-2007 campaigns. More than 700 plasma shots were included and after a careful validation, around 250 entries remained. On the basis of this dataset, dependencies of the density profile gradient on a variety of parameters were investigated. The previous observations done on the JET and AUG tokamaks were generally confirmed. Extrapolation of the derived scaling laws to ITER plasma conditions suggests a peaked density profile, also confirming previous observations. It was also shown that the experimental results do not depend on which of the main density measurement diagnostics (LIDAR or FIR inversion) are used for the analysis.
The next chapter of the thesis work is dedicated to linear gyrokinetic simulations of particle fluxes using the GS2 code. To model the dependencies of the experimentally observed density gradients, a set of linear runs was executed on the PLEIADES2 computing cluster at the EPFL. All the simulations were done with input plasma parameters characteristic of the JET H-mode operating domain. GS2 simulation

showed good agreement with the experimentally measured density gradient over the wide range of input parameters.
The last chapter of the thesis is devoted to TCV H-mode plasmas with full electron cyclotron heating. The first observations of density peaking behaviour in such plasmas were reported at the EPS conference in 2006. For the relatively high collisionality values the observed density peaking was significantly higher than the expectations based on the scaling laws produced on other tokamaks. That result was puzzling at the beginning, but the linear GS2 simulations, done for TCV parameter range in the same manner as described above, have shown that such low T_i/T_e values are consistent with strong density peaking if the ITG mode remains dominant. A follow-up study of the density peaking behaviour in TCV H-modes is still ongoing, with the aim of contributing towards a better understanding of particle transport in unfuelled, electron heated conditions.
As a general conclusion, in this thesis work, the density peaking observed on different tokamaks in H-modes plasmas is found to be consistent with theoretical expectations for anomalous transport due to dominant ITG modes, as indeed calculated to be unstable in these plasma conditions. Peaked density profiles are now expected in ITER instead of the flat ones assumed in the ITER conceptual design. Density peaking is expected to result in higher fusion power. The main part of the thesis (JET experimental data analysis versus GS2 simulations) was published in [M. Maslov et al. "Density profile peaking in JET H-mode plasmas: experiments versus linear gyrokinetic predictions", 2009 *Nucl. Fusion* 49 075037]

Nicolas MELLET: *"Propagation and absorption of low-frequency waves in two and three dimensional warm plasmas"* (EPFL Thesis 4398(2009)
In order to model a broader range of phenomena taking place in three-dimensional plasmas, the LEMan code has been extended to a warm formulation. As the wave propagation is strongly influenced by the parallel wave vector, special attention has been paid for its consistent computation. The choice to concentrate on this quantity has limited the complexity of the problem to the order "0" in the Finite Larmor Radius expansion.
Two methods have been implemented in LEMan. The first technique implies the inversion of a polynomial matrix and requires incorporating the dielectric tensor as a convolution in the linear system. It has been tested successfully and applied to a wide range of cases up to three-dimensional geometries in the Alfvén domain (JET-like equilibrium, straight helix, Large Helical Device,etc...). The frequency and damping of global modes that appear in the gaps formed by the breaking of symmetry can then be determined. Strong variations are observed depending on the presence, for example, of a mode conversion to the Kinetic Alfvén Wave. This method has however displayed numerical limitations in the Ion-Cyclotron Range of Frequencies (ICRF). A new technique based on the iterative evaluation of the parallel wave vector has then been developed. After having tested its agreement with the convolution method, computations in the ICRF domain have been undertaken in two and three-dimensional configurations including the Large Helical Device where the power deposition has been determined. In order to model the contribution of fast ions, a bi-Maxwellian distribution function has been added to the warm dielectric tensor. The fast ion population absorbs in this case an important fraction of the total power in the ICRF domain. In addition, a displacement of the Toroidicity-induced Alfvén Eigenmode frequency has been observed.
The code has been finally optimised and parallelised permitting to perform computations in complicated geometry such as stellarators in the ICRF domain. Furthermore, the approach used here yields a much shorter computation time than for most of the other codes dealing in this domain of frequency.

Pablo MUELLER: *"Finite element modelling and experimental study of brittle fracture in tempered martensitic steels for thermonuclear fusion applications"* (EPFL thesis 4518(2009))

In this work we have studied brittle fracture in high-chromium reduced activation tempered martensitic steels such as Eurofer97 and F82H. The most concerning drawback of these kind of steels is irradiation embrittlement. The aim of this work was to study brittle fracture in the ductile-brittle transition region of this kind of steels in the as-received condition. It is necessary to be able to transfer laboratory specimen fracture data to real components and structures in order to assess the performance of these steels in the different conditions they would find in a fusion reactor. In order to do so, the specimen geometry and size effects on measured fracture toughness need to be properly understood and predicted with an appropriate model. In particular, specimen size effect on measured toughness is a major concern for the nuclear materials research community owing to the limited irradiation volume in current and planed materials irradiation facilities.

The master-curve ASTM-E1921 standard is a method initially developed to determine the ductile-to-brittle transition reference temperature, T_0, in fission reactor ferritic steels from a small number of experiments. In this work the applicability of the master-curve method to reduced activation tempered martensitic steels was studied in detail. Fracture tests with pre-cracked sub-sized compact tension specimens (three different sizes, 0.18T, 0.35T and 0.87T of Eurofer97) were carried out in the temperature range [-196 C, -40 C]. The toughness-temperature behavior and scatter were shown to deviate from the ASTM-E1921 standard predictions near the lower shelf. The athermal component of the master-curve was calibrated to better fit our fracture toughness data from the lower to the middle transition region. We showed that these master-curve adjustments are necessary to make consistent a series of single T_0 determinations performed at different temperatures. The ASTM specimen size limitations were found to be too lenient for this kind of steels. This problem was especially evident in fracture toughness data of Eurofer97 and F82H obtained in the upper transition temperature range with two different specimen sizes. Thus a more stringent specimen size requirement was proposed to avoid inconsistent transition temperature determinations.

Finite element simulations were undertaken for compact, notched and tensile specimens of Eurofer97 steel tested from 20 C down to -197ºC. Three and two dimensional simulations were run in order to calculate the stress and strain fields at the onset of brittle fracture. For each tested temperature, the calculated load-displacement curves were found to reproduce very well those of the experiments. A local approach fracture criterion was studied. This criterion states that when the maximum principal stress is larger than a critical stress within a critical volume ahead of the crack tip, notch or neck, cleavage is triggered leading to macroscopic fracture of the specimen. It was shown that this model is able to predict the minimum fracture load of the notched specimens with the same values of critical stress and critical volume that were calibrated to predict the lower bound of fracture in compact specimens. This local approach model was also successfully used to predict the strong size effect observed experimentally in pre-cracked compact tension specimens in the upper transition region. The critical fracture stress determined in the standard tensile specimens was found higher than that of the fracture specimens. It was suggested that this difference stems from a significant difference in the stress state between the different specimens (triaxiality).

Alessandro MARINONI: *"Plasma fluctuation studies in the TCV tokamak: modelling of shaping effects and advanced diagnostic development"* (EPFL thesis 4516(2009))

One of the most important issues for magnetic-confinement fusion research is the so- called anomalous transport across magnetic field lines, i.e. transport that is in excess of that caused by collisional processes. The need to reduce anomalous

transport in order to increase the efficiency of a prospective fusion reactor must be addressed through an investigation of its fundamental underlying causes.
This thesis is divided into two distinct components: one experimental and instrumental, and the other theoretical and based on numerical modeling. The experimental part consists of the design and installation of a new diagnostic for core turbulence fluctuations in the TCV tokamak. An extensive conceptual investigation of a number of possible solutions, including Beam Emission Spectroscopy, Reflectometry, Cross Polarization, Collective Scattering and different Imaging techniques, was carried out at first. A number of criteria, such as difficulties in data interpretation, costs, variety of physics issues that could be addressed and expected performance, were used to compare the different techniques for specific application to the TCV tokamak. The expected signal to noise ratio and the required sampling frequency for TCV were estimated on the basis of a large number of linear, local gyrokinetic simulations of plasma fluctuations. This work led to the choice of a Zernike phase contrast imaging system in a tangential launching configuration.
The diagnostic was specifically designed to provide information on turbulence features up to now unknown. In particular, it is characterized by an outstanding spatial resolution and by the capability to measure a very broad range of fluctuations, from ion to electron Larmor radius scales, thus covering the ma jor part of the instabilities expected to be at play in TCV. The spectrum accessible covers the wavenumber region from $0.9cm^{-1}$ to $60cm^{-1}$ at 24 radial positions with 3MHz bandwidth. The diagnostic is an imaging technique and is therefore also well suited to investigate inhomogeneous spatial regions, where the need for an excellent spatial resolution is greatest. Additionally, it was also designed as translatable to broaden the region of study, which can extend up to the magnetic axis, in selected configurations. The translatable design combined with the flexibility of TCV in terms of plasma positioning in the vacuum vessel allows the phase contrast system to measure fluctuations across virtually the whole plasma minor radius. The diagnostic is sensitive both to radial and poloidal wave numbers, depending on the configuration. A parallel pro ject to the development and installation of the phase contrast imaging system was the installation of a prototype Doppler reflectometer operating in a homodyne configuration, both in X and in O mode polarization. The reflectometer was operated parasitically to assess its performance which proved to be excellent; it is now routinely available on TCV.
The theoretical part of the thesis consisted of extensive modeling of the effect of plasma shape, in particular triangularity, on turbulent transport by means of linear and nonlinear gyrokinetic simulations. This was motivated by experiments on TCV that had shown a vi dramatic improvement in confinement, up to a factor of two, in inverting the sign of the triangularity from positive to negative. Negative triangularity was indeed found to have a stabilizing influence on ion scale instabilities, specifically on the so called trapped electron mode (TEM). Simulations were carried out on actual TCV shots and the variation of the heat flux with triangularity calculated by the nonlinear simulations is in fair agreement with the experimental results. Linear simulations and a simple analytical model explain, in agreement with nonlinear runs, the resulting stabilization as a result of a rather complex modification of the toroidal precessional drift of trapped particles exerted by negative triangularity.

Gennady PLYUSHCHEV: *"Interaction of supra-thermal ions with turbulence in magnetised toroidal plasma"* (EPFL thesis 4543(2009))
This Thesis addresses the interaction of a supra-thermal ion beam with turbulence in the simple magnetized toroidal plasma of TORPEX.
The first part of the Thesis deals with the ohmic assisted discharges on TORPEX. The aim of these discharges is the investigation of the open to closed magnetic field line transition. The relevant magnetic diagnostics were developed. Ohmic assisted

discharges with a maximum plasma current up to 1kA are routinely obtained. The equilibrium conditions on the vacuum magnetic field configuration were investigated.
In the second part of the Thesis, the design of the fast ion source and detector are discussed. The accelerating electric field needed for the fast ion source was optimized. The fast ion source was constructed and commissioned. To detect the fast ions a specially designed gridded energy analyzer was used. The electron energy distribution function was obtained to demonstrate the efficiency of the detector.
The experiments with the fast ion beam were conducted in different plasma regions of TORPEX. In the third part of the Thesis numerical simulations are used to interpret the measured fast ion beam behavior. It is shown that a simple single particle equation of motion explains the beam behavior in the experiments in the absence of plasma. To explain the fast ion beam experiments with the plasma a turbulent electric field must be used. The model that takes into account this turbulent electrical field qualitatively explains the shape of the fast ion current density profile in the different plasma regions of TORPEX. The vertically elongated fast ion current density profiles are explained by a spread in the fast ion velocity distribution. The theoretically predicted radial fast ion beam spreading due to the turbulent electric field was observed in the experiment.

Christian SCHLATTER *"Turbulent ion heating in TCV tokamak plasmas"*, (EPFL thesis 4479 (2009))
Back in 1996, when a TCV plasma was first subjected to ECCD, a puzzling energisation of the ions, perpendicular to the confining magnetic field, was observed on the charge exchange spectrum measured with the vertical neutral particle analyser (VNPA). It was soon concluded that the ion acceleration was not due to power equipartition between electrons and ions, which, due to the absence of direct ion heating on TCV, has thus far been considered as the only mechanism heating the ions. However, although observed for more than ten years, little attention was paid to this phenomenon, whose cause has remained unexplained to date.
The key subject of this thesis is the experimental study of this anomalous ion acceleration, the characterisation in terms of relevant parameters and the presentation of a model simulation of the potential process responsible for the appearance of fast ions. The installation of a new compact neutral particle analyser (CNPA) with an extended high energy range (50keV) greatly improved the fast ion properties diagnosis.
The energisation and the properties of fast ions were studied in dedicated, low density, cold ion, hot electron plasmas, resonantly heated at the second harmonic of the electron cyclotron frequency. The ion acceleration occurs on a characteristic timescale in the sub-millisecond range and comprises up to 20% of the plasma ions. The number of fast ions n_i^s and their effective temperature T_i^s are found to depend strongly on the bulk and suprathermal electron parameters, in particular $T_i^s \quad T_e^b$ (electron bulk) and $n_i^s \approx v_{de}$ (toroidal electron drift speed). The suprathermal electrons, abundantly generated in plasmas subjected to ECCD, are diagnosed with perpendicular and oblique viewing electron cyclotron emission (ECE) antennas and the measured frequency spectra are reconstructed with the relativistic ECE radiation balance code NOTEC-TCV. With steady-state ECRH and ECCD, the fast ion population reaches an equilibrium state. The spatial fast ion temperature profile is broad, of similar shape compared to the bulk ion temperature profile. The hottest suprathermal temperature observed is T_i^s 6keV.
Various potential ion acceleration mechanisms were examined for relevance in the TCV parameter range. The simultaneous wave–electron and wave–ion resonances of ion acoustic turbulence (IAT) show the best correlation with the available experimental knowledge. Ion acoustic waves are emitted by the weakly relativistic circulating electrons and are mainly Landau damped onto the ions. Destabilisation

of IAT is markedly facilitated by the important degree of nonisothermicity T_e/T_i 40 of X2 EC heated TCV plasmas.
Efforts were undertaken to consistently model the experimental observations using a numerical experiment. The relevant physics describing IAT was implemented in a finite difference code solving the quasilinear diffusion equation describing the time evolution of the electron and ion distribution functions. The simulations, fed as far as possible with experimentally available information, confirm the growth and saturation of IAT. Electrons and ions are initially preferentially heated in the toroidal direction. As the ions gain energy, the ion waves are damped more efficiently and only modes propagating at oblique angles can still grow, thus accelerating ions into the radial perpendicular direction. The simulation shows that turbulence reaches a steady-state when the ions are sufficiently hot to permanently stabilise IAT. The parameters describing the tail of the modelled equilibrium ion distribution agree quantitatively well with the CNPA measurement.
Preliminary studies investigated on the interaction of fast ions with the sawtooth instability. It is found that the fast ion population in sawtoothing plasmas is transiently enforced with each sawtooth collapse. It is presently thought that the toroidal electric reconnection field lowers the IAT stability threshold thus producing more suprathermal ions.

Costanza ZUCCA: *"Modeling and control of the current density profile in tokamaks and its relation to electron confinement"*, (EPFL thesis 4360(2009))
The current density in tokamak plasmas strongly affects transport phenomena, therefore its understanding and control represent a crucial challenge for controlled thermonuclear fusion. Within the vast framework of tokamak studies, three topics have been tackled by the present thesis: 1. the modelling of the current density evolution in eITB discharges in TCV; 2. the study of current diffusion and inversion of electron transport properties observed during Swing ECCD discharges in TCV; 3. the analysis of the current density tailoring obtained by local ECCD driven by the improved EC system for sawtooth control and reverse shear scenarios in ITER.
The study of eITBs in TCV was undertaken to identify which of the main parameters related to the current density plays a relevant role in the confinement improvement created during these advanced scenarios. The current density has to be modeled, there being no measurement currently available on TCV. The ASTRA interpretative simulations showed that the thermal confinement improvement factor linearly increases with the absolute value of the minimum shear outside ρ>0.3, and therefore confirmed a general observation that the formation of the transport barrier is correlated with the magnetic shear reversal. The increase of confinement with the negative magnetic shear was observed to be gradual, but constant, and did not depend on specific values of the safety factor. Therefore, the transition from standard to improved confinement appeared to be smooth, although it can be very fast.
The flexible EC system in TCV also allowed performing transport studies on plasmas characterized by low confinement, in which we locally modified the magnetic shear profile around the deposition location. For instance, alternate and periodic injection of co- and counter-ECCD within the same plasma discharge was realized while maintaining the same total input EC power. Such a heating scheme is the basis of Swing ECCD experiments, which were initially carried out using nearly on-axis EC deposition locations in the plasma, in order to maximize the EC power absorption, and therefore the magnetic shear variation. The ASTRA simulations pointed out the effects of Swing ECCD on the magnetic shear and on the electron temperature profile around the radius at which the EC waves are absorbed. Both profiles turned out to be modulated at the same frequency as the frequency of the Swing ECCD. Moreover, the maximum magnetic shear variation was observed to be independent of the transport models used for the simulations, therefore underlying the robustness of the modeling. Additionally, the numerical

results motivated further experiments with more off-axis EC deposition, which were found roughly in agreement with recent gyrokinetic predictions, according to which, at higher positive values of the magnetic shear, an inversion of the transport properties should occur.
The aim of the ITER study was to analyse the capabilities of a possible variant of the EC system, recently proposed with the intent to optimize the combined action of the Upper and Equatorial EC Launchers and, therefore, to allow a broader operational domain for ITER. This variant will maintain the main goals for which the ITER EC system was originally designed, namely the stabilization of Neoclassical Tearing Modes (NTMs) and of the sawtooth instability. Besides, the suggested variant paves a way for further exploitation of EC waves for ITER. The present ITER base-line design has all EC launchers providing only co-ECCD. The performed numerical modeling showed that the possibility to drive counter-ECCD with one of the three rows of equatorial mirrors offers greater control of the plasma current density. The counter-ECCD may also be balanced with co-ECCD to provide pure EC heating, with no net driven current. This would be an additional asset if EC waves were found to be needed to assist the L-H transition during plasma ramp-up. The overall decrease in co-ECCD, by turning one row to counter-ECCD, is estimated to be negligible, because the difference between full off-axis co-ECCD using all 20MW from the Equatorial Launcher or co-ECCD driven by 2/3 from the Equatorial Launcher and 1/3 from the Upper Launcher is small. Therefore the latter analysis provides a strong evidence of the substantial gain in flexibility if the suggested variant of the ITER EC system were accepted as the base-line design.

Ph.D. Theses supervised by CRPP staff at the end of 2009

Mattia ALBERGANTE: *"Microtubulence driven transport of energetic ions"*
The question whether and to what level microturbulence can affect the transport of energetic ions has been addressed. The introduction of a velocity space dependent diffusivity, together with the parameters from the ITER steady state scenario, have been employed in the analysis. This allowed for a detailed description of the anomalous behaviour of fast ions in a burning plasma discharge.
The results indicate that neoclassical diffusivities, so far considered as being the dominant transport channel for suprathermal particles, are more than one order of magnitude smaller than anomalous expectations. This statement is particularly true for the electrostatic component of the turbulent transport, while magnetic components become important only at very large energies and high plasma beta. Finally, anomalous transport of energetic ions is expected to be subject to a local enhancement, being it stronger on the low field side of the tokamak.

Karim BESSEGHIR: *"Full tokamak simulations for ITER"*
Accurate knowledge of the magnetic fluxes and surfaces, which constitute the environment within which the plasma evolves, is necessary for efficient control of the plasma equilibrium. This information is foreseen to be extracted using the ITER magnetic diagnostics, which mainly consist of magnetic probes and flux loops. This technique suffers two principal sources of error, which are the drift of the integrators (the fields and fluxes being time-integrals of the probe signals) and the appearance of radiation and thermally-induced electromotive forces in the diagnostic sensors and cables due to the harsh environment that they will have to withstand. For these reasons, an alternative drift-free method for equilibrium estimation has been investigated, which involved modulation of the plasma position and current. Sinusoidal modulation of the plasma position and current around an ITER operating point induces measurable finite frequency responses observed within the magnetic diagnostics. These modulated responses allowed an estimation

of the plasma equilibrium without resorting to time-integration of diagnostics signals. This approach was thus guaranteed to avoid the drifts and offsets that appear when using conventional electronic integrators. At the same time, this method showed a considerable tolerance to noise. This work was performed using DINA-CH as a simulator. Further research will be carried out.
Efficient plasma control requires the full understanding of the functioning scheme of the control system implemented onto a given tokamak, and the sharing of this information amongst the scientific community may add considerable value to present and future research. The exchange of this data between institutions should be performed in a standardized manner, so that the misinterpretations and other kinds of error of communication are minimized. Therefore, a review of the present state of the ITER control scheme has been undertaken and supplied to the EU-ITM, which aims at providing a European platform for the exchange of tokamak-related data, among other tasks.
ITER is foreseen to possess twelve-phase PF coil power supplies. This implies that for any demand PF coil voltage, the PF coil power supplies DC output will not be constant but will include a voltage ripple, which amplitude depends on the demand PF coil voltages. This PF coil power supply voltage ripple may induce a non-negligible response in the in-vessel and ex-vessel pick-up coils, which needed to be estimated in order to state whether the present in- and ex-vessel pick-up coils design was appropriate. This work was performed using DINA-CH as a simulator.

Alice BURCKEL: *"Simulation of particle transport"*
The goal of this recently started project is to study particle transport in a tokamak from a theoretical and numerical point of view using nonlinear simulations. The first steps in this project have been to get familiar with gyrokinetic theory, learn how to run and analyze linear and nonlinear simulations using the local gyrokinetic GS2 code and the CHEASE interface for the calculation of the MHD equilibrium, and start to compare the linear and nonlinear results for basic cases. A comparison with GS2 simulations of some interesting nonlinear results for the heat and particle transports obtained by X. Lapillonne using the GENE code has also been started.

Ciro CALZOLAIO: *"Damages in Nb_3S n strands and wires*"
Nb_3S n is a A15 superconducting material which is the strongest candidate for the next generation accelerators magnets and it has already been utilized for the design of fusion magnets. The advantage of A15 conductors at high critical temperature T_c and high upper critical field H_{c2} is faced by the disadvantage of the brittle intermetallic A15 compounds and the reversible strain effect.
The analysis of these problems could be the starting point for my PhD thesis.

Michael CHESAUX: *"A new low ion energy bombardment PECVD reactor for the deposition of thin film silicon for solar cell applications"*
The deposition of thin film silicon solar cells done with PECVD using a CCP at VHF lead to a deposition rate of few Å/s and the film thickness is in the range of 0.2 to 3μm. To obtain higher deposition rates more power is often used but this causes an increase of the ion bombardment intensity thus creating higher defects density of the produced films. It is thus necessary to reduce this bombardment in order to increase solar cells efficiencies and satisfy industry demand in term of production yield. This research aims to reduce this ion bombardment by changing the reactor design.
The first tests demonstrate a difficulty of achieving plasma ignition in the firsts design because of low voltages on the electrode. The related problem was investigated and solutions were tested and proposed. The first milestone of the

project was archived by producing hydrogen plasma in the desired area. Currently different reactor geometries are being tested and measured by Langmuir probes.

Loïc CURCHOD: *"Heating of High Density Plasmas in the TCV Tokamak"*
In preparation of new electron Bernstein wave (EBW) experiments via O-SX-B double mode conversion in TCV, the Antenna-Mode-conversion-Ray-tracing code (AMR) coupled to the Fokker-Planck solver LUKE are used in a systematic analysis of the EBW heating and current drive performances. In this study, the main parameters influencing the EBW trajectory and absorption (e.g. the plasma-antenna relative position and the toroidal magnetic field) are scanned. For each configuration, the optimum injection angles for the O-SX-B double mode conversion are determined, the EBW ray-tracing is performed and the quasi-linear wave-plasma interaction is calculated. As expected, large toroidal injection angles are necessary for an efficient coupling of the EC power to the electrostatic mode. Central deposition is possible with injection close to the equator of the plasma, but the oscillatory behavior of the parallel refractive index N|| prevents efficient current drive. Injection away from the plasma midplane yields a N|| upshift and a net current drive is obtained. The versatility of the TCV heating system and magnetic configuration will then be used to experimentally test the optimum scenarios for central EBW heating (EBH) and EBW current drive (EBCD) in overdense ELM-free H-modes. In these experiments, the coupling efficiency is low when the optimum plasma edge conditions are not met, in particular when ELMs appear. The pedestal density gradient may be optimized by plasma shaping. A new stray power detection system has been designed using low-cost infrared sensors. Such a diagnostic provides a good indication of the power coupling efficiency, which is also useful for TCV EC safety purposes. Initial low power experiments with one gyrotron will allow the study of the lower-hybrid parametric instability at the SX-B mode conversion using a loop-antenna, as well as the search of the optimum EBH and EBCD scenarios with low duty-cycle modulated power prior to continuous wave injection of high power.

Cornelis DE MEIJERE: *"Experimental study of turbulence in the edge region of TCV plasmas"*
In the framework of a collaboration with A. Kraemer-Flecken, which will encompass joint experiments on both the Textor and TCV tokamaks, the candidate spent five weeks (May-June) working at Forschungzentrum Juelich. Correlation reflectometry measurements were performed during H-mode discharges, to study turbulence in the edge region of the Textor tokamak. To be able to correctly interpret the data, a literature study of correlation reflectometry was then undertaken and an attempt was made to apply various models to the system installed on Textor. Data analysis is currently underway and additional experiments are planned for next year to complete the dataset.
To allow for easy switching between reflectometer and ECE measurements on TCV, a new waveguide and support system was implemented. The TCV Doppler reflectometer system was operated during a few tens of shots, and the measurements partially analysed.
Finally, in September the candidate attended the joint annual meeting of the Swiss and Austrian physical societies, where he gave an oral presentation on the principles and capabilities of the tangential phase-contrast imaging diagnostic that is currently being installed on TCV.

Lucia FEDERSPIEL: 1)*"Observation of a critical pressure gradient for the stabilisation of interchange modes in simple magnetized toroidal plasmas"*
During the first semester of this year we investigate, from a theoretical and experimental point of view, the existence of a critical pressure gradient for the stabilisation of interchange modes in simple magnetised toroidal plasmas like those produced in the TORPEX device. This study led to the theoretical and experimental determination of such a critical threshold. Indeed, this critical gradient was reached during a scan of the neutral gas pressure pn: around a critical value for pn, depending on the magnetic configuration and the injected RF power, a small increase in the neutral gas pressure triggers a transition in the plasma behaviour. The pressure profile is locally flattened, stabilising the interchange mode observed at lower neutral gas densities. The measured value for the critical gradient is found to be close to the linear theory estimation.
2) "CXRS diagnostics and momentum transport studies on TCV"
The second part of this year was principally focused on getting known to the CXRS diagnostic in TCV and the related analysis tools as well as to the main theoretical models describing plasma rotation and momentum transport. During the last TCV opening, the alignment between the toroidal and poloidal system has been performed in order to reconstruct the observations chords for both systems and to compare them to the old alignment values. Moreover, complementary experiments with reversed toroidal magnetic field have been performed in TCV in order to complete previous density scan in ohmic diverted plasmas. Support has also been given during experiments performed to determine whether the up-down asymmetry of the magnetic configuration, producing a radial toroidal momentum flux, affects the toroidal rotation gradient in the outer region of TCV plasmas as theoretically predicted. Preliminary results show a variation in the toroidal velocity gradient for reversed plasmas shapes, which is in agreement with this prediction.

Federico FELICI: *"Control of ECH systems in Tokamaks aimed at Neoclassical Tearing Mode suppression"*
Work has progressed on physics modeling of NTM triggering in TCV. Combining the ASTRA transport code with PEST III and a cylindrical equilibrium code has allowed to analyze the effect of locally driven ECCD current on the classical tearing mode stability. The analyses have confirmed that the tearing mode stability is indeed very sensitive on the position of the driven current. This has been backed by experimental investigations, where we have shown that even a very small change in the deposition location can trigger a mode.
In parallel, there has been progress in other control issues related to the TCV ECRH system. First tests were performed of a method for profile control using line-integrated soft-X ray measurements as a reference and controlling the width and the peak of the emission profile by varying the power two gyrotrons having different deposition locations. Also, algorithms have been developed and tested to control the peak in the profile of an eITB plasma in real-time. Finally, methods for controlling the ECH polarization in real-time are being developed. A code has been written and benchmarked to allow calculations of the polarization with varying plasma conditions and injection angles. Fast rotating polarizers have been acquired and work is underway to install them in a TCV X2 transmission line.

Silvano GNESIN: *"Suprathermal electron dynamics in the TCV tokamak"*
Resonant wave heating and current drive in the TCV tokamak can generate a significant suprathermal electron population in an energy range from a few tens to hundreds of keV, resulting in hard-X ray (XHR) bremsstrahlung emission. Understanding suprathermal electron generation and dynamics is a key to achieving advanced plasma scenarios and to controlling MHD instabilities. A dedicated four camera (25 CdTe semiconductor detectors each) spectroscopic HXR

system is currently at an advanced stage of design and mechanical implementation. The cameras are to be distributed around the poloidal plane to provide the possibility of 2D tomographic inversion. Prototyping and extensive testing of the detector-collimator system and related electronics are underway in the laboratory as well as in the real condition of the TCV environment. Operation of a HXR pinhole camera on loan from CEA-Cadarache has proceeded in parallel. Preliminary results obtained with the Fokker-Plank code LUKE on X2/X3 synergy in EC-heated TCV plasmas have been presented at the 36th EPS conference in Sofia. Simulations are currently being performed to complete this study by investigating in detail the competing roles played by the radial transport and collisional slowing down of fast electrons in determining the current distribution and bremsstrahlung emission profiles.

Seyed Masood HAFEZ HAGHIGHAT: *"Multiscale modeling of irradiation induced effects on the plasticity of Fe and Fe-Cr alloys"*
The aim is to understand the effect of irradiation-induced defects on the plasticity of Fe(Cr) as model alloys for developing materials for future fusion reactors. We study the movement of an edge dislocation in Fe(Cr) and the interaction of a moving edge dislocation in pure Fe with a nanometeric defects such as void, He bubble and Cr precipitate using molecular dynamics simulation. It appears that a 2nm Cr precipitate is an easy defect for an edge dislocation relative to a 2nm void and He bubble. The flow stress to move the edge dislocation in a Fe(Cr) solid solution for a content of 2, 9 and 14% is not affected by a change in the strain rate in the range from 10^6 to $3\times10^7 s^{-1}$. However, the flow stress sensitivity to temperature rises with increasing the Cr concentration. It appears that with increasing Cr/Fe ratio in the Cr precipitate the strength of the precipitate may increase or decrease. Cr precipitate strength may depend not only on the Cr concentration of the precipitate but also on the short-range order of Fe-Cr in the precipitate. Concerning the interaction mechanism, when the edge dislocation reaches to the vicinity of the defects the Cr precipitate repels the edge dislocation whereas the void and He bubble attract it at the same distance from the defect. Difference between the shear modulus of the two phases, namely the matrix and the defect, is responsible for the image forces attracting or repulsing the dislocation. The results obtained by molecular dynamics simulation may be used in mesoscale study of irradiation defects strengthening by dislocation dynamics simulation.

Nazar ILCHUK: *"Plastic flow and fracture properties of degraded tempered martensitic steels"*
Experimental activities to investigate the constitutive behaviour of the as-received and cold rolled tempered martensitic steels Eurofer97 and F82H were undertaken. Characterization of the as-received material was performed by micro- and nano-indentation tests as well as by standard tensile tests. In addition, non-standard specimens such as compression micropillars were prepared using the focused ion beam technique. The dimensions of these micropillars were typically few micrometers in height with an aspect ratio (diameter/height) of about 0.5. They were compressed with a nano-indenter equipped with a flat tip. The results showed the capability to obtain a very good estimation of the flow curve of the material using such micropillars, which is of great importance in the case of irradiated materials characterization. Investigations of the degraded plate of Eurofer97 using the same techniques are in progress. Series of tensile tests of standard tensile specimens of Eurofer97 were also performed in order to get pre-deformed material. The evolution of the micro-hardness on the pre-deformed material was determined. Modeling of micro-mechanical tests (Brinell indentation and micropillar compression tests) using the finite element method was initiated.

Davoud IRAJI: *"Fast imaging of turbulent plasma in TORPEX"*
In order to use the camera easily and fix it at different alignments with respect to the plasma column, a suitable mechanical support prepared to observe the plasma from three different directions; tangential, vertical and lateral. Dependence of the mean values of the light emissions of the plasma upon the plasma density has been investigated. Different plasma scenarios and the influence of various parameters such as the vertical magnetic field BZ, Magnetron power and the neutral gas pressure on the light emission were studied. The results clearly show a linear dependence of the mean values of the light intensity upon the neutral gas pressure and the plasma density under the assumption of a constant electron temperature. To overcome the line integration effect and to increase the signal to noise ratio, development of a gas puffing system was considered and the gas puffing system was calibrated on a test bench. The first results of Gas Puff Imaging (GPI) clearly show an improvement of the level of the light by a factor of 5 which allows acquiring at higher acquisition frequencies up to 50k frames per second. This resulted better correlation between the HEXTIP and the GPI data. To benefit of higher frame rates of the camera and consequently resolving faster events in plasma, a Lambert- II25D image intensifier was tested.

Sudheer Kumar JAWLA: *"Infrared Measurements, Phase Retrieval and Gaussian Beam Mode Decomposition of the Millimetre Wave Paraxial RF-Output of a Gyrotron"*
A detailed analysis is done to completely characterize the millimetre wave paraxial RF-output of a gyrotron. This includes a phase reconstruction technique based on an accurate beam propagation method and an intermodal decomposition to identify the composition (power) of the fundamental and higher order modes based on the astigmatic Gaussian beam of higher order. The Gaussian beam mode decomposition method is established and tested on the theoretical and experimental data of 1st and 2nd prototype of the EU-170GHz/2MW coaxial cavity gyrotron for ITER and the experimental data of the 118GHz/500KW TCV gyrotron. We prove that the knowledge of the measured transverse intensity profile of such a beam in few locations is sufficient for evaluating the weights of each mode. We have shown that, in a given experimental situation where the beam profile is measured on a fixed plane size, the accuracy of the calculated fundamental mode Gaussian content is determined by the efficiency of the beam profile reconstruction. This requires an accurate estimation of other higher mode coefficients and beam parameters. The size of the measurement plane and its location along the direction of propagation restricts the number of modes used in the reconstruction. Taking all these restrictions into consideration, we have developed an efficient optimization technique which determines the mode contents by optimizing all beam parameters. The results are compared with the most commonly used technique which maximizes the power in the fundamental mode of a Gaussian beam without taking into account the other modes.

Martin JUCKER: *"Toroidal precession drift frequency in anisotropic pressure equilibria"*
Thanks to updates of the full-wave code LEMan, the wave fields and power deposition in the Ion Cyclotron Range of Frequencies (ICRF) can be computed using the exact value of the parallel wave vector (with an iterative method), in contrast to the widely used n/R approximation. Furthermore, the parallel and perpendicular wave vector calculation has been improved by using the electrostatic potential gradient directly. Thus, in the single particle Monte Carlo code VENUS, no approximations of the wave vectors or dispersion relation have to be used in the ICRF diffusion operators. Benchmarking efforts against the code SELFO form KTH,

Stockholm, are underway and preliminary results are encouraging. First ICRF heating computations show the emergence of asymmetric and ear-shaped distribution functions, which are characteristic for ICRF and result in anisotropic pressure and currents due to Ion Cyclotron Current Drive (ICCD).

Soumen KAR: *"Design, manufacture and testing of a HTS insert coil for high field generation"*
To study the safety of HTS current leads, the most severe possible accident is stoppage of the mass flow in the heat exchanger part needs to be considered. The transient behavior of EDIPO HTS current leads has been simulated using FlexPde, a commercially available FEM-based program to solve partial differential equations. First simulations considering only the heat exchanger part have been found to be in reasonably good agreement with solutions obtained by a finite differences method.
In addition, the use of first (Bi-2223) or second generation HTS (Y(RE)-123 Coated Conductors) for high magnetic field generation will be considered. In particular, the HTS magnet design has to be addressed. In the first step, the potential enhancement of the magnetic field of a Nb_3Sn laboratory magnet (12T) by means of a Bi-2223 or an Y-123 coated conductors insert coil has to be compared. This work is now under progress. As a basis for the design of the insert coil it is intended to characterize coated conductor properties experimentally. The HTS insert coil design could be the starting point of my PhD thesis.

Etienne KUENG: *"Active optical diagnostic and turbulence measurements in a basic toroidal plasma device"*
Turbulence studies in TORPEX are currently conducted mainly using Langmuir probes and therefore focusing on the electron behavior, but without information on the ions and their velocity. The Laser Induced Fluorescence (LIF) technique allows measuring the ion velocity distribution function in the plasma f(v). Knowing f(v), on can first determine parameters such as the ion temperature or drift velocity. Secondly, the ion linear response to an electrostatic wave results in a perturbation of f(v). By measuring f(v) with a good signal to noise ratio, it is possible to determine its perturbation due to the waves, and thus to study important aspects of the wave-particle interaction.
For LIF, we will use two lasers: an Argon laser which is used to pump a dye (Rhodamine 6G) laser. The first year of the thesis was devoted to the commissioning of the lasers, which includes the installation of a safety system, and the first reflection on the beam steering system and the injection into TORPEX.

Xavier LAPILLONNE: "*Global effects and simulations of microturbulence in realistic Tokamak geometry*"
Using the previously developed interface with the equilibrium code CHEASE, linear and nonlinear gyrokinetic simulations were carried out with the flux tube version of the GENE code with the aim of analyzing a TCV shot for which an electron internal transport barrier (eITB) was obtained. Starting from experimentally relevant parameters, scans in the density and ion temperature gradient were carried out in order to investigate their influence on particle transport. In particular one observes that there exist a temperature gradient value for which the particle flux cancels out.
In order to address the issue of non-local effects in turbulent transport, a global version of the GENE code has been developed. Radial variations of equilibrium quantities are now taken into account in the model, and the treatment of the radial direction has been modified from Fourier space to real space. The code has been benchmark against other global gyrokinetic codes in linear and nonlinear regime, showing a high level of agreement.

Boris LEGRADIC: “Arcing in Very Large Area Plasma-Enhanced Chemical Vapour Deposition Reactors - Breakdown in small gaps with irregular features”
RF breakdown has been extensively studied in parallel plate configurations. However, in capacitively coupled reactors for plasma-enhanced chemical vapour deposition, there are areas in the reactor where small gaps are used between RF electrode and ground that are meant to prevent RF breakdown – predominantly in the showerhead. They can be, as a first approximation, considered as parallel plates with holes and/or elevations, and are supposed to be narrow enough to prevent a glow discharge, but wide enough to prevent metal-vapour arcing between the electrodes.
These gaps have been shown to be vulnerable to damaging parasitic discharges when the reactor is used at higher powers and therefore higher RF voltages. In the last year I have investigated the behaviour of breakdown in these non-parallel surfaces. Numerous experiments with different geometrical configurations were made to separate the effect of edge-fields from other geometrical effects in determining the plasma breakdown voltage. Future work will focus on further analysing the data, and creating a fluid-simulation model of the breakdown in the finite-elements solver COMSOL.

Joaquim LOIZU: *"Simulation of plasma turbulence in the TORPEX basic plasma physics experiment"*
An effort is being put now in the improvement of the current 3D model that simulates the TORPEX device, first focusing on the physics of the plasma sheath. A kinetic model of the sheath is being developed and, by taking advantage of the detailed analysis of its results, more correct boundary conditions will be implemented in the TORPEX fluid code. The improvement of the 3D TORPEX simulation model will then be pushed further by studying the influence of neutrals on the plasma dynamics and by the development of a theory/experiment comparison framework.

Janos MARKI: *"Transient heat loads at the tokamak edge"*
The main task in view of achieving thesis goals, namely the experimental programme of this year started a bit late, due to a number of unfortunate events. First, the TCV transformer replacement and installation took until late April. However, in the down-time, the optics support was somewhat improved, resulting in less vignetting and a slightly larger field-of-view for the system. In this period, two new infrared filters were also acquired and tested, with the intention of reducing dust-, tile-covering layer- and hot-spot-caused effects on the calibration. Unfortunately, the shutter covering the port the vertical infrared system is installed on got stuck in a half-way position in the middle of April. Worse still, this could only be repaired during a machine opening, where it turned out that the soldering of the shutter has broken (its axis was moving without the covering metal). End of June, the machine was opened up, and the shutter assembly repaired by beginning of July.
Simultaneously, the loan of a longwave IR camera from the MAST group (for which an EU priority support contract was signed about a year ago) has finally become reality as the system arrived to CRPP in the middle of the summer. In the 6 weeks (15th July - 8th September) it has spent at CRPP before being sent back to MAST, a total of 28 TCV experimental sessions were dedicated to the edge physics programme. This has been split between 2 different, though linked tasks.
The first one was SOL characterisation of FWD- and REV-B ohmic and X3 ECRH heated, SNL diverted discharges, with the aim of deducing hitherto unknown power balance figures, as well as heat deposition time-scale differences for the two divertor

regions - these last two only being possible with the simultaneous operation of the two systems.
The other task was the investigation of filamentary heat deposition at the top of the machine, which could be of importance for an eventual redesign of the ITER upper dump plates, as the power deposition near the secondary X-point at the top of the machine could be too high for vessel elements not designed to withstand large heat loads. This investigation was carried out by using SNU plasmas - hence the field-of-view of the vertical system could observe the region of plasma-wall interaction which is usually at the top of the machine. By doing this experiment in a REV-B configuration, we covered the situation that goes in pair with the FWD-B SNL configuration, of greatest interest to the ITER design.
The calibrations for the two systems have been done at the time of writing this report, however, calculations of the heat fluxes and following physics analysis is still outstanding.

Theodoros PANIS: *"Alfvén Eigenmode stability in tokamak plasmas"*
The work on the technical aspects of the TAE antenna system on JET has been completed in 2009. Four of the matching units that were designed in 2007 for 4-antenna operation were built, installed and used for routine operation in plasma discharges. The TAE frequency range for typical values of the JET magnetic field and density can now be covered efficiently with high antenna currents. Another technical achievement has been the successful upgrade of the real-time resonance-tracking system that allows one to target in real time modes with specific n.
The advances made on the technical side have resulted in progress in the physics domain. During the JET 2008/9 experimental campaigns a damping rate database has been built that includes more than 10000 damping measurements for different plasma configurations and various ns. This database can now be used to systematically study the stability of AEs on JET by revealing possible dependencies on macroscopic plasma parameters and comparing the experimental findings to the theory predictions.
Experimental data has been collected spanning the range from $|n|=3$ to $|n|\sim 11$ TAEs, during parasitic operation and in dedicated experimental sessions. The antenna-plasma coupling decreases as function of n and observations of modes with $|n|=3$ 7 have been more frequent and more robust than those with $|n|>7$. Individual discharges have revealed information on the antenna-plasma coupling and the stability of intermediate-n TAEs. It has been observed that the antenna-plasma coupling in a case of $|n|=5$ TAEs, driven during the current ramp-up phase of a discharge, has a very sensitive dependence on the plasma profiles. In discharges with slow elongation scans during which the other macroscopic plasma parameters were stationary, the damping of $n=3$ TAEs was found to increase with increasing edge magnetic shear. In similar discharges, $n=4$ TAEs were found to be less damped than the $n=3$ TAEs by a factor 2-3 and their damping was found to be affected less or not at all by the increase in the edge magnetic shear.
The results for the n=3 TAEs have been compared to the codes LEMan and LIGKA in the framework of the International Tokamak Physics Activity (ITPA). LEMan estimations were close to the experimental measurements but the effect of the elongation on the damping was not captured because of the inability to simulate equilibria with strong up-down asymmetry. LIGKA predicted the scaling of the damping with the edge elongation but it estimated dampings a factor of 1.5-2 lower than the experimental ones. Such comparisons will continue in the future.

Francesco PIRAS: *"Plasma shape control of TCV"*
Plasma breakdown: The ohmic breakdown on TCV is studied using the sumac code. The magnetic configuration at the breakdown time is computed form the electro-magnetic model of TCV. During the ramp-up phase, a single filament model is used

to describe the plasma current evolution. Concerning the ECH assisted breakdown, new experiments are planned to investigate how the magnetic configuration can affect the ionization phase. From previous experiments, the ECH power threshold for a given magnetic configuration was evaluated.
Snowflake divertor: The snowflake divertor is an innovative configuration that has been studied on TCV. Different experiments have shown its compatibility with the tokamak operation in both standard regimes (L-mode) and high-confinement regimes (H-mode). New experiments are planned to investigate the physical properties of the snowflake.
Doublet: To create a doublet-shaped plasma, first the droplet configuration has to be achieved. The n=0 stability of this configuration is studied and a possible scenario for a doublet creation on TCV is setted-up. Experiments are carried on to create a droplet configuration from a double ECH breakdown.

Andreas PITSCHKE: *"Improvements in data analysis for the TCV Thomson scattering system and ideal MHD-stability simulations of the edge barrier in X3-heated ELMy H-mode discharges at TCV"*
First measurements of the electron temperature and density profiles in electron internal transport barriers were carried out with the new high spatial resolution Thomson scattering system. Comparison of the measurements with those of older experiments lacking the high spatial resolution principally confirmed the values of gradients and barrier width quoted earlier.
The properties of the edge pedestal barrier in the high confinement mode (H-mode) of discharges heated at the 3rd harmonical resonance frequency were measured. The edge barrier evolution during an ELM cycle was analyzed by statistical means, e.g. coherent averaging of measurements of comparable discharges. The obtained results are compared with those in purely ohmically heated H-mode discharges. Ideal magneto-hydrodynamic stability limits of the edge barrier were computed for both cases using the KINX code.
A real time control algorithm was developed for the Thomson scattering system to improve the probability to obtain a measurement of the edge electron temperature and density profile exactly at an ELM event. It is based on Simulink which can be easily implemented in the TCV control system. This algorithm is currently in the testing phase.

Anna Prokhodtseva: *"Primary Irradiation Damage in Ultra-High Purity Iron and Model Iron-Cromium Alloys"*
Ion irradiation/implantation experiments on UHP Fe and Fe Cr alloys were performed in JANNuS facility. Acquired doses range from 0.1 to 10 dpa with up to 1000 appm of implanted He. Produced defects were characterized using Transmission Electron Microscopy. In such a way, influence of He content and the amount of Cr on the defect accumulation was assessed.

Marina RICCI: *"Optimization of the plasma enhanced chemical vapor deposition (PECVD) process for the deposition of SiO_x barrier coatings on polymers"*
The plasma enhanced chemical vapor deposition (PECVD) process for coating polymer films has been used for producing SiO_x and SiN_x coatings. By studying processes made in BEPEX, it has shown that operating with different gas mixtures of hexamethyldisiloxane (HMDSO) and O_2, with Ar or N_2, keeping constant the total gas flux, the RF power and pressure values, it seems that an increase of Ar or N_2 reduces very well powder formation, promoting polymerization of the monomer. In the case of SiN_x coating deposition, hexamethyldisilazane (HMDSN) and H_2 have been used with N_2 or NH_3, keeping constant the total gas flux and modifying the values of power (from 30 to 200W). By the FTIR analysis of the recorded spectra, it

seems that the carbon content is well reduced at high power, but the final films are quite far from the ideal, because the SiN peak at 938cm^{-1} is still low in intensity.

Jonathan ROSSEL: *"Edge localized modes: analysis and control in TCV"*
An important part of the year has been dedicated to the development of the saddle coil system project, a component of the future upgrade of TCV aiming at ELM stabilization, error field correction and vertical control. This work included the description of the coil - vessel electrical system in the framework of linear system theory, in order to obtain a simplified characterization of the response functions describing the coils. The question of spectral characterization of the coil system was also addressed and a theory applicable to any coil configuration has been developed, allowing the determination of the number of simultaneously controllable target modes and the identification of the spectral degeneracy intrinsic to the system. The method of current distribution optimization has been largely enhanced, with features such as multi-mode optimization, unconstrained coil system geometry and optimization based on the maximum of a figure of merit. The calculation of magnetic forces has also been revisited to obtain a detailed description of the forces on the different parts of the coils.
In parallel, efforts have been made to take over the fast magnetic probe diagnostic on TCV and revisit its dedicated analysis tools. This is still an ongoing process.

Christian THEILER: "Basic investigations of turbulent structures and blobs of relevance for magnetic fusion plasmas"
This year, we have finalized the study on the cross-field motion of plasma filaments (blobs) in the *standard setup*, in which a plane steel limiter is inserted into the TORPEX vacuum vessel. In a next step, we have increased the complexity of the system by varying the angle between magnetic field lines and limiter. This was achieved by a specially designed tiltable plate limiter and, following theoretical predictions, should allow to actively influence the velocity of the filaments. So far, no such effect was observed in our experiments. Whether these results are disproving the theoretical prediction in general or if they are limited to our specific setup is still being explored.
Further, considerable effort has been devoted to the study of Langmuir probes, especially the *triple probe*. This probe provides in principle the time history of electron temperature, density and plasma potential. These quantities are not only needed for a more detailed study of filaments, but also for a continuation of the TORPEX turbulence code validation project. Several difficulties with the triple probe were encountered, such as phase delay errors due to a finite separation between tips or a limited bandwidth.

Lyubomira VELEVA: *"Development and Characterization of Tungsten-Base Materials for Fusion Reactor Applications"*
Recent activities were focused on manufacturing W-1Y_2O_3, W-2Y and W-1.7TiC materials (in weight percent) by conventional powder metallurgy methods including dry mechanical alloying of elemental powders in an argon atmosphere, followed by hot isostatic pressing at 1320 C under a pressure of 200MPa. The density of the compacted W-2Y material was found to be the highest, equal to about 98% of the theoretical density. Specimens for scanning electron microscopy and transmission electron microscopy (TEM) observations were prepared from the W-2Y and W-1.7TiC materials. TEM observations showed that the W-2Y material is composed of grains with a size between 20 and 40 nm, It also contains small oxide particles with a mean size up to 10 nm. The small particles appear homogeneously distributed in the tungsten matrix. The W-1.7TiC material was found to have a density equal to 95% of the theoretical density. It exhibits a bimodal grain size distribution (ADD

VALUES) and it contains small TiC particles (ADD VALUE) that appear non-homogenously distributed in the tungsten matrix.

Thibaud VERNAY: *"Collisions in delta f PIC methods"*
The simple collisional Particle-In-Cell code BIRDIE was written and tested. Its aim is to simulate electrostatic waves in 1D unmagnetised plasma, both in the linear and non-linear regime.
The main work was on the gyrokinetic code ORB5:

- Final tests of the new interface for the code CHEASE, which provides MHD equilibria and whose implementation has been started last year.
- Development of collision operators following Langevin's approach: the work started last year is extended with self-collision discretisation. The conservation properties of the algorithms are tested and the code is benchmarked against transport codes (CQL3D, FORTEC-3D) and gyrokinetic codes (GENE, GT5D) for neoclassical transport and collisional linear micro-instabilities growth rates. Preliminary runs for studying turbulence have been undertaken.
- Preliminary results of the collisions in ORB5 were presented on a poster at the European Fusion Theory Conference in Riga (October 2009).
- Important merging operations have begun, in order to have finally an electromagnetic version of the code with collisions and advanced noise-control procedure.

David WAGNER: *"Experimental and theoretical study of Impurity Transport on TCV"*
The commissioning of a new diagnostic, namely the Disruption Mitigation Valve (DMV) has been finished. It was demonstrated that this system is capable to deliver minor amounts of gaseous impurities in short, repetitive pulses into the plasma where their behaviour can be studied by charge exchange or soft X-ray spectroscopy. In a large database containing mostly ohmic and X3 heated shots it was found that at high collisionality the electron profiles have high gradients and these are mostly ohmic cases, while at low collisionalit both low and high gradients were observed despite of the strong similarities in the shot parameters. With help of large amount of gyrokinetic simulations it was shown that at the ohmic cases high peaking is caused by the neoclassical Ware-pinch. At low collisionality the α was identified as an important parameter, however its role is still under investigation.

Alexandra ZHUCHKOVA: *"Faraday rotation measurements of the poloidal magnetic field in the TCV Tokamak, using a far-infrared polarimeter"*
In 2009 a new far-infrared (FIR) polarimeter diagnostic began to operate on the TCV. It works at λ=432.5 μm and uses a dual cavity far-infrared laser optically pumped by a CO_2 laser.
For the measurements of the Faraday rotation angles this diagnostic uses a technique in which the polarization of the probing beam is modulated. For this purpose the cavities lengths of the FIR laser are detuned to obtain the difference in the frequencies of two cavities 750 kHz and to create a beat frequency. The FIR Polarimeter has to provide the measurements of the magnetic field distribution and hence the current density in the TCV plasmas. The current density j(r) is linked to the safety factor q which is a key parameter for the transport models as well as for the magnetohydrodynamic (MHD) stability theory of tearing modes, sawteeth and disruptions.
The installation of the diagnostic was completed in March of 2009. Then the calibration of the system was carried out and the results confirmed that the diagnostic works as it was expected.

The experiments with plasma showed that the changes in the magnitudes of the Faraday rotation angles, measured by the Polarimeter, correspond to the appropriate changes in the magnitudes of the currents and densities. However the noise level and the fluctuations of the signal pointed at the necessity to improve the system in order to achieve the resolution allowing to use the diagnostic for the study of the plasma phenomena. A number of steps for the diagnostic improvement was undertaken. First results of the upgraded FIR Polarimeter are expected next months.

7 PUBLIC RELATION ACTIVITIES IN 2009

The activities in the public relation domain were mainly dedicated to the general public and undergraduate students in the form of visits. A series of events also provided opportunities to present our work to a large public.

More than 1000 persons visited the CRPP in 2009. Most of them were adults belonging to professionnal or political groups which either were invited or asked for a visit. Besides that, one major event is the visit of 200 children (12-13 years old) in one morning. Classes visit different laboratories in the EPFL and the CRPP is a 'must go' destination !

The booklet presenting the CRPP activities has been completely renewed. The leaflet promoting the CRPP and dedicated the EPFL students has also been updated. Some papers have been published in the EPFL's internal newspaper. CRPP's collaborators also contributed to other booklets, newspapers (INTERfaces – Agence ITER France, for instance). Several talks were given at different large public meetings. Several pre-university students were coached in the frame of their 'Travail de Maturité'.

8 FUSION & INDUSTRY RELATION

A new position of Industrial Liaison Officer - ILO - was created with the mission of notifying firms likely to respond to a CfT (Call for Tender) for ITER of the existence of such an ongoing procedure. CfT's are issued by IO (ITER Organization in Cadarache), by F4E in Barcelona with respect to operational procurements and research assignments (GRANTS) as well as by third entities and domestic agencies across the world.

An Information Day was organized for Swiss Industry in Berne on September 28th, 2009, to which around 70 participants came. Presentations were given as well by officers of F4E from Barcelona as by representatives of Swiss firms having already participated in similar programs in the past (mainly with JET). The industrialists shared their experience and put forward the benefits gained from their involvements: an innovation impulse within the company, exposure to working in an international environment.

The ILO furthermore paid visits to institutions and companies, attended an F4E Information Day and two ILO meetings, updated and produced new information material and worked on the WEB-site. For all actions, a reliable list of potential suppliers is needed. The list was therefore elaborated and continuously updated; companies were also encouraged to register with F4E and IO. The support of Alliance-tt, within which the ILO deployed its activities, is very much appreciated for the wealth of knowledge on technological competences which is freely shared.

APPENDICES

APPENDIX A Articles published in Refereed Scientific Reviews during 2009

(see CRPP archives at http://crppwww.epfl.ch/archives)

M. Albergante, J.P. Graves, A. Fasoli, F. Jenko, T. Dannert, *Anomalous Transport of Energetic Particles in ITER Relevant Scenarios,* Physics of Plasmas **16**, 112301 (2009).

J.A. Alonso, P. Andrew, A. Neto, J.L. De Pablos, E. De La Cal, A. Fernandes, W. Fundamenski, C. Hidalgo, G. Kocsis, A. Murari, G. Petravich, R.A. Pitts, L. Rios, C. Silva, *Fast Visible Imaging of ELM-Wall Interactions on JET,* Journal of Nuclear Materials **390-91**, 797-800 (2009).

P. Angelino, X. Garbet, L. Villard, A. Bottino, S. Jolliet, P. Ghendrih, V. Grandgirard, B.F. Mcmillan, Y. Sarazin, G. Dif-Pradalier, T.M. Tran, *Role of Plasma Elongation on Turbulent Transport in Magnetically Confined Plasmas,* Physical Review Letters **102**, 195002 (2009).

C. Angioni, J. Candy, E. Fable, M. Maslov, A.G. Peeters, R.E. Waltz, H. Weisen, *Particle Pinch and Collisionality in Gyrokinetic Simulations of Tokamak Plasma Turbulence,* Physics of Plasmas **16**, Art. No. 060702 (2009).

C. Angioni, E. Fable, M. Greenwald, M. Maslov, A. Peeters, H. Takenaga, H. Weisen, *Particle Transport in Tokamak Plasmas, Theory and Experiment,* Plasma Physics and Controlled Fusion **51**, Art. No. 124017 (2009).

C. Angioni, A. Peeters, G.V. Pereverzev, A. Bottino, J. Candy, R. Dux, E. Fable, T. Hein, R.E. Waltz, *Gyrokinetic Simulations of Impurity, He Ash and Alpha Particle Transport and Consequences on ITER Transport Modelling,* Nuclear Fusion **49**, Art. No. 055013 (2009).

K. Appert, M. Azaiez, R. Gruber, *Modes of a Plasma-Filled Waveguide Determined by a Numerical Hp Method,* Communications in Computational Physics **5**, 413-425 (2009).

G. Arnoux, P. Andrew, M. Beurskens, A. Et, R.A. Pitts, *Divertor Heat Load in ITER-Like Advanced Tokamak Scenarios on JET,* Journal of Nuclear Materials **390-91**, 263-266 (2009).

M. Bagnasco, *Calorimetric Method Results for Current Sharing Temperature Measurements in ITER Conductor Samples in Sultan,* Fus. Eng. Des **84**, 423-426 (2009).

N. Baluc, *Material Degradation under Demo Relevant Neutron Fluences,* Physica Scripta **T138**, 014004 (2009).

M. Barnes, I. Abel, W. Dorland, D. Erns, G. Hammett, P. Ricci, B. Rogers, A. Schekochihin, T. Tatsuno, *Linearized Model Fokker-Planck Collision Operators for Gyrokinetic Simulations. Ii. Numerical Implementation and Tests,* Physics of Plasmas **16**, 072107 (2009).

S. Brezinsek, A.G. Meigs, S. Jachmich, M.F. Stamp, J. Rapp, R. Felton, R.A. Pitts, V. Philipps, A. Huber, R. Pugno, *The Impact of Divertor Detachment on Carbon Sources in JET L-Mode Discharges,* Journal of Nuclear Materials **390-391**, 267-273 (2009).

P. Bruzzone, B. Spepanov, R. Wesche, A. Della Corte, L. Affinito, M. Napolitano, A. Vostner, *Test Results of a Nb3Sn Cable-in-Conduit Conductor with Variable Pitch Sequence,* IEEE Trans. Appl. Supercond. **19**, 1448-1451 (2009).

P. Bruzzone, B. Stepanov, R. Wesche, *Qualification Tests for ITER TF Conductors in Sultan,* Fusion Engineering and Design **84**, 205-209 (2009).

P. Bruzzone, B. Stepanov, R. Wesche, R. Herzog, M. Calvi, M. Bagnasco, F. Cau, M. Vogel, *Qualification Tests and Facilities for ITER TF Superconductors,* Nuclear Fusion **49**, (2009).

P. Bruzzone, B. Stepanov, R. Wesche, Y. Ilyin, R. Herzog, M. Calvi, M. Bagnasco, F. Cau, *Methods, Accuracy and Reliability of ITER Conductor Tests in Sultan,* IEEE Trans. Appl. Supercond. **19**, 1508-1511 (2009).

E. Campitelli, P. Spätig, J. Bertsch, *Numerical Investigation by Finite Element Simulations of the Ball Punch Test: Application to Tempered Martensitic Steels,* Journal of Nuclear Materials, Proceedings of the 13th International Conference on Fusion Reactor Materials **386-388 909C0**, 319-322 (2009).

F. Cau, M. Bagnasco, P. Bruzzone, M. Calvi, F. Roth, *Interstrand Resistance and Current Redistribution in a Cable-in-Conduit Conductor (CICC) Termination,* IEEE Trans. Appl. Supercond. **19**, 1452-1456 (2009).

F. Cau, P. Bruzzone, *AC Loss Measurements in CICC with Different Aspect Ratio,* IEEE Trans. Appl. Supercond. **19**, 2383-2386 (2009).

F. Cau, P. Bruzzone, *Inter-Strand Resistance Measurements in the Termination of the ITER Sultan Samples,* Supercond. Sci. Technol. **22**, (2009).

F. Cau, P. Bruzzone, F. Staehli, *AC Loss Measurements on Cable in Conduit Conductor with Random- Changing Magnetic Fields,* Fusion Engineering and Design **84**, 569-572 (2009).

A.V. Chankin, D.P. Coster, G. Corrigan, S.K. Erents, W. Fundamenski, A. Kallenbach, K. Lackner, J. Neuhauser, R. Pitts, A.U. Team, JET Contributors, *Fluid Code Simulations of Radial Electric Field in the Scrape-Off Layer of JET,* Plasma Physics and Controlled Fusion **51**, 065022 (2009).

I.T. Chapman, V.G. Igochine, J.P. Graves, S.D. Pinches, A. Gude, I. Jenkins, M. Maraschek, G. Tardini, *Sawtooth Control and the Interaction of Energetic Particles,* Nuclear Fusion **49**, 035006 (2009).

R. Chavan, G. Chitarin, R.S. Delogu, A. Encheva, A. Gallo, E.R. Hodgson, L.C. Ingesson, A. Le-Luyer, J.B. Lister, P. Moreau, *The Magnetics Diagnostic Set for ITER,* Fusion Engineering and Design **84**, 295-299 (2009).

J. Chowdhury, R. Ganesh, S. Brunner, J. Vaclavik, L. Villard, P. Angelino, *A Comprehensive Gyrokinetic Description of Global Electrostatic Microinstabilities in a Tokamak,* Physics of Plasmas **16**, 052507 (2009).

J. Chowdhury, R. Ganesh, J. Vaclavik, S. Brunner, L. Villard, P. Angelino, *Short Wavelength Ion Temperature Gradient Mode and Coupling with Trapped Electrons,* Physics of Plasmas **16**, 082511 (2009).

A. Collazos, V.S. Udintsev, R. Chavan, F. Felici, F. Dolizy, M.A. Henderson, H. Shidara, *Progress on the ITER Upper Launcher Millimeter-Wave Design and Testing,* Fusion Science and Technology **55**, 84-93 (2009).

A.S. Collazos, R. Bertizzolo, R. Chavan, F.D.R. Dolizy, F. Felici, M.A. Henderson, J.-D. Landis, F. Sanchez, *Progress on the ITER ECRH Upper Launcher Steering Mirror Identification and Control,* Fusion Engineering and Design **84**, 618-622 (2009).

A.S. Collazos, F.O. Maréchal, C. Gähler, *Predictive Optimal Management Method for the Control of Polygeneration Systems,* Computers and Chemical Engineering **33**, 1584-1592 (2009).

J.W. Connor, A. Fasoli, C. Hidalgo, A. Kirk, V. Naulin, A.G. Peeters, T. Tala, *13th EU-US Transport Task Force Workshop on Transport in Fusion Plasmas,* Nuclear Fusion **49**, 047001 (2009).

G.A. Cooper, J.P. Graves, W.A. Cooper, R. Gruber, R.S. Peterson, *Becool: Ballooning Eigensolver with Cool Finite Elements,* Journal of Computational Physics **228**, 4911-4916 (2009).

W.A. Cooper, S.P. Hirshman, P. Merkel, J.P. Graves, J. Kisslinger, H.F.G. Wobig, Y. Narushima, S. Okamura, K.Y. Watanabe, *Three-Dimensional Anisotropic Pressure Free Boundary Equilibria,* Computer Physics Communications **180**, 1524-1533 (2009).

C. Darbos, M. Henderson, F. Albajar, T. Bigelow, T. Bonicelli, R. Chavan, G.G. Denisov, D. Fasel, R. Heidinger, J.P. Hogge, *Progress in Design and Integration of the ITER Electron Cyclotron H&CD System,* Fusion Engineering and Design **84**, 651-655 (2009).

C. Darbos, R. Magne, A. Arnold, H.O. Prinz, M. Thumm, F. Bouquey, J.-P. Hogge, R. Lambert, M. Lennholm, C. Liévin, E. Traisnel, *The 118-GHz Electron Cyclotron Heating System on Tore Supra,* Fusion Science and Technology **56**, 1205-1218 (2009).

I.R. Dixon, M.D. Bird, P. Bruzzone, B. Stepanov, *Current Sharing and AC Loss Measurements of Cable-in-Conduit Conductor with Nb3Sn Strands for the High Field Section of the Series-Connected Hybrid Outsert Coil,* IEEE Trans. Appl. Supercond. **19**, 2466-2469 (2009).

J.L. Dorier, P. Guittienne, C. Hollenstein, M. Gindrat, A. Refke, *Mechanisms of Films and Coatings Formation from Gaseous and Liquid Precursors with Low Pressure Plasma Spray Equipment,* Surface and Coatings Technology **203**, 2125-2130 (2009).

B. Elzendoorn, M. De Baar, R. Chavan, T. Goodman, C. Heemskerk, R. Heidinger, K. Kleefeldt, J. Koning, S. Sanders, P. Späh, *Analysis of the ITER ECH Upper Port Launcher Remote Maintenance Using Virtual Reality,* Fusion Engineering and Design **84**, 733-735 (2009).

A. Fasoli, *Overview of Physics Research on the TCV Tokamak,* Nuclear Fusion **49**, 104005 (2009).

F. Felici, T.P. Goodman, O. Sauter, T. Shimozuma, S. Ito, I. Mizuno, S. Kubo, T. Mutoh, *Real-Time Feedback Control of Millimeter-Wave Polarization for LHD,* Review of Scientific Instruments **80**, 013504 (2009).

J. Fikar, R. Schäublin, *Atomistic Simulations of Nanometric Dislocation Loops in Bcc Tungsten,* Nuclear Instruments and Methods in Physics Research Section B: Beam Interactions with Materials and Atoms **267**, 3218-3222 (2009).

J. Fikar, R. Schäublin, *Molecular Dynamics Simulation of Radiation Damage in Bcc Tungsten,* Journal of Nuclear Materials **386-388**, 97-101 (2009).

J. Fikar, R. Schaeublin, C. Bjoerkas, *Atomistic Simulation of 1/2<111> Screw Dislocations in Bcc Tungsten,* Advanced Materials Research **59**, 247-252 (2009).

N. Gao, C.-C. Fu, M. Samaras, R. Schäublin, M. Victoria, W. Hoffelner, *Multiscale Modelling of Bi-Crystal Grain Boundaries in Bcc Iron,* Journal of Nuclear Materials **385**, 262-267 (2009).

J.P. Graves, I.T. Chapman, S. Coda, L.G. Eriksson, T. Johnson, *Sawtooth-Control Mechanism Using Toroidally Propagating Ion-Cyclotron-*

Resonancewaves in Tokamaks, Physical Review Letters **102**, 065005 (2009).

B. Gulejovà, R.A. Pitts, D. Coster, X. Bonnin, M. Beurskens, S. Jachmich, A. Kallenbach, *SOLPS5 Simulations of Type I Elming H-Mode at JET,* Journal of Nuclear Materials **390-391**, 412-416 (2009).

S.M. Hafez Haghighat, M.C. Fivel, J. Fikar, R. Schaeublin, *Dislocation-Void Interaction in Fe: A Comparison between Molecular Dynamics and Dislocation Dynamics,* Journal of Nuclear Materials **386-388,** 102-105 (2009).

S.M. Hafez Haghighat, G. Lucas, R. Schaeublin, *State of a Pressurized Helium Bubble in Iron,* Europhysics Letters **85**, 60008 (2009).

S.M.H. Haghighat, G. Lucas, R. Schäublin, *Atomistic Simulation of He Bubble in Fe as Obstacle to Dislocation,* Materials Science and Engineering **3**, 012013 (2009).

R. Heidinger, R. Bertizzolo, A. Bruschi, R. Chavan, S. Cirant, A. Collazos, M. De Baar, B. Elzendoorn, D. Farina, U. Fischer, *Conceptual Design of the ECH Upper Launcher System for ITER,* Fusion Engineering and Design **84**, 284-289 (2009).

R. Herzog, M. Calvi, C. Marinucci, P. Bruzzone, *Helium Flow-Reversal in 3 M Long, Partially Heated Sections of Dual-Channel CICC for ITER,* IEEE Trans. Appl. Supercond. **19**, 1488-1491 (2009).

R. Herzog, R. Wesche, P. Bruzzone, *Ic Measurements on Nb3Sn Strands Extracted from ITER CICC Prototypes,* IEEE Trans. Appl. Supercond. **19**, 1440-1443 (2009).

G.T. Hoang, A. Bécoulet, J. Jacquinot, J.F. Artaud, Y.S. Bae, B. Beaumont, J.H. Belo, G. Berger-By, J.O.P.S. Bizarro, P. Bonoli, M.H. Cho, J. Decker, L. Delpech, A. Ekedahl, J. Garcia, G. Giruzzi, M. Goniche, C. Gormezano, D. Guilhem, J. Hillairet, F. Imbeaux, F. Kazarian, C. Kessel, S.H. Kim, J.G. Kwak, J.H. Jeong, J.B. Lister, X. Litaudon, R. Magne, S. Milora, F. Mirizzi, W. Namkung, J.M. Noterdaeme, S.I. Park, R. Parker, Y. Peysson, D. Rasmussen, P.K. Sharma, M. Schneider, E. Synakowski, A. Tanga, A. Tuccillo, Y.X. Wan, *A Lower Hybrid Current Drive System for ITER,* Nuclear Fusion **49**, 075001 (2009).

J.-P. Hogge, T. Goodman, S. Alberti, F. Albajar, K.A. Avramides, P. Benin, S. Bethuys, W. Bin, T. Bonicelli, A. Bruschi, S. Cirant, E. Droz, O. Dumbrajs, D. Fasel, F. Gandini, G. Gantenbein, S. Illy, S.K. Jawla, J. Jin, S. Kern, P. Lavanchy, C. Liévin, B. Marlétaz, P. Marmillod, A. Perez, B. Piosczyk, I. Pagonakis, L. Porte, T. Rzesnicki, U. Siravo, M. Thumm, M.Q. Tran, *First Experimental Results from the European Union 2 MW Coaxial Cavity ITER Gyrotron Prototype,* Fusion Science and Technology **55**, 204-212 (2009).

A.A. Howling, B. Strahm, C. Hollenstein, *Non-Intrusive Plasma Diagnostics for the Deposition of Large Area Thin Film Silicon,* Thin Solid Films **517**, 6218-6224 (2009).

A. Huber, R.A. Pitts, A. Loarte, V. Philipps, P. Andrew, S. Brezinsek, J.P. Coad, T. Eich, J.C. Fuchs, W. Fundamenski, S. Jachmich, G.F. Matthews, K. Mccormick, P. Mertens, J. Rapp, G. Sergienko, M.F. Tamp, *Plasma Radiation Distribution and Radiation Loads onto the Vessel During Transient Events in JET,* Journal of Nuclear Materials **390-391**, 830-834 (2009).

D.A. Humphreys, T.A. Casper, N. Eidietis, M. Ferrara, D.A. Gates, I.H. Hutchinson, G.L. Jackson, E. Kolemen, J.A. Leuer, J. Lister,

L.L. Lodestro, W.H. Meyer, L.D. Pearlstein, A. Portone, F. Sartori, M.L. Walker, A.S. Welander, S.M. Wolfe, *Experimental Vertical Stability Studies for ITER Performance and Design Guidance,* Nuclear Fusion **49**, 115003 (2009).

T.P. Intrator, X. Sun, G. Lapenta, L. Dorf, I. Furno, *Experimental Onset Threshold and Magnetic Pressure Pile-up for 3d Reconnection,* Nature Physics **5**, 521-526 (2009).

M.Y. Isaev, K.Y. Watanabe, W.A. Cooper, M. Yokoyama, H. Yamada, O. Sauter, T.M. Tran, A. Bergmann, C.D. Beidler, H. Maaberg, *Bootstrap Current Calculations with the SPBSC and the VENUS delta f Codes for the Large Helical Device,* Nuclear Fusion **49**, 075013-1-8 (2009).

S. Jachmich, Y. Liang, G. Arnoux, T. Eich, W. Fundamenski, H.R. Koslowski, R.A. Pitts, *Effect of External Perturbation Fields on Divertor Particle and Heat Loads During ELMs at JET,* Journal of Nuclear Materials **390-391**, 768-772 (2009).

M.W. Jakubowski, W. Fundamenski, G. Arnoux, T. Eich, R.A. Pitts, D. Reiter, R.C. Wolf, *ELM Filament Interaction with the JET Main Chamber* Journal of Nuclear Materials **390-391**, 781-784 (2009).

S. Jawla, J.-P. Hogge, S. Alberti, T. Goodman, B. Piosczyk, T. Rzesnicki, *Infrared Measurements of the RF Output of 170-GHz/2-MW Coaxial Cavity Gyrotron and Its Phase Retrieval Analysis,* Ieee Transactions on Plasma Science **37**, 414-424 (2009).

S. Jawla, J.P. Hogge, S. Alberti, *Theoretical Investigation of Iterative Phase Retrieval Algorithm for Quasi-Optical Millimeter-Wave RF Beams,* IEEE Transaction on Plasma Science **37**, 403-413 (2009).

S. Jolliet, B. McMillan, T. Vernay, L. Villard, A. Bottino, P. Angelino, *Quasisteady and Steady States in Global Gyrokinetic Particle-in-Cell Simulations,* Physics of Plasmas **16**, 052307-1 (2009).

S. Jolliet, B. Mcmillan, T. Vernay, L. Villard, R. Hatzky, A. Bottino, P. Angelino, *Influence of the Parallel Nonlinearity on Zonal Flows and Heat Transport in Global Gyrokinetic Particle-in-Cell Simulations,* Physics of Plasmas **15**, 072309 (2009).

A.N. Karpushov, Y. Andrebe, B.P. Duval, A. Bortolon, H. Zohm, *The Diagnostic Neutral Beam Injector with Arc-Discharge Plasma Source on the TCV Tokamak,* Fusion Engineering and Design **84**, 993-997 (2009).

S.H. Kim, J.F. Artaud, V. Basiuk, A. Bécoulet, V. Dokuka, G.T. Hoang, F. Imbeaux, R.R. Khayrutdinov, J.B. Lister, V.E. Lukash, *Lower Hybrid Assisted Plasma Current Ramp-up in ITER,* Plasma Physics and Controlled Fusion **51**, 065020 (2009).

S.H. Kim, J.F. Artaud, V. Basiuk, V. Dokuka, R.R. Khayrutdinov, J.B. Lister, V.E. Lukash, *Full Tokamak Discharge Simulation of ITER by Combining DINA-CH and CRONOS,* Plasma Physics and Controlled Fusion **51**, 105007 (2009).

S.H. Kim, M.M. Cavinato, V. Dokuka, A.A. Ivanov, R.R. Khayrutdinov, P.T. Lang, J.B. Lister, V.E. Lukash, Y.R. Martin, S.Y. Medvedev, L. Villard, *Comparing Magnetic Triggering of ELMs in TCV and Asdex Upgrade,* Plasma Phys. Control. Fusion **51**, 055021 (2009).

A. Kreter, S. Brezinsek, J.P. Coad, H.G. Esser, W. Fundamenski, V. Philipps, R.A. Pitts, V. Rohde, T. Tanabe, A. Widdowson, *Dynamics of Erosion and Deposition in Tokamaks,* Journal of Nuclear Materials **390-391**, 38-43 (2009).

A. Kreter, H.G. Esser, S. Brezinsek, J.P. Coad, A. Kirschner, W. Fundamenski, V. Philipps, R.A. Pitts, A. Widdowson, *Nonlinear Impact of Edge Localized Modes on Carbon Erosion in the Divertor of the JET Tokamak,* Physical Review Letters **102**, 045007 (2009).

R.J. Kurtz, A. Alamo, E. Lucon, Q. Huang, S. Jitsukawa, A. Kimura, R.L. Klueh, G.R. Odette, C. Petersen, M.A. Sokolov, P. Spätig, J.W. Rensman, *Recent Progress toward Development of Reduced Activation Ferritic/Martensitic Steels for Fusion Applications,* Journal of Nuclear Materials, Proceedings of the 13th International Conference on Fusion Reactor Materials **386-388 909C0**, 411-417 (2009).

J.D. Landis, R. Chavan, R. Bertizzolo, A. Collazos, F. Dolizy, F. Felici, F. Sanchez, M. Henderson, *Design Status of the ITER ECRH Upper Launcher mm-Wave System,* Fusion Engineering and Design **84**, 1151-1155 (2009).

X. Lapillonne, S. Brunner, T. Dannert, S. Jolliet, A. Marinoni, L. Villard, T. Goerler, F. Jenko, F. Merz, *Clarifications to the Limitations of the S-Alpha Equilibrium Model for Gyrokinetic Computations of Turbulence,* Physics of Plasmas **16**, 032308 (2009).

M. Lewandowska, M. Bagnasco, *Pressure Drop Measurements in Cable-in-Conduit Conductors (CICC's) for an Extended Range of Reynolds Number,* Electrical Review, **85**, 152-155 (2009).

B. Li, B. Rogers, P. Ricci, K. Gentle, *Plasma Transport and Turbulence in the Helimak: Simulation and Experiment,* Physics of Plasmas **16**, 082510 (2009).

G. Lucas, R. Schäublin, *Vibrational Contributions to the Stability of Point Defects in Bcc Iron: A First-Principles Study,* Nuclear Instruments and Methods in Physics Research Section B: Beam Interactions with Materials and Atoms **267**, 3009-3012 (2009).

G. Lucas, R. Schäublin, *Stability of Helium Bubbles in Alpha-Iron: A Molecular Dynamics Study,* Journal of Nuclear Materials **386-388**, 360-362 (2009).

N. Mellet, W.A. Cooper, *Parallelization of the Leman Code with MPI and OPENMP,* Advanced parallel processing technologies, Proceedings , Lecture notes in Computer Science **5737 909C0**, 356-362 (2009).

S.H. Müller, C. Theiler, A. Fasoli, I. Furno, B. Labit, G.R. Tynan, M. Xu, Z. Yan, J.H. Yu, *Studies of Blob Formation, Propagation and Transport Mechanisms in Basic Experimental Plasmas (TORPEX and Csdx),* Plasma Physics and Controlled Fusion **51**, 055020 (2009).

A. Marinoni, S. Brunner, Y. Camenen, S. Coda, J.P. Graves, X. Lapillonne, A. Pochelon, O. Sauter, L. Villard, *The Effect of Plasma Triangularity on Turbulent Transport:Modelling TCV Experiments by Linear and Non Linear Gyrokinetic Simulations,* Plasma Phys. Control. Fusion **51**, 055016 (2009).

C. Marinucci, L. Bottura, M. Calvi, *A Parametric AC Loss Model of the ITER Coils for Control Optimization,* Cryogenics **50(3)**, 187 (2009).

J. Marki, R.A. Pitts, J. Horacek, D. Tskhakaya, *ELM Induced Divertor Heat Loads on TCV,* Journal of Nuclear Materials **390-391**, 801-805 (2009).

E. Marmar, A. Bader, M. Bakhtiari, H. Barnard, W. Beck, I. Bespamyatnov, A. Binus, P. Bonoli, B. Bose, M. Bitter, I. Cziegler, G. Dekow, A. Dominguez, B. Duval, E. Edlund, D. Ernst, M. Ferrara, C. Fiore, T. Fredian, A. Graf, R. Granetz, M. Greenwald, O. Grulke, D. Gwinn, S. Harrison, R. Harvey, T.C. Hender, J. Hosea, K. Hill, N. Howard, D.F. Howell, A. Hubbard, J.W. Hughes, I. Hutchinson, A. Ince-Cushman, J. Irby, V. Izzo, A. Kanojia, C. Kessel, J.S. Ko, P.

Koert, B. Labombard, C. Lau, L. Lin, Y. Lin, B. Lipschultz, J. Liptac, Y. Ma, K. Marr, M. May, R. Mcdermott, O. Meneghini, D. Mikkelsen, R. Ochoukov, R. Parker, C.K. Phillips, P. Phillips, Y. Podpaly, M. Porkolab, M. Reinke, J. Rice, W. Rowan, S. Scott, A. Schmidt, J. Sears, S. Shiraiwa, A. Sips, N. Smick, J. Snipes, J. Stillerman, Y. Takase, D. Terry, J. Terry, N. Tsujii, E. Valeo, R. Vieira, G. Wallace, D. Whyte, J.R. Wilson, S. Wolfe, G. Wright, J. Wright, S. Wukitch, G. Wurden, P. Xu, K. Zhurovich, J. Zaks, S. Zweben, *Overview of the Alcator C-Mod Research Program,* Nuclear Fusion **49**, 104014 (2009).

N.N. Martovetsky, D.R. Hatfield, J.R. Miller, C.Y. Gung, J.S. Schultz, N. Cheggour, L.F. Goodrich, P. Bruzzone, B. Stepanov, *Test Results of the First US ITER TF Conductors in Sultan,* IEEE Trans. Appl. Supercond. **19**, 1478-1482 (2009).

M. Maslov, C. Angioni, H. Weisen, JET Contributors, *Density Profile Peaking in JET H-Mode Plasmas: Experiments Versus Linear Gyrokinetic Predictions,* Nuclear Fusion **49**, 075037 (2009).

K. Matsui, T. Isono, Y. Nunoya, T. Hemmi, Y. Okui, M. Oshikiri, N. Koizumi, Y. Takahashi, K. Okuno, B. Stepanov, P. Bruzzone, *Test Results of Japanese Sultan Sample and Conductor Procurement in Japan for ITER TF Coils,* IEEE Trans. Appl. Supercond. **19**, 1470-1473 (2009).

A. Matsuyama, M.Y. Isaev, K.Y. Watanabe, K. Hanatani, Y. Suzuki, N. Nakajima, W.A. Cooper, T.M. Tran, *Moment Approach to the Bootstrap Current in Nonaxisymmetric Toroidal Plasmas Using Deltaf Monte Carlo Methods,* Physics of Plasmas **16**, 052501-1-9 (2009).

G.F. Matthews, P. Coad, H. Greuner, M. Hill, T. Hirai, J. Likonen, H. Maier, M. Mayer, R. Neu, V. Philipps, R. Pitts, V. Riccardo, *Development of Divertor Tungsten Coatings for the JET ITER-Like Wall,* Journal of Nuclear Materials **390-391**, 934-937 (2009).

B.F. McMillan, S. Jolliet, T.M. Tran, L. Villard, A. Bottino, P. Angelino, *Avalanche-Like Bursts in Global Gyrokinetic Simulations,* Physics of Plasmas **16**, 022310 (2009).

P. Moreau, A. Le-Luyer, P. Hertout, F. Saint-Laurent, W. Zwingmann, J.M. Moret, Y. Martin, *Design and Performance Analysis of ITER Ex-Vessel Magnetic Diagnostics,* Fusion Engineering and Design **84**, 1344-1350 (2009).

P. Moreau, F. Saint-Laurent, J.B. Lister, *Drift-Free Magnetic Equilibrium Reconstruction Using the Response to Plasma Position Modulation,* Fusion Engineering and Design **84**, 1339-1343 (2009).

P. Mueller, P. Spätig, *3D Finite Element and Experimental Study of the Size Requirements for Measuring Toughness on Tempered Martensitic Steels,* Journal of Nuclear Materials **389**, 377-384 (2009).

P. Mueller, P. Spätig, R. Bonadé, G.R. Odette, D. Gragg, *Fracture Toughness Master-Curve Analysis of the Tempered Martensitic Steel Eurofer97,* Journal of Nuclear Materials **386-388**, 323-327 (2009).

A. Neto, C. Silva, J. Sousa, H.C. Fernandes, C. Hidalgo, J.L.D. Pablos, S. Salasca, J.-M. Travère, J.B. Lister, *ITER CODAC Interface for the Visible and Infra-Red Wide Angle Viewing Cameras,* Fusion Engineering and Design **84**, 1412-1415 (2009).

T. Nishitani, H. Tanigawa, S. Jitsukawa, T. Nozawa, K. Hayashi, T. Yamanishi, K. Tsuchiya, A. Möslang, N. Baluc, A. Pizzuto, *Fusion Materials Development Program in the Broader Approach Activities,* Journal of Nuclear Materials **386-388**, 405-410 (2009).

Z. Oksiuta, N. Baluc, *Role of Cr and Ti Contents on the Microstructure and Mechanical Properties of ODS Ferritic Steels,* 1st International Conference on New Materials for Extreme Environments **59 909C0**, 308-312 (2009).

Z. Oksiuta, N. Baluc, *Optimization of the Chemical Composition and Manufacturing Route for ODS Raf Steels for Fusion Reactor Application,* Nuclear Fusion **49**, 055003 (2009).

Z. Oksiuta, N. Baluc, *Effect of Mechanical Alloying Atmosphere on the Microstructure and Charpy Impact Properties of an ODS Ferritic Steel,* Journal of Nuclear Materials **386-388**, 426-429 (2009).

Z. Oksiuta, P. Olier, Y. De Carlan, N. Baluc, *Development and Characterisation of a New ODS Ferritic Steel for Fusion Reactor Application,* Journal of Nuclear Materials **393**, 114-119 (2009).

Z. Oksiuta, P. Olier, Y. Decarlan, N. Baluc, *Development and Characterisation of a New ODS Ferritic Steel for Fusion Reactor Application,* Journal of Nuclear Materials **393**, 114-119 (2009).

P. Olier, Z. Oksiuta, J.F. Melat, D. Hamon, T. Leblond, Y. Decarlan, N. Baluc, *Microstructural and Cold Workability Assessment of a New ODS Ferritic Steel,* Advanced Materials Research **59**, 313-318 (2009).

J.I. Paley, F. Felici, J. Berrino, S. Coda, N. Cruz, B.P. Duval, T.P. Goodman, Y. Martin, J.M. Moret, F. Piras, A.P. Rodriques, B. Santos, C.A.F. Varandas, *Real Time Control of Plasmas and ECRH Systems on TCV,* Nuclear Fusion **49**, 085017 (2009).

J.I. Paley, F. Felici, S. Coda, T.P. Goodman, *From Profile to Sawtooth Control: Developing Feedback Control Using ECRH/ECCD Systems on the TCV Tokamak,* Plasma Phys. Control. Fusion **51**, 124041 (2009).

J.I. Paley, F. Felici, S. Coda, T.P. Goodman, F. Piras, *Real Time Control of the Sawtooth Period Using EC Launchers,* Plasma Phys. Control. Fusion **51**, 055010 (2009).

F. Piras, S. Coda, I. Furno, J.M. Moret, R. Pitts, O. Sauter, B. Tal, G. Turri, A. Bencze, B. Duval, F. Felici, A. Pochelon, C. Zucca, *Snowflake Divertor Plasmas on TCV,* Plasma Physics and Controlled Fusion **51**, 055009 (2009).

R.A. Pitts, G. Arnoux, M. Beurskens, T. Eich, W. Fundamenski, A. Huber, A. Loarte, J. Marki, M.F. Stamp, P. Andrew, *The Impact of Large ELMs on JET,* Journal of Nuclear Materials **390-391**, 755-759 (2009).

F.M. Poli, M. Podesta, A. Fasoli, *A Robust Method for Measurement of Fluctuation Parallel Wavenumber in Laboratory Plasmas,* Review of Scientific Instruments **80**, 053501 (2009).

A. Portone, W. Baker, A. Vostner, E. Salpietro, P. Testoni, P. Bruzzone, E. Theisen, A. Della Corte, A. Baldini, *Status of the EDIPO Project,* IEEE Trans. Appl. Supercond. **19**, 1552-1556 (2009).

A. Ramar, N. Baluc, R. Schäublin, *On the Lattice Coherency of Oxide Particles Dispersed in EUROFER97,* Journal of Nuclear Materials **386-388**, 515-519 (2009).

J. Rapp, Y. Corre, Y. Andrew, M.R. De Baar, M. Beurskens, S. Brezinsek, M. Brix, S. Devaux, T. Eich, R. Felton, W. Fundamenski, C. Giroud, D. Howell, A. Huber, S. Jachmich, E. Joffrin, A. Korotkov, G.F. Matthews, D.C. Mcdonald, A. Meigs, P. Monier-Garbet, P. Morgan, I. Nunes, G.J. Van Rooij, O. Sauter, M.F. Stamp, G. Telesca, P.C. De Vries, R. Zagorski, *Integrated Scenario with Type-III ELMy H-Mode Edge: Extrapolation to ITER,* Nuclear Fusion **49**, 095012 (2009).

P. Ricci, B.N. Rogers, *Transport Scaling in Interchange-Driven Toroidal Plasmas,* Physics of Plasmas **16**, 062303 (2009).

P. Ricci, B.N. Rogers, *Three-Dimensional Fluid Simulations of a Simple Magnetized Plasma,* Physics of Plasmas **16**, 092307 (2009).

P. Ricci, C. Theiler, A. Fasoli, I. Furno, B. Labit, S. Muller, M. Podesta, F.M. Poli, *Langmuir Probe-Based Observables for Plasma-Turbulence Code Validation and Application to the TORPEX Basic Plasma Physics Experiment,* Physics of Plasmas **16**, 055703 (2009).

D. Ronden, M. De Baar, M. Van Den Berg, W. Bongers, R. Chavan, M. Graswinckel, M. Hannink, M. Houkema, F. De Vreede, *Finalization of the Conceptual Design of the Remote Steering ECH Launcher for ITER,* Fusion Engineering and Design **84**, 1645-1648 (2009).

F. Sanchez, R. Bertizzolo, R. Chavan, A. Collazos, M. Henderson, J.D. Landis, *Design and Manufacturing of the ITER ECRH Upper Launcher Mirrors,* Fusion Engineering and Design **84**, 1702-1707 (2009).

T. Shimozuma, S. Kubo, Y. Yoshimura, H. Igami, H. Takahashi, Y. Takita, S. Kobayashi, S. Ito, Y. Mizuno, H. Idei, T. Notake, M.A. Shapiro, R.J. Temkin, F. Felici, T.P. Goodman, O. Sauter, R. Minami, T. Kariya, T. Imai, T. Mutoh, *Handling Technology of Mega-Watt Millimeter-Waves for Optimized Heating of Fusion Plasmas,* Journal of Microwave Power and Electromagnetic Energy **43**, 43-1-60 (2009).

C. Silva, B. Gonçalves, C. Hidalgo, M.A. Pedrosa, W. Fundamenski, M. Stamp, R.A. Pitts, *Intermittent Transport in the JET Far-SOL,* Journal of Nuclear Materials **390-391**, 355-358 (2009).

F. Tavassoli, T. Hutter, P. Mueller, P. Spätig, R. Bonadé, G.R. Odette, D. Gragg, *Fracture Toughness Master-Curve Analysis of the Tempered Martensitic Steel Eurofer97,* Journal of Nuclear Materials, Proceedings of the 13th International Conference on Fusion Reactor Materials **386-388**, 323-327 (2009).

F. Tavassoli, T. Hutter, P. Spätig, R. Stoenescu, P. Mueller, G.R. Odette, D. Gragg, *Assessment of Irradiation Embrittlement of the Eurofer97 Steel after 590 Mev Proton Irradiation,* Journal of Nuclear Materials, Proceedings of the 13th International Conference on Fusion Reactor Materials **386-388**, 245-248 (2009).

D. Testa, C. Schlatter, M. Cecconello, *The Dependence of the Proton-Triton Thermo-Nuclear Fusion Reaction Rate on the Temperature and Total Energy Content of the High-Energy Proton Distribution Function,* Nuclear Fusion Letter **49**, 062004 (2009).

C. Theiler, I. Furno, P. Ricci, A. Fasoli, B. Labit, S.H. Müller, G. Plyushchev, *Cross-Field Plasma Blob Motion in an Open Magnetic Field Line Configuration,* Physical Review Letters **103**, 065001-1 (2009).

D. Tskhakaya, R.A. Pitts, W. Fundamenski, T. Eich, S. Kuhn, JET Contributors, *Kinetic Simulations of the Parallel Transport in the JET Scrape-Off Layer,* Journal of Nuclear Materials **390-391**, 335-338 (2009).

L. Veleva, Z. Oksiuta, U. Vogt, N. Baluc, *Sintering and Characterization of W–Y and W-Y203 Materials,* Fusion Engineering and Design **84**, 1920-1924 (2009).

G. Veres, R.A. Pitts, A. Bencze, J. Marki, B. Tal, R. Tye, *Fast Radiation Dynamics During ELMs on TCV,* Journal of Nuclear Materials **390-391**, 835-839 (2009).

C. Wahlberg, I.T. Chapman, J.P. Graves, *Importance of Centrifugal Effects for the Internal Kink Mode Stability in Toroidally Rotating Tokamak Plasmas,* Physics

of Plasmas **16**, 112512 (1-16) (2009).

P. Xanthopoulos, W.A. Cooper, F. Jenko, Y. Turkin, A. Runov, J. Geiger, *A Geometry Interface for Gyrokinetic Microturbulence Investigations in Toroidal Configurations,* Physics of Plasmas **16**, 082303-1-13 (2009).

J. Yu, G. Yu, *Fission-fusion Neutron Source,* Journal of Nuclear Materials **386-388**, 949-953 (2009).

R. Zanino, M. Bagnasco, D. Ciazynski, B. Lacroix, E.P.A. Van Lanen, S. Nicollet, A. Nijhuis, L. Savoldi Richard, C. Sborchia, A. Torre, A. Vostner, L. Zani, *EU Contribution to the Test and Analysis of the ITER Poloidal Field Conductor Insert and the Central Solenoid Model Coil,* Superconductor Science and Technology **22**, 085006 (2009).

C. Zucca, O. Sauter, S. Alberti, S. Cirant, T.P. Goodman, G. Turri, *Modulation of Electron Transport During Swing ECCD Discharges in TCV,* Plasma Phys. Control. Fusion **51**, 125009 (2009).

C. Zucca, O. Sauter, E. Asp, S. Coda, E. Fable, T.P. Goodman, M.A. Henderson, *Current Density Evolution in Electron Internal Transport Barrier Discharges in TCV,* Plasma Physics and Controlled Fusion **51**, 015002 (2009).

APPENDIX B Conferences and Seminars

(see CRPP archives at http://crppwww.epfl.ch/archives)

B.1 Conference and conference proceedings published in 2008

M. Bagnasco, D. Bessette, L. Bottura, C. Marinucci, *Progress in the Integrated Simulation of Thermal-Hydraulic Operation of the ITER Magnet System,* MT-21, Int. Conference on Magnet Technology, Hefei, China, October 17-23 2009 (2009).

M. Bagnasco, M. Lewandovska, *Pressure Drop Measurements in Cable-in-Conduit Conductors (CICC) with Different Layouts,* proceedings of the 22th International Cryogenic Engineering Conference, 865-870 (2009).

A. Bottino, B.D. Scott, R. Hatzky, S. Jolliet, B.F. McMillan, T.M. Tran, L. Villard, M. Mateev, *Global nonlinear particle-in-cell gyrokinetic simulations in tokamak geometry*, Proceedings of the 36th EPS Conference on Plasma Physics, vol. 33E, 2009, p. O2.005, European Physical Society, 2009.

A. Bruschi, T.P. Goodman, R. Chavan, A. Collazos, D. Farina, M.A. Henderson, A. Moro, P. Platania, P. Poli, G. Ramponi, C. Sozzi, V.S. Udintsev, *The ITER EC Upper Launcher with Internal Optics: Beam Characteristics, Tracing and Planned Tests,* 5th IAEA Technical meeting on ECRH Physics and Technology for Large Fusion Devices, Gandhinagar, India, 18-20 February 2009, Proc. of the 5th IAEA Technical meeting on ECRH Physics and Technology for Large Fusion Devices (2009).

P. Bruzzone, *Superconductors for Fusion: Achievements, Open Issues, Roadmap to Future, presented at* ISS2009 – 22nd Int. Symposium on Superconductivity, Tsukuba, Japan, November 2-4, 2009 (2009).

P. Bruzzone, B. Stepanov, R. Wesche, M. Bagnasco, F. Cau, R. Herzog, M. Calvi, M. Vogel, M. Jenni, M. Holenstein, H. Rajainmaki, *Status Report of the Sultan Test Facility,* presented at MT-21, Int. Conference on Magnet Technology, Hefei, China, October 17-23 2009 (2009).

P. Bruzzone, R. Wesche, F. Cau, *Results of Thermal Strain and Conductor Elongation Upon Heat Treatment for Nb3Sn Cable-in-Conduit Conductors,* presented at MT-21, Int. Conference on Magnet Technology, Hefei, China, October 17-23 2009 (2009).

M. Calvi, P. Bauer, F. Cau, C. Marinucci, P. Bruzzone, *Design Proposal for ITER Feeder Busbar System,* presented at MT-21, Int. Conference on Magnet Technology, Hefei, China, October 17-23 2009 (2009).

M. Calvi, P. Bruzzone, R. Wesche, M. Bagnasco, F. Cau, R. Herzog, M. Vogel, *Progress on the EDIPO Test Facility,* presented at MT-21, Int. Conference on Magnet Technology, Hefei, China, October 17-23 2009 (2009).

F. Cau, P. Bruzzone, *Dependence of the AC Loss on the Aspect Ratio in CICC,* presented at MT-21, Int. Conference on Magnet Technology, Hefei, China, October 17-23 2009 (2009).

F. Cau, P. Bruzzone, M. Calvi, *Interstrand Resistance and Contact Resistance Distribution on Terminations of ITER Short Samples,* presented at MT-21, Int. Conference on Magnet Technology, Hefei, China, October 17-23 2009 (2009).

F. Cau, P. Bruzzone, M. Vogel, *Design Study of a Superconducting Magnet System for the European Synchrotron Radiation Facility,* presented at MT-21, Int.

Conference on Magnet Technology, Hefei, China, October 17-23 2009 (2009).

L. Curchod, A. Pochelon, J. Decker, F. Felici, T.P. Goodman, J.M. Moret, J.I. Paley, T.C.V. Team, V. Bobkov, J.-M. Noterdaeme, *Simultaneous Power Deposition Detection of Two EC Beams with the Bis Analysis in Moving TCV Plasmas,* 18th Topical Conf erence on Radio Frequency Power in Plasmas, Gent, Belgium, 24-26 June 2009, Proceedings of the 18th Topical Conference on Radio Frequency Power in Plasmas **1187**, 515 (2009).

A.A. Colazos Gottret, R. Bertizzolo, R. Chavan, F.D.R. Dolizy, F. Felici, T. Goodman, J.-D. Landis, F. Sanchez, M. Henderson, *Progress on the ITER Electron Cyclotron Heating and Current Drive Upper Launcher Steering Mirror Control System,* 23rd IEEE/NPSS Symposium on Fusion Engineering, 647-650 (2009).

F. Felici, O. Sauter, T.P. Goodman, B. Labit, C. Zucca, *Self-Consistent Simulation of Tearing Modes During ECCD Experiments on TCV,* 36th European Physical Society Conference on Plasma Physics, Sofia, Bulgaria, 29 June - 03 July 2009 (2009).

G. Gantenbein, T. Rzesnicki, S. Alberti, T.P. Goodman, J.P. Hogge, S. Illy, J. Jin, S. Kern, B. Piosczyk, A. Samartsev, M. Thumm, *Status of Development of High Power Coaxial-Cavity Gyrotron at Fzk,* 5th IAEA Technical meeting on ECRH Physics and Technology for Large Fusion Devices, Gandhinagar, India, 18-20 February 2009, 5th IAEA Technical meeting on ECRH Physics and Technology for Large Fusion Devices, 2009 (2009).

S. Gnesin, J. Decker, T.P. Goodman, S. Alberti, S. Coda, Y. Peysson, *Synergy of 2nd and 3rd Harmonic Electron Cyclotron Absorption Mediated by Suprathermal Electrons in the TCV Tokamak,* 36th EPS Conference on Controlled Fusion and Plasma Physics, Sofia, Bulgaria, June 29-July 3, 2009, Europhysics Conference Abstracts **33E**, P-2.139 (2009).

T. Goodman, S. Alberti, E. Droz, D. Fasel, J.-P. Hogge, S. Jawla, L. Porte, U. Siravo, M,Q. Tran, F. Albajar, T. Bonicelli, P. Benin, S. Bethuys, C. Liévin, S. Cirant, O. Dumbrajs, G. Gantenbein, S. Illy, J. Jin, S. Kern, et al., *First expérimental results from the EU 2MW coaxial cavity ITER gyrtoron prototype*, *Proc.* 15th Workshop on Electron Cyclotron Emission and Electron Cyclotron Resonance Heating, Yosemite National Park, CA, USA, March 10-13, 2008, in Electron Cyclotron Emission and Elecron Cyclotron Resonance Heating, 2009, p. 515-522

T.P. Goodman, F. Felici, V.S. Udintsev, V. Bobkov, J.-M. Noterdaeme, *Polarization Issues with High Power Injection and Low Power Emission in Fusion Experiments,* 18th Topical Conf erence on Radio Frequency Power in Plasmas, Gent, Belgium, 24-26 June 2009, Proceedings of the 18th Topical Conference on Radio Frequency Power in Plasmas **1187** (2009).

J.P. Graves, I. Chapman, S. Coda, K. Crombe, L.G. Eriksson, T. Johnson, R. Koslowski, M. Lennholm, M.L. Mayoral, I. Nunes, *Sawtooth Control Mechanism on JET Using Off-Axis Toroidally Propagating Icrf Waves,* 36th EPS Conference on Controlled Fusion and Plasma Physics, Sofia, Bulgaria, June 29-July 3, 2009, Europhysics Conference Abstracts **33E**, P-5.176 (2009).

R. Herzog, M. Lewandowska, M. Calvi, D. Bessette, *Helium Flow and Temperatures in a Heated Sample of a Final ITER TF Cable- in-Conduit Conductor,* presented at EUCAS 2009, Dresde, September 13-17, 2009

S. Jawla, I. Pagonakis, J.P. Hogge, S. Alberti, T. Goodman, T.M. Tran, *Mode Content Analysis of the RF Output of a Gyrotron Based on the Astigmatic Gaussian Beams of High Order,* IRMMW THz 2009, Infra Red and Millimeter Waves, Busan, Korea, 11-15 September 2009 (2009).

A.N. Karpushov, B.P. Duval, J.M. Major, H. Weisen, M. Mateev, E. Benova, *Feasibility Studies of the Neutral Beam Heating System for the TCV Tokamak,* 36th European Physical Society Conference on Plasma Physics, Sofia, Bulgaria, 29 June - 03 July 2009, 36th European Physical Society Conference on Plasma Physics **33E**, P.2-140 (2009).

X. Lapillonne, S. Brunner, E. Fable, T. Goerler, F. Jenko, B.F. Mcmillan, F. Merz, O. Sauter, L. Villard, *Gyrokinetic Simulations of Microturbulence in Tokamak Plasmas Presenting an Electron Internal Transport Barrier, and Development of a Global Version of the Gene Code,* 36th European Physical Society Conference on Plasma Physics, Sofia, Bulgaria, 29 June - 03 July 2009, Proceedings of the 36th EPS Conference on Plasma Physics **33E**, P-4.125 (2009).

M. Lewandowska, M. Bagnasco, *Thermal-Hydraulic Analysis of the EDIPO Cool Down,* presented at MT-21, Int. Conference on Magnet Technology, Hefei, China, October 17-23 2009 (2009).

C. Marinucci, M. Calvi, L. Bottura, F. Cau, A. Portone, *Analysis of the EDIPO Ramp Rate Performance,* presented at MT-21, Int. Conference on Magnet Technology, Hefei, China, October 17-23 2009 (2009).

M. Mateev, E. Benova, A. Bottino, B.D. Scott, R. Hatzky, S. Jolliet, B.F. Mcmillan, T.M. Tran, L. Villard, *Global Nonlinear Particle-in-Cell Gyrokinetic Simulations in Tokamak Geometry,* 36th European Physical Society Conference on Plasma Physics, Sofia, Bulgaria, 29 June - 03 July 2009, Proceedings of the 36th EPS Conference on Plasma Physics **33E**, O2.005 (2009).

M. Mateev, E. Benova, S.Y. Medvedev, A.A. Ivanov, A.A. Martynov, Y.Y. Poshekhonov, Y.R. Martin, J.M. Moret, F. Piras, A. Pochelon, O. Sauter, L. Villard, *Stability of Snowflake Diverted and Negative Triangularity Plasmas in the TCV Tokamak,* 36th European Physical Society Conference on Plasma Physics, Sofia, Bulgaria, 29 June - 03 July 2009, Proceedings of the 36th EPS Conference on Plasma Physics **33E**, P2.143 (2009).

S.Y. Medvedev, Y. Hu, A.A. Martynov, L. Villard, *Tokamak Plasma Equilibria and Axisymmetric Stability with a Zero Total Toroidal Current,* 36th European Physical Society Conference on Plasma Physics, Sofia, Bulgaria, June 29 - July 3, 2009, Proceedings of the 36th EPS Conference on Plasma Physics **33E**, P1.130 (2009).

L. Muzzi, A. Della Corte, S. Di Zenobio, S. Turtu, P. Barabaschi, P. Bruzzone, A. Baldini, *The JT-60SA Toroidal Field Conductor Reference Sample: Manufacturing and Test Results,* presented at MT-21, Int. Conference on Magnet Technology, Hefei, China, October 17-23 2009 (2009).

Y. Narushima, K.W. Watanabe, R. Sakamoto, I. Yamada, K. Narihara, Y. Suzuki, S. Sakakibara, S. Ohdachi, H. Yamada, LHD Experimental Group, W.A. Cooper, J. Varela Rodriguez, *MHD Stability Analysis of IDB Plasma in LHD,* Proceedings of the 14th International Congress on Plasma Physics (ICPP2008) **8**, 1070-1074 (2009).

D.K. Oh, S.-H. Park, K. Kim, P. Bruzzone, *Performance Test of TFK02 Qualification Sample for ITER TF Conductor,* presented at MT-21, Int. Conference on Magnet Technology, Hefei, China, October 17-23 2009 (2009).

J.I. Paley, F. Felici, L. Curchod, S. Coda, T.P. Goodman, *Real Time Control of EC Heating and Current Drive Systems on TCV,* 5th IAEA Technical meeting on ECRH Physics and Technology for Large Fusion Devices, Gandhinagar, India, 18-20 February 2009, 5th IAEA Technical meeting on ECRH Physics and Technology for Large Fusion Devices (2009).

T. Panis, D. Testa, A. Fasoli, A. Klein, P. Blanchard, H. Carfantan, JET-EFDA Contributors, *Optimization of the Active MHD Spectroscopy System on JET for the Excitation of Individual Intermediate and High-n Alfvén Eigenmodes,* 11th IAEA Technical Meeting on "Energetic Particles in Magnetic Confinement Systems", Kyiv, Ukraine, 21-23 September 2009, Proceedings of the 11th IAEA technical meeting on energetic particles in magnetic confinement systems (2009).

F. Piras, A. Bencze, S. Coda, B.P. Duval, I. Furno, J.M. Moret, R.A. Pitts, O. Sauter, B. Tal, D. Wàgner, F. Felici, B. Labit, J. Marki, Y. Martin, S. Medvedev, A. Pitzschke, A. Pochelon, G. Turri, C. Zucca, *Snowflake Divertor Plasmas on TCV,* 36th European Physical Society Conference on Plasma Physics, Sofia, Bulgaria, 29 June - 03 July 2009, Europhysics Conference Abstracts **33E**, P-2.141 (2009).

J. Rossel, J.M. Moret, Y. Martin, *A Saddle Coil System for TCV and Rmp Spectrum Optimisation,* 36th European Physical Society Conference on Plasma Physics, Sofia, Bulgaria, 29 June - 03 July 2009, 36th EPS Conference on Plasma Phys. Sofia, June 29 - July 3, 2009 **33E** (2009 ECA), P-2.142 (2009).

F. Sanchez, R. Bertizzolo, R. Chavan, C. Gottret, A. Alfonso, M. Henderson, J.-D. Landis, *Progress on the Design and Manufacturing of the Mirrors for the ITER Electron Cyclotron Heating and Current Drive Upper Launcher,* 2009 23rd IEEE/NPSS Symposium on Fusion Engineering 2009, 190-193 (2009).

A. Shikov, V. Pantsyrny, A. Vorobieva, R. Vasilyev, N. Kozlenkova, K. Abramushin, V. Sytnikov, A. Taran, A. Rychagov, P. Bruzzone, B. Stepanov, *The Result of Russian ITER TF Conductor Sample Test in Sultan,* presented at MT-21, Int. Conference on Magnet Technology, Hefei, China, October 17-23 2009 (2009).

F. Simon, Y. Ilin, B. Su Lima, F. Cau, R. Herzog, B. Stepanov, *Reliability Considerations of the ITER Poloidal Field Coils,* presented at MT-21, Int. Conference on Magnet Technology, Hefei, China, October 17-23 2009 (2009).

B. Stepanov, P. Bruzzone, R. Wesche, N. Martovetsky, D. Hatfield, A. Vostner, A. Devred, *Impact of Sample Preparation Procedure on the Test Results of Four US ITER TF Conductors,* presented at MT-21, Int. Conference on Magnet Technology, Hefei, China, October 17-23 2009 (2009).

D. Testa, *The Magnetic Diagnostics Set for ITER,* 36th International Conference on Plasma Science and 23rd Symposium on Fusion Engineering, San Diego, California, 31 May - 05 June 2009, 23rd Symposium on Fusion Engineering (2009).

D. Testa, *Baseline System Design and Prototyping for the ITER High-Frequency Magnetic Diagnostics Set,* 36th International Conference on Plasma Science and 23rd Symposium on Fusion Engineering, San Diego, California, 31 May - 05 June 2009, 23rd Symposium on Fusion Engineering (2009).

D. Testa, T. Panis, P. Blanchard, H. Carfantan, A. Fasoli, EFDA-JET Collaborators, *Measurement of the Damping Rate of High-N Toroidal Alfven Eigenmodes in JET,* 11th IAEA Technical Meeting on "Energetic Particles in Magnetic Confinement Systems", Kyiv, Ukraine, 21-23 September 2009, 11th IAEA Technical Meeting on "Energetic Particles in Magnetic Confinement Systems" (2009).

C. Theiler, I. Furno, P. Ricci, A. Fasoli, B. Labit, *Study of Filament Motion and Their Active Control,* 36th European Physical Society Conference on Plasma Physics, Sofia, Bulgaria, 29 June - 03 July 2009, 36th European Physical Society Conference on Plasma Physics (2009).

A. Vostner, C. Sborchia, P. Bruzzone, B. Stepanov, R. Wesche, *Test*

Results of the European ITER TF Conductor Performance Qualification Samples, presented at MT-21, Int. Conference on Magnet Technology, Hefei, China, October 17-23 2009 (2009).

R. Wesche, M. Bagnasco, P. Bruzzone, M. Calvi, F. Cau, R. Herzog, C. Marinucci, B. Stepanov, E. Todesco, *Results of Conductor Testing in Sultan: A Review,* Proceedings of WAMSDO Accelerator magnet superconductors, design and optimization **2009-001**, 68-77 (2009).

B.2 Seminars presented at the CRPP in 2009

Dr. J.U. Brackbill, Particle solutions, Portland, USA, *"Coupling fluid and kinetic plasma models"*

Dr. F. Zonca, ENEA Frascati, Italy, *"Integrated burning plasma physics in FAST: scientific basis and plasma scenarios"*

J. Loizu, EPFL, Switzerland, *"Theoretical biophysics of light sensitive neurons: the quantum bump in Drosophila"*

Dr. Y. Camenen, Centre for Fusion, Space and Astronomy, Univ. of Warwick, United Kingdom, *"Transport of parallel momentum induced by current symmetry breaking in toroidal plasmas"*

Dr. D. Mazon, CEA Cadarache, France, *"Real-time determination of suprathermal electron local emission profile from hard X-Ray measurements on Tore Supra and associated feedback control"*

Dr. A. Klein, PSFC, MIT, Cambridge, USA, *"Intertial electrostatic confinement and the multipole ion beam experiment"*

A. Burckel, EPFL, Switzerland, *"Simulation of the dynamics and transport of fast ions in the TORPEX turbulent plasma"*

D. Yuan, KTH Engineering Science, Stockholm, Sweden, *"Modelling of the radiative power loss from the plasma of the Tore Supra Tokamak, comparison of predictions from onion-skin-collisional-radiative modelling with experimental data"*

C. Calzolaio, Univ. of Bologna, Italy, *"Performance analysis of the ITER superconductors"*

S. Kobayashi, Dartmouth College, Hanover NH, USA, *"Plasma turbulence and transport in a ring dipole system"*

Dr. T. Hellsten, KTH Stockholm, Sweden, *"Integrated modelling of RF heating"*

Dr. C. Zucca, CRPP-EPFL, Switzerland, *"Modelling and control of the current density profile in tokamaks and its relation to improved confinement"*

P. Rosini, Univ. degli Studi di Trieste, Italy, *"Polarization entanglement through noise"*

B. Baiocchi, Univ. Statale degli Studi di Milano, Italy, *"Drift modes instability excieted by the formation of a plasma sheath on material surface"*

Dr. N. Mellet, CRPP-EPFL, Switzerland, *"Propagation and absorption of low frequency waves in two and three dimensional warm plasmas"*

Dr. P. Mantica, IFP, CNR, Milano, Italy, *"Recent results on ITG driven ion heat and toroidal momentum transport in JET"*

Dr. R.A. Pitts, ITER Organisation, Fusion Science & Technology Dept., France, *"Status and physics basis of the ITER divertor"*

M. Agostini, Consorzio RFX, Ass. Euratom - ENEA Padova, Italy, *"Edge turbulence in RFX-mod reversed field pinch device and common features with tokamak experiments"*

Dr. D. Gambier, Head of Fusion for Energy, and **Dr. M. Gasparotto**, Chief Engineer, ITER Dept., Fusion for Energy, *"Presentation of Fusion for Energy"*

A. Matsuyama, Graduate School of Energy Science, Kyoto Univ., Japan, *"Moment-equation approach to the bootstrap current and the flows in stellarator/heliotrons using the Monte Carlo methods"*

Dr. M. Gilmore, Univ. of New Mexico, Albuquerque, New Mexico, USA, *"Basic experiments on drift turbulence/flows and magnetic relaxation in the HelCat Device"*

Dr. M. Maslov, CRPP-EPFL, Switzerland, *"Particle transport in JET and TCV H-mode plasmas"*

P. Drewelow, Max-Planck-Inst. für Plasmaphysik, Greifswald, Germany, *"3D-measurements of magnetic field lines at the WEGA stellarator"*

A. Szappanos, KFKI-Research Inst. for Particle and Nuclear Physics, Budapest, Hungary, *"Developing real time tomography"*

Dr. N. Kirneva, RRC Kurchatov Institute, Moscow, Russia, *"Density profile behavior in T-10 tokamak and effect of plasma self-organisation"*

Dr. M. Lesur, Japan Atomic Energy Agency, Tokyo, Japan & CEA, IRFM, St Paul-lez-Durance, France, *"Fully nonlinear features of the energetic beam-driven instability"*

Prof. A.O. Benz, ETH-Zürich, Switzerland, *"Plasma physics of the sun"*

Dr. T.A. Casper, ITER Organisation, Cadarache, France, *"Development of an ITER plasma control system"*

Dr. Ch. Schlatter, CRPP-EPFL, Switzerland, *"Turbulent ion heating in TCV tokamak plasmas"*

Dr. S.H. Kim, CRPP-EPFL, Switzerland, *"Full tokamak discharge simulation and kinetic plasma profile control for ITER"*

Dr. C. Roach, UKAEA Fusion, Culham Science Center, Abingdon, United Kingdom, *"Gyrokinetic simulations of spherical tokamaks"*

Dr. A. Krämer-Flecken, Inst. for Energy Research - Plasma Physics, Forschungszentrum Jülich, Germany, *"Poloidal rotation measurements at TEXTOR"*

Prof. W. Heidbrink, Univ. of California, Irvine, USA, *"Beam-ion confinement for different injection geometries including observation of fast-ion transport by drift waves"*

S. Khosh Aghdam, Univ. Pierre et Marie Curie, Paris, France, *"Linear and nonlinear study of tearing modes in inhomogeneous plasmas"*

Dr. G. Tonetti, CRPP-EPFL, Switzerland, *"L'aluminium, un vecteur d'énergie?"*

Dr. K. Gustafson, Theoretical Plasma Physics, Univ. of Maryland, USA, *"Subdiffusive radial transport in a gyrokinetic Z-pinch plasma with zonal flows"*

Dr. G. von Nessi, Plasma Research Lab., Research School of Physics Science & Engineering, ANU, Canberra, Australia, *"Analysis of MAST plasma discharges via Bayesian inference"*

Dr. E. Nardon, Culham Science Center, UK, *"Edge localized mode control by résonant magnetic perturbations : experiments and modelling"*

Dr. H. Reimerdes, Columbia University, New York, USA, *"Interaction between externally applied non-axisymmetric magnetic fields, the kink mode stability and plasma rotation in the DIII-D tokamak"*

S. Puddu, University of Study of Cagliari, Italie, *"Diagnostics for burning plasmas with GEM detectors"*

Dr. A. Casati, CEA-Cadarache, France, *"A quasi-linear gyrokinetic transport model for tokamak plasmas"*

Dr. A. Bortolon, CRPP-EPFL, Switzerland, *"Plasma rotation and momentum transport studies in the TCV tokamak based on charge exchange spectroscopy measurements"*

Dr. A. Moro, ENEA-CNR Milano, Italy, *"Development and optimization of complex optical systems for high power millimeter waves for fusion plasmas applications"*

APPENDIX C External activities of CRPP Staff during 2009

C.1 National and international committees and ad-hoc groups

MEMBERSHIP

N. Baluc	Member of the HPC-FF board International Organizing Committee of the SOFT Conference (Symposium on Fusion Technology) International Advisory Committee of the ICFRM Conference (International Conference on Fusion Reactor Materials) IEA Annex II Executive Committee IEA Fusion Materials Agreement Executive Committee Swiss Society for Optics and Microscopy (SSOM) Task Coordinator of the subproject entitled 'Radiation-Resistant Materials' of the EXTREMAT Integrated Project (IP) of the 6th European Framework Programme
P. Bruzzone	International Magnet Technology Conference Organizing Committee European Magnet Expert Group 21st Magnet Technology Conference, Programme Committee SST-1 (India), Magnet Review Group Series Connected Hybrid Magnet, Project Review Group GSI Magnet Advisory Group
A. Fasoli	Visiting Professor, MIT Physics Department EFDA Steering Committee ASDEX Upgrade Programme Committee, Germany International Tokamak Physics Activities: Energetic Particles Topical Group Scientific Committee, 11th IAEA Technical Meeting on Energetic Particles in Magnetic Confinement Systems, 2009 Expert for the Review of projects submitted to the French National Agency for Research (ANR) Member of visiting Committee for the Laboratory of Plasma Physics of the Ecole Polytecnique Paris (fusion of LPTP and CETP) President of a Committee for a nation wide search for researchers in plasma physics with the Italian National Research Council Member of Scientific Committee of the EFDA Transport Topical Group Scientific Expert for EFDA in the EU Facilities Review Member of the APS-DPP Programme Committee Member of the EFDA Satellite Tokamak Working Group
Ivo Furno	Member of the SPS Committee
Ch. Hollenstein	Member of the Wissenschaftlicher Beirat Leibniz-Institut für Oberflächenmodifizierung Leipzig Editorial Board Plasma Chemistry and Plasma Processing Kluwer Academic/Plenum Publisher Member of the IUVSTA Plasma Division President of the Swiss Vacuum society
J.B. Lister	International Tokamak Physics Activities: MHD, Disruption and Control Topical Group
C. Marinucci	CHATS-AS, Board

A. Pochelon	Member of the Committee of the SWISS NUCLEAR FORUM Member of the Commission for Training and Formation of the Swiss Nuclear Forum "Aussschuss Wissenschaft" Member of the FORATOM Committee, in particular of the "Research and Development Task Force (R&D.TF) Associate member of IUPAP (International Union of Physics and Applied Phyiscs), Commission C16: Commission on plasma physics
O.Sauter	Member of ITPA on Transport Physic
R. Schäublin	Member of the board of the Swiss Society for optics and microscopy
M.Q. Tran	Director of the Inst. of Physics of Energy and Particle, EPFL Consultative Committee for the Euratom Specific Research and Training Programme in the field of Nuclear Energy, Fusion (CCE-FU) Chairman of the Technical Advisory Panel of the Joint Undertaking Fusion for Energy (F4E) Swiss delegate to the Governing Board of F4E Member of the Core Commission for the nomination of Max-Planck Plasma Physics Director Standing Committee of the International Symposium on Fusion Nuclear Technology Member of the Steering Committee of the Center of Competence on Energy and Mobility of the the CEPF Member of the International Committee of the IRMWW and THZ conference Swiss delegate at the Fusion Power Coordinating Committee Member of the EU Delegation to ITER STAC
L. Villard	Expert Group on High Performance Computing, EFDA Special working group 1 of the HPC-IFERC-Broader Approach
H. Weisen	Seconded to EFDA-JET CSU, programme department Coordinator for particle transport ('spokesperson') of the working group on particle transport within the ITPA database and modelling workgroup Member of the Diagnostics Working Group within the ITPA Member of the expert panel for evaluating PhD and post-doc research proposals submitted to the Fonds National de la Recherche, Luxembourg

PARTICIPATION

B. Duval	Remote Participation Users Group, EFDA-JET 36th EPS Local Organising Committee EU-TTG Meeting, JET, UK
S. Coda	Programme Committee EPS 2009, Sofia, Bulgaria
Y.R. Martin	International Tokamak Physics Activity: Confinement Database and Modelling Topical Group

C.2 Editorial and society boards

S. Alberti	Guest Editor for the Special Issue on High-Power Microwave Generation, IEEE Transactions on Plasma Science, June 2010
S. Coda	Editorial Board of Plasma Physics and Controlled Fusion
Ch. Hollenstein	Editorial Board Plasma Chemistry and Plasma Processing Kluwer Academic/Plenum Publisher

J.B. Lister	Member of the International Advisory Board of Plasma Physics and Controlled Fusion
Y.R. Martin	Member of the EFDA Information Network (PIG) Chairman of the Association Vaudoise des Chercheurs en Physique
A. Pochelon	Auditor of the Swiss Physical Society Committee Set up of a "Network of Experts in the domain of Energy in Switzerland", Swiss Physical Society Committee
M.Q. Tran	Guest Editor for the Special Issue on High-Power Microwave Generation, IEEE Transactions on Plasma Science, June 2010

C.3 EPFL committees and commissions

N. Baluc	Commission Ecole Doctorale en Science et Génie des Matériaux Commission Ecole Doctorale en Physique
A. Fasoli	Commission d'Enseignement de la Section de Physique, FSB-EPFL Commission Stratégique de la Physique, EPFL Direction de la Faculté FSB Comité de Coordination Joint Doctoral Initiative EPFL-IST Lisbon
J-Ph. Hogge	Commission du Doctorat de la Section de Physique, FSB-EPFL
O. Sauter	Commission du Doctorat de la Section de Physique, FSB-EPFL
M.Q. Tran	Commission du Doctorat de la Section de Physique, FSB-EPFL Commission stratégique de la Section de Physique, EPFL Membre du Comité de Sélection du Prix de la meilleure thèse EPFL
T.M. Tran	Groupe de travail technique du Comité de Pilotage HPC/MPC, EPFL
L. Villard	Délégué à la mobilité, Section de physique, FSB-EPFL Commission d'Ethique, EPFL Commission d'Enseignement de la Section de Physique, FSB-EPFL Groupe de travail technique HPC (High Performance Computing) – EPFL Steering Committee, HPC (High Performance Computing) – EPFL Steering Committee, Blue Gene Project – EPFL

APPENDIX D The basis of controlled fusion

D.1 Fusion as a sustainable energy source

Research into controlled fusion aims to demonstrate that it is a valid option for generating power in the long term future in an environmentally, politically and economically acceptable way. Controlled fusion is a process in which light nuclei fuse together to form heavier ones: during this process a very large amount of energy is released. For a fusion reactor it is planned to use the two isotopes of hydrogen: deuterium (D) and tritium (T), which fuse together much more readily than any other combination of light nuclei according to the following reaction:

$$D^2 + T^3 \rightarrow He^4 + n + 17.6MeV$$

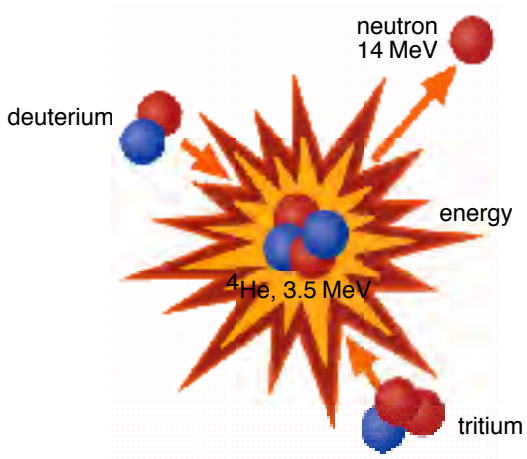

Fig. D.1 *Schematic of a fusion reaction between deuterium and tritium nuclei. The products are 3.5MeV ^{4}He, the common isotope of helium, and a 14MeV free neutron.*

The end products are helium and neutrons (n). The total energy liberated by fusing one gram of a 50:50% mixture of deuterium and tritium is 94000kWh, which is 10 million times more than from the same mass of oil. 80% of this energy is carried by the neutrons with an energy of 14MeV while the remaining 20% is carried by the helium nucleus. Most of this energy eventually becomes heat to be stored or converted by conventional means into electricity.

The temperature at which fusion reactions start to become significant are above a few tens of millions of degrees. For the D-T reaction, the optimal temperature is of the order of 70-200 million degrees. At such temperatures the D-T fuel is in the plasma state.

Deuterium is very abundant on the earth and can be extracted from water (0.034g/l). Tritium does not occur naturally, since its half-life is only 12.3 years, but it can be regenerated from lithium using the neutrons produced by the D-T fusion reactions. The two isotopes of natural lithium contribute to this breeding of tritium according to the reactions:

$$Li^6 + n \rightarrow He^4 + T^3 + 4.8MeV$$

$$Li^7 + n \rightarrow He^4 + T^3 + n - 2.5MeV$$

The relative abundance of the two lithium isotopes Li^6 and Li^7 are 7.4% and 92.6%, respectively. The known geological resources of lithium both in the earth and in the sea water are large enough to provide energy for an unlimited time.

D.2 Attractiveness of fusion as an energy source

The inherent advantages of fusion as an energy source are:

- The fuels are plentiful and their costs are negligible because of the enormous energy yield of the reaction;
- The end product of the reaction is helium, an inert gas;
- No chain reaction is possible: at any time only a very small amount of fuel is in the reacting chamber and any malfunction would cause an immediate drop of temperature and the reaction would stop;
- No after-heat problem can lead to thermal runaway;
- None of the materials required by a fusion power plant are subject to the provisions of the non-proliferation treaties.

Its further potential advantages are:

- Radioactivity of the reactor structure, caused by neutrons, can be minimised by careful selection of low-activation materials resulting in a manageable quantity of long lived radioactive waste;
- The release of tritium in normal operation can be kept at a very low level. The inventory of tritium in the breeding section of the reactor and on the site can be sufficiently small so that the worst possible accident could not lead to a harmful release to the environment requiring evacuation of the nearby population.

APPENDIX E Sources of Financial Support

The work carried out at the CRPP and presented in this annual report was financed from several sources. The major financial support is provided by the Ecole Polytechnique Fédérale de Lausanne (EPFL), EURATOM, ITER F4E, the Paul Scherrer Institute (PSI), which hosts the supraconductivity and materials science activities, and the Swiss National Science Foundation and the Centre de Compétence "Energie-Mobilité" of the CEPF. Other public and private organisations which contributed funding for our research in 2009 include, in alphabetical order: Charmilles SA,, OC Oerlikon, Ruag, the Secrétariat d'Etat à l'Education et à la Recherche (SER), Sulzer Metco AG, the Swiss Commission pour la Technologie et l'Innovation (CTI), Swiss Electric AG and Tetra Pak SA.

The CRPP is the Host of Euratom Fellows:

- MM. A. Collazos and M. da Silva, EC-TECH “Electron cyclotron system technology for ITER”
- F. Cau, M. Bagnasco, MATEFU “Magnet Technology for Fusion”
- Dr. A. Bencze, WP08-FRF-HAS “Spatio-temporal characterization of edge localised mode filamentary and turbulent transport in tokamaks”

APPENDIX F Glossary

The following is a general purpose glossary for the field of controlled fusion and plasma physics.

Additional heating: Usually with reference to a plasma which is initially heated by a toroidal current induced in the plasma (ohmic heating), additional heating designates other means of heating a plasma (absorption of electromagnetic waves or of injected fast neutral particles).

Advanced Tokamak Scenarios: Tokamaks normally generate natural profiles of plasma current and plasma pressure. External non-inductive current drive and local control of the current and pressure profiles can allow access to enhanced regimes and even steady state operation, generally referred to as Advanced Tokamak Scenarios.

ALCATOR C-MOD: High field, high density tokamak at MIT (USA) with an elongated, diverted plasma and metallic walls.

Alfvén gap modes: The toroidal nature of tokamak plasmas produces gaps in the otherwise continuous spectrum of Alfvén waves, populated by discrete, weakly damped Alfvén gap modes. Under certain conditions these modes can be destabilised by resonant energy transfer from energetic particles, e.g. α-particles from fusion reactions.

Alfvén waves: A fundamental plasma wave, which is primarily magneto-hydrodynamic in character with an oscillation of the magnetic field and, in some cases, plasma pressure. In tokamaks, these waves are typically strongly damped. See also fast Alfvén wave.

Alfvén velocity: The velocity of propagation of Alfvén waves in the direction of the magnetic field; it is proportional to the magnetic field strength, and inversely proportional to the square root of the mass density.

alpha particle, or α-particle He^4: The nucleus of the helium atom, composed of two protons and two neutrons, is one of the two products of the DT fusion reaction (the other one is a neutron). The α-particles, being electrically charged, are trapped by the magnetic confinement field and therefore can release their energy to the plasma contrary to the neutrons which escape from the plasma and transfer their energy in the blanket surrounding the plasma core. The plasma heating which is provided by these α-particles as they slow down due to collisions is essential for achieving ignition.

Alternative lines: Magnetic confinement development other than the tokamak.

Analytic/Computational modelling: Analytic: algebraic solution of basic equations. Computational: numerical solution of basic equations.

Anomalous transport: Measured heat and particle loss is anomalously large compared with collisional theory of heat transport in toroidal plasmas.

ASDEX-Upgrade: Medium-sized Tokamak at Garching (Association Euratom-IPP, Germany) with an elongated, diverted plasma.

Aspect ratio: The ratio between the large radius and the small radius of a torus.

Auxiliary heating: See additional heating.

Ballooning instability: A local instability which can develop in the tokamak when the plasma pressure exceeds a critical value; it therefore constrains the maximum β that can be achieved. It is analogous to the unstable bulge which develops on an over-inflated tyre.

Beta (β): Ratio of plasma pressure to magnetic field pressure. One of the figures of merit for magnetic confinement: the magnitude of the magnetic field pressure determine the cost of the field coil that generates it; since fusion reactivity increases with the square of the plasma pressure, a high value of β indicates good performance. The highest values achieved in tokamaks reach 40% (START).

Beta-normalised (β_N): The ratio of plasma current (in MA) to the product of minor radius (in m) and magnetic field (in T) characterises the limit to the achievable β imposed by ideal MHD. β -normalised is the ratio of β (as a percentage) to the above ideal MHD parameter. Generally β_N ~3 should be achievable, but techniques for obtaining higher values have been found experimentally.

Blanket: A structure containing lithium or lithium compounds surrounding the plasma core of a fusion reactor. Its functions are to breed tritium, via lithium-neutron reactions, and to absorb most of the fusion energy to be used for electricity generation.

Bootstrap current: Theory developed in 1970 predicted that a toroidal electric current will flow in a tokamak which is fuelled by energy and particle sources that replace diffusive losses. This diffusion driven "Bootstrap current", which is proportional to β and flows even in the absence of an applied voltage, could be used to provide the poloidal magnetic field: hence the concept of a Bootstrap tokamak, which has no toroidal voltage. A Bootstrap current consistent with theory was observed many years later on JET and TFTR; it now plays a role in optimising advanced tokamaks.

Breakeven: The fusion performance of a power plant is denoted by Q, which is the ratio of the power released by fusion reactions to that used to heat the plasma. As a convention, scientific breakeven corresponds to Q=1 and ignition to Q=infinity. A fusion power plant would operate at Q~50.

Breeding ratio: The number of tritium atoms produced in the blanket of a fusion power station per tritium nucleus burned in the fusion plasma.

Burn: The fusion process of consuming DT fuel in a reactor, releasing energy.

CCE-FU: The Consultative Committee for the Euratom Specific Research and Training Programme in the field of Nuclear Energy, Fusion. Formerly the CCFP.

CEA: Commissariat à l'Energie Atomique, France. Partner in the Association EURATOM-CEA which operates the TORE SUPRA tokamak.

CFI: Committee on Fusion-Industry.

Charge exchange measurement: Measures the plasma ion temperature. Neutral atoms in the plasma (for example from a neutral beam) donate electrons to hot plasma ions, which are thereby neutralised. These hot atoms are no longer confined by the magnetic field and leave the plasma. Their energy is measured by a neutral particle analyser.

CIEMAT: Centro de Investigaciones Energéticas Medioambientales y Tecnológicas, Spain. Partner in the Association EURATOM-CIEMAT. Operates the flexible heliac stellarator TJ-II.

Classical transport: Collisions between the individual particles of a plasma allow them to move across the magnetic field. Theories which describe this mechanism are called "classical" (or "neo-classical" when additional effects due to the toroidal geometry are included). The measured heat and particle transport is usually higher than predicted by these theories.

Collisionality: Non-dimensional parameter, which is the inverse ratio of the mean free path of plasma particles between collisions to a characteristic length of the magnetic field configuration.

Compact torus: Class of closed magnetic configurations in which no material elements (coils, conductors or walls) need to link through the bore of the plasma torus. Thus the vessel of compact tori can be spherical or cylindrical.

COMPASS: COMPact ASSembly, a tokamak for studies of plasma stability, at Culham, UK (Association EURATOM-UKAEA). Originally with circular vessel (COMPASS-C), later with D-shaped vessel (COMPASS-D).

Confinement time: In a fusion plasma neither particles nor energy are perfectly confined. Particle confinement time is the time during which the particles, on average, stay confined. The energy confinement time, which is usually shorter than the particle confinement time, is defined in steady state as the ratio of the plasma energy content to the total power input to the plasma and is a measure of how fast a plasma would cool if there were no heating.

CRPP: Centre de Recherches en Physique des Plasmas. Fusion laboratories of the Association EURATOM-Swiss Confederation at the Ecole Polytechnique Fédérale de Lausanne and the Paul-Scherrer Institute, Villigen (CRPP-Fusion Technology).

Current drive (non-inductive): In a tokamak, plasma current can be driven inductively, with the toroidal plasma acting as a secondary winding of a transformer whose primary coil is at the central column of the device. Continuous current cannot be driven by transformer action. 'Non-inductive' current drive methods are

applied either by injecting particles with directed momentum into the plasma or by accelerating electrons by electromagnetic waves so that they carry the current. Also being applied to control instabilities and to optimise confinement by modifying the current profile. The bootstrap effect also drives current.

Current profile (current distribution): The distribution of current density across the minor radius of the plasma.

Current ramp-up (down): The increase (decrease) of plasma current either at the start of operation or during operation.

Cyclotron frequency: Charged particles in a magnetic field have a natural frequency of gyration in the plane perpendicular to the magnetic field - the cyclotron frequency. For electrons in a tokamak, the cyclotron frequency is typically a few tens of GHz (28GHz per Tesla), and for ions, a few tens of MHz (7.5MHz per Tesla for deuterium).

Cylindrical approximation: An approximation to the true tokamak geometry in which the torus is straightened, so that the toroidal direction becomes the cylinder axis. There are two directions of symmetry: along the axis (the 'toroidal' direction) and about the axis (the 'poloidal' direction).

DCU: Dublin City University, Ireland. Partner in the Association EURATOM-DCU.

DEMO: Demonstration Reactor (the first device in the European fusion strategy intended to produce significant amounts of electricity).

Deuterium: A stable isotope of hydrogen, whose nucleus contains one proton and one neutron. In heavy water, normal hydrogen is replaced by deuterium. Sea water contains, on average, 34g deuterium per m^3. Deuterium plasmas are used routinely in present-day experiments; in a fusion power plant the plasma will consist of a mixture of deuterium and tritium which fuse more readily then two deuterium nuclei.

DG Research (DG RTD): The Directorate-General of the European Commission, Brussels, responsible for Research and Development. Formerly DG XII.

Diagnostic: Apparatus used for measuring one or more plasma quantities (temperature, density, current, etc.).

Diffusion, thermal (or particle): The random flow of heat (or particles) in the presence of a thermal (or density) gradient.

DIII-D: The largest operating US tokamak, run by General Atomics, San Diego. It has a flexible configuration and studies core and divertor physics with intense additional heating.

D-He^3: Deuterium-^{3}Helium: A potential fuel mix for fusion with low release of neutrons, but which would require a much higher fusion triple product ($n T \tau$) than DT to reach ignition. ^{3}Helium is an isotope of helium which is not available in appreciable quantities on Earth.

Disruption, Disruptive instability: A complex phenomenon involving MHD instability which results in a rapid release of energy to the wall and strong electromechanical forces in a tokamak. Plasma control may be lost, triggering a VDE (q.v.). This phenomenon places a limit on the maximum density, pressure and current in a tokamak.

Distribution function: Describes both the space and velocity distribution of plasma particles.

Divertor: A magnetic field configuration with a separatrix, affecting the edge of the confinement region, designed to remove heat and particles from the plasma, i.e. divert impurities and helium ash to divertor plates in a target chamber. Alternative to using a limiter to define the plasma edge.

Double null: See Single/double null divertors.

Drift kinetic theory: Kinetic theory which describes plasma processes which have spatial scales much greater than the particle Larmor radii.

Drift orbits: Particle motion is tied to straight magnetic field lines. However, electric fields and gradients of the magnetic field give an additional drift perpendicular to the magnetic field creating drift surfaces displaced from the magnetic surfaces.

Driven current: Plasma current produced by a means external to the plasma, inductively or non-inductively.

Driver: In inertial confinement fusion, the laser or particle beam system used to compress a target pellet.

DTE: The deuterium-tritium experiment at JET which in 1997 set new records for fusion power production. Followed the Preliminary Tritium Experiment of 1991.

ECCD: Electron Cyclotron Current Drive. Non-inductive current drive technique using directed electron cyclotron resonance waves.

ECE: Electron Cyclotron Emission. Radiation emitted by electrons as a result of their cyclotron motion around magnetic field lines. Used to measure electron temperature.

ECH: Electron-Cyclotron Heating. Radio wave heating near the resonance frequency (or its multiple) of the electron gyration in a magnetic field. In present and future machines ECH is at typically 60-170GHz, depending on the magnetic field strength in a machine.

EFDA: European Fusion Development Agreement. The organisational framework of the EU fusion activities for the exploitation of the JET Facilities, international collaboration (including ITER) and supporting technology.

EFET: European Fusion Engineering & Technology: a fusion technology oriented European Economic Interest Grouping.

Electron temperature: A measure of electron thermal energy in units of degrees or electron volts (1eV ~ 10^4 degrees Kelvin).

ELM: Edge localised mode. An instability which occurs in short periodic bursts during the H-mode in divertor tokamaks. It modulates and enhances the energy and particle transport at the plasma edge. These transient heat and particle losses could be damaging in a reactor.

ENEA: Ente per le Nuove Tecnologie, l'Energia e l'Ambiente, Italy. Partner in the Association EURATOM-ENEA.

Energetic particle: In terms of energy, the particles in a plasma can be divided into two classes. The more numerous thermal particles are characterised by a temperature typically in the range 1–30keV for modern tokamaks. The less numerous class of energetic particles has significantly higher energy up to several MeV. Energetic particles can be created by electric fields, fusion reactions, neutral beam injection or RF heating.

EPS: European Physical Society. Its Plasma Physics Division hosts the major European annual conference on Plasma Physics.

Error fields: The magnetic coils of a tokamak are designed to give the desired magnetic field configuration. The finite number of coils and imperfections in their construction lead to unwanted deviations from this configuration known as error fields. These could lead to disruptions and are of particular concern for larger tokamaks.

EXTRAP T-II: External Trap II, a medium-sized reversed field pinch (RFP) at the Royal Institute of Technology, Stockholm (Association EURATOM-NFR), built for RFP transport and shell stabilisation studies in support of RFX.

EURATOM: European Atomic Energy Community.

Faraday rotation: The rotation of the plane of polarisation of light passing through a magnetised plasma.

Fast Alfvén wave: The fast Alfvén wave exists over a broad frequency spectrum, from the ion cyclotron range of frequencies (ICRF) where its character is electromagnetic, down to magnetohydrodynamic frequencies. Its velocity is comparable to the Alfvén velocity. The fast Alfvén wave is used routinely for high-power (~20MW) ICRF heating on JET, as it is efficiently absorbed in the plasma by the mechanism of ion cyclotron resonance. Although usually stable in tokamaks, the wave can be excited by energetic ion populations.

Fast wave current drive: Current drive produced by a fast wave. The wave can penetrate the plasma more easily than a lower hybrid wave.

Feedback: Use of measurements of plasma parameters to control the parameters, shape or profiles of the plasma to obtain desired conditions.

Field lines, Flux surfaces: Imaginary lines marking the direction of a force field. In a tokamak these define a set of nested toroidal surfaces, to which particles are approximately constrained, known as flux surfaces.

Field reversed configuration: A compact torus with a strongly elongated plasma. The plasma is contained in a cylindrical vessel inside a straight solenoid. The confining magnetic field usually has

only a poloidal component. Not to be confused with reversed field pinch.

FIR: Far infra-red (e.g. wavelength ~ 0.2 to 1mm). FIR lasers are used to measure the magnetic field and plasma density.

"Fishbones": Rapid bursts of MHD activity sometimes observed when neutral beam heating is used in tokamaks (fishbone refers to the shape of the bursts in oscillating magnetic field when plotted as a function of time).

First wall: The first material boundary that surrounds the plasma. Today, the first wall in many machines is protected by low-Z materials (such as carbon tiles, boron or beryllium coating). Future tokamaks will require metallic walls.

Flat-top current: Constant current during quasi-stationary operating conditions.

Fokker-Planck Code: A computer code to calculate the velocity distribution of plasma particles allowing for collisional relaxation and plasma heating. Calculates distribution functions (q.v.).

FOM: Stichting voor Fundamenteel Onderzoek der Materie (Foundation for basic investigations of matter), The Netherlands. Partner in the Association EURATOM-FOM.

FTU: Frascati Tokamak Upgrade, a high density, high current tokamak at Frascati, Italy (Association EURATOM-ENEA).

Fusion triple product: Product of (ion) density, (ion) temperature and energy confinement time. A measure of the proximity to break-even and ignition.

Fusion product: The product of a fusion reaction, for example an α-particle or neutron in a deuterium-tritium plasma.

Fusion reactivity: Fusion reaction rate. For present typical tokamak conditions, it increases with the square of the density and the ion temperature of the plasma.

Full wave theory: Wave theory which includes complete accounting of wave energy (transmitted, reflected and absorbed, including energy transferred to other waves) for studying RF heating.

FZK: Forschungszentrum Karlsruhe, Germany. Partner in the Association EURATOM-FZK, active in fusion technology and, with the development of gyrotrons, in plasma engineering.

FZJ: Forschungszentrum Jülich GmbH, Germany. Partner in the Association EURATOM-FZJ, operating the tokamak TEXTOR.

GSI: Gesellschaft fuer Schwerionenforschung, Darmstadt, Germany. Studying heavy-ion physics, and driver physics with possible application for inertial confinement fusion.

Gyro-kinetic theory: Version of kinetic theory in which the Larmor radius is not assumed to be small. An essential theory for investigating fine-scale instabilities which might be responsible for driving turbulence, which may in turn be responsible for anomalous transport.

Gyrotron: Device used for generating high power microwaves in the electron cyclotron range of frequencies (50 - 200GHz). This UHF wave is mostly used to heat the plasma at the electron cyclotron resonance frequency. It also could be used to diagnose the plasma.

Heliac: Stellarator configuration with a central toroidal coil around which the plasma column is wound helically. Because of its high capability of investigating a wide range of stellarator configurations, it is used for TJ-II.

Helias: Optimised stellarator configuration, used with modular coils for Wendelstein VII-X (Germany) and SHEILA (Australia).

H-mode: A High confinement regime that has been observed in tokamak plasmas. It develops when a tokamak plasma is heated above a characteristic power threshold, which increases with density, magnetic field and machine size. It is characterised by a sharp temperature gradient near the edge (resulting in an edge “temperature pedestal”), ELMs and typically a doubling of the energy confinement time compared to the normal “L” regime. Today, a variety of high confinement modes have been identified in divertor and in limiter configurations (e.g. the I-mode), which, in part, have been obtained by special tailoring of the radial plasma current profile.

H-transition (or L-to-H transition): Transition into the H-regime from the L-regime, usually quite sudden, at a certain threshold power of additional heating and specific plasma parameters.

Halo currents: See Vertical Displacement Event.

Helicity injection: The helicity of a toroidal plasma is related to a linkage of toroidal and poloidal magnetic fluxes, and is approximately conserved throughout a discharge. If additional helicity can be injected, the plasma current could be sustained or even increased.

Helium ash: Fusion reactions in a deuterium-tritium plasma produce energetic α-particles (helium nuclei), which heat the plasma as they slow down. Once this has happened, the α-particles have no further use: they constitute helium ash, which dilutes the fuel and must be removed to maintain a burning plasma.

High beta (β): Condition in which the plasma energy is a significant fraction of the energy in the magnetic field. An alternative measure is the ratio between the plasma energy and the energy in the poloidal magnetic field, the poloidal β.

High field ECH launch: Electron cyclotron waves can be launched from the inside of the plasma torus. This allows higher density plasma to be heated.

Hydrogen: The lightest element; the nucleus consists of only one proton, the atomic shell of one electron. Isotopes of hydrogen, with one or two additional neutrons in the nucleus, are deuterium and tritium respectively.

IAEA: International Atomic Energy Agency (of the United Nations), Vienna, Austria. The ITER-EDA is undertaken under the auspices of the IAEA.

ICE: Ion Cyclotron Emission. Observed in JET and TFTR as a suprathermal signal, apparently driven by collective instability of energetic ion populations such as fusion products and injected beam ions.

ICF: Inertial Confinement Fusion. Intense beams of laser light or light or heavy ion beams are used to compress very rapidly and heat tiny target pellets of fusion fuel to initiate fusion burn in the centre. Sufficient fusion reactions must occur in the very short time before the fuel expands under its own pressure. The inertia of the pellet's own mass determines the time scale during which fusion reactions occur, hence the name inertial confinement.

Ideal: In the context of MHD, 'ideal' implies that the magnetic field and the plasma always move together. For this to occur, the electrical resistivity of the plasma must be negligible.

Ideal internal kink modes: An MHD instability of the central region of a tokamak. This, or its close relative the resistive internal kink mode, may be involved in the Sawtooth disruptions which occur in most Tokamaks.

IEA: International Energy Agency (of the OECD), Paris, France. Implementing agreements for international collaboration on specific topics in fusion have been set up in the frame of the IEA.

Ignition condition: Condition for self-sustaining fusion reactions: heat provided by fusion α-particles replaces the total heat losses. External sources of plasma heating are no longer necessary and the fusion reaction is self-sustaining. Ignition is not required for energy gain in a power station. Retaining a level of external heating or current drive will be required to control the plasma pressure and current profiles, to optimise the performance, leading to a so-called "driven burn".

Impurities: Ions, other than the basic plasma ion species, which are unwanted as they lose energy by radiation and dilute the plasma.

Impurity screening: The prevention of impurities from entering the plasma.

Internal kink: A type of MHD instability that can occur within the central region of the plasma (where $q < 1$) reducing the peak temperature and density.

Internal Reconnection Event (IRE): An instability which breaks magnetic field lines and reconnects them with a different topology to reduce the system to a lower energy state - associated with the operating limits of spherical tokamaks.

Ion Bernstein wave: A wave which only exists in a hot plasma and is supported by the ions. It propagates at right angles to the magnetic field, when it is undamped, at harmonics of the ion cyclotron frequency. There is also an electron Bernstein wave which propagates at harmonics of the electron cyclotron frequency.

Ion Cyclotron Current Drive (ICCD): Non-inductive current drive using ICRH.

Ion Cyclotron Resonance Heating (ICRH)/Ion Cyclotron Resonance Frequencies (ICRF): Additional heating method using RF waves at frequencies (~ 20-50MHz) matching the frequency at

which ions gyrate around the magnetic field lines.

IPP: Max-Planck-Institut fuer Plasmaphysik, Garching, Germany. Partner in the Association EURATOM-IPP, operating the tokamak ASDEX-Upgrade and the stellarator Wendelstein VII-AS. Also has sites in Berlin and in Greifswald, where the construction of the large superconducting stellarator Wendelstein VII-X is in progress. The name is also used for the Czech Republic Association.

IR: Infra Red part of the electromagnetic spectrum.

IRE: Internal Reconnection Event.

IST: Instituto Superior Técnico, Portugal. Partner in the Association EURATOM-IST.

ISTTOK: Tokamak, for study of non-inductive current drive, at the Instituto Superior Técnico (IST), Lisbon, Portugal.

ITER: International Thermonuclear Experimental Reactor (the next step as a collaboration between EURATOM, Japan, China, India, Korea, the Russian Federation and the USA, under the auspices of the IAEA). After a conceptual design phase - CDA (1988-1990), and engineering design activities (ITER-EDA, 1992-2001), now under the Coordinated Technical Activities (CTA).

JAEC: Japan Atomic Energy Commission, Tokyo, Japan.

JAEA: Japan Atomic Energy Agency. Headquarters in Tokyo, Japan.

JET: Joint European Torus. The largest tokamak in the world, sited at Abingdon, UK. Operated as a Joint Undertaking (JET Joint Undertaking), until the end of 1999. The scientific exploitation of the JET facilities is now guaranteed by the Euratom fusion Associations within the EFDA framework. The operation of the facility is the responsibility of the Association Euratom-UKAEA.

JT-60U: Japanese tokamak at Naka. The largest Japanese tokamak and second largest operating experiment after JET, but not designed for use with D-T fuel.

keV: Kilo-electronvolt. Energy which an electron acquires passing a voltage difference of 1000 volts. Also used to measure the temperature of a plasma (1 keV corresponds to 11.8 million degrees Kelvin).

Kinetic instability: Oscillation which is unstable as a result of the energy distribution of ions or electrons.

Kinetic theory: A detailed mathematical model of a plasma in which trajectories of electrons and ions are described. More complex than fluid and two-fluid theories, it is necessary in the study of RF heating and some instabilities, particularly when energetic particles are involved.

L-H transition: Change from L regime to H regime (usually quite sudden).

L-mode: As opposed to the H mode. Regime with degradation of confinement, in additionally heated plasmas, with respect to plasmas heated ohmically by the plasma current.

Langmuir probe: Electrical probe inserted into the edge of a plasma for measurements of density, temperature and electric potential.

Larmor radius: Radius of the gyratory motion of particles around magnetic field lines.

Large scale ideal modes: A large scale mode has a wavelength which is a significant fraction of the plasma dimensions and assumes ideal MHD.

Laser ablation: Use of lasers to produce a sudden influx of impurities into the plasma from a solid surface.

Last closed flux surface: The boundary separating those magnetic field lines that intersect the wall (open lines) from the magnetic field lines that never intersect the wall (closed lines).

Lawson criterion: The value of the confinement time multiplied by the ion density (at the required temperature) which must be exceeded in a fusion reactor to reach ignition.

Limiter: A material surface within the tokamak vessel which defines the edge of the plasma and thus avoids contact between the plasma and the vessel. A pumped limiter can also be used to remove heat and particles and is an alternative exhaust system to the divertor.

LLNL: Lawrence Livermore National Laboratory, Livermore, USA.

Locked modes: MHD modes that cease rotating (though they can still grow).

Low-activation materials: Materials which do not develop high, long-lived radioactivity under neutron irradiation.

Low aspect ratio: Low ratio of major to minor radius of the torus.

Lower hybrid current drive (LHCD): Non-inductive current drive using lower hybrid waves.

Lower hybrid heating (LHRH): Plasma heating by radio frequency waves at the "lower hybrid" resonance frequency in the plasma. Typical frequencies are a few GHz.

Lower hybrid (LH) wave: A plasma wave of frequency between the ion and electron cyclotron frequencies. It has a component of electric field parallel to the magnetic field, so it can accelerate electrons moving along the field lines.

Magnetic axis: The magnetic surfaces of a tokamak form a series of nested tori. The central 'torus' defines the magnetic axis.

Magnetic Confinement Fusion (MCF): Confinement and thermal insulation of a plasma within the reactor core volume by the action of magnetic fields. In toroidal magnetic confinement, usually both toroidal and poloidal components of the magnetic field are needed (the field lines are threaded like the filaments of a cable which is bent into a ring).

Magnetic islands: Islands in the magnetic field structure caused either by externally applied fields or internally by unstable current or pressure gradients. See tearing magnetic islands.

Magnetic surfaces (flux surfaces): In toroidal magnetic confinement, the magnetic field lines lie on nested toroidal surfaces. The plasma pressure, but not the amplitude of the magnetic field, is a constant on each magnetic surface.

Magneto-acoustic cyclotron instability: This instability results from an exchange of energy between the fast Alfvén wave (or magneto-acoustic wave) and an ion Bernstein wave which has a source of free energy through the presence of a population of energetic (non-thermal) ions, e.g. fusion products. The instability occurs for propagation perpendicular to the equilibrium magnetic field.

Major radius: The distance from the tokamak symmetry axis to the plasma centre.

Marfe: A localised and radiating thermal instability sometimes observed near the edge of tokamak plasmas.

Marginal Stability: Close to the transition from stability to instability.

MAST: Mega Amp Spherical Tokamak at Culham (Association EURATOM-UKAEA), twice as big as START. Began operation in 1999.

MeV: Mega-electronvolt, unit for nuclear energies. Energy which an electron acquires passing a voltage difference of 1 million volts.

MHD (Magnetohydrodynamics): A mathematical description of the plasma and magnetic field, which treats the plasma as an electrically conducting fluid. Often used to describe the bulk, relatively large-scale, properties of a plasma.

MHD instabilities: Unstable distortions of the shape of the plasma/magnetic field system.

Microinstabilities: Instabilities with characteristic wave-lengths similar to the ion Larmor radii, rather than to the tokamak dimensions. These are thought to be responsible for the fine scale turbulence in tokamaks, and hence anomalous transport.

Minor radius: Half the small diameter of the tyre-shaped toroid.

Mirnov coils: Pick-up coils at the edge of the plasma for measuring the time variation of magnetic fields arising from instabilities.

Mirror: A linear magnetic confinement concept with a weaker magnetic field in a central region and with strong fields at both ends which reflect contained particles by the mirror effect. Some variants exist to increase the magnetic field in all directions from the centre or to improve the closure of the bottlenecks. The Tandem Mirror confinement concept also involves electrostatic fields.

MIT: Massachusetts Institute of Technology, Boston, USA. Operates the high-field divertor tokamak ALCATOR C-MOD.

Mode: A resonant wave or oscillation in a plasma. Also used as a synonym for an operating regime.

Mode number: Characterises the wavelength of a mode normalised to the device size.

Monte Carlo code: A statistical technique used in numerical calculations where events may occur many times, each with a certain probability.

Motional Start Effect (MSE): The measurement of shifts and splitting of spectral lines emitted from particles moving in a local electric field. This can be interpreted to give the local magnetic field inside the tokamak if the particle velocity is known, and is a major diagnostic on some tokamaks to deduce the current profile.

MPQ: Max-Planck-Institut fuer Quantenoptik, Garching, Germany. Active, within its programme, in ICF (laser fusion) related physics. Partially supported by Euratom, for a "keep in touch activity" in ICF.

Negative ion beam: To produce neutral beams, negative ions (obtained by the addition of electrons to neutral atoms) are accelerated and then neutralised before entering the plasma. The efficiency of creating neutral beams from positive ions is too low at the beam energy required for a fusion power station, of the order of 1 MeV.

Neo-classical theory: Classical collisional plasma transport theory, corrected for toroidal effects. The neoclassical theory predicts the existence of the bootstrap current.

Neo-classical tearing mode: The magnetic island produced by a tearing mode perturbs the bootstrap current which further amplifies the island and degrades confinement or leads to a disruption.

NET: Next European Torus, a design for the Next Step which had been prepared by the NET team (located at the Association EURATOM- IPP in Garching) and which largely influenced the ITER design.

Neural network: A computer algorithm that uses incoming data to derive plasma parameters, having previously been "trained" on a series of examples of a non-linear input-output mapping.

Neutrons: Neutral particles in the nucleus. Products of Deuterium-Tritium and other fusion reactions.

Neutral beams: Since charged particles cannot easily penetrate the magnetic confinement fields of the plasma, high energy beams of neutral atoms are injected into the plasma for fuelling, heating and current drive. Within the plasma, the atoms of the beam are ionized and are then confined.

Neutron multiplier: The fusion of deuterium and tritium consumes one tritium nucleus per reaction, producing one neutron. Since in the blanket of a power station not every neutron reacts with lithium to produce a new tritium atom, a neutron multiplying element may be used in the blanket to enhance the tritium production so as to make the power station self-sufficient in tritium supply.

Next Step: The next experimental device in the strategy of the European Fusion Programme. Presently pursued via the ITER EDA, with a European activity as a fall-back option. The generic name for an experimental reactor with a long pulse burning plasma at high fusion gain.

NFR: Naturvetenskapliga Forskningsrädet (Natural Science Council), Sweden. Partner in the Association EURATOM-NFR.

NIFS: National Institute for Fusion Science, Nagoya, Japan.

NRIM: National Research Institute for Metals, Sakura-mura, Japan.

Non-inductive heating and current drive: See additional heating and current drive.

NSTX: Spherical tokamak at Princeton, USA. A similar size to MAST, but of different design. Started operation in 1999.

Ohmic heating (OH): The resistive heating resulting from a current flowing within the plasma corresponding to the heating of a wire by a current flowing through it. Ohmic heating in a tokamak is insufficient to reach thermonuclear temperatures since, contrary to a wire, the resistance of a plasma decreases strongly with increasing temperature, thus making Ohmic heating weak at high temperatures.

ORNL: Oak Ridge National Laboratory, USA.

Operating limits: See tokamak operating boundaries.

Optimised shear: Adjusting the current profile to optimise tokamak.

PbLi: Eutectic lithium-lead alloy considered for use as blanket breeding material.

Peeling mode: An edge MHD instability which exists when the current density at the plasma edge is non-zero. It may be associated with ELMs.

Pellet: In inertial confinement concepts, the fuel is contained in tiny spheres, called pellets, which are compressed by laser or particle beams. In magnetic fusion, pellets of frozen hydrogen, deuterium, tritium, accelerated up to several kilometres per second, are used to refuel the plasma and to obtain very high densities.

PIREX: Proton Irradiation Experiment, material test facility (Association Euratom-Switzerland, CRPP-FT, PSI, Villigen, CH).

Plasma: State of matter above a few thousand degrees where atoms are broken into their constituents, ions and electrons, thereby creating an electrically conducting medium. Plasmas can therefore interact strongly with electric and magnetic fields.

Plasma confinement: Retention of plasma energy or particles within a given region, including the heat and particle losses from the plasma.

Plasma parameters: Physical quantities which characterise the plasma and which must be measured experimentally, such as current, density, temperature, confinement time, β.

Plasma pressure: Proportional to the product of plasma density and temperature. There is an electron and an ion pressure and the plasma pressure is the sum of the two. In magnetic confinement devices, this pressure is counterbalanced by magnetic pressure.

Plasma shape: Describes the plasma vertical cross-section, circular, elongated, D-shape, diverted, single null, double null.

Polarimetry: Measurement of the rotation of the plane of polarisation of light passing through a magnetically confined plasma; used to measure the local magnetic field and thus the safety factor (see Faraday rotation).

Poloidal field: Component of the magnetic field perpendicular to the toroidal direction and the major radius. The poloidal field is essential for confinement and is generated in a tokamak by the plasma current and the external coils.

Power threshold: The L-H transition and improved performance regimes related to reversed shear occur when the power exceeds a certain threshold value - the power threshold.

PPPL: Princeton Plasma Physics Laboratory, New Jersey, USA.

Preliminary Tritium Experiment (PTE): Three plasma discharges on JET, November 1991, into which a significant amount of tritium was injected for the first time in a tokamak. The power liberated from fusion reactions (~ 2MW for ~ 2 seconds) was in accordance with expectations. Followed by the more ambitious DTE in 1997.

Profile: Variation of plasma parameters with minor radius.

Profile control: Controlling the profiles of pressure, density or current, in order to control instabilities.

PSI: Paul-Scherrer-Institut, Villigen, Switzerland, active, in muon physics among others fields. The Association EURATOM-Swiss Confederation has their fusion technology activities working in superconductor and materials technology located at Villigen.

Pumped divertor: Divertor field lines directed into a pumped chamber surrounding the target plate.

q, q_{95}: See Safety factor.

Q: Ratio of fusion power to total additional heating power. At Q= , no external power is required and the plasma is said to be ignited. A power station should operate with Q~50 to be economical.

Radial electric field: Arises when there is a charge imbalance in the plasma.

Radio frequency (RF) heating: Heating with waves in the radiofrequency range at resonance frequencies of the plasma (see ECH, ICRH, LHH).

Reflectometry: Use of reflected microwaves to measure plasma density.

Relaxation: The evolution of a plasma to a lower energy state.

Resistive ballooning modes: A class of ballooning mode which would be stable in the absence of resistivity, but can be

unstable in its presence. Related to tearing modes, but topologically different.

Resistive instability: Instability due to diffusion and rearrangement of magnetic field lines. When the plasma resistivity is small, these instabilities have a slow growth rate.

Resistivity: The tendency to resist the flow of electric current, thereby dissipating energy. Plasmas are very good conductors of electric current, so that their resistivity can often be neglected. In this case, 'ideal' magnetohydrodynamics may be applied.

Resonant ions/electrons: Resonance occurs when one of the characteristic frequencies of particle motion in the plasma (for example, the cyclotron frequency) matches the frequency of some applied perturbation (for example, an RF wave).

Resonant magnetic perturbation (RMP): An externally applied magnetic perturbation matched to the spatial structure and optionally the frequency and phase of an instability.

Reverse Field Pinch (RFP): A toroidal magnetic confinement device, similar to a tokamak, in which the poloidal and toroidal fields are of comparable magnitude. Capable of higher plasma current and pressure for a given external magnetic field. They require a conducting shell close to the plasma for stabilisation.

Reverse (magnetic) shear: In a tokamak the current density is usually greatest at the magnetic axis, in which case the safety factor increases from the centre to the edge of the plasma. Using non-inductive current drive and/or the bootstrap current the current density can be made to increase away from the centre. In this "reverse shear" case, the safety factor has a minimum away from the plasma centre. Using reverse or low shear ("optimised shear") some tokamaks, notably DIII-D and TFTR in the US and more recently JT-60U in Japan and JET, have shown greatly improved plasma performance. Reverse shear is an attractive option for advanced tokamak scenarios.

RF: Radio-Frequency.

RFX: Reversed Field pinch Experiment at CNR-Padova, Italy (Association EURATOM-ENEA).

RISØ: Forskningscenter Risø, Denmark. Partner in the Association EURATOM-RISØ.

Rotational transform: Measure of the ratio of poloidal to toroidal flux defining the pitch of the helical field lines. The q-value of the tokamak is proportional to the reciprocal of the rotational transform.

RTP: Rijnhuizen Tokamak PETULA, for study of transport in a plasma, at Nieuwegein (Rijnhuizen), the Netherlands (Association EURATOM-FOM). Ceased operation in 1998, the activities of the Association being transferred to TEXTOR, as part of the Tri-lateral Euregio Cluster.

Runaway electron: An electron with a very high energy has a decreasing probability of colliding with another charged particle and of losing its energy. Such a particle then gains more and more energy in the electric field of a tokamak, reaching 10's of MeV.

Safety factor: Number of turns the helical magnetic field lines in a tokamak make round the major circumference for each turn round the minor circumference, denoted q. Has no connection with the ordinary sense of "safety" other than q=1 surfaces are ideally unstable. For diverted plasmas q goes to infinity at the separatrix, so instead q_{95} is used to describe the safety factor near the edge, which is the safety factor of the plasma surface which contains 95% of the poloidal flux.

Sawtooth: A cyclically recurring instability which causes an energy loss from the central region of tokamak discharges. The temperature periodically falls abruptly, then slowly recovers. The jagged trace produced by plotting temperature against time gives the instability its name.

Sawtooth crash: The rapid collapse of the central temperature in a tokamak during a sawtooth cycle.

Scaling laws: Empirical or theoretical expressions for how various plasma phenomena (eg confinement, power threshold, etc) vary with tokamak parameters. They are particularly used for predicting the performance of future tokamaks.

Scrape-off-layer (SOL): The residual plasma between the "edge" of the plasma (defined by the limiter radius or the separatrix) and the tokamak vessel wall.

Semi-empirical: A theoretical approach in which the behaviour of some key quantities

is deduced from experiment, rather than a priori.

SEAFP: The Safety and Environmental Assessment of Fusion Power is an extensive study conducted by several teams in the associated laboratories, NET, industry and the JRC, published in June 1995.

SEAL: The Safety and Environmental Assessment of Fusion Power Long-term is a programme, launched in 1995, being undertaken for the European Commission in the framework of the Fusion Programme.

Separatrix: Magnetic surface at which the rotational transform vanishes and the safety factor becomes infinite.

Shear: The safety factor usually varies from magnetic surface to magnetic surface across the plasma cross-section; this variation is measured by the non-dimensional quantity called "shear". Also refers to the variation of plasma flow (flow shear). If the type of shear is not specified, it usually means magnetic shear.

Single/double null: Points of zero poloidal magnetic field where the separatrix crosses itself are the X-points or nulls. Usually sited above and/or below the plasma. Tokamak divertor configurations have either one or two nulls.

Single fluid model: The set of equations which represent a plasma as a magnetised, electrically conducting fluid with the usual fluid properties of viscosity, thermal conductivity, etc. The possibility of distinct behaviour of electrons and ions (i.e. 2 "fluids") is excluded.

Small aspect ratio: Same as Low aspect ratio.

Spectroscopy: The detection and analysis of the spectrum of radiation emitted by a plasma. This can yield information about temperatures, impurities, rotation, using different parts of the electromagnetic spectrum (IR, visible, VUV, XUV, etc.)

Spherical tokamak (ST): A very low aspect ratio tokamak - it appears almost spherical, though topologically it remains a torus with a centre column. The spherical tokamak is being further investigated, with larger experiments, MAST and NSTX.

Spheromak: A spherical plasma in which comparable toroidal and poloidal currents flow. The toroidal current is not driven by transformer action.

Stability theory: The theory of how small perturbations to a system evolve in time. Spontaneous growth is due to instability. Instabilities can saturate at some small amplitude, in which case they may degrade confinement, or grow uncontrollably, in which case the equilibrium is lost leading to a disruption.

START: Small Tight Aspect Ratio Tokamak, a "spherical" tokamak with a very small aspect ratio at the Association EURATOM-UKAEA (Culham). This very fat ring-shaped configuration showed experimentally a lesser tendency to disruptions and is efficient in its use of magnetic energy. Ceased operation in 1998, replaced by MAST.

Start-up assist: Assisting plasma formation to cross a range of plasma temperature at which impurities radiate strongly, with the aim of minimising the start-up delay and transformer requirements, usually using ECH.

STAC: Scientific and Technical Advisory Committee set up by EURATOM.

Steady state power plant: A continuously (as opposed to cyclically) operated power plant.

Stellarator: Closed configuration having the shape of a three-dimensionally distorted ring in which the plasma is confined principally by an externally generated magnetic field (produced by non-planar coils outside the plasma vessel). The coils can be arranged in a modular fashion. Stellarators do not need a transformer; they need an additional heating system for the plasma start-up. Due to the fact that no toroidal plasma current is needed to maintain the confinement configuration, they naturally provide steady state operation.

SULTAN: Supra Leiter Test ANlage. Large Superconductor Test Facility, CRPP at PSI Villigen, Switzerland (Association EURATOM-Swiss Confederation).

Super Alfvénic velocity: A velocity greater than the Alfvén velocity. In a tokamak, only energetic particles have super Alfvénic velocities; because they

satisfy this condition, they may resonantly transfer their energy to magnetohydrodynamic modes, which may grow as a result (eg TAE modes).

Superthermal radiation: Electromagnetic radiation produced by energetic particles, as opposed to thermal particles.

Survey spectrometer: An instrument which gives information concerning the radiated spectrum over a large range of frequencies.

TAE modes: Toroidal Alfvén Eigenmodes. One class of Alfvén gap modes.

Target plates: See Divertor.

TCV: "Tokamak à Configuration Variable", for study of elongated and strongly shaped plasmas, at Lausanne, Switzerland (Association EURATOM-Swiss Confédération).

TEKES: Technology Centre Finland. Partner in the Association EURATOM-TEKES.

Tearing magnetic islands: The disturbance caused by a tearing mode which alters the topology of the confining magnetic field and causes transfer of heat across the affected region.

Tearing mode: A class of resistive MHD instability which has been predicted theoretically in tokamaks and positively identified in experiments.

Temperature pedestal: In an H-mode discharge there is a region of steep temperature gradient at the plasma edge. The temperature at the top of this steep gradient region is the temperature pedestal.

Tesla: Unit of magnetic field strength (more exactly the magnetic induction). $1T = 1Vs/m^2 = 10{,}000$Gauss.

TEXTOR: Torus Experiment for Technology Oriented Research. Tokamak at Jülich, Germany (Association EURATOM-FZJ). Refurbished and upgraded, in 1994, as TEXTOR-94.

TFTR: "Tokamak Fusion Test Reactor" at Princeton, the largest US device with a major campaign using deuterium-tritium fuel from 1993 - 1997. Ceased operation in March 1997.

Thermal cycling: Successive heating and cooling of materials can lead to cracks or rupture, particularly at boundaries between materials that expand at different rates.

Thermal particles: As a result of collisional energy exchange, the energy of most plasma particles falls within a Maxwellian distribution which is described by a single temperature (typically 1-30keV for tokamaks). These are the thermal particles, as distinct from energetic particles which lie outside the thermal distribution.

Thomson scattering diagnostic: Diagnostic to measure temperature and density by detecting laser light scattered and Doppler shifted by the thermal plasma electrons.

Tight aspect ratio: Same as Low aspect ratio.

TJ-II: A heliac stellarator at Madrid, Spain (Association EURATOM-CIEMAT). (TJ-IU was a torsatron at CIEMAT, built and operated in preparation for TJ-II).

Tokamak: Magnetic configuration with the shape of a torus. The plasma is stabilised by a strong toroidal magnetic field. The poloidal component of the magnetic field is produced by an electrical current flowing toroidally in the plasma. This current is induced via transformer action and, for steady state, must be maintained by non-inductive current drive and by self-generation of bootstrap current inside the plasma.

Tokamak operating boundaries: The set of plasma parameters, beyond which it is impossible to operate a tokamak. Careful choice of plasma cross-sectional shapes and current and pressure profiles can increase the operating regime.

TORE SUPRA: Large tokamak with superconducting toroidal magnetic field coils and a circular plasma cross-section at the Association EURATOM-CEA in Cadarache, France. It features long high total energy plasmas.

Toroidal Alfvén Eigenmodes: See TAE modes.

Toroidal field: The component of the magnetic field along the major circumference of the torus. The largest magnetic field component in a tokamak.

Toroidal stability: Stability analysis taking account of effects due to the toroidal geometry. These are sometimes neglected to identify possible instabilities, but must

usually be included for accurate predictions of stability boundaries.

Toroidal turbulence code: A turbulence code which includes effects due to the toroidal geometry.

TOSKA: Large testing facility for superconductors (Association EURATOM-FZK, Karlsruhe, Germany).

Transformer drive: The use of a transformer action to induce plasma current.

Transport: The processes by which particles and energy move across magnetic surfaces.

Transport barrier: In certain operational scenarios (e.g. the H-mode or ITB-mode) a region of low transport exists giving rise to a steep local pressure gradient. Such a region is referred to as a transport barrier.

Transport scaling: The magnitude of heat transport may be expressed, empirically or theoretically, in terms of a simple functional dependence on a few plasma parameters. This allows us to model how the heat transport varies (scales) in response to changes in the value of these parameters.

Trapped particles: The outside (large major radius) of a tokamak plasma has a lower magnetic field than the inside. Particles with low velocity parallel to the magnetic field compared with the velocity perpendicular to the magnetic field may not enter the higher field (inside) region and become trapped on the outside. They are not free to circulate toroidally but instead bounce back and forth, performing so-called banana orbits.

Tri-lateral Euregio Cluster (TEC): A collaboration between the Associations Euratom-FZJ, -FOM and –Etat Belge, to exploit the TEXTOR tokamak at FZJ, Julich, Germany.

Tritium: An isotope of hydrogen, whose nucleus consists of one proton and two neutrons. Tritium is unstable to radioactive decay with a half-life of 12.3 years. Due to its rapid decay, tritium is almost absent on earth. For a fusion reactor, tritium will be produced in the breeding blanket surrounding the core of a fusion power station. Special tritium-handling technology is required whenever the use of deuterium-tritium plasmas is contemplated and has been developed on TFTR and JET.

Tritium inventory: The amount of tritium contained in a fusion power station or in a specified part of it.

Turbulence: Randomly fluctuating, as opposed to coherent, wave action. For example, the turbulent water beneath a waterfall can only be described in terms of its averaged properties, such as the scale and duration of fluctuations; whereas a more systematic description can be given to waves on the surface of a still pond.

Turbulent transport: Anomalous heat transport associated with plasma turbulence.

Two-fluid model and multi-fluid model: The extended set of equations which represent a plasma as interpenetrating and interacting fluids of electrons and ions, impurity ions etc.

UKAEA: United Kingdom Atomic Energy Authority. Partner in the Association EURATOM-UKAEA which operates the tokamak COMPASS-D and the spherical tokamak MAST. Also charged with the operation of the JET facilities under EFDA.

Vertical Displacement Event (VDE): An event which arises when control of the plasma is lost and the plasma moves vertically. It can lead to a "halo current" in components which surround the plasma resulting in large, potentially damaging, forces on these components. The forces are much larger in larger tokamaks and are therefore of particular concern for JET and ITER.

VUV: The "Vacuum Ultra Violet" range of the electromagnetic spectrum.

Warm plasma refuelling: Fuelling of plasma using medium energy particles or particle clusters.

WEC: World Energy Council.

WENDELSTEIN VII-AS: Advanced stellarator, at Garching, Germany (Association EURATOM-IPP).

WENDELSTEIN VII-X: Large advanced superconducting stellarator, optimised to produce a reactor-relevant plasma configuration, designed at Garching. Construction is in progress at Greifswald, Germany (Association EURATOM-IPP).

X-point: See single/double null.

XUV: The “Extreme Ultra Violet” range of the electromagnetic spectrum. Shorter wavelengths than VUV.

<u>Acknowledgement:</u> This glossary was adapted from the “Glossary of fusion terms” by UKAEA Culham, UK, and from the glossary of “Fusion programme evaluation”, 1996, EUR 17521, European Commission.